Use of the RAFT technique as an efficient method to synthesise well-defined polymer–clay nanocomposites with improved properties

By

Austin Samakande

Dissertation presented in partial fulfillment of the requirements for the degree of Doctor of Philosophy (PhD) in Polymer Science

at the

University of Stellenbosch

Promoter: Prof. R.D. Sanderson

Copromoter: Dr. P.C. Hartmann

December 2008

Declaration

I, the undersigned, hereby declare that the work contained in this dissertation is my own original work and that I have not previously in its entirety or in part submitted it at any university for a degree.

Signature:  Date: 1-12-2008

Austin Samakande

Abstract

Synthesis and structural characterization of two novel cationic and three new neutral reversible addition–fragmentation chain transfer (RAFT) agents is described. The cationic RAFT agents bear a quaternary ammonium group: N,N-dimethyl-N-(4-(((phenylcarbonothionyl)thio)methyl)benzyl)ethanammonium bromide (PCDBAB) and N-(4-((((dodecylthio)carbonothioyl)thio)methyl)benzyl)-N,N-dimethylethanammonium bromide (DCTBAB). The three neutral RAFT agents synthesized are 1,4-phenylenebis(methylene)dibenzene carbodithioate (PCDBDCP), didodecyl-1,4-phenylenebis(methyllene)bistrithiocarbonate (DCTBTCD) and 11-(((benzylthio)carbonothioyl)thio)undecanoic acid (BCTUA). The self-assembly behaviour in diluted aqueous solutions of the cationic RAFT agents, PCDBAB and DCTBAB, is described. The self-assembly behaviour was promoted by the presence of the thiocarbonyl-thio group on the RAFT agents, in addition to the overall chemical structure of the surfactant that also influence self-assembly.

The RAFT agents were used for the bulk or miniemulsion RAFT-mediated controlled free-radical polymerization in the presence of clay to yield polymer–clay nanocomposites (PCNs). Bulk polymerization resulted in PCNs with better control of molar mass and polydispersity index (PDI) values when compared to PCNs prepared by miniemulsion polymerization. In both bulk and miniemulsion polymerizations the molar masses and PDI values were dependent on the amount of clay and RAFT agent present in the system.

Free-radical bulk neutral RAFT agent-mediated polymerization resulted in PCNs with predominantly intercalated morphology. This was attributed to radical–radical coupling of the initiator anchored onto the clay galleries on which polymerization took place. On the other hand, when the cationic RAFT agent anchored onto clay, i.e. RAFT-modified clay was used, bulk polymerization resulted in predominantly

exfoliated PCNs. However, miniemulsion polymerization carried out in the presence of the RAFT-modified clays resulted in PCNs with a morphology that ranged from partially exfoliated to intercalated morphology, as the clay loading was increased. The changing morphology for miniemulsion-based PCNs was attributed to the decreasing molar mass as the clay loading was increased.

The PCNs obtained had enhanced thermo-mechanical properties as a result of the presence of clay. The thermo-mechanical properties depended on the molar mass, PDI, clay loading, and the morphology of the PCNs.

Opsomming

Die bereiding en strukturele karakterisering van twee nuwe kationiese en drie neutrale RAFT-verbindings word bespreek. Die kationiese RAFT-verbinding bevat ’n vierdelige ammonium groep, N,N-dimetiel-N-(4-(((fenielkarbonotioniel)tio)metiel)-bensiel)etaanammonium bromied (PKDBAB) en N-(4-((((dodesieltio)karbonotioiel)-tio)metiel)bensiel-N,N-dimetieletaanammonium bromied (DKTBAB). Die drie neutrale RAFT-verbindings wat berei is, is 1,4-fenielienbis(metieleen)dibenseen karboditioaat (PKDBDKP), didodesiel-1,4-fenieleenbis(metieleen)bistritiokarbonaat (DKTBTKD), en 11-(((bensieltio)-karbonotioiel)tio)undekanoiese suur (BKTUS). Die eiesamestelling-sgedrag van verdunde water oplossings berei met die kationiese RAFT-verbindings, PKDBAB en DKTBAB word beskryf. Afgesien van die seeplengte, hoofgroep en chemiese samestelling word die eiesamestellingsgedrag bevorder deur die tio-karboniel-tio groep teenwoordig in die RAFT-verbinding.

Die RAFT-verbindings is gebruik om massa of miniemulsie RAFT-bemiddelde beheerde vryradikaal polimerisasie uit te voer in die teenwoordigheid van klei om sodoende polimeer-klei-nanosamestellings (PKNs) te vorm. Massapolimerisasie in PKNs het getoon daar beter beheer is oor die molêre massa sowel as die poliverspreidingsindeks (PVI) in vergelyking met miniemulsie polimerisasie. In beide polimerisasie tegnieke is die molêre massa en PVI afhanklik van die hoeveelheid klei en RAFT-verbinding teenwoordig in die sisteem.

Vryradikaal massa neutrale RAFT-verbinding bemiddelde polimerisasie het oorheersend ’n inskakelingsmorfologie. Dit kan toegeskryf word aan die radikaal-radikaal koppeling van die afsetter wat aan die klei vasgeanker is en waarop die polimerisasie plaasvind. In teenstelling hiermee is gevind dat, wanneer die kationiese RAFT-verbinding aan die klei vasgeanker word, i.e. waar RAFT-gewysigde klei gebruik is, het die massapolimerisasie getoon dat oorheersend afgeskilferde

morfologie PKNs gevorm word. Miniemulsie polimerisasie, uitgevoer in die teenwoordigheid van die RAFT-gewysigde klei, het egter PKNs gevorm wat gewissel het van gedeeltelik afgeskilferde morfologie tot inskakelingsmorfologie soos wat die kleilading verhoog is. Die verandering in morfologie, in die geval van die miniemulsie gebaseerde PKNs, word toegeskryf aan die verlaging in die molêre massa soos wat die kleilading verhoog word.

Die PKNs wat berei is het verhoogde termiese-meganiese eienskappe as gevolg van die klei wat teenwoordig is. Die termiese-meganiese eienskappe is afhanklik van die molêre massa, PVI, kleilading en die morfologie van die PKNs.

Acknowledgements

Firstly, I would like to give praise and worship to God, for with Him nothing is unfeasible. With faith we can move mountains …Mark 11 vs 24 and Hebrews 11.

Secondly the Department of Chemistry and Polymer Science, the UNESCO centre for Macromolecules, NRF, MONDI Packaging South Africa (MPSA) and THRIP are thanked for funding this very exciting project.

To my promoter Professor Sanderson, Sir, your unwavering support, being a visionary and your endless intellect during the time I have spent at the University of Stellenbosch is highly acknowledged. Moreover, you believed in me; that gave me strength and confidence in my work.

To Dr Hartmann (Boss), my copromoter, I say thank you for all your input. You were there whenever I needed you, even when you were on holiday you had time for me. Boss, it was indeed a pleasure working with you.

My friends in Stellenbosch and beyond, you indeed inspired me and you played a very crucial role in my completing my studies. The paper coatings group at Polymer Science is also thanked for their help and support. The people at the Polymer science department are thanked for their warm and tender hearts towards me.

I thank my family for their patience, and support for my wish to realize my dreams.

Dr Margie Hurndall is thanked for helping me with editing this document. Mum, thank you for your time and energy.

Lastly, to Miriam, my beautiful living angel, indeed we endured through thick and thin. It wasn't easy for us to be endless miles away from each other but here we are; still

standing, going strong and weathering each and every storm together. Honey, this one (document) is for you!

List of contents

List of abbreviations

ABS	acrylonitrile-butadiene-styrene
ABS-graft-MAH	acrylonitrile-butadiene-styrene grafted maleic anhydride
AIBA	azo*bis*isobutyramidine hydrochloride
AIBN	azo*bis*isobutyronitrile
ATRP	atom transfer radical polymerization
BCTUA	11-(((benzylthio)carbonothioyl)thio)undecanoic acid
CAD	4-cyanopentanoic acid dithiobenzoate
Calc M_n	calculated theoretical molar mass
$CDCl_3$	deuterated chloroform
CDDA	10-Carboxylic acid-10-dithiobenzoate-decyltrimethylammonium bromide
cec	cation-exchange capacity
cmc	critical micelle concentration
CT	chain transfer
CTAB	cetyltrimethylammonium bromide
DBX	α, α-dibromo-p-xylol

DCTBAB	N-(4-((((dodecylthio)carbonothioyl)thio)methyl)benzyl)-N,N-dimethylethanammonium bromide
DCTBAB-MMT	N-(4-((((dodecylthio)carbonothioyl)thio)methyl)benzyl)-N,N-dimethylethanammonium bromide-modified montmorillonite clay
DCTBTCD	dodecyl-1,4-phenylenebis(methylene)bistrithiocarbonate
DLS	dynamic light scattering
DMA	dynamic mechanical analysis
DSC	differential scanning calorimetry
ELS	evaporative light scattering
ESMS	electrospray mass spectroscopy
Exp M_n	experimental molar mass
FT-IR	fourier-transform infrared
G^I	storage modulus
G^{II}	loss modulus
GPC	gel permeation chromatography
HLB	hydrophilic–lipophilic balance
HPLC	high performance liquid chromatography
I	initiator
Inisurf	initiator surfactant
ITP	iodine transfer polymerization
LDH	layered double hydroxide
MMT	montmorillonite clay
M_n	number average molar mass

M_{RAFT}	molar mass of RAFT agent
M_S	molar mass of styrene
M_W	weight average molar mass
MMD	molar mass distribution
M_W/M_n	polydispersity index
m/z	mass per unit charge ratio
n_I	number of moles of initiator
Na^+-MMT	montmorillonite clay containing predominantly sodium ions
NaOH	sodium hydroxide
n-BA	n-butyl acrylate
NMP	nitroxide-mediated polymerization
NMR	nuclear magnetic resonance
PAS	photoacoustic spectroscopy
PBA	poly(butyl acrylate)
PCDBAB	N, N-dimethyl-N-(4-(((phenylcarbonothionyl)thio)methyl)benzyl)-ethanammonium bromide
PCDBAB-MMT	N, N-dimethyl-N-(4-(((phenylcarbonothionyl)thio)methyl)benzyl)-ethanammonium bromide-modified montmorillonite clay
PCDBDCP	1,4-phenylenebis(methylene)dibenzenecarbodithioate
PCNs	polymer–clay nanocomposites
PDI	polydispersity index
PEO	poly(ethylene oxide)
PRE	persistent radical effect

PMMA	poly(methyl methacrylate)
PS–CNs	polystyrene–clay nanocomposites
P(S-co-BA)	polystyrene-co-butyl acrylate
RAFT	reversible addition–fragmentation chain transfer
RAFT-MMT	RAFT-modified MMT clay
S	styrene
SANS	small angle neutron scattering
SAXS	small angle X-ray scattering
SDS	sodium dodecyl sulphate
SEC	Size-exclusion chromatography
SFRP	stable free-radical polymerization
Surfmer	polymerizable surfactant
TEM	transmission electron microscopy
TEMPO	2,2,6,6-tetramethyl-1-piperidinyloxy free-radical
T_g	glass transition temperature
TGA	thermogravimetric analysis
THF	tetrahydrofuran
Transurf	transfer surfactant
UV	ultraviolet
VA060	2,2'-azo*bis*(2-(1-(2-hydroxyethyl)-2-imidazolin-2-yl)propane)di-hydrochloride monohydrate
WAXD	wide angle X-ray diffraction
wt	weight

XRD	X-ray diffraction

List of symbols

d	interlayer distance
$\Delta_{dil}H_{cum}$	cumulative enthalpies of dilution
ω	angular frequency
a_0	surfactant head group surface area
ΔG_{mic}	fee energy of micellization
ΔH_{mic}	enthalpy of micellization
ΔS_{mic}	etropy of micellization
$\Delta_{dil}H$	molar enthalpy of dilution
Γ_m	surface excess concentration
$[RAFT]_0$	initial concentration of RAFT agent
$\frac{[S]_0}{[R]_0}$	initial ratio of the number of moles of styrene to RAFT
α	micelle ionization degree
λ	wavelength

Chapter 1: Introduction and objectives

Abstract

This chapter gives a brief introduction and the objectives of this study.

1.1 Introduction

Nanotechnology has caught the scientific community by storm; many discoveries have been reported and many practical applications envisaged. Nanotechnology has also been embraced by polymer scientists, who, with others, are at the forefront of some recent ingenious developments. In the polymer science arena, one of the most interesting research area in nanotechnology focuses on the inclusion of nanoparticles in polymers in order to enhance their chemical resistance, thermal stability, barrier properties and mechanical properties. Some of the nanoparticles studied to date include nanofibres, silica nanoparticles, carbon nanotubes, graphene sheets and clays. Of all these fillers, the most interesting and arguably the most studied are the clays. Not only do they provide most of the advantages offered by nanometer-size dispersions but they can be incorporated in both hydrophilic and hydrophobic polymers with relative ease. Moreover, the clays are naturally available and thus their use is generally cost effective.

Clays in their natural state are crystalline, inorganic layered compounds. These compounds are divided, into two main families, i.e. the non swellable clays and the swellable clays (i.e. they can expand along the c axis in order to accommodate foreign species in-between their clay layers). It is the swellable clays that are used as nanofillers for polymers. Due to crystalline defects, which cause a charge imbalance in the crystalline latice, the swellable clays exhibit negative charges on their surface, which are counterbalanced by hydrated inorganic cations such as K^+, Na^+ and Mg^{2+}. These small cations reside in-between the clay layers. Naturally occuring clays are hydrophilic and can thus be dispersed in hydrophilic polar polymers like polyethylene oxide, to readily yield polyethylene oxide–clay nanocomposite. However, for hydrophobic polymers the clay needs to be modified to become hydrophobic, to render it compatible with and thus dispersible in the continuous polymer matrix.

In the early 1990s the Toyota research group showed that the hydrated cations within the clay layers can be replaced by alkyl ammonium compounds. The resultant organically modified-clay was then dispersed in ε-caprolactam,

followed by an *in situ* intercalative polymerization process to yield nylon 6 polymer–clay nanocomposite (Nylon 6-PCN).[1] The Nylon 6-PCNs they prepared had exceptional thermal and mechanical properties, relative to the neat Nylon 6 polymer, and hence the Nylon 6-PCN found application in the automobile industry.

Many other researchers followed suit, and over the next decade numerous reports on various aspects of PCNs were reported, from their synthesis to applications. Significant findings to date include the following: for a complete and homogeneous dispersion of clay in the polymer matrix there must be complete miscibility between the clay and the polymer, and for exceptional property enhancement, (i.e. physical, chemical, thermal and mechanical) the clay modifier (i.e. normally reactive or non-reactive surfactants) should preferably be reactive towards the polymeric matrix. A reactive clay modifier leads to a strong interfacial adhesion between the clay and the polymer, and subsequently the exceptional mechanical properties during load bearing.

Thus a new era had begun in which various reactive surfactants were used for the modification of clay. These surfactants included polymerizable surfactants, initiator surfactants and transfer surfactants. To date, most of the reports on the use of functionalized surfactants focused on the use of polymerizable surfactants as clay modifiers.[2] However, only a few research efforts were focused on the use of transfer surfactants and initiator surfactants as clay modifiers and the subsequent preparation of PCNs.

The use of transfer agents in free-radical polymerization reactions allow one to achieve control of the polymerization process.[3] This results in polymers with low polydispersity indices and predictable molar masses. The discovery of the controlled polymerization techniques, and in particular reversible addition–fragmentation chain transfer (RAFT) agents, has been an outstanding achievement.[4] RAFT polymerization now allows the preparation of polymer architectures that were never before envisaged to be possible. Thus a combination of RAFT technology and clay nanotechnology for the synthesis of PCNs by RAFT-mediated polymerization is expected to allow the preparation of tailor-made materials with specific properties for niche applications. To date

the synthesis of RAFT based transurfs has not been extensively reported, save for reports by Baussard *et al*. and Levesque *et al.*[5,6] This can be attributed to the presence of the thio-carbonyl-thio group on the RAFT agents. The thio-carbonyl-thio group is reactive towards nucleophiles, hence complicating the synthesis of the RAFT–transurfs. On the other hand, the use of RAFT-based positively charged RAFT agents for the modification of clay and the subsequent synthesis of PCNs by bulk polymerization has recently been reported by Di and Sogah and, most recently, Zhang *et al.*[7,8] reported on a similar approach using solution polymerization. They achieved clay layers that were homogeneously dispersed in the polymer matrix. The polymer chains had low polydispersity indices. The efficiency of the RAFT anchored onto clay was dependent on the RAFT/clay amount within the reaction mixture. The nanocomposites thus prepared had enhanced thermal stability. They did not report on the use of aqueous based miniemulsion polymerization, and no reports in the open literature describe using RAFT agents and clay in miniemulsion polymerization.

Salem and Ship reported on the use of a clay modified by a polymerizable surfactant in the presence of a free RAFT agent to control the polymerization process.[9] They observed that the incorporation of a free RAFT agent for the control of PCN synthesis does not alter the nanocomposite morphology nor the ability of the RAFT agent to control the polymerization process. However, no reports are available on the use of an initiator anchored onto clay, and the subsequent polymerization process by an *in situ* intercalative process in the presence of a free RAFT agent.

1.2 Objectives

The main objective of this study was to combine the latest RAFT technology and clay nanotechnology for the synthesis of PCNs. Thus novel RAFT agents had to be synthesized and characterized. Such RAFT agents we choose should be able to control the polymerization reactions of styrene monomer. Styrene was used as a model monomer because of its vast literature that is available, thus easy to find references. PCNs were to be synthesized, making use of *in situ* intercalative free-radical polymerization in the presence of RAFT

agents in bulk and then applying the knowledge gained to aqueous based polymerization in miniemulsion. The miniemulsions obtained should be stable and the polymer chains RAFT controlled, without any adverse effects as often reported for RAFT-mediated miniemulsion polymerizations, such as miniemulsion instability. For stable RAFT-mediated miniemulsions I aimed to use the positively charged RAFT agents only. This was necessary because neutral RAFT agents have been found to lead to aqueous phase polymerization and destabilization. However, the use of free, neutral and ionic RAFT agents in bulk polymerization is proposed to proceed smoothly and information obtained from bulk polymerization of styrene could be applied to the miniemulsion based polymerization of styrene and copolymers of styrene and butyl acrylate.

Thus the specific objectives of the study were the following:-

- Synthesis and structural characterization of novel, positively charged and neutral RAFT agents.
- Determination of the aqueous behavior of the positively charged RAFT transurfs under dilute conditions.
- Modification of clay by an initiator, 2,2'-azo*bis*(2-(1-(2-hydroxyethyl)-2-imidazolin-2-yl)propane)dihydrochloride monohydrate (VA060). Dispersion of the initiator-modified-clay in styrene followed by *in situ* intercalative bulk polymerization to yield PS–VA060-clay nanocomposites. Evaluation of the effect of the use of the RAFT-mediated polymerization on the control of the PS–VA060-clay nanocomposites' morphology and properties.
- Modification of clay by the positively charged RAFT agents synthesized. Dispersion of the RAFT-modified-clays in styrene followed by *in situ* intercalative bulk polymerization to yield PS–RAFT-clay nanocomposites. Characterization of the modified-clays and the various PS–RAFT-CNs obtained.
- Preparation of PCNs by controlled free-radical polymerization in miniemulsion using RAFT-surface modified-clay. Two polymer systems will

be considered: polystyrene (PS), and poly(styrene-co-butyl acrylate) [P(S-co-BA)]. Characterization of PCNs obtained in terms of colloidal properties, PCN structure, polymer matrix composition, molar mass, thermal stability and thermo-mechanical properties.

1.3 Layout of dissertation

This dissertation was intentionally written in the “publication style”, in fact Chapters 4–8 are publications in their published form.

1.3.1 Chapters layout

In Chapter 1, a brief introduction on polymer–clay nanocomposites (PCNs) and the objectives of this study are presented.

Chapter 2, literature review of PCNs with emphasis on those based on polystyrene (PS) is addressed. In addition factors that influence the formation of a PCN are given together with techniques for PCN characterization.

Chapter 3, documents a literature review on the controlled free-radical polymerization techniques and their applicability to PCN synthesis. Emphasis is placed on the reversible addition–fragmentation chain transfer (RAFT) technique as it is the technique chosen in this study.

Chapter 4, details the synthesis and characterization of novel cationic (two) and neutral (three) RAFT agents. A study of the self-assembly of the cationic RAFT agents in dilute aqueous environment is also outlined.

In Chapter 5, bulk polymerization of styrene in the presence of an initiator-modified-clay and neutral RAFT agents’ to yield PCNs is outlined. The effectiveness of the initiator-modified-clay and the neutral RAFT agents to initiate and control the polymerization, respectively is documented. Moreover, the characterization of the obtained PCNs was included.

Chapter 6, details the use of cationic RAFT agents for the modification of clay and the subsequent use of the RAFT-modified-clay for the control of styrene

polymerization to yield PCNs is outlined. Characterization of the PCNs obtained is documented.

Chapter 7 and 8, details the synthesis and characterization of PCNs obtained by making use of miniemulsion polymerization. A comparison of the PCNs obtained in bulk and those obtained in miniemulsion is outlined in terms of control of polymerization and thermo-mechanical properties.

Chapter 9, gives conclusions of this study and recommendations for future work.

1.4 References

[1] A. Usuki, Y. Kojima, M. Kawasumi, A. Okada, Y. Fukushima, T. Kurauchi, O. Kamigaito. *J Mater Res* **1993**, *8*, 1179-1184.

[2] A. Samakande, P. C. Hartmann, V. Cloete, R. D. Sanderson. *Polymer* **2007**, *48*, 1490-1499.

[3] W. A. Braunecker, K. Matyjaszewski. *Prog Polym Sci* **2007**, *32*, 93-146.

[4] T. P. Le, G. Moad, R. Ezio, S. H. Thang. *PCT Int Appl WO 9801478* **1998**, 88.

[5] J. Baussard, J. Habib-Jiwan, A. Laschewsky, M. Mertoglu, J. Storsberg. *Polymer* **2004**, *45*, 3615-3626.

[6] G. Levesque, P. Arsene, V. Fanneau-Bellenger, T. Pham. *Biomacromolecules* **2000**, *1*, 387-399.

[7] J. B. Di, D. Y. Sogah. *Macromolecules* **2006**, *39*, 1020-1028.

[8] B. Q. Zhang, C. Y. Pan, C. Y. Hong, B. Luan, P. J. Shi. *Macromol Rapid Commun* **2006**, *27*, 97-102.

[9] N. Salem, D. A. Shipp. *Polymer* **2005**, *46*, 8573-8581.

Chapter 2: Literature review

Abstract

This chapter details the background and literature review of the study I carried out. Focus is emphasized on the aspects that are paramount to this study.

2.1 Introduction

In many situations polymers are either too expensive to produce viably or their properties fail for the intended application. To circumvent this, either fillers to reduce cost or additives to enhance properties are incorporated into polymers. There are many different classes of fillers and additives available but of particular interest are the fillers that contribute to improved polymer properties, namely carbon nanonotubes, nanofibres and clays. The most interesting of these filler additives are the clays. Clays have received much attention in the past decade because they can be dispersed in a polymer matrix at nanometer level yield particle reinforced polymers known as polymer–clay nanocomposites (PCNs).[1] PCNs have superior barrier, chemical, thermal and mechanical properties relative to neat polymers. PCN applications include areas where tough and high temperature durability is required, coatings, electronics.[2]

2.2 Types of Clay

There are two major classes of clays, the non-swelling clays and the swelling clays. The non-swelling clays, also known as the 1:1 family, are not swellable because the forces that hold two adjacent clay layers (platelets) in place are colossal that the layers cannot move away from each other to accommodate any foreign species between them. The most common non-swelling clay is kaolinite. The swelling clays, also known as the 2:1 family, have the ability to expand (along their c axis) by incorporating foreign species in-between adjacent clay tactoids.

2.3 Clay structure

Clay consists of small-sized crystalline particles comprising aluminosilicates of various compositions, with possible iron and magnesium substitutions by alkaline earth elements.

The basic unit is a silicon atom, surrounded by four oxygen atoms forming a tetrahedron, as shown in Fig. 2.1. The tetrahedra are then linked in two dimensions to form a sheet of hexagonal rings. There is also an octahedron of aluminium surrounded

by oxygen atoms, and the octahedra link to form a more closely packed two-dimensional sheet.

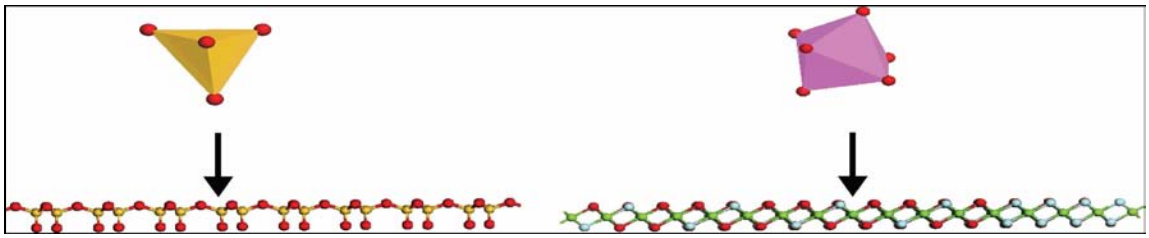

tetrahedral sheet octahedral sheet

Fig. 2.1 Basic units of clay minerals.

The non-swelling clay family composes of alumina octahedra sitting on top of a sheet of tetrahedral silica, forming a dioctahedral (hence the name 1:1 family). The apical oxygen atoms from silica are shared with the aluminium atoms of the upper layer. The swelling clay family comprises two sheets of silica to one of alumina (parent compound is the pyrophyllite) or two sheets of silica to one of magnesium oxide (hence the name 2:1 family). See Fig. 2.2.

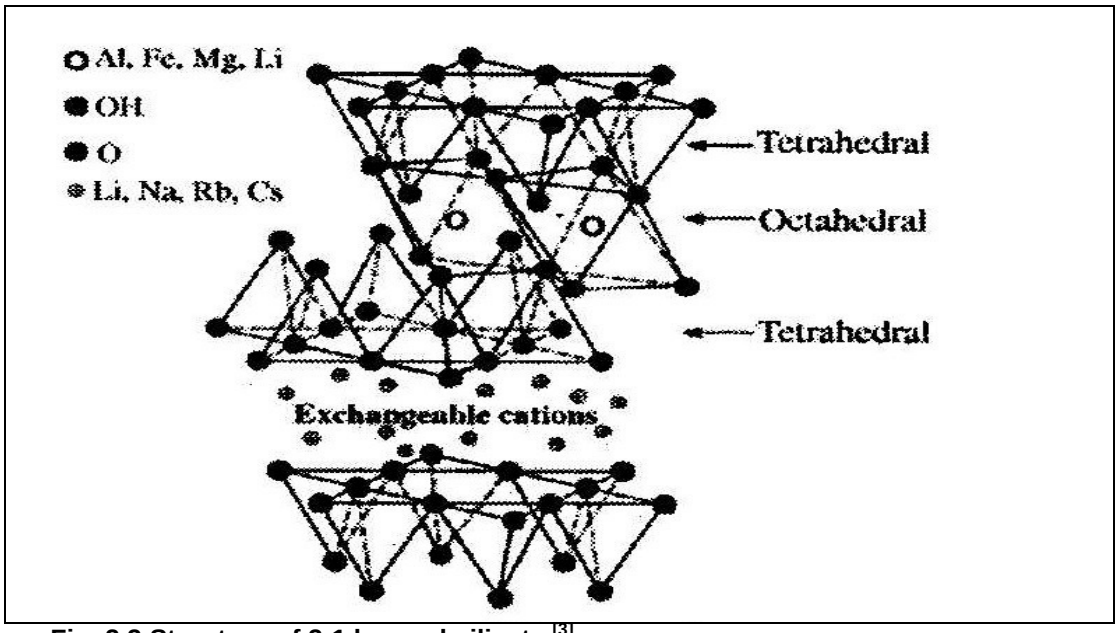

Fig. 2.2 Structure of 2:1 layered silicate.[3]

Clays used in the preparation of PCNs belong to the 2:1 family. The layer thickness of an individual tactoid is around 1 nm and the lateral dimensions may vary from 30 nm to several micrometers and even larger, depending on the type of the layered silicate. Stacking of the layers then leads to a regular gap between the clay layers, called the

interlayer distance. Naturally occurring isomorphic substitution within the layers (e.g. Al^{3+} replaced by Mg^{2+} or Fe^{2+}, or Mg^{2+} replaced by Li^{+}) generates negative charges that are counterbalanced by hydrated alkali and alkaline earth cations situated inside the clay galleries. The commonly used layered silicates are montmorillonite (MMT), hectorite and saponite.[4] Their chemical formulae are given in Table 2.1. The type of clay is characterized by a moderate charge called the cation-exchange capacity (cec), which ranges from 80–120 meq/100 g.

Table 2.1 Chemical structure of commonly used 2:1 layered phyllosilicates [5]

2:1 phyllosilicate	General formula
Montmorillonite	$M_x (Al_{4-x} Mg_x) Si_8O_{20} (OH)_4$
Hectorite	$M_x (Mg_{6-x} Li_x) Si_8O_{20} (OH)_4$
Saponite	$M_x [Mg_x] (Si_{8-x} Al_x)O_{20} (OH)_4$

M is the counterbalancing ion, and x is the degree of isomorphous substitution (between 0.5 and 1.3).

One of the most interesting and widely investigated clays for PCN is MMT. MMT comprises one octahedral alumina sheet sandwiched between two tetrahedral silica sheets. About one in six of the aluminum ions in the octahedral layers of MMT is isomorphously substituted by a magnesium ion or other divalent ions. The resulting negative charges are counterbalanced by cations (e.g. Na^+, K^+ or Ca^{2+}) residing in the interlayer spaces.

The forces that hold the stacks together are relatively weak, resulting in easy intercalation of small hydrophilic molecules between the layers. At this point the clay is only miscible with hydrophilic species, e.g. water-soluble polymers such as polyethylene oxide. In order to improve miscibility with hydrophobic species it is necessary to convert the hydrophilic silicate surfaces to organophilic surfaces. Modification of the clay surfaces also increases the distance between adjacent clay platelets and thus more room for larger foreign species to penetrate.[6] Clay modification can be achieved by any of the four processes detailed below.

2.4 Modification of clay

The four methods of clay modification are by ion-exchange reactions, adsorption, edge-wise and *in situ* synthesis.

2.4.1 Ion-exchange

The most commonly used method for clay modification is ion-exchange reactions. In pristine clay, small inorganic cations can be replaced by any positively charged species. The latter can be simple inorganic cations, such as Cd^{2+}.[7] The total number of replaceable small inorganic cations is governed by the moderate negative surface charge called the cation-exchange capacity (cec) i.e. the maximum number of exchangeable sites. The cec values are different for different types of clays; they range from 80–120 meq/100 g of clay.[5] During PCN preparation the small hydrated inorganic cations in the clay gallery spaces are usually ion-exchanged by organic cationic surfactants, such as primary, secondary, tertiary, quaternary alkyl ammonium or alkyl phosphonium cations. The organic cations reduce the surface energy and decrease the cohesive energy by expanding the interlayer distance, thus facilitating wetting and intercalation of monomer or polymer onto the clay surfaces and into the galleries, respectively. The ion-exchange of cationic surfactants onto MMT clay dispersed in water is independent of the size of the hydrophilic head group of cationic surfactants.[8] The ion-exchange reaction is affected by pH. Lagaly reported that due to broken bonds on the clay edges, depending on the pH, these edges can also take part in the ion-exchange reaction.[9] This results in more surfactant than the cec binding onto the clay. The cec is approximately equal to the total amount of surfactant that can be adsorbed as a monolayer. The surfactant's chemical structure, the reaction temperature and the charge density of the clay determine the orientation of the surfactant in the galleries. Increasing the surfactant's chain length or the clay's charge density leads to a larger *d* spacing and interlayer volume.

There are many possible orientations of the surfactants in gallery spacings. These orientations vary from solid-like to liquid-like. The liquid-like dominates at higher temperatures, as the surfactant chain length decreases, or as the interlayer density

decreases.[3,4,8] Other factors that influence the orientation of the surfactants in the galleries include the surfactant's number of tails and branching. A schematic representation of the ion-exchange reaction is shown in Fig. 2.3.

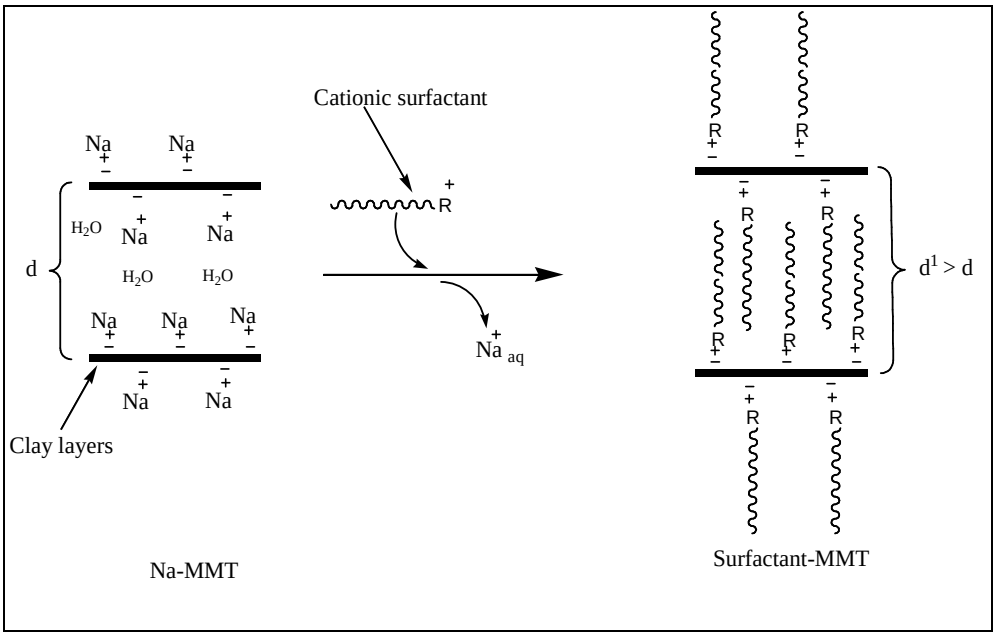

Fig. 2.3 Ion-exchange reaction of Na-MMT and a cationic surfactant.

The modification of clay by organic cations was reported as early as 1949, when Jordan reported on the use of various aliphatic ammonium salts for the modification of hydrophilic bentonite to prepare organophilic bentonite.[10] Since then, other researchers have used various modifying agents, mainly quaternary ammonium salts, to modify the surfaces of clay from hydrophilic to hydrophobic.[11,12] In 1965 Dekking used an azo based, ammonium initiator.[13] His work marked the beginning of a new era in which the use of functionalized ammonium salts, not only yielded hydrophobic clay surfaces but were also able to take part in the initiation, chain transfer or copolymerization with the main monomer during the course of a polymerization reaction. In essence, these are functionalized quaternary ammonium compounds or surfactants that participate in free-radical polymerization. These compounds are divided into three main classes: (i) Surfmers, i.e. surfactants that can also act as monomers, (ii) Transurfs, i.e. surfactants that have the ability to transfer a radical from a growing chain to another chain, and (iii) Inisurfs, i.e. surfactants that can initiate polymerization process.

There are also reports on the modification of clay by the ion-exchange process that involve the use of quaternary ammonium compounds that can take part in non-radical polymerization processes such as condensation polymerization and ionic polymerization.[14]

2.4.2 Adsorption

Adsorption takes place when small molecules, that can undergo dipole–dipole, ion–dipole interactions,[12,15-17] or hydrogen bonding, interact with the hydrated cations in the gallery space. An example of such a molecule is ethylene glycol.[12] In some cases even negatively charged species have been reported to adsorb onto clay surfaces. The mode of adsorption is however debatable. Greesh *et al*. have reported on the adsorption of various modifiers on montmorillonite clay using neutral and negatively charged molecules.[17] The amount of material adsorbed onto the clay surfaces by this method is however difficult to predict. A simplified schematic diagram of this mode of clay modification is shown in Fig. 2.4.

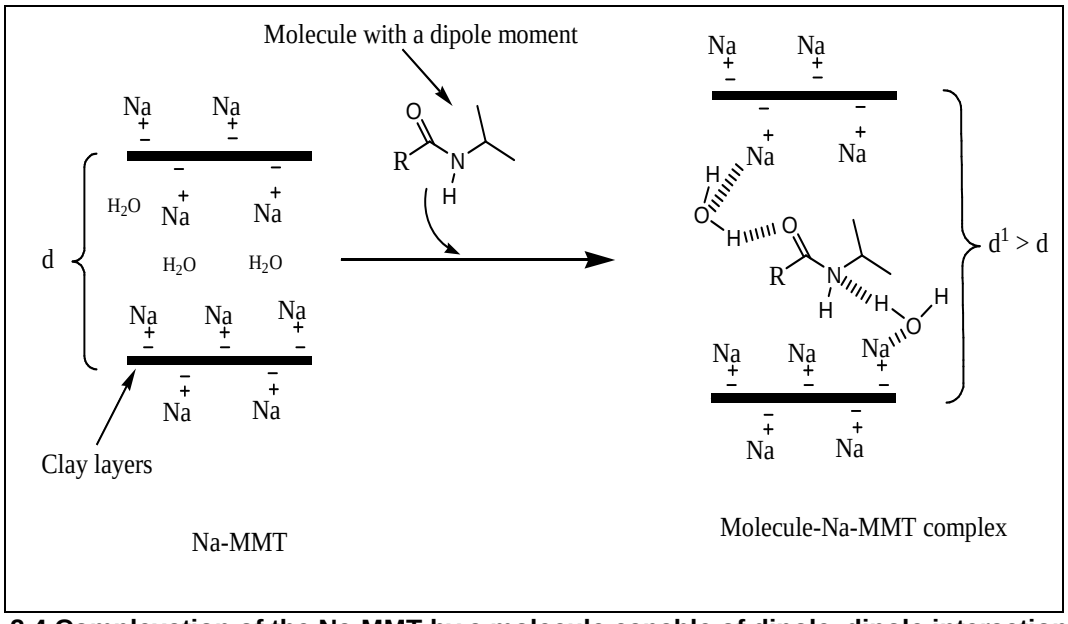

Fig. 2.4 Complexation of the Na-MMT by a molecule capable of dipole–dipole interaction.

2.4.3 Edge-wise modification

Edge-wise modification takes place when advantage is taken of the hydroxyl groups on aluminium or silica on the edges of clay platelets. The hydroxyl groups are reacted with

organic species to yield, in most cases, ether linkages. Most researchers have used mainly silanes,[2,11,12,16,18,19] and titanates[18] for the formation of the ether linkages during edge-wise modification. Here there is no change in the interlayer distances (*d*), given that the modification process is restricted to the edges. A schematic representation of edge-wise modification is shown in Fig. 2.5.

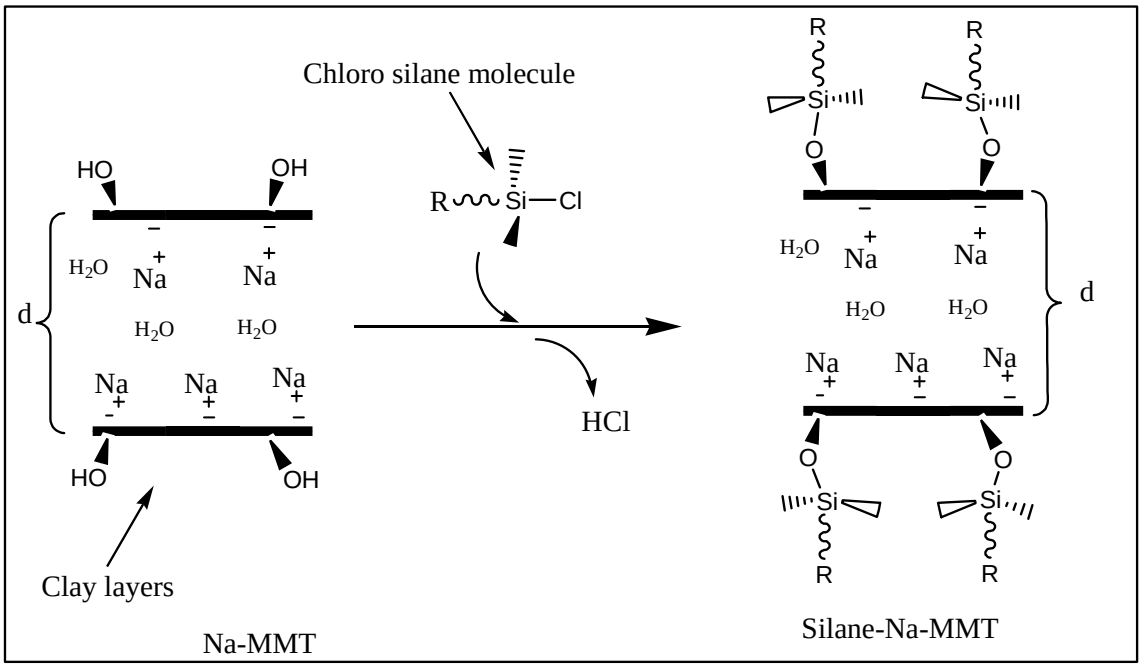

Fig. 2.5 Edge-wise modification of clay using chloro silane molecules.

2.4.4 *In situ* synthesis of modified-clays

Chastek *et al.* reported on the *in situ* synthesis of already modified-clays.[20,21] Here synthetic modified-clays are prepared with alkyl modifying groups already attached to the clay layers (i.e. modification takes place *in situ* during the clay synthesis). This method is however not popular, and is rarely reported on.

2.5 Polymer–clay nanocomposites

Polymer–clay nanocomposites are a new class of two-phase composite materials obtained by the dispersion of clay platelets at nanometer level in a polymer matrix. PCNs were revolutionized by the Toyota research group in the early 1990s when, for the first time, they reported on the successful synthesis and characterization of a nylon

6 polymer–clay nanocomposite (Nylon 6-PCN).[1] The Nylon 6-PCN exhibited exceptional thermo-mechanical properties. Nylon 6-PCN has subsequently been commercialized and has found wide use in the automotive industry. Interest in the area of PCNs has increased significantly from both the academic and industrial perspectives as seen by the numerous journal articles, patents and commercialized products.

In order to attain a nanocomposite structure several requirements have to be met. Firstly, there has to be sufficient compatibility between the clay particles and the polymer matrix, e.g. polyethylene oxide and pristine clay are water soluble and miscible, hence a PCN can be obtained. However, no nanocomposite will result from a hydrophobic polymer and the hydrophilic clay. In such a case one of the components of the composite has to be modified to become compatible with the other. In most cases the clay has to be surface modified, as explained above. Secondly, from a thermodynamic point of view, there has to be a negative free energy associated with nanocomposite formation.

Once a PCN is formed the morphology of clay particles within the continuous polymer matrix depends on the type of interactions between the clay and the polymer matrix. Since the degree of these interactions differs from one PCN to another the morphology of the clay platelets is then used to classify the nanocomposites in question as described below.

2.6 Degree of clay dispersion in a polymer–clay nanocomposite

The degree of clay dispersion in a polymer matrix determines the nanocomposite structure. There are three main general classes of polymer–clay composites that have been widely agreed upon: Conventional microcomposite, intercalated nanocomposite and exfoliated nanocomposite.

2.6.1 Conventional microcomposites

In conventional microcomposites the polymer chains have failed to penetrate the clay galleries during the PCN synthesis and the clay particles exist as agglomerates within the polymer matrix (c.f. Fig. 2.6).

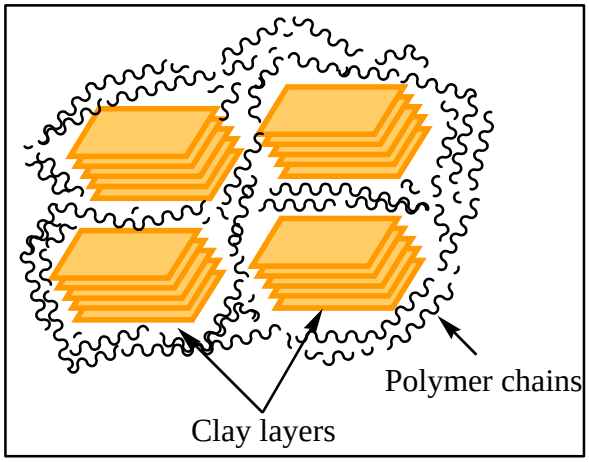

Fig. 2.6 Polymer–clay microcomposite.

This clay morphology normally gives rise to weakened polymer material because the agglomerated clay now acts as imperfections. The material normally fails, commencing with the polymer material surrounding these aggregates due to little or no interaction between the clay and the polymer. This type of clay morphology is not that of a nanocomposite but rather phase-separated material, and is typical of the ancient way of dispersion of inorganic material in a polymer matrix.[5]

2.6.2 Intercalated nanocomposites

In intercalated nanocomposites the polymer chains have penetrated between the clay galleries, resulting in a regular alternating pattern of polymer chain(s) and clay platelets (c.f. Fig. 2.7).

True nanocomposite structure is obtained here. This morphology is easier to achieve than the exfoliated structure (Section 2.6.3) and has been reported on by many researchers.[22]

The benefits of a nanometer-size dispersion of the clay layers start here and the physico-chemical properties of PCNs are superior to those of virgin polymers as well as those of the microcomposites.[4]

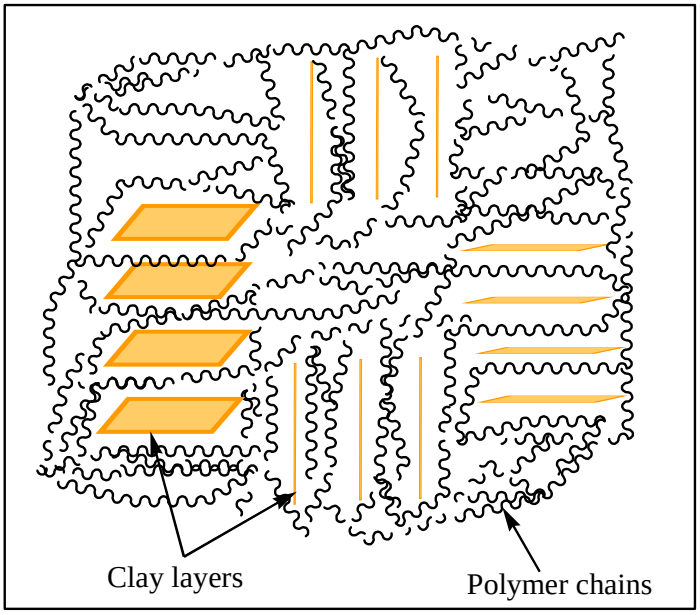

Fig. 2.7 Intercalated polymer-clay nanocomposite.

2.6.3 Exfoliated/delaminated nanocomposite

In exfoliated/delaminated nanocomposites there is a loss of order of the clay platelets relative to each other (c.f. Fig. 2.8).

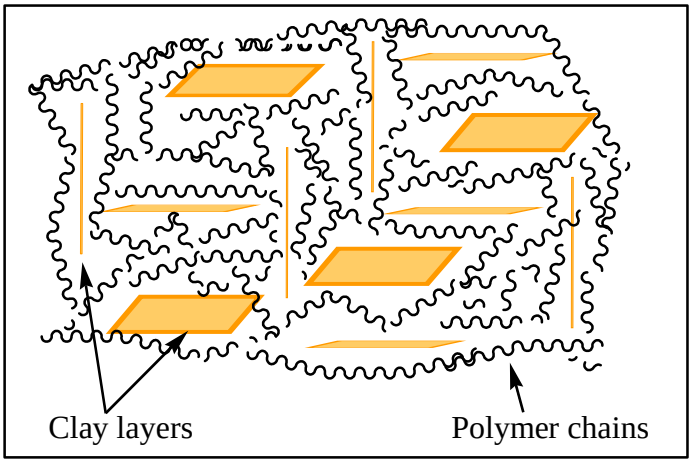

Fig. 2.8 Exfoliated polymer–clay nanocomposite.

The disorder in the clay platelets relative to one another is due to the polymer growth within the galleries, causing massive pressure on the clay platelets, and extensive movement of the clay platelets during copolymerization of the main monomer and the surfmer attached to clay platelets. Fischer reported that modification of clay using zwiter-ions causes repulsion of the adjacent clay platelets. [6] These repulsions lead to

the exfoliated clay structure in a PCN. However, researchers generally agree that the exfoliated structure results in the best enhancement in physico-chemical properties compared to the other two types of composite materials.

It is to be noted that between these three main types of composite structures there are other hybrid clay morphologies that exist in which there is a mixture of clay morphologies within the same sample. The nanocomposite structure and properties depend on the surfactant used during the clay modification and the method by which the nanocomposite was made. In this study an initiator and two transurfs (i.e. RAFT agents) are used in the modification of MMT clay prior to the use of the modified-clays in the synthesis of PCNs. As the type and chemical structure of the modifying agent/surfactant plays a critical role in the overall morphology and properties of the PCN synthesized, I have deliberately included a brief background to surfactants and the various aspects pertaining to the preparation of PCNs.

2.7 Surfactants

The word surfactant comes from the two words “surface” and “active”, meaning that surfactants can be described as surface-active agents. The surface activity of surfactants arises from their amphiphilic nature. The word amphiphilic means that surfactants contain hydrophilic (”water loving”) and hydrophobic (“water hating”) groups in their chemical structures. The general structure of a surfactant is shown in Fig. 2.9.

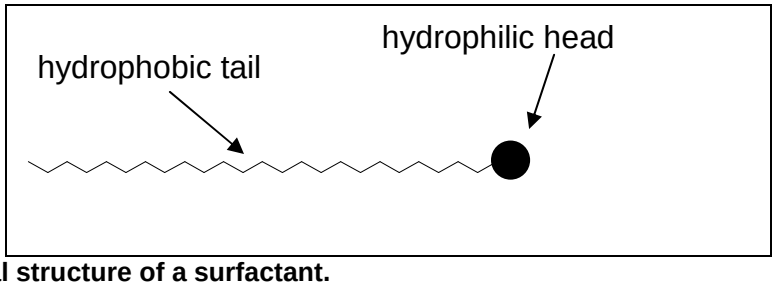

Fig. 2.9 General structure of a surfactant.

Thus, surfactants can interact with both hydrophilic and hydrophobic species, hence they are adsorbed at interfaces thus decreasing the interfacial tension. In general, each surfactant is characterized by its critical micelle concentration (cmc) value, which

correspond to the concentration at which it starts to self assemble into micelles when dissolved in solution.

Surfactants can be divided into two groups: non-reactive surfactants and reactive surfactants. The hydrophilic part (head group) of both the non-reactive and the reactive surfactants can be positively, negatively charged or neutral.

2.7.1. Non-reactive surfactants

Non-reactive surfactants are the conventional surfactants that have found many applications: from household use, as soaps and detergents, to academic and industrial use, as stabilizers/compatibilizers. Stabilizers for reactions such as polymerization, e.g. in emulsion, miniemulsion, suspension, etc., are used to control particle size and particle size distribution, as well as to ensure the stability of the dispersion during the polymerization process. The most remarkable aspect about non-reactive surfactants is that they do not take part in the reaction process itself, apart from acting as stabilizers. On the other hand, the major drawback associated with this group of surfactants is that they can be desorbed from the particle surface as they are not bound to the polymer particles.[23] A common example of this group of surfactants is sodium dodecyl sulphate (SDS).

2.7.2 Reactive surfactants

Reactive surfactants, on the other hand, can play a role in the free-radical polymerization process. Free-radical polymerization involves initiation (formation of radicals), propagation (growing of the polymer chain), or a transfer reaction (a radical that moves from a growing chain to a non-radical species, which itself is able to reinitiate the polymerization of a new chain), and termination (destruction/death of radicals). Depending on their behaviour during a free-radical polymerization reactive surfactants can further be divided into three subgroups: transurfs, inisurfs and surfmers. Upon taking part in the polymerization reaction these surfactants become covalently attached to the polymer particles and thus cannot desorb from the surface. These surfactants replace non-reactive surfactants in requirements where desorption of

surfactants from particles is otherwise a problem. They also find use in other novel applications where thermal, chemical or mechanical specific properties are required, as they become chemically bound to the main polymer chain. Because of their unique properties these reactive surfactants are also highly attractive for use in the preparation of PCNs as described below.

Nitrogen-containing positively charged surfactants are the most widely used for the modification of clay for the synthesis of PCNs. This is due to the fact that clay has negative surface charges that can interact with positively charged species by electrostatic interaction.

2.8 Post modification of clay

After the modification of clay (by any one of the methods mentioned in Section 2.4), the surface of clay becomes hydrophobic, and thus compatible with the monomer, prepolymer or the polymer matrix. Of importance to the final nanocomposite structure is the type of the modifier used for the modification. Its chemical structure should be compatible with both the clay and the polymer matrix, thus providing for favourable interactions (ionic, hydrogen bonding or van der Waals) between surfactant–clay and surfactant–polymer. If favourable interactions are achieved then an exfoliated structure will be obtained. On the other hand, if poor interactions exist then a conventional composite will generally be obtained.[24-26] It has been shown that surfmer-, transurf- or inisurf-modified-clays generally result in an exfoliated structure because during the polymerization process, growth of the polymer chains in the case of transurf- and inisurf-modified-clay starts from the surface of clay.[22,27,28] In the case of the surfmer-modified-clay the broad movement of the clay platelets during the copolymerization of the main monomer and the surfmer on the clay surface results in the exfoliated structure.[28] Edge-wise modification also yields similar results, especially when functional modifying species are used.[11,19] When there is a good interaction between the polymer and the modified-clay, as is the case when a classical surfactant is used to modify clay, only an intercalated nanocomposite is obtained.

2.9 Surfactants used for the synthesis of polystyrene–clay nanocomposites

Surfactants used for the synthesis of polystyrene–clay nanocomposites (PS–CNs) range from alkyl- and aromatic-containing ammonium surfactants,[1,24-27,29-38] to alkyl phosphonium surfactants[39], inisurfs,[14,40], transurfs,[22,41] and surfmers.[27,42-47] Fig. 2.10 shows examples of surfactants that have been used in the synthesis of PS–CNs of varying clay morphologies.

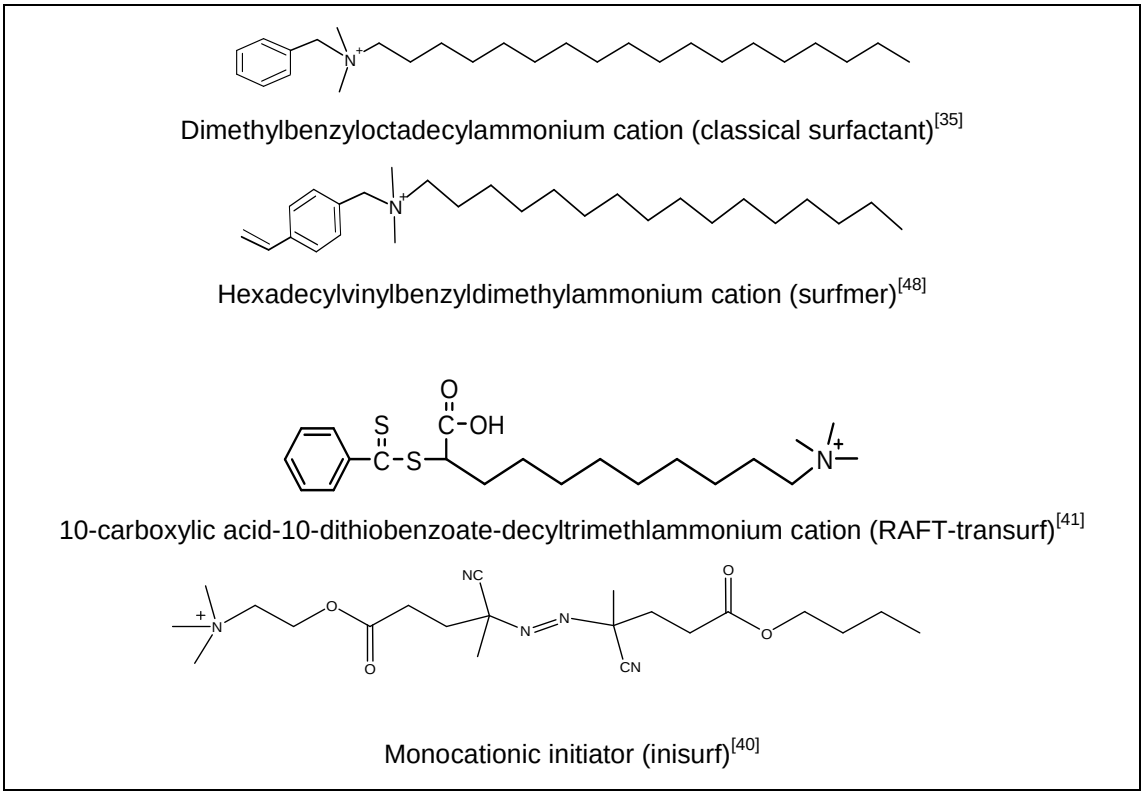

Fig. 2.10 Surfactants used for the modification of clay in the synthesis of PS–CNs.

2.10 Effect of modifying the surfactant on the properties of a polymer–clay nanocomposite

The use of a surfactant during the modification of clay and the subsequent use of the modified-clay in the preparation of a PCN affects especially the physical, chemical and mechanical properties of the prepared nanocomposite. The polymerizable group in the surfmer takes part in the polymerization reaction, resulting in a copolymer rather than a homopolymer. Classic surfactants have been extensively used for clay modification, in the synthesis of PCNs. However, most efforts have mainly resulted in the preparation of

intercalated nanocomposites.[24-26,30,31,33,35,38] The successful use of surfmers, inisurfs and transurfs for the modification of clay, and subsequently the synthesis of exfoliated PS–CNs, has been widely reported.[27,40,44,46,49-52] It is believed that the polymerization of the surfmer and styrene in-between the clay galleries provides the driving force for the clay exfoliation. Inisurf- and transurf-modified-clays result in polymer growth from the clay surfaces, resulting in exfoliated clay structures due to the pressure exerted onto the clay platelets by the growing polymer.

Many researchers have used benzene ring containing surfactants for the modification of clay, mainly because the benzene ring of the surfactant interacts by van der Waals forces, with the benzene rings of styrene and polystyrene.[32,44,45] However, other non benzene ring containing surfactants have also been used for the modification of clay and the subsequent preparation of PS–CNs.[27,35,37,50]

2.11 Techniques relevant to the synthesis of nanocomposites

2.11.1 Template synthesis

Template synthesis is rarely used in the synthesis of PCNs. During template synthesis the building blocks of clay layers and the polymer (normally water soluble) are mixed together under specific conditions, of pH, temperature, ionic concentration, etc. The polymer in solution then acts as a nucleus for layered silicate crystal growth, and becomes trapped between the layers as the clay platelets grow. After the solvent is removed a nanocomposite material is obtained. This method of PCN synthesis is being used by Carrado and coworkers.[53-60] The method has however, found limited applicability because many polymers in use today are not water soluble.

2.11.2 Exfoliation adsorption

In this technique the modified-clay and the polymer are dispersed in a solvent under very dilute conditions and are mixed under shear for a long time. A very low viscosity is required to allow polymer diffusion. During mixing, the polymer diffuses into the clay galleries to yield nanocomposites. See Fig. 2.11.

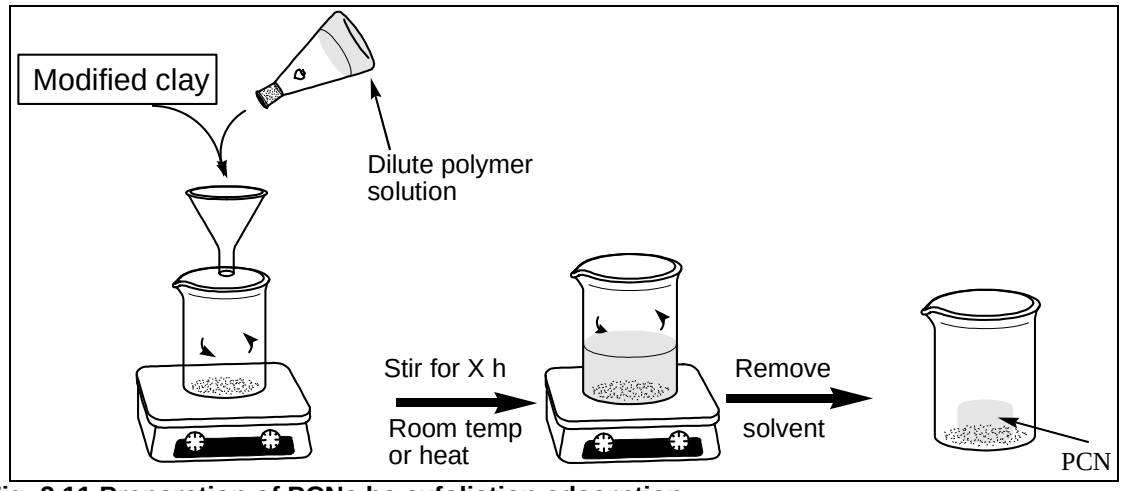

Fig. 2.11 Preparation of PCNs be exfoliation adsorption.

Although this method has been used it has many disadvantages from both academic and industrial points of view.[4,5] In practical terms only low solid contents can be used per each cycle and each cycle requires a long time to yield a nanocomposite. From an industrial point of view, the method is neither financially nor environmentally friendly as, in most cases, organic solvents are used.

2.11.3 Melt intercalation

The melt intercalation technique has been widely used as it holds huge potential for industrial applications.[24,25] In this approach polymer(s) and modified-clay(s) are mixed together under very high shear conditions, normally in an extruder. See Fig. 2.12.

In the extruder the polymer is melted and forced into the galleries of the modified-clay, to yield a PCN. Melt intercalation however does have its disadvantages:

- During the melt intercalation the surfactants used to modify the clay surface may decompose before the polymer penetrates the galleries, leading to a microcomposite.
- There is need for compensation of energy, given that the polymer moves from a region of high entropy outside the galleries to a confined region inside the galleries.

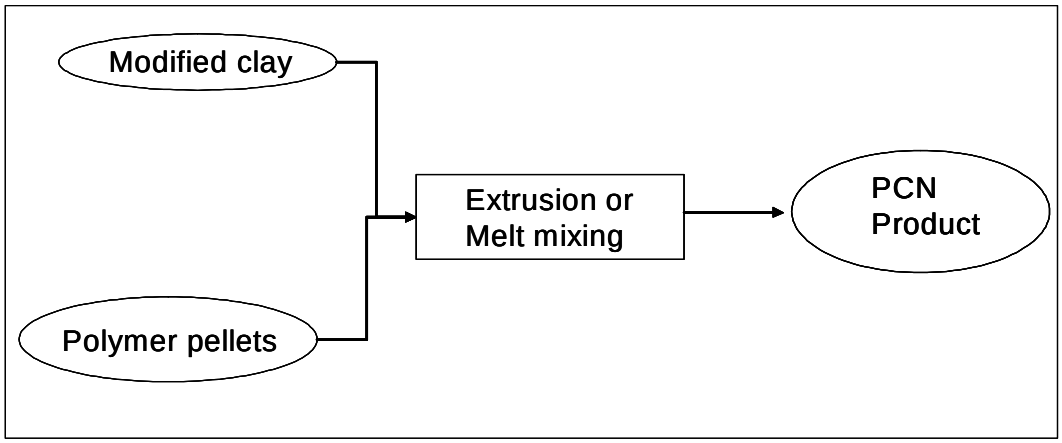

Fig. 2.12 Preparation of PCNs by the melt intercalation technique.

- The clay particles quickly wear out the extruder as the inorganic clays are in contact with the extruder, hence more robust extruders are required, such as those coated with titanium dioxide, which are expensive.

Notwithstanding disadvantages many commercially available PCNs have been synthesized using this method, including; polyolefin, nylon and polyimide based PCNs.

2.11.4 *In situ* intercalative polymerization

The *in situ* intercalative polymerization method requires that the modified or unmodified-clay be dispersed in the monomer or prepolymer system prior to the polymerization step. During polymerization the clay is incorporated in the polymer matrix, yielding the desired PCN. See Fig. 2.13.

This method has received much attention from an academic perspective and some from industry. This is mainly because most of the polymers in use today are polyolefin based, and are not compatible with *in situ* intercalative polymerization. Some of the key advantages of the technique are the following.

- ❖ It is especially attractive to academic research because it allows the modification of clay to be performed using functional modifiers that take part in various stages of a polymerization reaction (see modification of clay above Section 2.4).

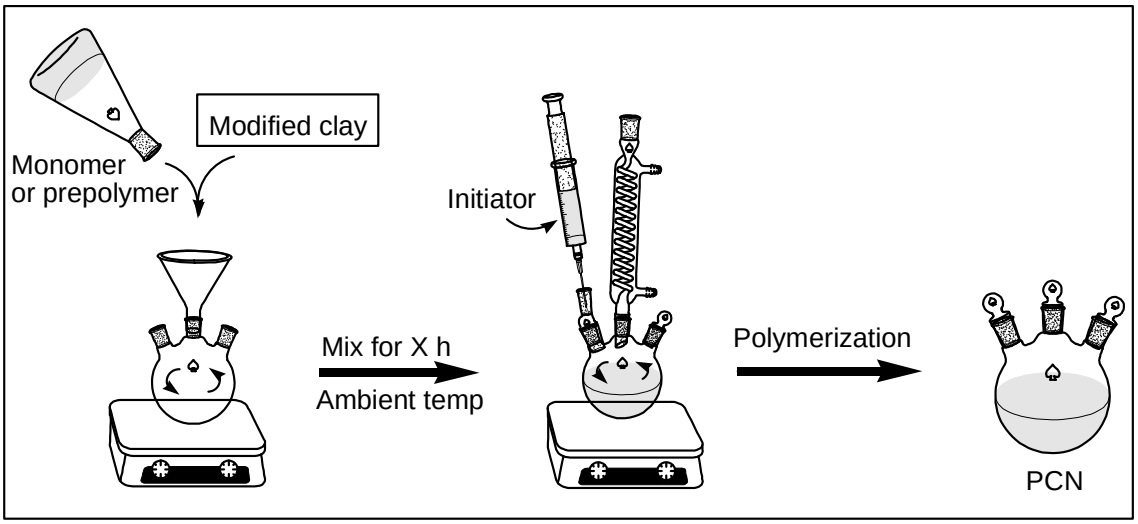

Fig. 2.13 Preparation of PCNs by the *in situ* intercalative polymerization technique.

- It is the only method that can be used for dispersed polymerization methods (i.e. polymerization in emulsion, miniemulsion, dispersion, suspension, etc), as well as in bulk and solution.

- It allows the synthesis of polymers that are tethered to the clay platelets.

- The obtained PCNs can be further processed or used as master batches without the fear of surfactant degradation and the extensive wear on the extruder as the clay particles are already homogeneously dispersed in a polymer matrix.

- Kinetic and thermodynamic parameters can be determined as in non-clay containing conventional systems.

Having all these advantages over the other methods, *in situ* intercalative polymerization was the method used to prepare the PCNs described in this study.

2.12 The fate of the modifier during and after the polymerization process

The modifier may or not take part during the polymerization process. In the case of classical surfactants, apart from compatibilizing the clay, the monomer and the polymer matrix, they are merely spectators in the reaction mixture.[28] On the other hand,

surfmers compatibilize and take part in the polymerization process, resulting in the clay becoming permanently attached to the polymer matrix.[28]

Inisurfs compatibilize the clay and initiate the polymerization process and, like surfmers, permanently become part of the polymer matrix. The use of initiator-bound clay in the initiation of polymerization has been shown to be a useful method for creating PCNs with polymers bound to the clay surfaces. In the mid-1960s Dekking anchored an azo initiator, azo*bis*isobutyramidine hydrochloride (AIBA), onto clay layers, thus forming an initiator-modified-clay. The latter was subsequently used in the initiation of styrene or methyl methacrylate (MMA) polymerization, giving rise to PCNs with over 80% of the polymer chains attached to the clay layers. Dekking investigated the kinetics of the decomposition of the bound initiator and of the polymerization process.[13,61] Meier *et al*.[62] and Bourgeat-Lami *et al*.[12] also reported on the use of AIBA initiator-modified-clays during the preparation of PCNs. Fan *et al*. compared the use of a monocationic initiator versus a bicationic initiator in modified-clays on the resultant clay morphology and molar masses of the resultant PS–CNs.[40] The monocationic initiator-modified-clay resulted in exfoliated PCNs whereas bicationic initiator-modified-clay resulted in PCNs with intercalated morphology.

The same can be said for transurfs and, in particular, RAFT agents: they become part of the polymer matrix by transferring a radical from an active chain to a dormant chain. By so doing, the RAFT agent is able to control the polymerization process, as described in more detail in Chapter 3. Ideally, the polymer chains produced have a predictable molar mass and a narrow polydispersity index (PDI). The use of such agents that are able to control molar mass has attracted great interest, in both academia and industria.

2.13 Nanocomposite characterization

There are many methods by which nanocomposites can be characterized.

2.13.1 XRD analysis

Most important of which are X-ray diffraction (XRD) either in the form of wide angle X-ray diffraction (WAXD) or small angle X-ray scattering (SAXS). The clay platelets are

crystalline ordered material and thus give rise to Bragg peaks, which give the interlayer distance commonly referred to as the *d* spacing. XRD measurents give an average *d* spacing of the bulk sample. When organic species such as surfactants or polymers are introduced into the galleries the adjacent clay platelets move away from each other along the c axis. It is this shift that is recorded in the XRD analysis. The 001 Bragg peak shifts to the left in the XRD spectrum, according to the Bragg formula in Equation 2.1.

$$2d\sin\theta = n\lambda \qquad \textbf{Equation 2.1}$$

where n is the order of interference, λ corresponds to the wavelength of the X-ray radiation used in the diffraction experiment, *d* is the spacing between diffractional lattice planes and θ is the measured diffraction angle or glancing angle. Thus an increase in the *d* spacing results in a decrease in the angle θ. Fig. 2.14 shows typical XRD patterns of clay as one moves from organically modified-clay, to intercalated morphology, to a mixture of morphologies, and finally to the exfoliated structure.

The disappearance of the Bragg peak is an indication of loss in order of the clay layers, relative to each other; hence the possibility of an exfoliated structure. Disappearance of the Bragg peak can also be due to too little clay in the sample that is below the detection limit of the XRD apparatus. Hence a complimentary technique, e.g transmission electron microscopy (TEM) is needed to confirm conclusions made from XRD results. XRD results can also be misleading: sometimes, when a mixed morphology of clay in a PCN is present, it is seen as ill defined Bragg peaks, which is the case in most situations. Hence complementary techniques (e.g. TEM), are very useful in facilitating the elucidation of the morphology of PCNs.

Some researchers used 2D XRD and 2D WAXS, alone or simultaneously, for quantitative determinations and the determination of the three-dimensional orientations of various organic and inorganic structures in PCNs.[3] However the 2D techniques have not been used extensively.

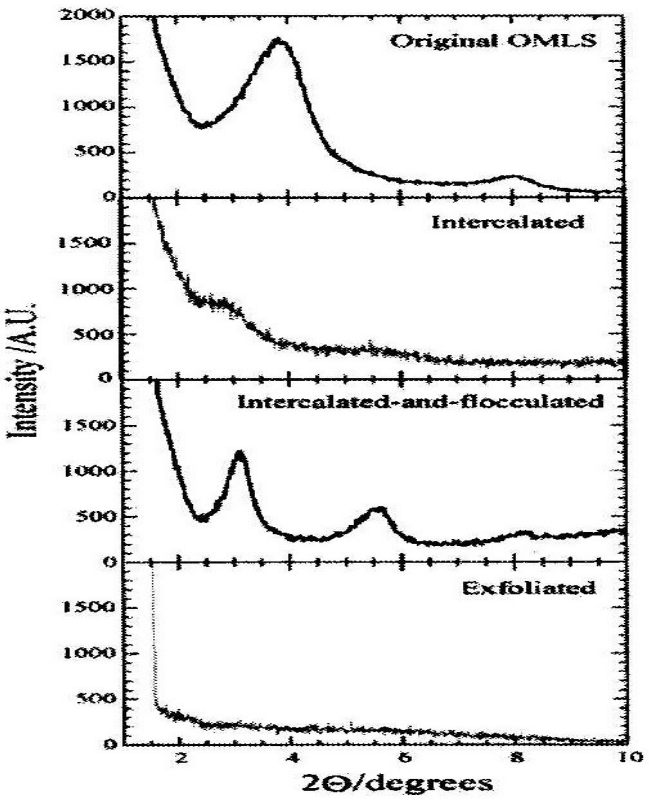

Fig. 2.14 The XRD patterns of different clay morphologies, WAXD patterns of three layered silicates structures. original OMLS is an organically modified layered silicate for reference.[3]

In this document SAXS measurements were used for the characterization of polymer–clay nanocomposites. Below the relationship between XRD and SAXS is outlined.

From XRD (Section 2.13.1) the Bragg's law is given as:

$$2d\sin\theta = \lambda \qquad \textbf{Equation 2.2}$$

Whereas from SAXS measurements the wave vector q is related to θ by the relation:

$$q = \frac{4\pi\sin\theta}{\lambda} \qquad \textbf{Equation 2.3}$$

From relations (Equation 2.2) and (Equation 2.3), the following can be deduced:

$$d = \frac{2\pi}{q} \qquad \textbf{Equation 2.4}$$

were the *q* value corresponds to the associated Bragg peak position, hence from the SAXS measurements, the q value can be used for measuring changes in the intergallery spacing in polymer–clay nanocomposites.

2.13.2 TEM analysis

TEM analysis is a visual technique that looks at the clay morphology at nanometer level. If TEM is used in combination with the XRD, the true structure of the nanocomposite can be elucidated. TEM analysis does not provide a true representation of an entire sample since it looks only at a very small portion of the whole sample, This is its major disadvantage. Fig. 2.15 shows an example of a TEM image of a microtomed sample of an exfoliated PCN.

The clay layers are seen as the randomly distributed hair-like particles. Here the angle at which the TEM looks at the particles is from the edges and the polymer chains are not seen in the image.

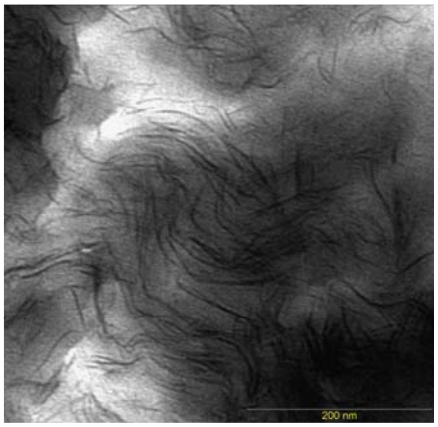

Fig. 2.15 TEM image of an exfoliated polymer–clay nanocomposite (Bar 200 nm).[28]

2.13.3 Other characterization techniques

Other important analytical techniques that have been used for characterizing nanocomposites include size-exclusion chromatography (SEC), infrared spectroscopy (IR), nuclear magnetic resonance spectroscopy (NMR), dynamic mechanical analysis (DMA), melt rheology and thermogravimetric analysis.

2.13.3.1 Infrared spectroscopy and nuclear magnetic resonance spectroscopy

Since the clay platelets and most polymers are IR active, IR has been used for simple identification purposes. The correlation between the IR absorption frequencies and particular vibration modes can also be used to determine the microstructure of polymer molecules confined in the clay platelets.[3] Thus IR can be used for both structural characterization and identification.[42,44] Solid-state nuclear magnetic resonance spectroscopy (NMR) (^{1}H and ^{13}C) has also been used by some researchers to gather information on the morphology, surface structure chemistry and, to a lesser extent, the dynamics of nanocomposites.[3]

2.13.3.2 Size-exclusion chromatography

SEC is a valuable tool for the nanocomposites elucidation. It is mainly used for the determination of molar mass, molar mass distribution and the PDI of the polymer matrix of a PCN. SEC can therefore be used to determine the effect of clay on the molar mass and PDI. Moreover, the application of controlled/living radical polymerization to PCNs has seen the use of SEC becoming increasingly important. A major drawback of using SEC to characterize PCNs is the fact that it may be difficult to separate the polymer chains from the nanoclay particles. However, if successful separation of the polymer chains from the clay particles is achieved, valuable information on the differences in molar mass and molar mass distribution of the polymer chains unattached and those freed after separation from clay particles may be obtained, which could be useful in elucidating the kinetics of polymerization inside the clay platelets relative to the continuous phase (i.e. outside the clay galleries).

2.13.3.3 Dynamic mechanical analysis

DMA technique measures the dynamic mechanical properties of PCNs samples as a function of temperature. There are three main parameters that are used to express DMA results: (i) the storage modulus (G^{I}), which is a measure of elastic response to the deformation; (ii) the loss modulus (G^{II}), which is a measure of the plastic response; and (iii) tan δ, i.e. the ratio of G^{II}/G^{I}. Tan δ is used for the determination of molecular

mobility. The interaction taking place at the interface between the polymer matrix and silicate layers decreases the macromolecule's mobility in the polymer segments near the interface,[63] which leads to improved mechanical properties. In general, G^{I} values increase with an increase in clay loading for nanocomposites at temperatures below the glass transition temperature (T_g) (i.e. glassy state). The same effect occurs in the rubbery region as well, relative to pristine polymers and conventional composites.[44,50,64,65] This can be attributed to the large aspect ratio of the structural hierarchy on the nanoscale level. Due to its sensitivity towards small changes, even at the nanoscale, DMA has been used to differentiate between different morphologies of clay in the nanocomposite samples, at the same clay loading but having different morphologies.[27] DMA is sensitive to the level of clay dispersion in the nanocomposite samples. G^{II} and the tan δ peaks broaden and shift to higher temperatures as a result of the presence of the nanoclay in the PCN sample. This has been attributed to restricted chain mobility,[64,66-68] associated with an increase in T_g of the PCN relative to the neat polymer.

2.13.3.4 Melt rheology

Melt rheology measures the flow properties of PCNs at temperatures far above the T_g. The principles behind the operation of melt rheology and DMA are however similar, yet more structural information of PCNs may be obtained. The rheological properties of polymer melts are important as they give indications of the processibility of the material as a function of the temperature. The melt rheological properties of PCNs are dependent on the molar mass, PDI, clay loading and PCN morphology.[50,69-73]. Moreover, when all the other parameters are constant apart from the distribution of the clay layers in a PCN, rheology measurements like DMA detect these disparities. Hence it can also be used to confirm the clay morphology in a PCN.[74] The complex viscosity of PCNs has generally been shown to be typically non-Newtonian in behaviour.[69,74] Typical variation in complex viscosity as a function of angular frequency is shown in Fig. 2.16.

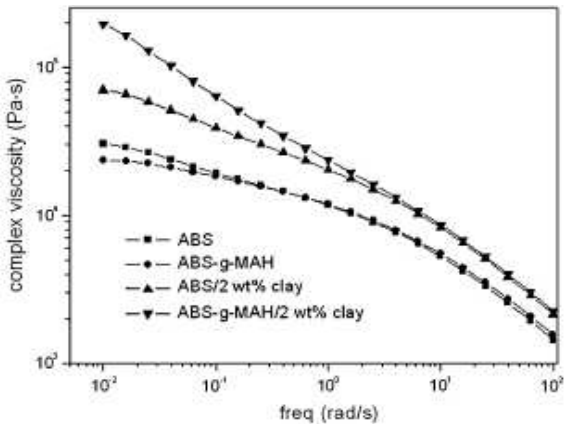

Fig. 2.16 Change in complex viscosity as a function of angular frequency for ABS based nanocomposites.[75]

The storage and loss moduli of PCNs have been reported to show non-terminal solid-like behaviour at low frequencies due to the presence of the clay platelets.[66,71-77] In the high frequency region however, monotonic increases in G^{I} and G^{II} have been observed as clay loading increases.[66,71-73,78] Typical variation of storage and loss moduli as a function of angular frequency is shown in Fig. 2.17.

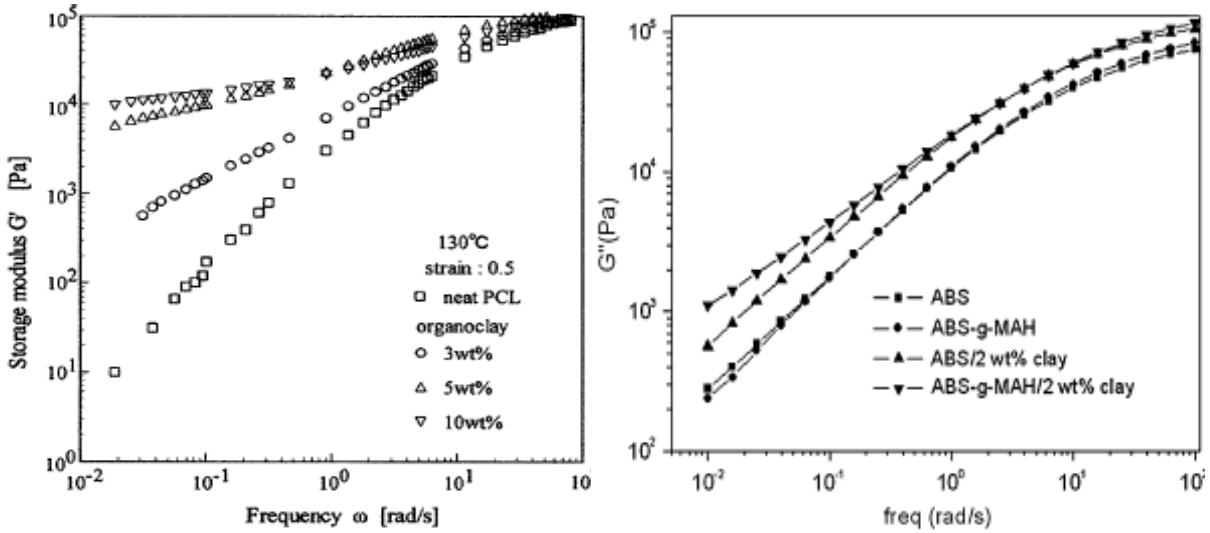

Fig. 2.17 Variation of storage modulus as a function of angular frequency for polycaprolactam based nanocomposites (left).[72] Variation of loss modulus as a function of angular frequency for ABS based nanocomposites (right).[75]

2.13.3.5 Thermogravimetric analysis

Thermogravimetric analysis measures the weight loss of a material as a function of temperature. The first report on the thermal stability of PCNs was published as early as 1965, by Bluimstein.[79] Since then many reports on the thermal stability of PCNs have

been published.[3,4,8,28] The general notion on the issue of thermal stability of PCNs is the following: an increase in clay loading results in an increase in thermal stability.[3-5] This is due to an increase in the number of clay platelets hindering diffusion of gasified polymers.[27,28,36] Improvement in thermal stability has also been attributed to restricted thermal motion of the polymer between the clay galleries.[79] The homogeneous distribution of the clay layers within the polymer matrix also improves thermal stability because almost all nanocomposite samples become homogeneous and almost all the polymer chains are in contact with the clay particles. However, since most of the available literature is based on uncontrolled free-radical polymerization, many researchers attribute the net increase in thermal stability only to clay loading. Correlation between the morphology of clay in the nanocomposites with the thermal stability still remains controversial. The general agreement on this is that an exfoliated clay structure results in optimal thermal stability with regards to the other morphologies.[27] However, in some specific cases, an intercalated clay structure has been reported to offer better thermal stability than exfoliated ones.[28,80,81] To date, reports on the impact of clay loading and the morphology of clay in a PCN on the thermal stability and the molar mass has not clearly been outlined. There is nonetheless agreement that molar mass does have an effect on thermal stability, up to a certain point, where entanglements start to form. Beyond this critical molar mass, the thermal stability becomes independent of molar mass. On the issue of clay loading, there exists a limiting clay loading that gives a huge improvement in thermal stability. Doh and Choh reported that this limiting clay loading for the PCNs they prepared was 0.3%.[43] Once the limiting clay loading is surpassed further thermal stability enhancements are minimal.

2.14 References

[1] A. Usuki, Y. Kojima, M. Kawasumi, A. Okada, Y. Fukushima, T. Kurauchi, O. Kamigaito. *J Mater Res* **1993**, *8*, 1179-1184.

[2] R. Advincula, Q. Y. Zhou, Y. Nakamura, S. Inaoka, M. K. Park, Y. F. Wang, J. Mays. *Abstr Pap Am Chem Soc* **2000**, *219*, U498-U498.

[3] S. S. Ray, M. Okamoto. *Prog Polym Sci* **2003**, *28*, 1539-1641.

[4] M. Okamoto. *Encyclopedia of Nanoscience and Nanotechnology*; American Scientific Publishers: California, 2004.

[5] M. Alexandre, P. Dubois. *Mater Sci Eng A* **2000**, *28*, 1-63.

[6] H. Fischer. *Mater Sci Eng C* **2003**, *23*, 763-772.

[7] F. Bergaya, G. Lagaly. *Appl Clay Sci* **2001**, *19*, 1-3.

[8] M. Rosorff. *Nano Surface Chemistry*; Marcel Dekker: New York-Basel, 2002.

[9] G. Lagaly. In *Coagulation and flocculation*, Second ed.; H. Stechemesser,B. Dobias, Eds.; CRC Press: FL., 2005; pp 427-704.

[10] J. W. Jordan. *J Phys Colloid Chem* **1949**, *53* 294-306.

[11] P. A. Wheeler, J. Z. Wang, L. J. Mathias. *Chem Mater* **2006**, *18*, 3937-3945.

[12] E. Bourgeat-Lami, N. N. Herrera, J.-L. Putaux, S. P. Reculusa, A. Perro, S. Ravaine, C. Mingotaud, E. Duguet. *Macromol Symp* **2005**, *229*, 32-46.

[13] H. G. G. Dekking. *J Appl Polym Sci* **1965**, *9*, 1641-1651.

[14] X. W. Fan, Q. Y. Zhou, C. J. Xia, W. Cristofoli, J. Mays, R. Advincula. *Langmuir* **2002**, *18*, 4511-4518.

[15] G. W. Beall, M. Goss. *Appl Clay Sci* **2004**, *27*, 179-186.

[16] N. Takahashi, H. Tamura, D. Mochizuki, T. Kimura, K. Kuroda. *Langmuir* **2007**.

[17] N. Greesh, P. C. Hartmann, V. Cloete, R. D. Sanderson. *J Colloid Interf Sci* **2008**, *319*, 2-11.

[18] D. J. Voorn, W. Ming, A. M. Van Herk. *Macromolecules* **2006**, *39*, 4654-4656.

[19] P. A. Wheeler, J. Z. Wang, J. Baker, L. J. Mathias. *Chem Mater* **2005**, *17*, 3012-3018.

[20] T. T. Chastek, E. L. Que, J. S. Shore, R. J. Lowy, C. Macosko, A. Stein. *Polymer* **2005**, *46*, 4421-4430.

[21] T. T. Chastek, A. Stein, C. Macosko. *Polymer* **2005**, *46*, 4431-4439.

[22] A. Samakande, J. J. Juodaityte, R. D. Sanderson, P. C. Hartmann. *Macromol Mater Eng* **2008**, 293, 428-437.

[23] M. J. Unzue, H. A. S. Schoonbrood, J. M. Asua, A. M. Goni, D. C. Sherrington, K. Stahler, K. H. Goebel, K. Tauer, M. Sjoberg, K. Holmberg. *J Appl Polym Sci* **1997**, *66*, 1803-1820.

[24] R. A. Vaia, E. P. Giannelis. *Macromolecules* **1997**, *30*, 7990-7999.

[25] R. A. Vaia, E. P. Giannelis. *Macromolecules* **1997**, *30*, 8000-8009.

[26] R. A. Vaia, K. D. Jandt, E. J. Kramer, E. P. Giannelis. *Macromolecules* **1995**, *28*, 8080-8085.

[27] W. A. Zhang, D. Z. Chen, H. Y. Xu, X. F. Shen, Y. E. Fang. *Eur Polym J* **2003**, *39*, 2323-2328.

[28] A. Samakande, P. C. Hartmann, V. Cloete, R. D. Sanderson. *Polymer* **2007**, *48*, 1490-1499.

[29] G. Chigwada, C. A. Wilkie. *Polym Degrad Stabil* **2003**, *80*, 551-557.

[30] C. I. Park, O. O. Park, J. G. Lim, H. J. Kim. *Polymer* **2001**, *42*, 7465-7475.

[31] P. Pinnavaia. *Appl Clay Sci* **1999**, *15*, 11-29.

[32] D. R. Robello, N. Yamaguchi, T. Blanton, C. Barnes. *J Am Chem Soc* **2004**, *126*, 8118-8119.

[33] J. G. Ryu, S. W. Park, H. Kim, J. W. Lee. *Mat Sci Eng C-Bio S* **2004**, *24*, 285-288.

[34] S. Sadhu, A. K. Bhowmick. *J Appl Polym Sci* **2004**, *92*, 698-709.

[35] C. Tseng, J. Wu, H. Lee, F. Chang. *J Appl Polym Sci* **2002**, *85*, 1370-1377.

[36] J. Wang, J. Du, J. Zhu, C. A. Wilkie. *Polym Degrad Stabil* **2002**, *77*, 249-252.

[37] D. Yei, S. Kuo, Y. Su, F. Chang. *Polymer* **2004**, *45*, 2633-2640.

[38] D. B. Zax, D. K. Santos, H. Hegemann, E. P. Giannelis, E. Manias. *J Chem Phys* **2000**, *112*, 2945-2951.

[39] J. Zhu, A. B Morgan, F. J. Lamelas, C. A. Wilkie; *Chem. Mater* **2001**, *13*, 3774-3780.

[40] X. W. Fan, C. J. Xia, R. C. Advincula. *Langmuir* **2003**, *19*, 4381-4389.

[41] B. Q. Zhang, C. Y. Pan, C. Y. Hong, B. Luan, P. J. Shi. *Macromol Rapid Commun* **2006**, *27*, 97-102.

[42] A. Akelah, A. Moet. *J Mater Sci* **1996**, *31*, 3589-3596.

[43] J. G. Doh, I. Cho. *Polym Bull* **1998**, *41*, 511-518.

[44] X. Fu, S. Qutubuddin. *Polymer* **2001**, *42*, 807-813.

[45] X. A. Fu, S. Qutubuddin. *J Colloid Interf Sci* **2005**, *283*, 373-379.

[46] C. Zeng, L. J. Lee. *Macromolecules* **2001**, *34*, 4098-4103.

[47] S. A. Zerda, C. T. Caskey, J. A. Lesser. *Macromolecules* **2003**, *36*, 1603-1608.

[48] J. Zhu, A. B. Morgan, F. J. Lamelas, C. A. Wilkie. *Chem Mater* **2001**, *13*, 3774-3780.

[49] C. I. Park, H. Kim, O. O. Park. *Polymer* **2004**, *45*, 1267-1273.

[50] M. Xu, Y. S. Choi, Y. K. Kim, K. H. Wang, I. J. Chung. *Polymer* **2003**, *44*, 6387-6395.

[51] J. B. Di, D. Y. Sogah. *Macromolecules* **2006**, *39*, 1020-1028.

[52] M. W. Weimer, H. Chen, E. P. Giannelis, D. Y. Sogah. *J Am Chem Soc* **1999**, *121*, 1615-1616.

[53] K. A. Carrado. *Abstr Pap Am Chem Soc* **1993**, *206*, 74.

[54] K. A. Carrado, K. Song, G. W. Zajac. *Abstr Pap Am Chem Soc* **1997**, *213*, 237.

[55] K. A. Carrado, P. Thiyagarajan, D. L. Elder, G. W. Zajac. *Abstr Pap Am Chem Soc* **1995**, *209*, 78.

[56] K. A. Carrado, P. Thiyagarajan, R. E. Winans, R. E. Botto, J. E. Forman. *Abstr Pap Am Chem Soc* **1991**, *201*, 341.

[57] K. A. Carrado, L. Xu, D. M. Gregory, K. Song, S. Seifert, R. E. Botto. *Chem Mater* **2000**, *12*, 3052-3059.

[58] K. A. Carrado, L. Q. Xu. *Abstr Pap Am Chem Soc* **1998**, *216*, U308-U309.

[59] K. A. Carrado, L. Q. Xu. *Chem Mater* **1998**, *10*, 1440-1445.

[60] K. A. Carrado, G. W. Zajac, K. Song, J. R. Brenner. *Langmuir* **1997**, *13*, 2895-2902.

[61] H. G. G. Dekking. *J Appl Polym Sci* **1967**, *11*, 23-26.

[62] L. P. Meier, R. A. Shelden, W. R. Caseri, U. W. Suter. *Macromolecules* **1994**, *27*, 1637-1642.

[63] J. Luo, I. M. Daniel. *Compos Sci Technol* **2003**, *63*, 1607-1616.

[64] H. Tyan, K. Wei, T. Hsieh. *J Polym Sci Part B: Polym Phys* **2000**, *38*, 2873-2878.

[65] W. Zhang, D. Z. Chen, Q. B. Zhao, Y. Fang. *Polymer* **2003**, *44*, 7953-7961.

[66] T. H. Kim, S. T. Lim, C. H. Lee, H. J. Choi, M. S. Jhon. *J Appl Polym Sci* **2003**, *87*, 2106-2112.

[67] M. W. Noh, D. C. Lee. *Polym Bull* **1999**, *42*, 619-626.

[68] Y. Yu, J. Yeh, S. Liou, Y. Chang. *Acta Mater* **2004**, *52*, 475-486.

[69] T. D. Fornes, P. J. Yoon, H. Keskkula, D. R. Paul. *Polymer* **2001**, *42*, 9929-9940.

[70] G. Galgali, C. Ramesh, A. Lele. *Macromolecules* **2001**, *34*, 852-858.

[71] R. Krishnamoorti, E. P. Giannelis. *Macromolecules* **1997**, *30*, 4097-4102.

[72] K. Okada, T. Mitsunaga, Y. Nagase. *Korea-Aust Rheol J* **2003**, *15*, 43-50.

[73] J. X. Ren, A. S. Silva, R. Krishnamoorti. *Macromolecules* **2000**, *33*, 3739-3746.

[74] J. Zhao, A. B. Morgan, J. D. Harris. *Polymer* **2005**, *46*, 8641-8660.

[75] H. Y. Ma, L. F. Tong, Z. B. Xu, Z. P. Fang. *Polym Degrad Stabil* **2007**, *92*, 1439-1445.

[76] S. T. Lim, C. H. Lee, H. J. Choi, M. S. Jhon. *J Polym Sci Part B: Polym Phys* **2003**, *41*, 2052-2061.

[77] R. P. Moraes, A. M. Santos, P. C. Oliveira, F. C. T. Souza, M. Amaral, T. S. Valera, N. R. Demarquette. *Macromol Symp* **2006**, *245-246*, 106-115.

[78] M. J. Solomon, A. S. Almusallam, K. F. Seefeldt, A. Somwangthanaroj, P. Varadan. *Macromolecules* **2001**, *34*, 1864-1872.

[79] A. Bluimstein. *J Polym Sci A* **1965**, *3*, 2665-2673.

[80] E. Giannelis. *Adv Mater* **1996**, *8*, 29-31.

[81] J. W. Gilman, T. Kashiwagi, A. B. Morgan, R. H. Harris, L. D. Brassell, M. R. Vanlandingham, C. L. Jackson. *NISTIR 6531* **2000**, 1-55.

Chapter 3: Controlled/Living polymerization with emphasis on the RAFT process

Abstract

Controlled/living polymerization techniques are discussed in this Chapter. Focus is emphasized on their applicability to the synthesis of polymer–clay nanocomposites. More emphasis was given to the RAFT technique given this document is based on it.

3.1 Introduction

Since the discovery of conventional free-radical polymerization, there were huge efforts devoted to its research, development and commercialization. To date, most of the polymers in use are prepared by this polymerization method. However, conventional free-radical polymerization offers little control over architecture, functionality, molar mass and molar mass distribution (MMD). The lack of control is attributed to irreversible termination processes,[1] and the continual radical generation throughout the polymerization process, which results in different initiation times of chains.[2] During the polymerization process the radical lifetime is not more than a few seconds,[1,2] and within a few minutes of the polymerization process, high molar mass polymers have already formed.[1]

Conventionally polymerized polymers are of no use in some specialized areas, pertaining to such biomedical applications, and as compatibilizers of polymer blends. Bearing in mind the ever-increasing demand for polymers with specific functionality, architecture, molar mass and MMD, the concept of living/controlled polymerization was developed. In 1955 Michael Szwarc presented to the science community the first ever article on the synthesis of living polymers by the anionic polymerization technique.[3] Polystyrene with controlled molar mass and narrow polydispersity index (PDI, a measure of the broadness of the MMD) was described. Several controlled free-radical polymerization techniques were subsequently reported.[2]

3.2 Fundamentals of controlled radical polymerization techniques

A stumbling block to the realization of controlled radical polymerization is the ability to decrease the termination rate. This requirement emanates from the fact that the termination process is a second-order reaction and that the propagation step is first-order. Thus a decrease in the radical concentration during the polymerization process should indeed decrease the termination rate to a greater extent than it decreases the rate of propagation, hence resulting in a better control of polymerization. This is the fundamental requirement upon which all controlled radical polymerization techniques are based. The reduction of termination and fast chain end transfer of the active radicals results in polymer chains that all grow at the same time, until all the monomer is consumed. If more monomer is then added, the polymerization continues or if a different monomer is added then to the system a

block copolymer is formed. Hence in all controlled radical polymerization methods there is a dynamic equilibrium between the propagating species and the various dormant species. However, for effective control there is need for fast exchange between the active and dormant species, i.e. the transfer constant should be greater than the propagation constant. The requirements for a perfect controlled radical polymerization can be reduced to the following requirements, according to Quirk and Lee.[4]

- Polymerization should progress until all monomer has been consumed. If more monomer is added then the polymer chains should grow further without any new ones being initiated, i.e. block copolymer synthesis.

- There should be a linear increase of molar mass with conversion, and at any time during the polymerization process the molar masses should be predictable. As in conventional polymerization there is a decrease in molar mass with increased conversion due to monomer consumption. However, in most controlled systems there is linear dependency, although termination reactions are present, as is seen by a broadening MMD.

- The number of living species must remain constant during the entire polymerization process. The conformance of a system to this requirement can be followed by assaying the linearity of the curve $\ln([M]_0/[M]_t)$ against time. This criterion is also met in some conventional polymerizations in the steady state, i.e. when the rate of termination equals the rate of initiation, normally in the intermediate conversions. In the case of controlled systems it should start from the onset of polymerization and the intercept of the curve should be zero.

- The MMD should be narrow.

- End groups must be retained, thus yielding end-functionalized polymers in quantitative yields.

3.3 Common controlled radical polymerization methods

The most common controlled radical polymerization methods that have been reported to date are: stable free-radical polymerization (SFRP), atom transfer radical polymerization (ATRP) and reversible addition–fragmentation chain transfer (RAFT).

3.3.1 Stable free-radical polymerization (SFRP)

The SFRP technique is based on a persistent radical effect (PRE), where, growing radicals are continuously trapped in a reversible activation–deactivation process by another species. Activation is brought about by heat, light, or by a catalyst.[2] SFRP is normally adequately represented by nitroxide mediated polymerization (NMP).[5] NMP was derived from the realization that nitroxide based radicals are able to scavenge for carbon centered radicals by reacting with them reversibly, at near diffusion rates, to form alkoxyamines. As in the case of all controlled techniques, irreversible termination leads to dead chains. The NMP mechanism is given in Scheme 3.1.

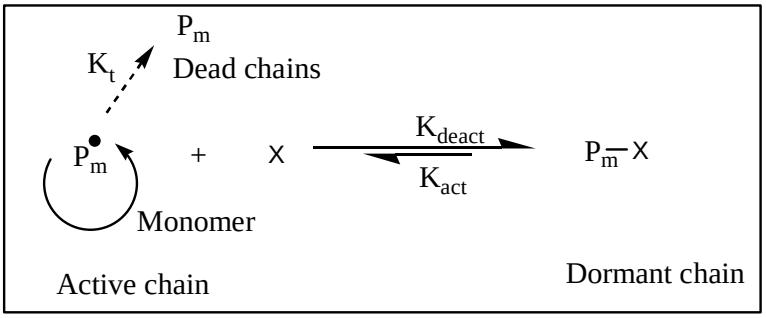

Scheme 3.1 Schematic presentation of the NMP process.

The nitroxide species here is represented by an X, the most commonly known of which is the 2,2,6,6-tetramethyl-1-piperidinyloxy (TEMPO) free-radical. Many other nitroxides have been used. A detailed account of NMP is given in a review by Solomon.[5] The success of various nitroxides is based on the degree of steric compression around the carbon–oxygen bond formed between growing chains and nitroxide radicals. NMP has been successful used with styrene and acrylates but has generally been ineffective with methacrylates. Major disadvantages of this method are its stringent reaction conditions, and that some of the nitroxides show susceptibility towards thermal degradation.

3.3.2 Atom transfer radical polymerization (ATRP)

ATRP, like NMP, is based on PRE. ATRP relies on the addition of halocarbons across a double bond via a reversible radical chain process, through the catalytic action of a transition metal complex (Mt^n / L), as shown in Scheme 3.2 .

Copper is often used as the transition metal although other metals have been used. ATRP has been applied to a broad range of monomers it has been shown to be a

versatile technique, but has the major drawback of requiring the removal of the toxic transition metal from the final polymer.

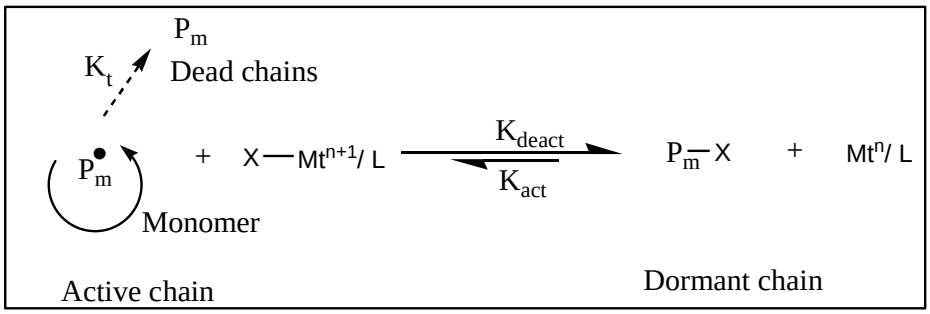

Scheme 3.2 Schematic representation of the ATRP process.

ATRP is also sensitive towards any redox species in the system.[6] A detailed account of ATRP is given in a review by Braunecker and Matyjaszewski.[2]

3.3.3 Reversible addition–fragmentation chain transfer (RAFT)

As the RAFT process is the basis of this document the author has endeavored to give an adequate account of the process. The RAFT technique is one of the fastest growing and most robust controlled radical polymerization techniques.[1,7] This is due to its versatility, such as tolerance to impurities, and the numerous types of monomers that can be polymerized in a controlled manner. Furthermore, the experimental setup required for RAFT controlled radical polymerization is relatively simple. The RAFT technique owes its success to a family of organic molecules containing the thio-carbonyl-thio group, known as RAFT agents.[8-10] The general structure of a RAFT agent is shown in Scheme 3.3 below.

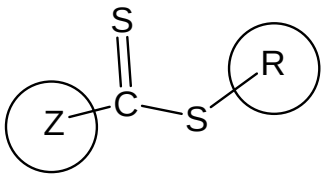

Scheme 3.3 General RAFT agent structure.

The control of polymerization in RAFT is significantly influenced by both the leaving group (R) and the stabilizing group (Z), which makes their choice, to match the selected monomer, very important.[11,12] The (Z) group acts as an activator for the thio-carbonyl-thio group to react with radicals. It also acts as a stabilizing group for the transition state radical that is formed between the thiocarbonyl group and a free-radical. On the other hand, the (R) group should be a good leaving group by

undergoing a homolytic sission: once it leaves the main RAFT agent as a free-radical it should be able to reinitiate polymerization by reacting with monomer units.

In the RAFT process, addition of a transfer agent (RAFT agent) in larger amounts relative to the initiator, results in control of the polymerization process. The RAFT agent transfers the radical from a growing chain to itself to form the dormant form, which results in equilibrium between growing and dormant chains, with the equilibrium far to the dormant state. There are thus few active chains (radicals) and hence control is achieved. In RAFT the product of chain transfer is also a chain transfer agent with similar activity to the precursor transfer agent. Because RAFT agents are added to a conventional polymerization set up, there has to be initiation and propagation. The generally accepted RAFT mechanism is outlined in Scheme 3.4.[12]

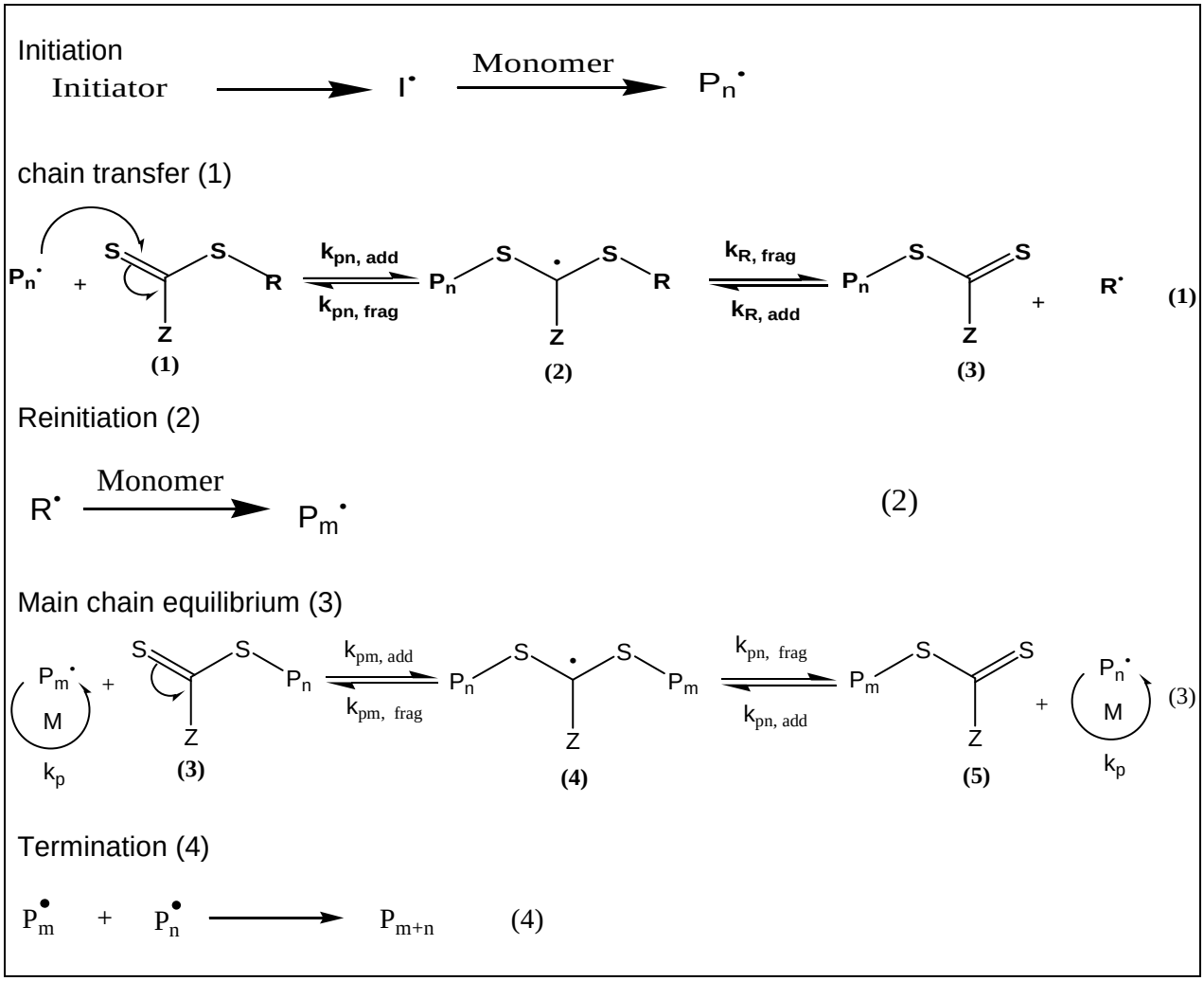

Scheme 3.4 The RAFT mechanism.

As is with other controlled polymerization techniques the RAFT process also undergoes termination reactions, either by radical coupling or disproportionation, as well as other unwanted side reactions. The thio-carbonyl-thio group can be hydrolyzed by basic species such as hydroxide ions, and primary and secondary amines.[2,13-16] The RAFT process also suffers from inhibition and retardation. Radical termination and side reactions have been reported to cause broadening of the MMD. The theoretical polymer molar masses in RAFT-mediated polymerizations are calculated using Equation 3.1. These theoretical molar masses are then compared to those obtained from size-exclusion chromatography (SEC), from where the level of control of the polymerization is determined.

$$M_n = \frac{[M]_0 M_{MW} x}{[RAFT]_0} + RAFT_{MW}$$ [17] **Equation 3.1**

where $[M]_0$ = initial monomer concentration, M_{MW} = molecular weight of monomer, x = conversion, $RAFT_{MW}$ = molecular weight of RAFT, $[RAFT]_0$ = initial concentration of RAFT.

The mechanism of control in the RAFT process, i.e. reversible transfer, is also applicable to iodine transfer polymerization (ITP),[18-24] and Telluride mediated polymerization (TERP).[25]

3.4 Controlled radical polymerization techniques and their applicability to polymer–clay nanocomposites with special emphasis on the RAFT technique

To date, most of the research carried out into the polymer architecture in PCNs has focused mainly on the use of uncontrolled radical polymerization.[26-29] The few articles available on the use of controlled living radical polymerization in PCNs has focused on NMP.[30,31] Clay in its native state is hydrophilic, and hence incompatible with hydrophobic monomers. Consequently, a prerequisite in preparing most PCNs is to modify the clay surface in order to make it compatible with the monomer/polymer system involved. This is generally done by ion-exchange, using positively charged organic species such as quaternary ammonium surfactants.[29] In NMP the control of polymerization is based on a nitrogen containing species that can easily be quaternized and anchored on clay surfaces, resulting in a modified-clay, which can subsequently be used in a controlled free-radical polymerization reaction. This leads to nanocomposites with both the polymer and clay architectures being controlled. This idea was pioneered by Weimer *et al*., who synthesized PS–CNs with controlled molar masses by first anchoring a TEMPO derivative onto clay layers prior

proceeding with the free-radical polymerization of styrene.[31] Di and Sogah prepared their nanocomposites based on this idea, with minor changes in the nitroxide mediating species. They also successfully synthesized block copolymers by the same method.[30]

Other types of controlled living polymerization methods, such as ionic polymerization,[32,33] ATRP,[34,35] borane chemistry,[36,37] and RAFT techniques,[38-40] have not been widely used in the preparation of PCNs. There are several reasons for this, particularly the technique's susceptibility to impurities: e.g. the propagating species in ionic polymerization is destroyed by even small amounts of water (small amounts of water are always present in clays).[38] Notwithstanding the disadvantages of ionic polymerization in the presence of clay, Fan *et al*. and Advincula *et al*. synthesized PS–CNs under harsh conditions of high temperature and vacuum in order to remove any moisture in the system.[32,33] ATRP suffers from the presence of redox species,[6] the presence of which in clays is well known, as these might lead to the undesired reduction of the ionic copper species to copper zero. This technique also suffers from a limited number of monomers that can be successfully synthesized under controlled conditions, as well as the presence of toxic copper in the final product.[2] Although very little is known about controlling polymerization using borane chemistry, Yang *et al*. successfully used this technique to synthesize PS–CNs with controlled molar masses.[36]

Given the susceptibility of RAFT towards basic nucleophiles like hydroxide ions, primary and secondary amines,[2,13-16] the synthesis of positively charged RAFT agents that can be anchored onto clay by an ion-exchange process is a great challenge. This is because of the inherent instability of the thio-carbonyl-thio group in a basic environment, given that most of the positively charged organic species originate from amines. Because of the advantages of the RAFT technique over other controlled radical polymerization techniques I considered it worthwhile to endeavor to synthesize positively charged RAFT agents and apply the RAFT technique to the synthesis of PCNs to control both the clay morphology and the polymer architecture.

Although it is difficult to synthesize positively charged RAFT agents,[14] they can be anchored onto clay layers, thus allowing the synthesis of controlled RAFT-mediated PCNs, with the polymer growth taking place from the clay surfaces, as has been reported by Di *et al*.[38] Most of the work reported in literature to date is on the use of

free RAFT agents (i.e. the RAFT agent is not attached to the clay layers). Moad *et al*. have used RAFT-mediated polar polymers that are miscible with polypropylene and then melt blended both polymers (i.e. polymers and polypropylene) in the presence of sodium montmorillonite to yield polypropylene-clay nanocomposites.[40-42] Salem and Shipp have shown the ability of free RAFT agents to control the polymerization in the preparation of polystyrene-, poly(methyl methacrylate)- and poly(butyl acrylate)-clay nanocomposites by the *in situ* intercalative polymerization method.[39] They used polymerizable surfactant-modified-clays and copolymerized these anchored polymerizable surfactants with the main monomer in a controlled manner. The monomer-clay system they investigated had previously been studied and results showed that the nanocomposite structure obtained was not changed by the presence of the RAFT agent.[43] PCNs synthesized using positively charged RAFT agents have been reported by Zhang *et al*. who anchored a cationic RAFT agent 10-Carboxylic acid-10-dithiobenzoate-decyltrimethylammonium bromide (CDDA) onto clay and then used the modified-clay for the controlled solution-based *in situ* intercalative polymerization of styrene, and obtained exfoliated PCNs.[44] Ding *et al*. reported on the use of a negatively charged RAFT agent, 4-cyanopentanoic acid dithiobenzoate (CAD), onto a layered double hydroxide (LDH) (i.e. a positively charged layered clay like material) and then used the modified LDH in the *in situ* intercalative polymerization of styrene to obtain exfoliated LDH nanocomposites.[37] Di and Sogah,[38] used a dithiocarbamate-based modified-clay for the synthesis of PS–CNs. However, dithiocarbamates are well known for their poor ability to control polymerization, save for the polymerization of specific monomer systems. The poor control is because the dithiocarbamyl radicals generated undergo several side reactions.[2] The use of positively charged RAFT agents based on the more general and versatile dithiocarbonates and trithiocarbonates has still to be researched and described.

3.5. References

[1] G. Moad, E. Rizzardo, S. H. Thang. *Aus J Chem* **2005**, *58*, 379-410.

[2] W. A. Braunecker, K. Matyjaszewski. *Prog Polym Sci* **2007**, *32*, 93-146.

[3] M. Szwarc. *J Polym Sci Part A: Polym Chem* **1998**, *36*, IX-XV.

[4] R. P. Quirk, B. Lee. *Polym Int* **1992**, *27*, 359-367.

[5] D. H. Solomon. *J Polym Sci Part A: Polym Chem* **2005**, *43*, 5748-5764.

[6] P. Bera, S. K. Saha. *Polymer* **1998**, *39*, 1461-1469.

[7] E. Rizzardo, J. Chiefari, R. Mayadunne, G. Moad, S. Thang. *Macromol Symp* **2001**, *174*, 209-212.

[8] J. Chiefari, R. T. A. Mayadunne, G. M. Catherine L. Moad, E. Rizzardo, A. Postma, M. A. Skidmore, S. H. Thang. *Macromolecules* **2003**, *36*, 2273-2283.

[9] B. Y. K. Chong, J. Krstina, T. P. T. Le, G. Moad, A. Postma, E. Rizzardo, S. H. Thang. *Macromolecules* **2003**, *36*, 2256-2272.

[10] S. H. Thang, B. Y. K. Chong, R. T. A. Mayadunne, G. Moad, E. Rizzardo. *Tetrahedron Lett* **1999**, *40*, 2435-2438.

[11] S. Perrier, P. Takolpuckdee. *J Polym Sci Part A: Polym Chem* **2005**, *43*, 5347-5393.

[12] A. Favier, M. T. Charreyre. *Macromol Rapid Commun* **2006**, *27*, 653-692.

[13] J. Baussard, J. Habib-Jiwan, A. Laschewsky, M. Mertoglu, J. Storsberg. *Polymer* **2004**, *45*, 3615-3626.

[14] A. Samakande, R. D. Sanderson, P. C. Hartmann. *Synthetic Commun* **2007**, *37*, 3861-3872.

[15] G. Levesque, P. Arsene, V. Fanneau-Bellenger, T. Pham. *Biomacromolecules* **2000**, *1*, 400-406.

[16] G. Levesque, P. Arsene, V. Fanneau-Bellenger, T. Pham. *Biomacromolecules* **2000**, *1*, 387-399.

[17] A. Postma, T. P. Davis, G. X. Li, G. Moad, M. S. O'Shea. *Macromolecules* **2006**, *39*, 5307-5318.

[18] C. Boyer, P. Lacroix-Desmazes, J. J. Robin, B. Boutevin. *Macromolecules* **2006**, *39*, 4044-4053.

[19] P. Lacroix-Desmazes, R. Severac, B. Boutevin. *Macromolecules* **2005**, *38*, 6299-6309.

[20] P. Lacroix-Desmazes, R. Severac, B. Otazaghine, B. Boutevin. *Abstr Pap Am Chem Soc* **2003**, *226*, U398-U398.

[21] J. Tonnar, P. Lacroix-Desmazes, B. Boutevin. *Abstr Pap Am Chem Soc* **2005**, *230*, U4126-U4126.

[22] J. Tonnar, P. Lacroix-Desmazes, B. Boutevin. *Macromol Rapid Commun* **2006**, *27*, 1733-1738.

[23] J. Tonnar, P. Lacroix-Desmazes, B. Boutevin. *Macromolecules* **2007**, *40*, 6076-6081.

[24] J. Tonnar, P. Lacroix-Desmazes, B. Boutevin. *Macromolecules* **2007**, *40*, 186-190.

[25] A. Goto, T. Fukuda. *Prog Polym Sci* **2004**, *29*, 329-385.

[26] M. Okamoto. *Encyclopedia of Nanoscience and Nanotechnology*; American Scientific Publishers: California, 2004.

[27] B. Ray, Y. Isobe, K. Morioka, S. Habaue, Y. Okamoto, M. Kamigaito, M. Sawamoto. *Macromolecules* **2003**, *36*, 543-545.

[28] M. Rosorff. *Nano Surface Chemistry*; Marcel Dekker:: New York-Basel, 2002.

[29] A. Samakande, P. C. Hartmann, V. Cloete, R. D. Sanderson. *Polymer* **2007**, *48*, 1490-1499.

[30] J. B. Di, D. Y. Sogah. *Macromolecules* **2006**, *39*, 5052-5057.

[31] M. W. Weimer, H. Chen, E. P. Giannelis, D. Y. Sogah. *J Am Chem Soc* **1999**, *121*, 1615-1616.

[32] X. W. Fan, Q. Y. Zhou, C. J. Xia, W. Cristofoli, J. Mays, R. Advincula. *Langmuir* **2002**, *18*, 4511-4518.

[33] R. Advincula, Q. Y. Zhou, Y. Nakamura, S. Inaoka, M. K. Park, Y. F. Wang, J. Mays. *Abstr Pap Am Chem Soc* **2000**, *219*, U498-U498.

[34] P. A. Wheeler, J. Z. Wang, J. Baker, L. J. Mathias. *Chem Mater* **2005**, *17*, 3012-3018.

[35] P. A. Wheeler, J. Z. Wang, L. J. Mathias. *Chem Mater* **2006**, *18*, 3937-3945.

[36] Y. Y. Yang, J. C. Lin, W. T. Yang, G. J. Jiang. *Polym Prepr* **2003**, *44*, 855-856.

[37] P. Ding, M. Zhang, J. Gai, B. Qu. *J Mater Chem* **2007**, *17*, 1117-1122.

[38] J. B. Di, D. Y. Sogah. *Macromolecules* **2006**, *39*, 1020-1028.

[39] N. Salem, D. A. Shipp. *Polymer* **2005**, *46*, 8573-8581.

[40] G. Moad, G. Li, E. Rizzardo, S. H. Thang, R. Pfaendner, H. Wermter. *Polym Prepr* **2005**, *46*, 376.

[41] G. Moad, K. Dean, L. Edmond, N. Kukaleva, G. X. Li, R. T. A. Mayadunne, R. Pfaendner, A. Schneider, G. Simon, H. Wermter. *Macromol Symp* **2006**, *233*, 170-179.

[42] G. Moad, G. Li, R. Pfaendner, A. Postma, E. Rizzardo, S. Thang, H. Wermter. *ACS Symp Ser* **2006**, *944*, 514-532.

[43] C. Zeng, L. J. Lee. *Macromolecules* **2001**, *34*, 4098-4103.

[44] B. Q. Zhang, C. Y. Pan, C. Y. Hong, B. Luan, P. J. Shi. *Macromol Rapid Commun* **2006**, *27*, 97-102.

Chapter 4: Synthesis and characterization of RAFT agents

The work described in this chapter has been published in the following two papers:

Synthesis and Characterization of Novel Quaternary Ammonium RAFT Agents.
Austin Samakande, Ronald D. Sanderson and Patrice C. Hartmann
Synthetic Commun. 2007, 37, 3861–3872.

and

Aqueous behaviour of cationic surfactants containing a cleavable group.
Austin Samakande, Radhouane Chaghi, Gaelle Derrien, Clarence Charnay and Patrice C. Hartmann
J Colloid Interface Sci. 2008, 320, 315–320.

Abstract

This chapter details the synthesis and characterization of reversible addition–fragmentation chain transfer (RAFT) agents. Behaviour of the positively charged RAFT agents in water is also investigated. Emphasis is placed on the use of these RAFT agents as chain transfer agents during the synthesis of polymer–clay nanocomposites (PCNs).

4.1 Introduction

The industrial demand for novel synthetic materials with specific properties is constantly growing. From an academic point of view, this results in tremendous efforts in the research and development of new methods of polymerization that yield polymers that have tailored structures with the desired properties. Many nanocomposite materials have inorganic nanofillers dispersed in an organic polymer continuous matrix. Emphasis is most frequently on the control of the nature, the shape, and the dispersion of the inorganic nanoparticles.[1,2] In nanocomposites, the control of the polymer structure itself is generally neglected. Good control of the polymer architecture can however influence the morphology of the nanofiller itself.[3-5] This is the case in the preparation of polymer–clay nanocomposites(PCNs) using *in situ* intercalative polymerization methods. Here, as the polymerization takes place, the chain growth itself is one of the main driving forces of clay exfoliation.[1] Good control of the macromolecular chain growth could therefore directly impact on the degree of exfoliation of clay.

Preparation of polymers with fairly controlled architectures can be achieved by making use of controlled polymerization techniques such as ionic polymerization, nitroxide-mediated polymerization (NMP), atom transfer radical polymerization (ATRP) and, lately, reversible addition–fragmentation chain transfer polymerization (RAFT).[6] Of all these methods, RAFT polymerization is often reported as being the most versatile, as it is fairly tolerant to impurities and can be used with a wide range of monomers. The control in RAFT-mediated polymerization is achieved by using thio-carbonyl-thio (i.e. dithio) compounds.[7,8]

Thio-carbonyl-thio compounds are unstable when exposed to heat, light, oxygen, basic media, or amines (primary and secondary).[9-14] However, due to the important role their structure plays in controlling (or not) the polymerization of specific monomer systems, great efforts have been made to prepare tailored RAFT agents with a variety of structures. Very good reviews are available in the literature, and many, mostly neutral, RAFT agents are described.[12,15,16]

RAFT agents bearing an ionic group have been used in controlled free-radical polymerization. The following, anionic containing compounds have been described: sodium carboxylate,[17-21] sodium sulfonate,[22,23] or carboxylic acid.[18,22,24-33] Recently Ding *et al*. reported on the use of a negatively charged RAFT agent, 4-

cyanopentanoic acid dithiobenzoate (CAD), onto a layered double hydroxide (i.e. a positively charged layered clay like material) and the use of the modified layered double hydroxide (LDH) in the *in situ* intercalative polymerization of styrene and obtained exfoliated LDH nanocomposites.[34]

To the best of our knowledge, only three cationic RAFT agents have been reported to date.[3,9,35] The first reference described the synthesis of 4-(*N,N*-diethyldithiocarbamylmethyl)benzyltrimethylammonium bromide, its use in the modification of montmorillonite clay, and the preparation of polymer–clay nanocomposites(PCNs) by *in situ* intercalative free-radical polymerization of acrylic monomers and styrene.[3] The second reference describes the synthesis of 10-carboxylic acid-10-dithiobenzoate-decyltrimethylammonium bromide (CDDA) and its anchoring onto clay, and the use of the modified-clay in the RAFT-mediated solution based *in situ* intercalative controlled free-radical polymerization of styrene resulting in exfoliated PCNs.[35] The third reference describes the synthesis of a RAFT agent containing a morpholinium cationic group, and its use in controlling the free-radical polymerization of *N*-vinylbenzyl-*N*,*N*,*N*-trimethylammonium chloride in aqueous solution.[9]

A dithioester with a cationic quaternary ammonium group has been prepared for protein thioacetylation purposes.[11] However, the chemical structure of this dithioester compound makes it a poor candidate for use as a RAFT agent for controlled free-radical polymerization of monomers.

This chapter deals with the preparation of neutral thio-carbonyl-thio compounds (RAFT agents) as well as those that bear positive charges, i.e. quaternary ammonium groups. The RAFT agents containing the positive charges should be able to attach onto the surfaces of clay and also control the free-radical polymerization of monomers according to the RAFT process. However, as the compounds described here are also water soluble, and have surface-active properties, they may also be used in the controlled polymerization of water-soluble monomers or as transfer surfactants (‘transurf’) in emulsion polymerizations. Hence, the determination of their surface activity and self-assembly properties in diluted aqueous solutions is reported, with particular emphasis on the thermodynamic parameters associated with their micellization behaviour. Numerous studies on the aqueous behaviour of conventional cationic surfactants, e.g. mono-, di- and tri-valent quaternary ammonium have been

published.[36-40] However, to our knowledge there is no previous report on the aqueous micellization process of any dithio-group-containing surfactants. Both quaternary ammonium transurfs described here can also be used in water-based polymerization systems.[41]

Determination of the thermodynamic parameters controlling surfactant's partitioning between the water and organic phases is therefore essential as the surfactant micelle structure has an influence on the rate of polymerization and the molar mass distribution of the synthesized polymer chains. In addition, modern use of conventional RAFT agents in emulsion polymerizations present problems because poor transportation of the RAFT agent through the water phase leads to secondary particle nucleation and hence loss of control of polymerization.[26] Thus the physicochemical properties of the two synthesised cationic RAFT agents will be investigated, as the performance of the transurf surfactants is related to their self-association properties. Their aggregation behaviour was compared to that of a commercially available conventional cationic surfactant, cetyltrimethylammonium bromide (CTAB), in order to investigate the influence of the molecular structure on the surface activity and aggregation behaviour. The effects of the insertion of a bulky group and non-hydrocarbon functionality (S-C=S- linkage) within the hydrophobic moiety are also discussed.

4.2 Materials

4.2.1 Part A: Reagents used for the synthesis and characterization of RAFT agents

Magnesium turnings, dodecanethiol, thionyl chloride, 32% HCl and methyl iodide (Riedel-de-Haen); iodine crystals, bromobenzene, benzylbromide, N,N-dimethylethylamine, N,N-dimethylethanol amine and α,α-dibromo-p-xylene (Fluka); carbon disulphide and 11-mercaptoundecanoic acid (Aldrich). Aliquote 336 (Acros), NaOH pellets and anhydrous magnesium sulphate (Merck). Dry tetrahydrofuran (THF) was obtained by distillation of THF (HPLC grade, Sigma) over lithium aluminium tetrahydride. All the other solvents (p.a. grade or higher) were used as received from Sigma.

4.2.2 Part B: Reagents used for the determination of the aqueous behaviour of the cationic RAFT agents

All the reagents and solvents used were of the highest commercially, available grade and used after purification and drying, or freshly distilled, as required. The water used throughout the experiments was purified with a Millipore Super Q System. Cetyltrimethylammonium bromide (CTAB) was obtained from Aldrich and used without further purification. *N*,*N*-dimethyl-*N*-(4-(((phenylcarbonothionyl)thio)methyl)-benzyl)ethanammonium bromide (PCDBAB) and *N*-(4-((((dodecylthio)carbono-thioyl)thio)methyl)benzyl)-*N*,*N*-dimethylethanammonium bromide (DCTBAB) (>95%) were synthesized as described in Section 4.1.1.

4.3 Analytical equipment

Nuclear magnetic resonance (NMR) spectroscopy was performed at 20 ºC using a Varian VXR-Unity 300 MHz. Fourier transform infrared spectroscopy (FTIR) was carried out on a Nexus FTIR instrument, by averaging 32 scans, with a wave number resolution of 4 cm^{-1}. Electrospray mass spectroscopy (ESMS) and electron impact mass spectroscopy (EIMS) were carried out using a Waters-Micromass QTOF Ultima API instrument and an AMD 604 high resolution mass spectrometer, respectively. Melting points were carried out on a Stuart melting point SMP 10 instrument and a Perkin Elmer lambda 20 UV spectrometer was used for UV analysis.

The critical micelle concentration (cmc) of the surfactants was determined at 303 K by measuring electrical conductivity and the surface tension of surfactant solutions of different concentrations. A Multilab 540 conductimeter was used for determining the electrical conductivity and the Wilhelmy plate method, using a Kruss digital tensiometer K 12, was used for determining the surface tension. Differential molar enthalpies of dilution ($\Delta_{dil}\mathrm{H}$) were measured using a “Calostar” microcalorimeter.

4.3.1 Operation of a “Calostar” microcalorimeter

The “Calostar” microcalorimeter measures thermal effects, which allow us to determine dilution, adsorption and micellization thermodynamic parameters. The calorimetric cell was filled with a known volume of water (~8g) and predetermined volumes of a concentrated solution of the surfactant (about 10 times the cmc) were injected using a syringe. The cell was allowed to equilibrate for 12 h before injections

were made, and equilibrated again 30 min between each injection. During each injection of the concentrated solution of surfactant into the calorimetric cell, the micelles are destroyed by dilution and the thermal effects recorded. A sufficient number of injections are made during which the concentration inside the cell will be above the cmc value. From the thermal effects, the enthalpy of dilution is determined by integration of the peaks that are obtained.[42] A new analysis of such data, recently proposed,[43] allows one to easily calculate the enthalpy of micellization per mole of surfactant, ΔH_{mic}^{0}, and the cmc value. The plot of the cumulative enthalpies of dilution, $\Delta_{dil}H_{cum}$, against the injection number, *i*, is composed of two linear parts, and their slopes provide the constant values of the apparent molar enthalpy of the surfactant in the premicellar and postmicellar regions. Within the framework of the pseudo-phase transition model, the micellization enthalpy is calculated straight from the difference between these two slopes.

4.4 Part A: Synthesis and characterization of RAFT agents

4.4.1 Experimental and results

4.4.1.1 N,N-dimethyl-N-(4(((phenyl-carbonothioyl)thio)methylbenzyl)ethanammonium bromide (5)

Dry THF (5 g), magnesium (Mg^0) turnings (1 g; 0.04 mol), a small crystal of iodine and bromobenzene (1 g; 0.0064 mol) were stirred with gentle heating (below 40 ºC) until the reaction commenced. Then an additional amount of bromobenzene (5.28 g; 0.0336 mol) and THF (25 g) were added dropwise, whilst keeping the temperature below 40 ºC by using an ice bath. After all the magnesium disappeared, carbon disulphide (3.05 g; 0.04 mol) was slowly added over 30 min at 0 ºC. The solution turned red and the contents were left to stir at room temperature for a further 15 min. The resulting Grignard reagent solution was heated at 40 ºC then added dropwise, over 2 h, to a solution of α,α-dibromo-p-xylene (15.84 g; 0.06 mol) in dry THF (200 ml), at 60 ºC. After the last drop of the Grignard reagent was added the reaction mixture was kept at 60 ºC for a further 2 h.

Ice cold water (150 ml) was then added to stop the reaction and the resultant mixture was extracted with ether (3 x 100 ml). The combined organic phases were washed with 100 ml water, and 2 x 40 ml brine, then dried over anhydrous magnesium sulphate. Solvents were evaporated off under reduced pressure, yielding a crude oil.

Purification was performed using column chromatography with hexane:chloroform (8:1) as eluent, and the peach-coloured band was collected. Column chromatography is however not necessary as the impurities present (i.e. unreacted α,α-dibromo-p-xylene and 1,4-phenylenebis(methylene)dibenzenecarbodithioate do not interfere with the next reaction step.

The crude oil was dissolved in acetone, and an excess of dimethylethylamine (26.28 g; 0.360 mol) was added dropwise to the solution. The reaction was stirred at ambient temperature for 48 h. The solvent was then removed under reduced pressure. The obtained residue was washed several times with ether. Dry acetone was used to extract the desired product from the insoluble material (i.e. the bi-quaternary ammonium compound). The acetone phase was collected, evaporated to dryness, and the residual solid product was washed with ether and dried, to yield hygroscopic red crystals of the desired RAFT agent i.e. *N*,*N*-dimethyl-*N*-(4(((phenyl-carbonothioyl)thio)methylbenzyl)ethanammonium bromide (**5**) (10.88 g; 66.36% yield).

The melting point could not be determined because the reagent was too hygroscopic. ^{1}H NMR (300 MHz, $CDCl_3$) δ (ppm): 7.98, 7.65 and 7.53 (d, d and t, 5H, aromatic =CH̃), 7.40 (m, 4H, p-phenylene aromatic =CH–), 5.04 (s, 2H, S–CH_2–Φ), 4.56 (s, 2H, Φ–CH_2–N^+), 3.66 (q, 2H, N^+–$\underline{CH_2}$–Me), 3.19 [s, 6H, $N^+(CH_3)_2$], 1.40 (t, 3H, –CH_3); ^{13}C NMR (300 MHz, $CDCl_3$) δ (ppm): 227.41 (C=S), 144.86, 138.80, 133.88, 133.00, 130.31, 128.74, 127.22, 66.72, 59.35, 49.06, 41.02, 8.54; ESMS *m/e*: 330.1 (M^+, 100); IR (neat): 1044 cm^{-1} (C=S); UV: λ_{max} 304 nm (C=S, π–π*). c.f. Appendix, Figs. 1-5.

4.4.1.2 1,4-phenylenebis(methylene)dibenzenecarbodithioate (3)

The ether soluble component (byproduct) was evaporated to dryness to obtain the neutral difunctional RAFT agent 1,4-phenylenebis(methylene)dibenze-necarbodithioate (**3**) (4.950 g; 30.19% yield).

Melting point: 33 ºC. ^{1}H NMR (300 MHz, $CDCl_3$) δ (ppm): 8.02, 7.35-7.52 (d and m, 10H, aromatic =CH–), 7.35 (s, 4H, p-phenylene aromatic =CH–), 4.58 (s, 4H, –CH_2–Φ–CH_2–);^{13}C NMR (300 MHz, $CDCl_3$) δ (ppm): 228.07 (C=S), 145.08, 135.03, 132.76, 129.97, 128.67, 127.22, 41.77; EIMS *m/e*: 410 (M^+); IR (neat): 1044 cm^{-1} (C=S); UV: λ_{max} 305 nm (C=S, π–π*). c.f. Appendix, Figs. 6-10.

4.4.1.3 N-(4-((((dodecylthio)carbonothioyl)thio)methyl)benzyl)-N,N-dimethylethanammonium bromide (10)

To a stirred solution of dodecanethiol (25.5 g; 0.126 mol) and Aliquote 336 (2 g) in a 160/60 ml acetone/water mixture, NaOH (11.16 g; 0.279 mol) was added dropwise as a 50% aqueous solution. The resulting mixture was further stirred at room temperature for 1 h and then cooled to 0 ºC using an ice bath. Carbon disulphide (9.88 g; 0.130 mol) was added very slowly over 30 min. The temperature was then slowly increased to 40 ºC and the reaction mixture held at that temperature for a further 15 min, resulting in a reddish-tinted solution. The resultant solution was added dropwise to a stirred solution of α,α-dibromo-p-xylene (50 g; 0.189 mol) in 250 ml THF maintained at 60 ºC. Upon completion of the addition, the mixture was immediately cooled to room temperature (rt) then stirred at rt overnight. The solvents were removed under reduced pressure and the crude product dissolved in 100 ml chloroform:acetone (80:20 v/v). Dimethylethyl amine (55.29 g; 0.756 mol) was slowly added and the resulting mixture was stirred for 48 h at rt. The precipitate that formed was filtered off. The filtrate was collected and washed with water, then concentrated under reduced pressure and precipitated in ether. The obtained powder was washed several times with ether, dried, and then recrystallized from acetone to yield yellow crystals of *N*-(4-((((dodecylthio)carbonothioyl)thio)methyl)-benzyl)-*N*,*N*-dimethylethanammonium bromide (**10**) (25,63 g; 38% yield).

Melting point: 79-81 ºC. ^{1}H NMR (300 MHz, $CDCl_3$) δ (ppm): 7.63 and 7.38 (d and d, 4H, p-phenylene aromatic =CH–), 5.04 (s, 2H, S–CH_2–Φ), 4.59 (2s, 2H, Φ–CH_2–N^+), 3.66 (t, 2H, N^+–CH_2–), 3.34 (t, 2H, –CH_2–S), 3.20 [s, 6H, $N^+(CH_3)_2$], 1.66 (m, 2H, –$\underline{CH_2}$–CH_2–S), 1.37 [m, 5H, –CH_2– and –CH_3 (head group)], 1.22 (m, 18H, –$(CH_2)_9$–), 0.83 [t, 3H, –CH_3 (main chain)]; ^{13}C NMR (300 MHz, $CDCl_3$) δ (ppm): 223.69 (C=S), 139.03, 133.88, 130.26, 126.96, 66.78, 59.30, 49.04, 40.29, 37.34, 31.88, 29.58, 29.52, 29.41,29.30, 29.08, 28.91, 27.92, 22.62, 14.00; ESMS *m/e*: 454.2 (M^+, 100); IR (neat): 1060 cm^{-1} (C=S); UV: λ_{max} 309 nm (C=S, π–π*). c.f. Appendix, Figs. 11-15.

4.4.1.4 Didodecyl-1,4-phenylenebis(methylene)bistrithiocarbonate (8)

The ether phases (obtained from the product washing) were combined and evaporated to yield yellow crystals of a difunctional neutral RAFT agent (a by-

product), didodecyl-1,4-phenylenebis(methylene)bistrithiocarbonate (**8**) (5.469 g; 8.1% yield).

Melting point: 63-64 ºC. ^{1}H NMR (300 MHz, $CDCl_3$) δ (ppm): 7.28 (s, 4H, p-phenylene aromatic =CH–), 4.57 (s, 4H, $–CH_2–Φ–CH_2–$), 3.34 (t, 4H, $–CH_2–S$), 1.66 (m, 4H, $–\underline{CH_2}–CH_2–S$), 1.12-1.40 (m, 36H, $–(CH_2)_9–$), 0.84 (t, 6H, $–CH_3$); ^{13}C NMR (300 MHz, $CDCl_3$) δ (ppm): 223.41 (C=S), 134.61, 129.36, 40.66, 36.95, 31.74, 29.45,29.37, 29.26, 29.16, 28.92, 28.73, 27.78, 22.51, 13.85; EIMS *m/e*: 658 (M^+); IR (neat): 1062 cm^{-1} (C=S); UV: λ_{max} 311 nm (C=S, $\pi–\pi^*$). c.f. Appendix, Figs. 16-20.

4.4.1.5 11-(((benzylthio)carbonothioyl)thio)undecanoic acid (13)

A solution containing 11-mercaptoundecanoic acid (20.61 g; 0.094 mol), Aliquote 336 (1.52 g) and THF (40 g; 44.5 ml) was prepared at rt. Sodium hydroxide (7.55 g; 0.189 mol) was slowly added as a 50% aqueous solution over 30 min. Then an additional volume of water (30 ml) was added and the clear brownish solution was stirred for an additional 30 min. The mixture was cooled to 0 ºC, using an ice bath and carbon disulphide (7.17g; 0.094 mol) was added slowly over 30 min. The resultant solution was stirred at rt for a further 30 min. Benzyl bromide (16.73 g; 0.094 mol) was slowly added and the mixture stirred for 24 h at rt. The aqueous phase was acidified to pH 2 using 32% HCl, and extracted using chloroform (3 x 100 ml). The organic phases were combined, washed with 100 ml water, dried over magnesium sulphate, and concentrated. The RAFT compound was precipitated in a petroleum ether/ethyl acetate mixture (7:1) and the precipitate dried under high vacuum, to yield yellow crystals of 11-(((benzylthio)carbonothioyl)thio)undecanoic acid **(13)** (31.23 g; 87.51%).

Melting point: 57 ºC. ^{1}H NMR (300 MHz, $CDCl_3$) δ (ppm): 7.27-7.35 (m, 5H, aromatic =CH–), 4.59 (s, 2H, $S–CH_2–Φ$), 3.35 (t, 2H, $–CH_2–S$), 2.32 (t, 2H, $–CH_2–CO$), 1.55-1.72 (m, 4H, $S–CH_2–\underline{CH_2}–$ and $\underline{CH_2}–CH_2–CO$), 1.20-1.42 [m, 12H, $–(CH_2)_6–$]; ^{13}C NMR (300 MHz, $CDCl_3$) δ (ppm): 224.42 (C=S), 135.50, 129.58, 129.01, 128.04, 37.08, 33.88, 29.28, 29.16, 29.03, 28.85, 27.96, 24.65; EIMS *m/e*: 474 (M^+); UV: λ_{max} 307 nm (C=S, $\pi–\pi^*$). c.f. Appendix, Figs. 21-25.

4.4.2 Discussion on the synthesis of RAFT agents

4.4.2.1 Monofunctional cationic RAFT agents

Positively charged RAFT agents: *N*,*N*-dimethyl-*N*-(4-(((phenylcarbonothionyl)thio)-methyl)benzyl)ethanammonium bromide (PCDBAB) (**5**) and *N*-(4-((((dodecylthio)-carbonothioyl)thio)methyl)benzyl)-*N*,*N*-dimethylethanammo-nium bromide (DCTBAB), (**10**) and the neutral RAFT agents:- 1, 4-phenylenebis(methylene)-dibenzenecarbo-dithioate (PCDBDCP) (**3**) and didodecyl-1,4-phenylenebis(methyle-ne)bistrithiocarbo-nate (DCTBTCD) (**8**) were prepared following a simple strategy (c.f. Scheme 4.1 and Scheme 4.2).

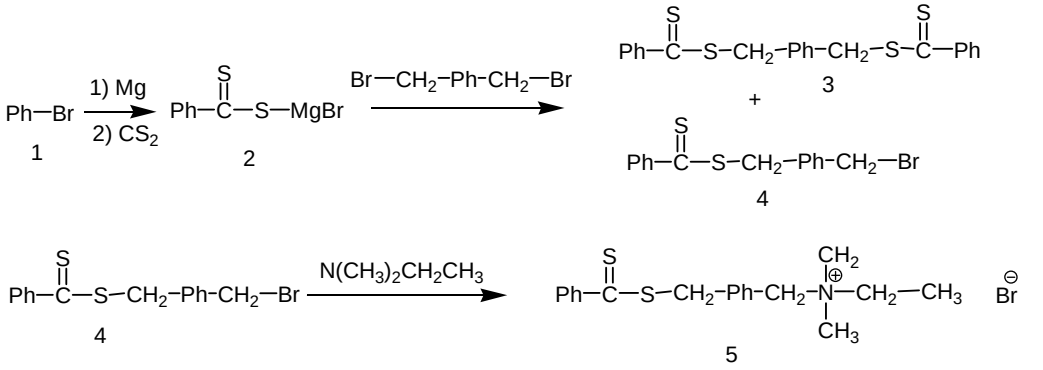

Scheme 4.1 Synthesis Method A: 1, 4-phenylenebis(methylene)dibenzenecarbodithioate (3) and *N*,*N*-dimethyl-*N*-(4-(((phenylcarbonothionyl)thio)methyl)benzyl)ethanammonium bromide (5).

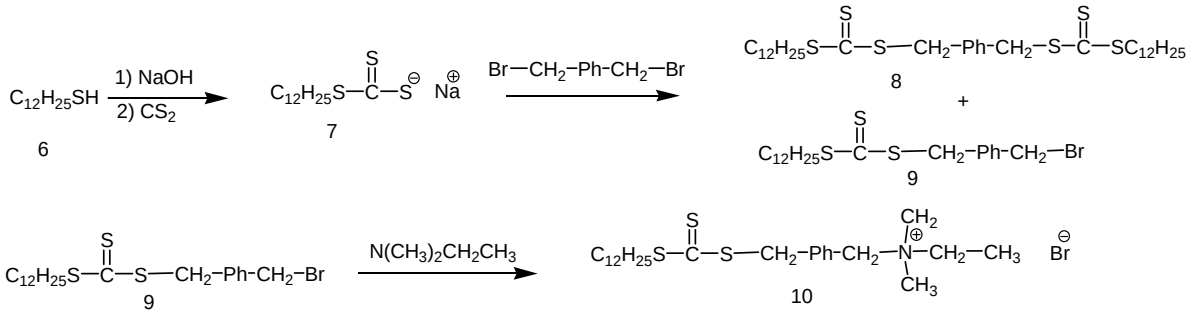

Scheme 4.2 Synthesis Method B: Didodecyl-1,4-phenylenebis(methylene)-bistrithiocarbonate (8) and N-(4-((((dodecylthio)carbonothioyl)thio)methyl)benzyl)-N,N-di-methylethanammonium bromide (10).

A Grignard reagent (**2**)[44] or sodium salt (**7**)[28] were first prepared following methods similar to those described in literature. Separately, (**2**) and (**7**) were further reacted with α,α-dibromo-p-xylene as described elsewhere.[9] One and a half equivalents of α,α-dibromo-p-xylene (relative to (**2**) or (**7**)) were used so as to favour the formation of the monofunctional adducts, ((**4**) or (**9**)). Reaction of intermediates (**4**) or (**9**) with dimethylethylamine yielded the quaternary ammonium salts (**5**) and (**10**) respectively.

The desired salts were purified by extraction using acetone so as to remove traces of double salts originating from the reaction of dimethylethylamine and α, α-dibromo-p-xylene (unreacted from the previous step).

4.4.2.2 Difunctional RAFT agents obtained as byproducts

The synthesis pathways outlined for the RAFT agents (in methods A and B) also yielded byproducts, i.e. R-CS_2-CH_2PhCH_2-S_2C-R (where R is phenyl in Method A or dodecyl in Method B), which are also interesting RAFT agents as they can be used in the preparation of ABA block copolymer by controlled free-radical polymerization. They have also been reported to be efficient in controlling the free-radical homopolymerization of styrene and butyl acrylate.[45] 1,4-phenylenebis-(methylene)dibenzenecarbodithioate **(3)** has been reported before,[45] whereas didodecyl-1,4-phenylenebis(methylene)bis-trithiocarbonate **(8)** is a novel RAFT agent.

11-(((benzylthio)carbonothioyl)thio)undecanoic acid (**13**) is a RAFT agent with a trithiocarbonate group. The synthesis route shown in Scheme 4.3.

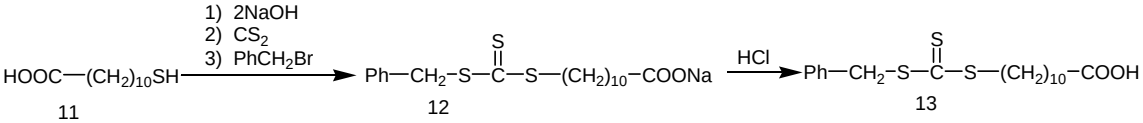

Scheme 4.3 Synthesis Method C: 11-((benzylthio)carbonothioyl)thio)undecanoic acid (13).

11-(((benzylthio)carbonothioyl)thio)undecanoic acid (BCTUA) (**13**) was synthesized following a procedure similar to one reported elsewhere.[46-48]

Neutral RAFT agents have been shown to be useful in the control of molar masses and the molar mass distribution during the synthesis of PCNs.[49]

4.5 Part B: Determination of the aqueous behaviour of cationic RAFT agents

Due to the surface activity of the two cationic RAFT agents (**5**) and (**10**) a study of their aqueous behaviour was carried out.

4.5.1 Experimental, results and discussion

4.5.1.1 Surface tension

The surface activity of the two synthesized RAFT agents, PCDBAB and DCTBAB, was first characterized by surface tension measurements. Fig. 4.1 displays the results of surface tension against the logarithm of the concentration for aqueous solutions of PCDBAB, DCTBAB and CTAB.

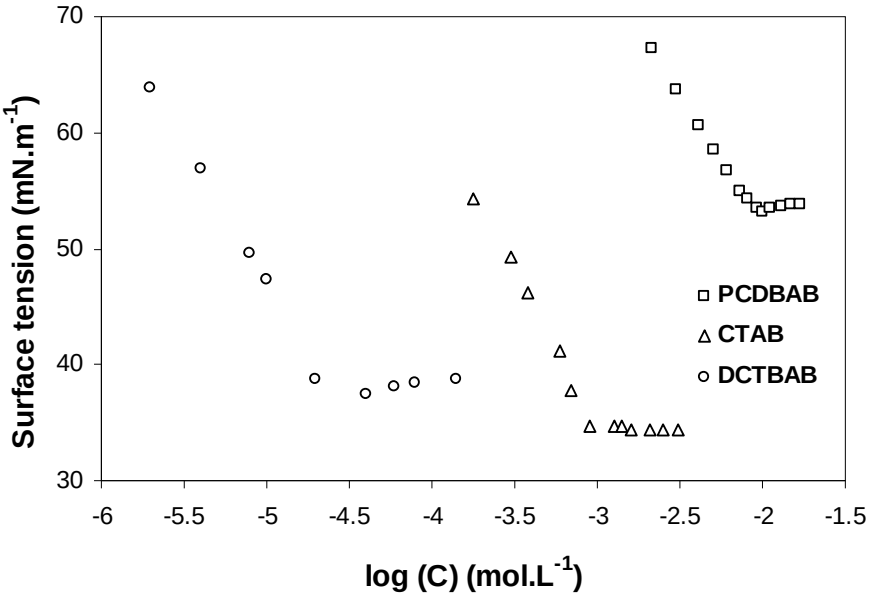

Fig. 4.1 Change in the surface tension with the log concentration of DCTBAB, CTAB and PCDBAB at 303 K.

The change in the surface tension of the two synthesized molecules, PCDBAB and DCTBAB, is typical of surface active molecules. The decrease in surface tension with increasing surfactant concentration is explained by the adsorption of the surfactant molecules at the solution/air interface. Above the cmc there is no further change in the surface tension of the solution as the water/air interface becomes saturated. The curves show breaks sharp enough to allow the exact determination of the cmc, which is taken as the concentration at the point of intersection of the two linear portions of the γ = f (log c) plots. The cmc values of PCDBAB, DCTBAB and CTAB were found to be 8.1, 0.032 and 0.8 mmol.L^{-1}, respectively. The few studies concerning cationic surfactants with para-substituted benzene rings, such as $C_nH_{2n+1}\Phi C_mH_{2m+1}N^+(CH_3)_3Br^-$ surfactant series,[50] report higher cmc values than that of DCTBAB. This indicates that the presence of a dithiocarbonothionyl group is expected to play an essential role in the control of the self-assembling properties.

Indeed, the polarity of the benzene rings leads to a higher hydration of the molecules, which is not favourable for micelle formation.

The cross-sectional area of surfactant head group, a_0, was calculated from the maximum value of the surface excess of Γ_m, according to equations below:

$$a_0 = \frac{1}{\Gamma_m . N_A}$$ **Equation 4. 1**

where the surface excess concentration Γ_m was calculated from the following Gibbs adsorption isotherm relation:

$$\Gamma = -\frac{1}{2.3nRT}\frac{d\gamma}{d(\log C)}$$ **Equation 4. 2**

with N_A being the Avogadro number, R = 8.32 J.mol^{-1}.deg^{-1}, T = 303 K, with γ expressed in N.m^{-1}, and n being the sum of the charge numbers of all ions resulting from the ionization of the surfactant molecule (n = 2 for monomeric surfactants).

All the cmc and head group surface area (a_0) values are tabulated in Table 4.1.

Table 4.1 cmc values of PCDBAB, DCTBAB and CTAB, determined using surface tension and the respective surfactant head group area

Surfactant	*cmc* (mmol.L^{-1})*	*Surfactant head group area (a_o), Å^2*
PCDBAB	8.200	89
DCTBAB	0.032	89
CTAB	0.890	62

PCDBAB and DCTBAB have a cross-sectional area of 89 Å^2 while for CTAB the value is 62 Å^2. The chemical structure of the head group of PCDBAB and DCTBAB comprises of a dimethylethylammonium bromide instead of a trimethylammonium bromide for CTAB. However, it has been shown that the introduction of a methylene group into a cationic headgroup has a negligible effect on the hydrophobicity of the cation.[51] The larger values of the surface area for PCDBAB and DCTBAB relative to CTAB suggest a bent conformation of the two surfactants at the air–water interface. A similar trend was observed in ammonium amphiphiles with para-substituted benzene rings, in which both the benzene ring and the polar head group contribute to the adsorption as hydrophilic parts.[50] Thus, the benzene ring in the vicinity of the quaternary ammonium for the DCTBAB and PCDBAB molecules may partly adsorb at the air–water interface, increasing the cross section of the polar head group compared with the quaternary ammonium of the conventional CTAB surfactant. Moreover, the final surface tension values for DCTBAB and PCDBAB, 38 and 54

$mN.m^{-1}$ respectively, are higher than obtained with CTAB, suggesting a hindered packing of the molecules at the interface. In addition, the π-π interaction among the benzene rings of the molecules at the interface may contribute to the increase of the final surface tension as this type of interaction is stronger than hydrophobic interaction among the CTAB molecules.[50,52]

The cmc of DCTBAB is 25-fold lower than that of CTAB. This result suggests that DCTBAB may be much more hydrophobic, despite its dithiocarbonothionyl group. Moreover, the dithiocarbonothionyl group is attached to a long alkyl chain that exhibits a hydrophobic behaviour. PCDBAB has the highest cmc relative to DCTBAB and CTAB because of the moderate hydrophobicity of its two benzene rings. As a consequence of the direct correlation between the cmc and the surfactant hydrophobicity, the logarithm values of the cmc vary linearly with the number of carbon atoms in the hydrophobic group (Kleven's rule) for surfactant homolog (same polar head group).[53] Such plots for alkyltrimethylammonium bromide are shown in Fig. 4.2, allowing the determination of the equivalent carbon number for the two surfactants PCDBAB and DCTBAB. From Fig. 4.2, PCDBAB and DCTBAB molecules have an equivalent carbon number of 13 and 21, respectively.

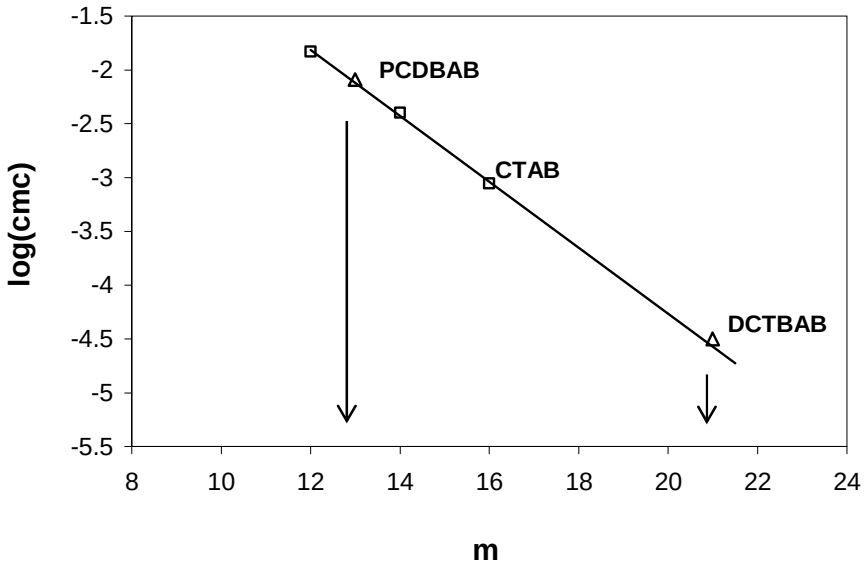

Fig. 4.2 log cmc vs alkyl chain carbon number (m) of n-alkyltrimethylammonium bromide surfactant at 303 K. Data for C_{12} and C_{14} molecules taken from Nagamura *et al*. [50].

4.5.1.2 Electrical conductivity

The electrical conductivity measurements of the three surfactants, PCDBAB, DCTBAB and CTAB are shown in Fig. 4.3.

Each plot of the electrical conductivity versus the surfactant concentration exhibits two straight lines that intersect at the concentration corresponding to the micelle formation, allowing identification of the cmc. Below the cmc the surfactants in solution conducts as simple single ions, whereas above the cmc the surfactants conducts as less mobile aggregates (micelles).

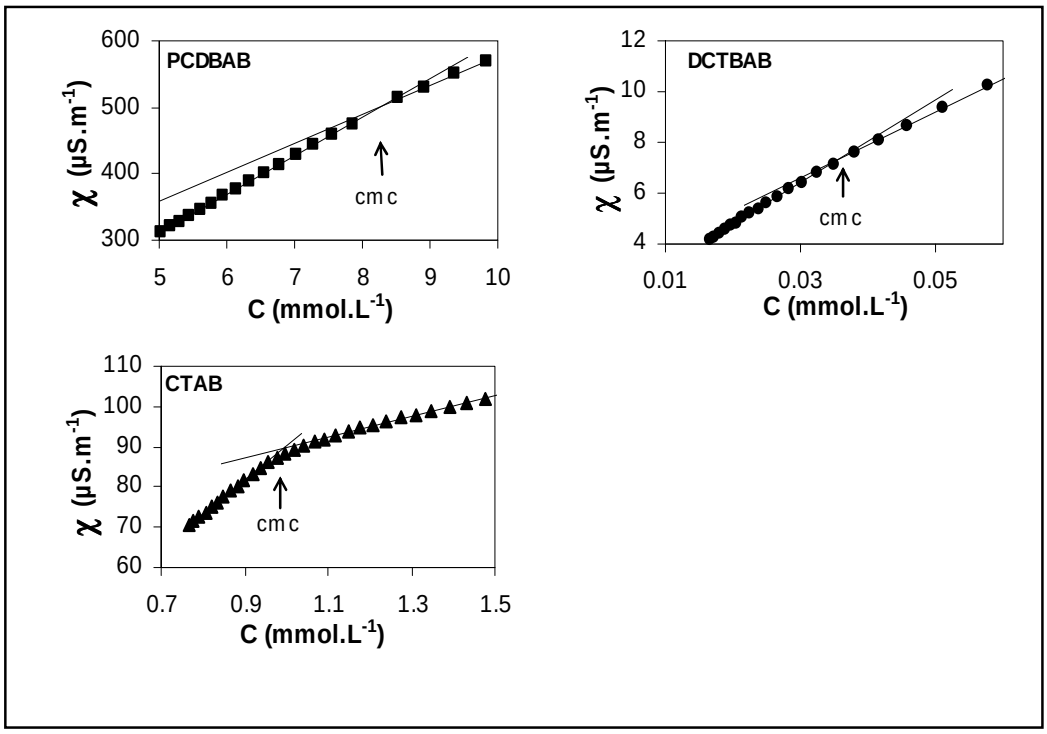

Fig. 4.3 Change in electrical conductivity with concentration of PCDBAB, DCTBAB and CTAB at 303 K.

The values of the cmc determined using electrical conductivity were in agreement with those obtained using surface tension and followed the same order i.e. 8.2, 0.033 and 0.98 mmol.L^{-1} for PCDBAB, DCTBAB, and CTAB, respectively (c.f. Table 4.2). The approximate value of the micelle ionization degree at the cmc (α) is usually determined from the electrical conductivity-concentration plot as the ratio of the slopes above and below the cmc. This method is a useful approximation when N_{agg} is not available, although the value of the micelle ionization degree is overestimated because the conductivity of the micelles is underestimated.[54-56] Table 4.2 lists the values of α calculated by this method.

The value of α is the smallest for CTAB indicating a higher binding of counterions to CTAB micelles (in agreement with a close packing of the headgroups), and therefore a higher surface charge density at the micelle-solution interface.[57]

Table 4.2 cmc values determined using electrical conductivity and the respective micelle ionization degree

Surfactant	*cmc (mmol.L^{-1})*	*Micelle ionization degree (α)*
PCDBAB	8.10	0,73
DCTBAB	0.033	0.78
CTAB	0.980	0.28

The values of α for PCDBAB and DCTBAB are higher, suggesting a less compact structure of the micelle and a low aggregation number. This picture is supported by the higher values of the headgroup surface area for these surfactants (Table 4.2).

4.5.1.3 Calorimetry

Fig. 4.4 Molar cumulative enthalpies of dilution for DCTBAB, PCDBAB and CTAB at 303 K. shows the cumulative molar enthalpies of dilution for the surfactant series as determined from the dilution calorimetric measurements.

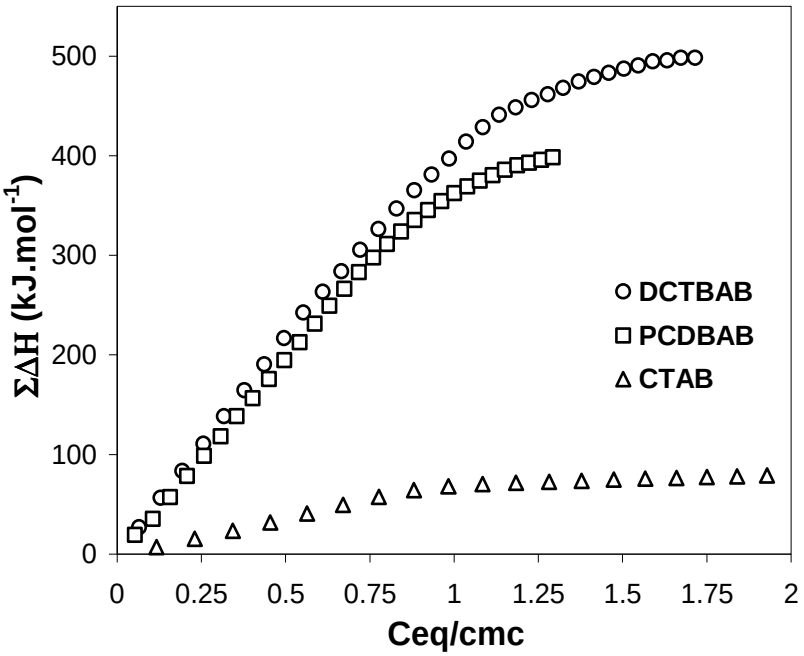

Fig. 4.4 Molar cumulative enthalpies of dilution for DCTBAB, PCDBAB and CTAB at 303 K.

This representation yields a change in the slope at the cmc. The cumulative molar enthalpies are plotted as a function of the reduced concentration as the cmc of the three investigated surfactants cover two orders in concentration. Table 4.3 lists the different thermodynamic parameters of micellization in aqueous solution at 303 K.

All ΔH_{mic} values in Table 4.3 are negative indicating that micelle formation is an exothermic process. The, DCTBAB surfactant exhibits the most negative value of ΔH_{mic} and CTAB the least, despite its long alkyl chain with 16 methyl groups.

Table 4.3 Thermodynamic parameters of micellization in aqueous solution at 303 K

Surfactant	cmc^* ($mmol.L^{-1}$)	ΔH_{mic} ($kJ.mole^{-1}$)	ΔG_{mic} ($kJ.mole^{-1}$)	$T\Delta S_{mic}$ ($kJ.mole^{-1}$)
PCDBAB	8.10	-12.64	-15.40	2.8
DCTBAB	0.033	-15.95	-31.81	15.86
CTAB	0.98	-7.24	-29.84	22.6

*: results from conductivity

These results clearly suggest that the micelle formation is energetically more favourable for DCTBAB and PCDBAB than for CTAB. This will be discussed further. The values of the free energy of micellization, $\Delta G_{mic}°$, and those of the entropy of micellization, $\Delta S_{mic}°$, give additional information on the thermodynamics of the surfactant micellization. These values are calculated using the following equations:

$$\Delta G_{mic} = (2 - \alpha)RT\ln (cmc) \qquad \textbf{Equation 4.3}$$

where cmc is expressed in the molarity of surfactant.

The entropy of micellization is derived from ΔG_{mic} and ΔH_{mic} by:

$$T\Delta S_{mic} = \Delta H_{mic} - \Delta G_{mic} \qquad \textbf{Equation 4.4}$$

All $T\Delta S_{mic}$ values in Table 4.3 are positive and the conventional CTAB surfactant exhibits the highest ΔS_{mic} while PCDBAB the smallest. These results indicate that the micelle formation is entropically more favourable for the conventional CTAB surfactant. The entropy change associated with the transfer of the surfactant monomers from an aqueous to a micellar environment involves different contributions.[58] The main contribution arises from the release of a large part of the solvating water molecules around the hydrophobic tail of the amphiphilic molecule (hydrophobic effect). In this way, the ΔS_{mic} is expected to increase with the chain's alkyl length. Some other processes that may contribute to ΔS_{mic} are the variation of the hydration of the headgroups according to the surface charge density of the micelle (number of associate monomers and condensed counterion to the micelle), the increase of the degrees of movement of the hydrophobic tail and restriction of the movement of the headgroups. The sum of the different contributions gives rise to a positive value of ΔS_{mic}.

PCDBAB displays the smallest hydrophobic moiety of the investigated molecules and the presence of the two benzene rings may increase its rigidity. Hence, the entropy change that occurs during the micellization process of PCDBAB is expected to be the smallest (Table 4.3). In the case of DCTBAB, its ΔS_{mic} value is lower than that of CTAB, although DCTBAB displays a higher carbon equivalent number (Fig. 4.2) in its

hydrophobic moiety. However, the molecular structure of the hydrophobic part of the two investigated molecules is different: DCTBAB exhibits a dithiocarbonothionyl group attached to a phenyl group and a C12 alkyl chain (Scheme 4.2) whereas the CTAB hydrophobic moiety consists of a C16 alkyl chain. So, the contribution to ΔS_{mic} owing to the release of water molecules from the alkyl chain will be higher for CTAB.[59] Moreover, the phenyl group linked to the dithiocarbonothionyl group may restrict the flexibility of the hydrophobic part into the core of the micelle. The sum of these two factors, smaller degrees of freedom of the chain motion and a reduced fraction of released water molecules, may result in a less positive value of ΔS_{mic} for DCTBAB. Thus the hydrophobic effect of the two investigated surfactants with benzene rings and a dithiocarbonothionyl moiety are weaker than that of the CTAB surfactant with an even long alkyl chain.

In contrast, the micellization processes give rise to enthalpic effects that are more exothermic for PCDBAB and DCTBAB than for CTAB (Table 4.3). The numerous energetic contributions to the enthalpy of micellization may be broken down into various terms.[60] The main contribution is associated with the transfer of the hydrocarbon chain of the surfactant monomer from the aqueous environment to the core of the micelle. This process is accompanied by the release of a fraction of the water molecules solvating the hydrophobic group of the amphiphilic molecule. This effect is expected to be exothermic. The second contribution arises from the electrostatic interactions at the micelle surface. This contribution involves several effects, including the repulsions between head groups and between bound counterions and the attractive interactions between the oppositely charged head groups and counterions. The net contribution to ΔH_{mic} of these electrostatic interactions is expected to be negative.[59,60] Other processes may occur and their contributions to ΔH_{mic} are more or less significant in relation to the molecular structure of the surfactant. These contributions may arise from the conformation changes of the hydrophobic moiety into the micelle core, the steric interactions between head groups and from specific interactions such as H bonding for surfactants that carry amide groups,[58] or π-π interactions among adjacent phenyl groups of surfactants that carry benzene rings.[3,52,61]

In this work, it is assumed that among these contributions, it is only those associated with the hydrophobic moiety that may explain the differences observed for the values of ΔH_{mic} (Table 4.3). Indeed, it has been shown that the effect of a trimethyl or

dimethylethylammonium bromide head group does not alter the values of ΔH_{mic} for surfactants with the same alkyl tail.[51] Moreover, an increase in the value of α associated with a larger headgroup surface area may be related to a less negative value of ΔH_{mic},[60] because of the electrostatic repulsion decrease and the headgroup hydration level. This trend is opposed to the more negative values of ΔH_{mic} obtained for DCTBAB and PCDBAB surfactants. Since the increase of the length of the alkyl tail contributes to a more negative ΔH_{mic},[60] an extra contribution to ΔH_{mic} may arise from the benzene rings and dithiocarbonothionyl moiety introduced into the hydrophobic group of DCTBAB and PCDBAB surfactants. The introduction of a bulky group into the hydrophobic part of amphiphilic molecules has been investigated for different classes of surfactant.[52,61] The reported microcalorimetric studies point out that the micellization of surfactant molecules bearing one or more benzene rings within their hydrophobic chain leads to a higher exothermic effect compared to surfactants with an even hydrophobic chain.[52,61] This effect may arise from the π-π interactions among the phenyl adjacent groups localised into the micelle. Therefore, the more negative values of ΔH_{mic} observed for DCTBAB and PCDBAB are consistent with this phenomenon. In addition, as assumed above the π-π interactions among adjacent benzene rings support the higher surface tension obtained for DCTBAB and PCDBAB (Fig. 4.1).

Cmc values of DCTBAB and PCDBAB and calorimetric data clearly indicate that the insertion of a di- or tri-thiocarbonothionyl moiety within the hydrophobic tail improves the surfactant properties of the molecule. Indeed the hydrophobic behaviour of the S-CS- linkage contributes to an increased tendency for DCTBAB and PCDBAB to self-assemble. Despite their molecular structure, DCTBAB and PCDBAB exhibit lower cmc values than their homolog alkyl ammonium surfactant. Moreover, the large negative values of ΔH_{mic} suggest that the release of the solvating water molecules around the dithio or trithio groups may be an exothermic process too. In this way, the insertion of the dithio or trithio cleavable functionalities greatly contributes to the negative value of $\Delta G_{mic,}$ and consequently to the micellization.

4.6. Conclusions

Quaternary ammonium functionalized RAFT agents, *N*,*N*-dimethyl-*N*-(4-(((phenylcarbonothionyl)thio)methyl)benzyl)ethanammonium bromide (PCDBAB) and *N*-(4-((((dodecylthio)carbonothioyl)thio)methyl)benzyl)-*N*, *N*-dimethylethanammonium

bromide (DCTBAB), and the neutral RAFT agents 1,4-phenylenebis(methylene)-dibenzenecarbodithioate (PCDBDCP), didodecyl-1,4-phenylenebis(methylene)bistri-thiocarbonate (DCTBTCD) and 11-(((benzylthio)carbonothioyl)thio)undecanoic acid (BCTUA), were successfully synthesized in acceptable yield and purity.

The self-assembling properties of the two novel positively charged transfer surfactants (transurfs), DCTBAB and PCDBAB, in dilute aqueous solutions have also been outlined. Their behaviour was compared to that of the conventional surfactant cetyltrimethylammonium bromide (CTAB) in order to explain the different structural relationships. It was observed that the presence of the dithio or trithio group on surfactants greatly alters surfactant properties in aqueous environments. DCTBAB and PCDBAB had lower cmc values than their homologue alkyl trimethylammonium surfactant. In fact, the hydrophobic behaviour of the S–C=S– linkage promotes the micellization and contributes to the negative value of $\Delta G_{mic,}$ as this group plays a role in the negative values of ΔH_{mic}.

The study also supports the concept that the introduction of a benzene ring in the vicinity of a quaternary ammonium headgroup leads to a more negative value of ΔH_{mic} due to the π-π interactions among the phenyl adjacent groups within the micelle core. In addition, the π-π interactions among the benzene rings at the water solution/air interface may contribute to increase the surface tension as this type of interaction is stronger than hydrophobic interaction among the CTAB molecules. Moreover, the values of a_0 for DCTBAB and PCDBAB were higher than that obtained for CTAB, suggesting a hindered packing of the molecules at the interface associated with the benzene ring.

4.7. References

[1] M. Alexandre, P. Dubois. *Mater Sci Eng A* **2000**, *28*, 1-63.

[2] M. Biswas, S. S. Ray. *Adv Polym Sci* **2001**, *155*, 170-221.

[3] J. B. Di, D. Y. Sogah. *Macromolecules* **2006**, *39*, 1020-1028.

[4] G. Moad, G. Li, E. Rizzardo, S. H. Thang, R. Pfaendner, H. Wermter. *Polym Prepr* **2005**, *46*, 376.

[5] M. W. Weimer, H. Chen, E. P. Giannelis, D. Y. Sogah. *J Am Chem Soc* **1999**, *121*, 1615-1616.

[6] J. Qiu, B. Charleux, K. Matyjaszewski. *Prog Polym Sci* **2001**, *26*, 2083-2134.

[7] A. Bowes, J. B. McLeary, R. D. Sanderson. *J Polym Sci Part A: Polym Chem* **2007**, *45*, 588-604.

[8] S. E. Shim, Y. Shin, J. W. Jun, K. Lee, H. Jung, S. Choe. *Macromolecules* **2003**, *36*, 7994-8000.

[9] J. Baussard, J. Habib-Jiwan, A. Laschewsky, M. Mertoglu, J. Storsberg. *Polymer* **2004**, *45*, 3615-3626.

[10] G. Levesque, P. Arsene, V. Fanneau-Bellenger, T. Pham. *Biomacromolecules* **2000**, *1*, 400-406.

[11] G. Levesque, P. Arsene, V. Fanneau-Bellenger, T. Pham. *Biomacromolecules* **2000**, *1*, 387-399.

[12] G. Moad, E. Rizzardo, S. H. Thang. *Aus J Chem* **2005**, *58*, 379-410.

[13] G. Moad, E. Rizzardo, S. H. Thang. *Aust J Chem* **2006**, *59*, 669-692.

[14] A. Samakande, R. D. Sanderson, P. C. Hartmann. *Synthetic Commun* **2007**, *37*, 3861-3872.

[15] C. Barner-Kowollik, T. P. Davis, J. P. A. Heuts, M. H. Stenzel, P. Vana, M. Whittaker. *J Polym Sci Part A: Pol Chem* **2003**, *41*, 365-375.

[16] S. Perrier, P. Takolpuckdee. *J Polym Sci Part A: Polym Chem* **2005**, *43*, 5347-5393.

[17] J. Chiefari, Y. K. B. Chong, F. Ercole, J. Krstina, J. Jeffery, T. P. T. Le, R. T. A. Mayadunne, G. F. Meijs, C. L. Moad, G. Moad, E. Rizzardo, S. H. Thang. *Macromolecules* **1998**, *31*, 5559-5562.

[18] E. Rizzardo, J. Chiefari, R. T. A. Mayadunne, G. Moad, S. H. Thang. *ACS Symp Ser* **2000**, *768*, 278-296.

[19] B. S. Sumerlin, A. B. Lowe, D. B. Thomas, C. L. Mccormick. *Macromolecules* **2003**, *36*, 5982-5987.

[20] A. Favier, M. T. Charreyre. *Macromol Rapid Commun* **2006**, *27*, 653-692.

[21] T. P. Le, G. Moad, R. Ezio, S. H. Thang. *PCT Int Appl WO 9801478* **1998**, 88.

[22] D. B. Thomas, A. J. Convertine, L. J. Myrick, C. W. Scales, A. E. Smith, A. B. Lowe, Y. A. Vasilieva, N. Ayres, C. L. Mccormick. *Macromolecules* **2004**, *37*, 8941-8950.

[23] D. B. Thomas, B. S. Sumerlin, A. B. Lowe, C. L. Mccormick. *Macromolecules* **2003**, *36*, 1436-1439.

[24] A. J. Convertine, N. Ayres, C. W. Scales, A. B. Lowe, C. L. Mccormick. *Biomacromolecules* **2004**, *5*, 1177-1180.

[25] C. J. Ferguson, R. J. Hughes, D. Nguyen, B. T. T. Pham, R. G. Gilbert, A. K. Serelis, C. H. Such, B. S. Hawkett. *Macromolecules* **2005**, *38*, 2191-2204.

[26] C. J. Ferguson, R. J. Hughes, B. T. T. Pham, B. S. Hawkett, R. G. Gilbert, A. K. Serelis, C. H. Such. *Macromolecules* **2002**, *35*, 9243-9245.

[27] X. Jiang, P. J. Schoenmakers, J. L. J. Van Dongen, X. Lou, V. Lima, J. Brokken-Zijp. *Anal Chem* **2003**, *75*, 5517-5524.

[28] J. T. Lai, D. Filla, R. Shea. *Macromolecules* **2002**, *35*, 6754-6756.

[29] H. Matahwa, J. B. McLeary, R. D. Sanderson. *J Polym Sci Part A: Polym Chem* **2006**, *44*, 427-442.

[30] R. T. A. Mayadunne, E. Rizzardo, J. Chiefari, J. Krstina, G. Moad, A. Postma, S. H. Thang. *Macromolecules* **2000**, *33*, 243-245.

[31] G. Moad, Y. K. Chong, A. Postma, E. Rizzardo, S. H. Thang. *Polymer* **2005**, *46*, 8458-8468.

[32] B. T. T. Pham, D. Nguyen, C. J. Ferguson, B. S. Hawkett, A. K. Serelis, C. H. Such. *Macromolecules* **2003**, *36*, 8907-8909.

[33] Y. Y. Yang, J. C. Lin, W. T. Yang, G. J. Jiang. *Polym Prepr* **2003**, *44*, 855-856.

[34] P. Ding, M. Zhang, J. Gai, B. Qu. *J Mater Chem* **2007**, *17*, 1117-1122.

[35] B. Q. Zhang, C. Y. Pan, C. Y. Hong, B. Luan, P. J. Shi. *Macromol Rapid Commun* **2006**, *27*, 97-102.

[36] A. Bendjeriou, G. Derrien, P. Hartmann, C. Charnay, S. Partyka. *Thermochim Acta* **2005**, *434*, 165-170.

[37] K. Esumi, K. Taguma, Y. Koide. *Langmuir* **1996**, *12*, 4039-4041.

[38] E. Jungerman. *Cationic Surfactants*; Marcel Dekker: New York, 1969.

[39] X. Wang, J. Wang, Y. Wang, H. Yan, P. Li, R. K. Thomas. *Langmuir* **2004**, *20*, 53-56.

[40] R. Zana. *Adv Colloid Interface Sci* **2002**, *97*, 205-253.

[41] A. Guyot, K. Tauer, J. M. Asua, S. Van Es, C. Gauthier, A. C. Hellgren, D. C. Sherrington, A. Montoya-Goni, M. Sjoberg, O. V. Sindt, F., M. Unzue, H. Schoonbrood, E. Shipper, P. Lacroix-Desmazes. *Acta Polymerica* **1999**, *50*, 57-66.

[42] S. Lagerge, A. Kamyshny, S. Magdassi, S. Partyka. *J Therm Anal Calorim* **2003**, *71*, 291-310.

[43] H. Benalla, J. Zajac. *J Colloid Interface Sci* **2004**, *272*, 253-261.

[44] W. G. Weber, J. B. McLeary, R. D. Sanderson. *Tetrahedron Lett* **2006**, *47*, 4771-4774.

[45] D. L. Patton, M. Mullings, T. Fulghum, R. C. Advincula. *Macromolecules* **2005**, *38*, 8597-8602.

[46] M. Jesberger, L. Barner, M. H. Stenzel, E. M. M, T. P. Davis, C. Barner-Kowollik. *J Polym Sci Part A: Polym Chem* **2003**, *41*, 3847-3861.

[47] M. H. Stenzel, T. P. Davis. *J Polym Sci Part A: Polym Chem* **2002**, *40*, 4498-4512.

[48] M. H. Stenzel, T. P. Davis, A. G. Fane. *J Mater Chem* **2003**, *13*, 2090-2097.

[49] N. Salem, D. A. Shipp. *Polymer* **2005**, *46*, 8573-8581.

[50] T. Nagamura, T. Kurlhara, T. Matsuo. *J Phys Chem* **1982**, *86*, 1886-1890.

[51] J. J. Galan, A. Gonzalez-Perez, J. R. Rodriguez. *J Therm Anal Calorim* **2003**, *72*, 465-470.

[52] Y. R. Fan, Y. J. Li, G. C. Yuan, Y. L. Wang, J. B. Wang, C. C. Han, H. K. Yan, Z. X. Li, R. K. Thomas. *Langmuir* **2005**, *21*, 3814-3820.

[53] L. D. Song, M. J. Rosen. *Langmuir* **1996**, *12*, 1149-1153.

[54] H. C. Evans. *J Chem Soc* **1956**, 579-586.

[55] G. Sugihara, A. A. Nakamura, T. H. Nakashima, Y. I. Araki, T. Okano, M. Fujiwara. *Colloid and Polym Sci* **1997**, *275*, 790-796.

[56] R. Zana. *J Colloid Interface Sci* **2002**, *246*, 182-190.

[57] R. Zana. *J Colloid Interface Sci* **2002**, *248*, 203-220.

[58] S. Shimizu, P. A. R. Pires, O. A. El Seoud. *Langmuir* **2004**, *20*, 9551-9559.

[59] G. Y. Bai, J. B. Wang, H. K. Yan, Z. X. Li, R. K. Thomas. *J Phys Chem B* **2001**, *105*, 3105-3108.

[60] L. Grosmaire, M. Chorro, C. Chorro, S. Partyka, R. Zana. *J Colloid Interface Sci* **2002**, *246*, 175-181.

[61] Y. J. Li, J. Reeve, Y. L. Wang, R. K. Thomas, J. B. Wang, H. K. Yan. *J Phys Chem B* **2005**, *109*, 16070-16074.

Chapter 5: RAFT-mediated polystyrene–clay nanocomposites prepared by making use of initiator-bound montmorillonite clay

The work described in this chapter has been published in the following paper:

RAFT-mediated polystyrene–clay nanocomposites prepared by making use of initiator-bound montmorillonite clay.

Samakande, Ronald D. Sanderson and Patrice C. Hartmann

European Polymer Journal (DOI: 10.1016/j.eurpolymj.2008.11.014)

Abstract

The initiator, 2,2'-azo*bis*(2-(1-(2-hydroxyethyl)-2-imidazolin-2-yl)propane)dihydrochloride monohydrate (VA060) was used to surface-modify sodium montmorillonite clay (Na-MMT). The obtained organically-modified-clay was then used as a macro-initiator in the preparation of PCNs by *in situ* free-radical polymerization of styrene in bulk. The polymerization was carried out in the presence of three different RAFT agents: 1,4-phenylenebis(methylene)dibenzenecarbodithioate (PCDBDCP), didodecyl-1,4-phenylenebis(methylene)bistrithiocarbonate (DCTBTCD) and 11-(((benzylthio)-carbonothioyl)thio)undecanoic acid (BCTUA). All of the nanocomposites prepared were found to have intercalated morphologies as determined by SAXS and TEM. In the absence of RAFT agents, typical uncontrolled free-radical polymerization occurred, yielding polystyrenes with high molar masses and high polydispersity indices. In contrast, when the polymerization was conducted in the presence of A RAFT agent, the polymerization was found to occur in a controlled manner, as the polystyrene–clay nanocomposites obtained contained polymer chains of narrow

polydispersities. The influences of clay loading and molar mass of the polymer chains in the PCN, on thermal stability of the polystyrene–clay nanocomposites (PS–CNs) were investigated. Increases in the clay loading or the molar masses resulted in improvement of the thermal stability of the nanocomposites.

5.1. Introduction

The discovery of living/controlled polymerization techniques that yield polymers with controlled architecture, functionality and composition has resulted in the preparation of specific polymer products that were traditionally considered impossible to make.[1-5] Moreover, the inclusion of species such as metals and inorganic particles into the polymers can be now achieved by making use of any one of the following available techniques:[6] ionic polymerization, stable free-radical polymerization (SFRP), atom transfer radical polymerization (ATRP), and reversible addition–fragmentation chain transfer (RAFT).[1-5,7,8] The RAFT-mediated controlled radical polymerization technique is one of the fastest growing, most versatile and robust, due to its tolerance of impurities,[2-5] and to the broad range of monomers that it can be applied to. However, the thio-carbonyl-thio group of the RAFT agent can be easily hydrolyzed by basic species such as hydroxide ions, and primary and secondary amines.[9-12] This is one of the few limitations of the RAFT technique.

Regardless of all its advantages over other techniques used to date, the RAFT technique has not been extensively utilized for the synthesis of polymer–clay nanocomposites(PCNs), probably due to the complexity of the resulting heterogeneous system. Notwithstanding this, Moad *et al*. used the RAFT technique indirectly to prepare PCNs.[13-15] In their work they blended polypropylene (PP) with a compatibilizer polymer prepared by RAFT-mediated free-radical polymerization to prepare PCNs by blending. Salem and Shipp reported that RAFT agents can be successfully used to synthesize polystyrene, poly(methyl methacrylate) (PMMA) and poly(butyl acrylate) (PBA) nanocomposites with controlled molar masses. [16] They used clay modified by polymerizable surfactants and performed copolymerization with common monomers (e.g. styrene, butyl acrylate or methyl methacrylate) in a controlled manner. The various monomer-clay systems they investigated had previously been studied by Zeng and Lee,[17] emerging from which Salem and Shipp found that the nanocomposites structure obtained was not changed by the presence of the RAFT agent. Tethering of a RAFT agent onto a clay surface prior its use in the

preparation of PCNs and the subsequent good control of the polymerization has been reported.[18-20]

In this chapter we report on the use of an initiator-bound clay in the initiation of new RAFT-mediated PS–CNs polymerization reactions. The use of initiator-bound clay in the initiation of polymerization has already been shown to be a very useful method for creating PCNs with polymers bound to the clay surfaces. In the mid-1960s Dekking anchored an azo initiator, azo*bis*isobutyramidine hydrochloride (AIBA), onto clay layers, thus forming an initiator-modified-clay, which he subsequently used in the initiation of polystyrene and PMMA polymerization. PCNs with polymer chains attached to the clay layers resulted.[21,22] He also investigated the kinetics of the decomposition of the bound initiator and of the polymerization process. Fan *et al*. and Meier *et al*. also reported a similar approach to the synthesis of PCNs initiated by a clay-bound initiator.[23-25]

The thermal stability of PCNs has been widely studied. The first article on this was published as early as 1965, by Bluimstein.[26] The general notion on the issue of thermal stability of PCNs is that an increase in clay loading results in an increase in thermal stability because of an increase in the number of clay tactoids hindering diffusion of gasified polymer degradation products.[27-29] Since most of the available literature is based on uncontrolled free-radical polymerization studies, many researchers attribute the net increase in thermal stability only to clay loading. In some cases researchers did try to relate the morphology of clay in the nanocomposites to the thermal stability. Here a general agreement is that an exfoliated clay structure results in better thermal stability.[30] However, several groups have questioned this general finding and proved that, in certain cases, the intercalated clay structure results in better thermal stability.[31-33]

Clearly, studies of the impact of the amount of clay and the morphology of PCNs on the thermal stability and molar masses have yielded conflicting results. Surprisingly, the molar mass generally also fluctuates as the amount and degree of intercalation/exfoliation of clay changes.[18] Since molar mass also contributes to changing thermal stability,[34,35] direct correlations between PCN morphology and thermal stability are sometimes difficult to establish.

This chapter reports on an investigation of the effect of clay loading on the thermal stability of the nanocomposites prepared in a controlled manner, i.e. by RAFT-

mediated *in situ* bulk polymerization. The influence of the clay content, whilst keeping the clay morphology and the molar mass relatively constant, is considered. Such a study has not been reported before and hence the work described here contributes to a better general understanding of the important correlation between the structure and properties of PCNs, i.e. structure/property relationships.

5.2 Experimental

5.2.1 Materials

Styrene (99%, Aldrich) was purified by washing with 0.3 M KOH, followed by distillation at 40 ºC under reduced pressure. 2,2'-azo*bis*(2-(1-(2-hydroxyethyl)-2-imidazolin-2-yl)propane)dihydrochloride monohydrate (VA060, 95%, Wako) and sodium montmorillonite (Na-MMT, Southern Clay Products, USA) were used as received. Deionized water was obtained from a Millipore Milli-Q-purification system. 1,4-phenylenebis(methylene)dibenzenecarbodithioate (PCDBDCP) didodecyl-1,4-phenylenebis(methylene)bistrithiocarbonate (DCTBTCD) and 11-(((benzylthio)carbonothioyl)thio)undecanoic acid (BCTUA) were synthesized as described in Chapter 4, Section 4.3.[12]

5.2.2 Modification of clay

A typical modification of Na-MMT clay (by an ion-exchange reaction) is described as follows. Na-MMT (5.021 g) was dispersed in deionized water (500 ml) and stirred for 1 h. A solution of VA060 (2.592 g; 6.035 10^{-3} mol) in deionized water (200 ml) was slowly added to the suspension of clay over 30 min. The mixture was further stirred for 3 h at room temperature. The suspended solids were then collected by filtration. The resulting cake was washed several times until a negative test to silver nitrate was obtained.[33] The filtrate was analyzed using high performance liquid chromatography (HPLC). The washed solids were then freeze dried for 4 days to yield a very finely dispersed powder of VA060-modified-clay (VA060-MC).

5.2.3 RAFT-mediated polymerization of styrene

In a typical procedure, predetermined quantities of RAFT agent and styrene were placed in a Schlenk tube. The contents were then freeze-vacuum-thawed three times before being placed in an oil bath at 90 ºC. The polymerization was carried out for 72 h. The solid polymer obtained was dissolved in chloroform and then precipitated in a

10-fold excess volume of methanol. The obtained monomer-free polymer was dried overnight in a vacuum oven at 55 ºC to yield a powdered polymer.

A similar procedure was followed for the synthesis of the nanocomposites, the only difference being that the VA060-MC initiator/clay was added, and that the monomer clay suspension was stirred overnight prior to polymerization so as to allow time for the monomer to swell the clay. Polymerization was carried out at 60 ºC in order to minimize self initiation.

5.2.4 Characterization of the polymer chains using high performance liquid chromatography (HPLC)

HPLC analyses were carried out on a C12 (250 x 460 mm, 4 µm) column in reverse phase mode, using a Kontron instruments HPLC system, which was automatically controlled by Geminyx software. Detection of analytes was done using a quasi online evaporative light scattering (ELS) detector system, model PL-ELS 2100, obtained from Polymer Laboratories. The detector parameters were set at: evaporator 50 ºC, nebuliser 30 ºC, and N_2 gas flow rate 1.60 ml/min. A mixture of two solvents was used as the mobile phase: 94.53/4.97/0.5 v/v/v HPLC grade acetonitrile/water/trifluoroacetic acid (B solvent) and 94.53/4.97/0.5 v/v/v water/acetonitrile/trifluoroacetic acid (A solvent), at a flow rate of 1 ml/min. The analyte injection volume was set at 20 µl. The filtrate from the ion-exchange reaction of clay was analyzed by HPLC with the solvent composition (B:A) optimized as follows: the initial ratio of B:A was 70:30, which was then linearly ramped to 100:0 over 25 min, kept constant at 100:0 for 5 min, then linearly ramped back to 70:30 over 5 min. As ELS detectors do not give a linear response to concentration,[36] an exponential calibration curve was created for a range of initiator standards of varying concentrations in water. Experimental concentrations were determined by extrapolation from the calibration curve.

5.2.5 Size-exclusion chromatography (SEC)

SEC was carried out using a Waters 600E system controller equipped with a Waters 610 Fluid Unit pump and a Waters 410 differential refractometer as detector. Prior to analysis, samples were vigorously stirred in tetrahydrofuran (THF) for a week. The samples were then filtered through a 0.20-µm filter membrane. However, it was soon discovered that even after filtering the polymer-clay suspension through Celite particles and the 0.20-µm filter membrane some polymer-grafted clay particles still

passed through and were detected in the RI signal. In order to overcome this, all of the samples were reverse ion-exchanged prior to the SEC analysis of the samples. The reverse ion-exchange method was carried out as follows. Polymer–clay nanocomposite (0.2 g) and LiCl (0.06 g) were dissolved in THF (10 ml) and refluxed at 70 ºC for 3 h. The solution was filtered through Celite. The polymer was then precipitated in methanol and dried. The absence of clay was determined by dynamic light scattering (DLS), which showed no peak that is characteristic of clay particles. SEC analysis was performed on samples of solutions of 5 mg/ml polymer in THF.

5.2.6 Small angle X-ray scattering (SAXS)

SAXS scattering measurements were carried out in transmission configuration, at 298 K. A copper rotating anode X-ray source (functioning at 4 kW) with a multilayer focusing "Osmic" monochromator giving high flux (10^8 photons/sec) and punctual collimation was used. An "image plate" 2D detector was used. Scattering curves were obtained, giving diffracted intensity as a function of the wave vector q. The calculation of q values is described elsewhere.[37]

5.2.7 Transmission electron microscopy (TEM)

TEM was used to directly visualize the morphology of the clay particles in PCNs at the nanometer level. Bright field TEM images were recorded on a LEO 912 transmission electron microscope at an accelerating voltage of 120 kV. Prior to analysis, samples of PCNs were embedded in epoxy resin and cured at 60 ºC for 24 h. The embedded samples were then ultra-microtomed with a diamond knife using a Reichert Ultracut S ultra microtome, at room temperature. This resulted in sections with a nominal thickness of about 100 nm. The sections were transferred from water at room temperature onto 300-mesh copper grids, which were then transferred into the TEM apparatus.

5.2.8 Thermogravimetric analysis (TGA)

TGA measurements were carried out using a Perkin Elmer TGA 7 instrument. Samples of less than 20 mg were used for all analyses. Analyses were carried out using a temperature sweep of 20 to 600 ºC, at a heating rate of 20 ºC/min. All TGA analyses were carried out in an air atmosphere.

5.3 Results and discussion

5.3.1 Modification of clay by VA060 initiator

The clay modification was carried out using a 1:1.3 ratio of the modifier to cation-exchange capacity cec. The cec value of the Na-MMT used was 92.6 meq/100g clay. HPLC and TGA results, which were further supported by the change (i.e. increase) in *d* spacing of the modified-clay relative to that of unmodified-clay, indicated that the ion-exchange reaction was a success.

From the HPLC measurements and extrapolation from the calibration curve it was determined that only 45.4% (relative to cec) of clay sites was ion-exchanged by the VA060 initiator. This is in close agreement with the value of 44.4%, as calculated from the weight loss determined on the TGA thermogram of the modified-clay VA060-MMT (see Fig. 5.1). The calculation was based on the difference in weight loss between pristine clay and the modified-clay at 800 ºC.[33,38-42]

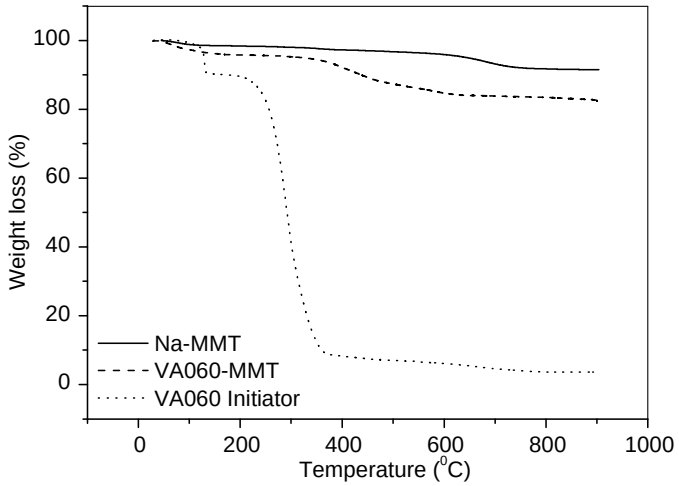

Fig. 5.1 TGA thermograms of Na-MMT and initiator-modified-clay (VA060-MMT).

The structure of VA060 has two positive charges per molecule (difunctional), which implies that each VA060 initiator molecule can theoretically bind to two sites, i.e. as a di-cation rather than as a mono-cation. This implies that only 50% cec of VA060 initiator should participate in the ion-exchange reaction, as is seen in this study. This inference agrees well with the findings of Dekking (in 1965), who also observed that azo*bis*isobutyramidine hydrochloride (AIBA) was similarly ion-exchanged as a di-cation.[21] Fan *et al*. synthesized a difunctional initiator based on 4,4'-azo*bis*(4-cyanovaleric acid) and observed that it was adsorbed either on two adjacent clay sheets or on the same clay sheet.[23]

The successful ion-exchange reaction was further confirmed by results of XRD analysis (c.f. Fig. 26 in Appendix) that showed a *d* spacing of 1.41 nm for the VA060-modified-clay relative to 1.19 nm for pristine Na-MMT (the *d* spacing of 1.19 nm has been frequently reported by others[30,40,43-45]). Furthermore, the FTIR of the VA060-MMT clay is shown in Fig 27 in Appendix. The appearance of new peaks in the spectra of the modified-clay relative to the virgin clay is a qualitative indication that the ion-exchange process was indeed a success.

5.3.2 Preparation of polystyrene-VA060-MC nanocomposites by free-radical bulk polymerization

An important aspect of this study was to synthesize PS–CNs with control of both the morphology of the PCN and the polymer architecture. In a preliminary study, polymerization of styrene was performed without RAFT agent, using only VA060-MMT, in order to prove that this initiator-modified-clay is able to efficiently initiate polymerization. The results are presented in Table 5.1 below, which shows the attained conversion, Mn, PDI, amount of clay and the initiator bound to it.

Table 5.1. Polysyrene-VA060-MC nanocomposites prepared in this study

Polymer	$\frac{[MC]_0}{[S]_0} x100$ ***(%)***	n_I ***x10^5 (mol)***	***Conv. (%)***	***Calc Mn x10^{-3} (g/mol)***	***Exp Mn x10^{-3} (g/mol)***	***PDI***
PS	-	-*	92.00	-	168.0	2.99
PS-VA060-1	0.500	3.310	21.60	3 386	347.5	3.10
PS-VA060-2	1.010	6.750	29.80	2 303	336.9	3.15
PS-VA060-3	5.000	33.47	23.20	361.0	288.6	2.74

Key: $\frac{[MC]_0}{[S]_0}$ = initial ratio (by mass) of modified-clay to styrene; nI = number of moles of initiator; Calc Mn = calculated theoretical molar mass, calculated using the Equation $M_n = \left[\frac{[S]_0 - [S]_t}{[I]_0}\right] M_S$,[3] where [S] and [I] = styrene and initiator concentrations respectively; MS = molar mass of styrene; Exp Mn = experimental molar mass; and PDI = polydispersity index. *Thermal self-initiation of styrene at 90 ºC (no initiator used).

As shown in Table 5.1, PCNs prepared using initiator-bound clay were found to have higher molar masses relative to polystyrene prepared according to the same procedure but without clay and without VA060 (thermal self initiation at 90 ºC). As VA060 is not soluble in styrene monomer it could not be used to initiate the polymerization of styrene to prepare clay-free polystyrene. However, styrene swells VA060-modified-clay well (as seen by the viscosity increase during the mixing of the modified-clay and the styrene monomer prior to polymerization process). This is understandable, since once ion-exchanged on the clay surface the charge of VA060

becomes shielded, whereas its non-polar organic part radiates away from the surface, hence increasing its affinity for organic molecules such as styrene. Polystyrene-VA060-MC-nanocomposites showed the typical free-radical polymerization features, i.e. high molar masses and high polydispersity indices (PDIs). As the clay level increased so did the initiator (bound to the clay layers), which resulted in the molar mass decreasing. The low conversions obtained are ascribed to both the low efficiency of VA060 when bound onto the clay surface, and to the glassy nature of polystyrene. The viscosity of the bulk polymerization system is further increased by the presence of clay, hence limiting the diffusion of monomers taking part in the polymerization.[33,46]

5.3.3 Preparation of polystyrene prepared by RAFT-mediated free-radical bulk polymerization

The choice of (R) and (Z) groups of any RAFT agent is crucial to the successful control of the free-radical polymerization of a given monomer within an acceptable reaction time.[2,4] The widely accepted RAFT mechanism is outlined in Scheme 5.1 below.

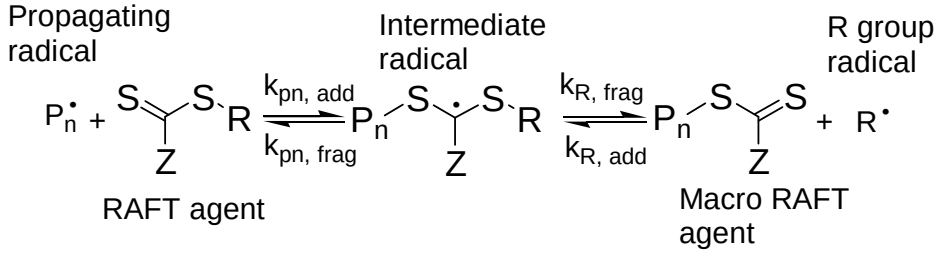

Scheme 5.1. Addition-fragmentation equilibrium between propagating radicals and dormant chains.

Accordingly, the three RAFT agents that were designed for the use in this study (see Scheme 5.2) bear derivatives of a benzyl (R) group, which has also been shown to be able to effectively reinitiate styrene polymerization.

The (Z) group was varied from a phenyl to a thio-alkyl chain, both of which have been reported to be effective for RAFT-mediated styrene polymerization.[2,3,5,47] The influence of the type, dithio- or trithio-, of RAFT agent on the control of the system was studied: PCDBDCP has a dithio- group whereas DCTBTCD and BCTUA have a trithio- group.

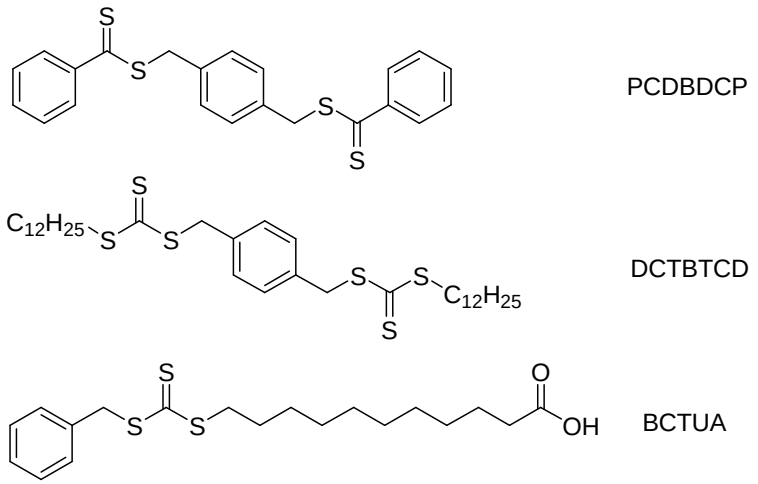

Scheme 5.2. RAFT agents: PCDBDCP, DCTBTCD and BCTUA.

Table 5.2 shows SEC data of the polymers mediated by the three RAFT agents in the absence of clay. All the SEC traces were unimodal. The PDI values of the final polymers were below 1.5 and the predicted M_n values were close to the expected calculated ones, showing that the polymerization occurred in a controlled manner.[16] Two major differences were noticed when the dithio and trithio RAFT agents were used. Firstly, after the same polymerization times, the conversion was found to be lower when the dithio compound (PCDBDCP) was used, i.e. 58%, relative to the trithio compounds (DCTBTCD and BCTUA), i.e. 80% and 82%, respectively. Zhao and Perrier have also reported that the polymerization of dithiobenzoates is slower than that of trithiocarbonates.[48]

Table 5.2. RAFT-mediated polymerization of styrene

Polymer	$\frac{[S]_0}{[R]_0}$	***Conv. (%)***	***Calc Mn (g/mol)***	***Exp Mn (g/mol)***	***PDI***
PS		92.0	-	168,000	2.99
PS-P0	284.0	57.9	17,480	20,340	1.30
PS-D0	275.0	79.2	23,320	20,800	1.31
PS-B0	260.0	82.2	22,930	19,950	1.17

Key: PS = uncontrolled polystyrene standard; PS-P0, PS-D0 and PS-B0 = polystyrene prepared by PCDBDCP, DCTBTCD, and BCTUA RAFT-mediated polymerization, respectively; $\frac{[S]_0}{[R]_0}$ = initial ratio of number of moles of styrene to RAFT; Calc Mn = calculated theoretical molar mass using the Equation $M_n = \frac{[S]}{[RAFT]_0}.M_S.conversion + M_{RAFT}$,[50] where [S] = initial concentration of styrene, Ms = molar mass of styrene used, MRAFT = molar mass of RAFT agent, [RAFT]0 = initial concentration of RAFT agent and Exp Mn = experimental mass; and PDI = polydispersity index.

This was attributed to the fact that dithio RAFT agents suffer from significant initialization, inhibition and retardation[49] and undergo a range of undesired reactions, which leads to a partial loss of control of polymerization, i.e. addition of more than

one monomer unit before deactivation. It has been suggested that these disadvantages do not occur when trithiocarbonates RAFT agents are used. Secondly, the experimental molar masses obtained with the trithio RAFT agents were found to be lower than the predicted ones.

5.3.4 Preparation of polystyrene-VA060-MC nanocomposites by RAFT-mediated free-radical bulk polymerization

All the RAFT-mediated nanocomposites were synthesized with control of the molar masses of the polystyrene matrix (see Tables 5.3–5.5), while the SEC traces for the nanocomposites were unimodal.

Table 5.3. PS-VA060-MC nanocomposites mediated by PCDBDCP

Polymer	$\frac{[MC]_0}{[S]_0} x100$ *(%)*	$\frac{[R]_0}{[I]_0}$	$\frac{[S]_0}{[R]_0}$	*Conv. (%)*	*Calc Mn (g/mol)*	*Exp Mn (g/mol)*	*PDI*
PS-P0	-	-	284.0	57.9	17,480	20,340	1.30
PS-VA060-P1	0.500	5.070	283.7	25.7	7,981	10,370	1.30
PS-VA060-P2	1.010	2.510	288.4	24.1	7,544	9,128	1.49
PS-VA060-P3	2.500	1.020	281.8	14.2	4,565	6,672	1.44

Key: $\frac{[MC]_0}{[S]_0}$ = initial ratio by mass of modified-clay to styrene; $\frac{[S]_0}{[R]_0}$ = initial ratio of number of moles of styrene to RAFT; $\frac{[R]_0}{[I]_0}$ = initial ratio of number of moles of RAFT to initiator; Calc Mn = predicted number average molar mass, calculated using the Equation $M_n = \frac{[S]}{[R]_0} .M_s .conversion + M_{RAFT}$,[50] where [S] = concentration of styrene, [S]MW = molar mass of styrene used, M_{RAFT} = molar mass of RAFT agent, $[R]_0$ = initial concentration of RAFT and Exp Mn = experimental number molar mass and the polydispersity indices (PDI) were obtained from SEC.

Table 5.4. Polystyrene-VA060-MC nanocomposites mediated by DCTBTCD

Polymer	$\frac{[MC]_0}{[S]_0} x100$ *(%)*	$\frac{[R]_0}{[I]_0}$	$\frac{[S]_0}{[R]_0}$	*Conv. (%)*	*Calc Mn (g/mol)*	*Exp Mn (g/mol)*	*PDI*
PS-D0	-	-	275.0	79.2	23,320	20,800	1.31
PS-VA060-D1	0.500	5.300	270.2	28.9	8,785	8,021	1.42
PS-VA060-D2	1.010	2.610	272.6	26.9	8,284	7,317	1.52
PS-VA060-D3	4.990	0.540	268.0	23.2	7,241	6,878	1.50

Key: same as for **Table 5.3**.

Relative to that of the non-clay-containing RAFT-mediated polystyrene, the PDI was found to increase slightly as the clay loading increased. As previously observed for the non-clay-containing system, the experimental molar masses of the products of PCDBDCP-mediated polymerization were always found to be slightly higher than the predicted ones, unlike in the cases of DCTBTCD- and

BCTUA-mediated polymerization systems, where the predicted and experimental molar masses were similar.

Table 5.5. PS-VA060-MC nanocomposites mediated by BCTUA

Polymer	$\frac{[MC]_0}{[S]_0} x100$ *(%)*	$\frac{[R]_0}{[I]_0}$	$\frac{[S]_0}{[R]_0}$	*Conv. (%)*	*Calc Mn (g/mol)*	*Exp Mn (g/mol)*	*PDI*
PS-B0	-	-	260.0	82.2	22,930	19,950	1.17
PS-VA060-B1	0.510	5.460	260.5	48.5	13,620	13,720	1.25
PS-VA060-B2	1.010	2.740	260.4	31.3	8,962	9,371	1.45
PS-VA060-B3	5.010	0.560	258.5	38.0	10,680	9,703	1.44

Key: as for **Table 5.3**.

Conversion was seen to decrease with an increase in clay loading, implying that the presence of clay layers has an effect on the polymerization kinetics. The decrease in conversion could also be due to the glassy nature of the polystyrene that is being exacerbated by the presence of clay, hindering diffusion of the monomer.[33,40] Another interesting aspect is that as the clay loading increased the initiator level increased. A loss of control of the polymerization could have been expected as the clay loading increased but this was not observed experimentally: fairly low PDI values (1.50 and less) were recorded for molar ratios of RAFT to initiator as low as 0.54. A possible cause of this could be the very low initiator efficiency due to substantial initiator-to-initiator recombination,[23] commonly referred as the "cage effect".

5.3.5 Morphology of polystyrene–clay nanocomposites

SAXS analysis of the PCNs showed that all had an intercalated morphology with a *d* spacing in the range 1.39–1.48 nm (see Fig. 5.2).

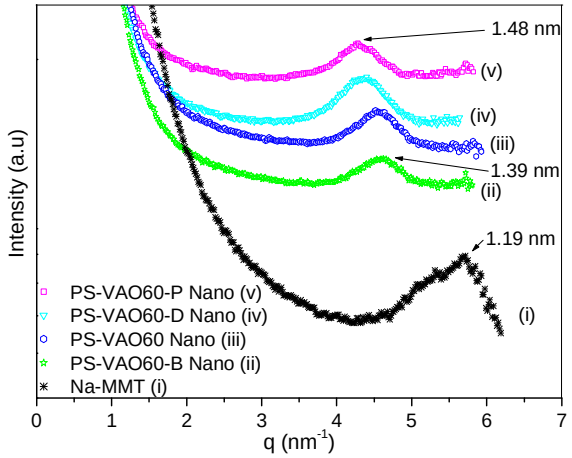

Fig. 5.2 SAXS patterns for polystyrene-VA060-clay based nanocomposites.

These intergallery spacing values are in line with our expectations, as free-radical initiation from clay grafted with a difunctional initiator has been reported to yield intercalated structures due to termination by recombination of growing radicals attached on facing clay layers, thus preventing further increase of the interlayer spacing.[22,23] TEM analysis, a technique commonly used to support SAXS results,[33,51] confirmed that intercalated morphologies were obtained (see Fig. 5.3).

Fig. 5.3 TEM images of PS-VA060-1, scale bar = 200nm.

5.3.6 Thermal stability of polystyrene–clay nanocomposites

The influence of clay loading and clay morphology (i.e. degree of exfoliation/intercalation) on thermal stability has been extensively studied for various PCN materials.[28,29,33,52] However, since in the studied systems the polymer architecture was not controlled, the impact that the polymer molar mass has on the thermal stability has always been assumed to be negligible. Nevertheless, the longer the polymer chains the greater are the intra- and inter-molecular forces. This manifests itself in the properties of a polymer, up to a certain molar mass limit where chains start to form entanglements at a critical molar mass equal to M_c, after which there is no further variation in the thermo-mechanical properties. In the present work, a series of PCNs were prepared by *in situ* polymerization with increasing amounts of clay whilst keeping the molar mass of the polymer relatively low and constant so as to eliminate the very significant contribution of varying molar masses to thermal stability.

5.3.6.1 PS-VA060-MC nanocomposites

One of the most studied thermo-mechanical properties of nanocomposites is their thermal stability. It is believed that during decomposition the clay platelets hinder diffusion of the gasified polymer's decomposition byproducts,[30,33,53] by forming a

char at the air–sample interface and thus preventing further decomposition. Thermal stability of PCNs has also been reported to be enhanced by the restricted thermal motion of the polymer chains within the clay galleries.[26] In general, PCNs have exceptional thermal stabilities relative to the virgin polymer. Bluimstein has reported a 40 to 50 ºC increase in the temperature of thermal decomposition of nanocomposites relative to virgin polymer.[26]

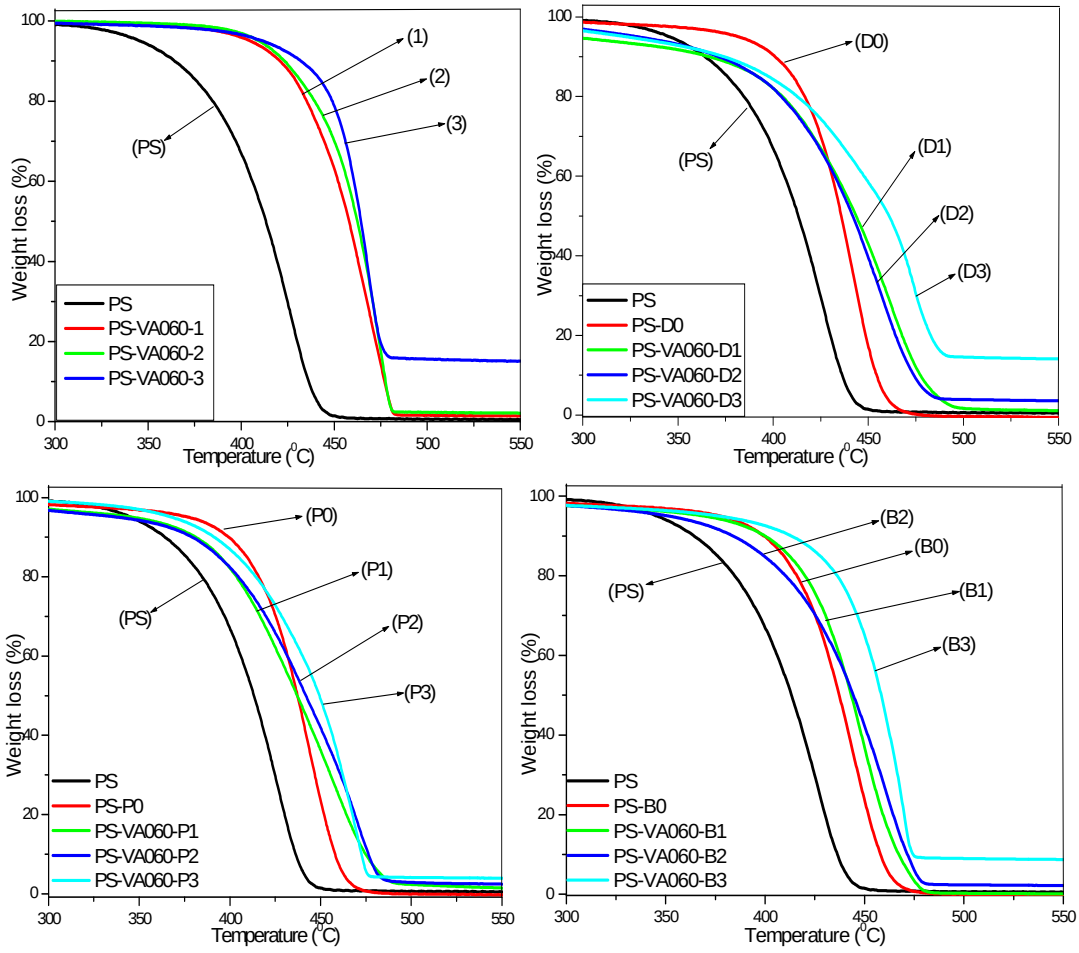

Fig. 5.4 TGA thermograms of PCNs and standards.

Table 5.6. Thermal decomposition rates of uncontrolled PS-VA060-MC nanocomposites

Polymer	*Exp. clay load (%)*	*Exp Mn (g/mol)*	*10% decomp*	*50% decomp*	*90% decomp*
PS	-	168,000	362.0	412.0	436.0
PS-VA060-1	1.300	347,500	420.0	458.0	477.0
PS-VA060-2	2.300	336,900	423.0	462.0	477.0
PS-VA060-3	14.60	288,600	428.0	462.0	473.0

In this study the focus was on the impact of the clay loading on the thermal stability. The thermal stabilities of the PS-VA060 nanocomposites (molar masses were not controlled in this series) were first evaluated as a function of the clay content. With an

experimental clay loading of only 1.3% the temperature of decomposition of the nanocomposite PS-VA060-1 was found to increase by 41 to 58 ºC, when compared to virgin PS, at equivalent percentages of decomposition (see Table 5.6 and Fig. 5.4). A further increase in clay loading resulted in only a slight improvement of the thermal stability, relative to the case of the lowest clay loading of 1.3%. It should nevertheless be remarked here that the molar masses of the nanocomposites decreased slightly as the clay loading increased, such that the molar mass of the polymer might also counteract the effect of the increase of clay loading on thermal stability. Doh and Cho report however that the enhancement in thermal stability does not increase linearly as a function of clay loading; they found that as little as 0.3% clay is sufficient to achieve optimum thermal stability in PCNs.[54] This behaviour has also been reported by Zhong *et al*.[55]

5.3.6.2 RAFT-mediated PS-VA060-MC nanocomposites

Although all RAFT-mediated polystyrenes PS-P0, PS-D0 and PS-B0 (no clay) have lower molar masses relative to virgin uncontrolled PS they displayed better thermal stability (see Table 5.7). This was attributed to the presence of very low molar mass PS chains generated by uncontrolled polymerization,[56-58] which degrade at lower temperature relative to high molar mass chains. Such an early generation of radicals, generated by the degradation of short chains, promotes the degradation of longer chains by initiating the mechanism of thermal decomposition. The effect of low molar mass species has been reported by Ding *et al*.,[59] who found a decrease in thermal stability with an increase in the amount of layered double hydroxide in the nanocomposites, due to the presence of the low molar mass sodium dodecyl sulfate (SDS) surfactant used as the clay modifier. This is not the case in the controlled systems where all the chains are (theoretically) of similar size. The slight differences in the thermal degradation of the RAFT-mediated polymers could be due to the end group effect, whereby the stability of the RAFT moiety becomes important.

The temperatures at which 10% weight loss occurred by decomposition were compared between controlled PS prepared in the presence as well as in the absence of clay, using three different RAFT agents. In all cases the temperatures of 10% decomposition were found to be higher for RAFT-mediated PS without clay relative to the equivalent RAFT-mediated PS clay nanocomposites. This was however not observed for the temperatures determined for the 50% and 90% decompositions, where the presence of clay clearly improved the thermal stability of controlled PS.

There are two possible explanations for this. First, the molar mass of PS-P0 is higher than that of the nanocomposite PS-VA060-P1-3, hence decomposition of the PS–CNs could commence at a lower temperature. Second, at 10% decomposition the clay platelets have not yet formed a char at the surface of the decomposing sample to effectively hinder diffusion of gasified material emerging from the decomposing polymer.

Although the molar mass is known to be critical to thermal stability,[34] here nanocomposites were seen to have better thermal stability relative to virgin polystyrene (c.f. uncontrolled PS-VA060-MC nanocomposite series), which is in agreement with what is reported in literature.[16,30,33,40,44,60-62] Furthermore, an increase in clay loading resulted in only a slight improvement in the thermal stability relative to the PCN containing the smaller clay loading. This shows that there is a minimum amount of clay that brings about the biggest increase in thermal stability; this lower clay loading is probably less than 1.0%. In a comparison of non-controlled nanocomposites relative to the RAFT-mediated nanocomposites it was seen that at 10% decomposition the uncontrolled system presents greater thermal stability than the controlled ones. However, thermal stabilities at 90% decomposition are roughly the same for both the controlled and uncontrolled systems. These results can be explained by either the molar mass differences or by the fact that in non-RAFT systems the amount of chains attached to the clay surfaces is far greater than the amount in the RAFT systems. Dekking showed that 83% of the polymer chains were bound to the clay surfaces when using initiator-grafted modified-clays.[22] This makes the entire polymer system therefore a near interface. In this study, polymerizations were performed in a system where the initiator is anchored to clay whereas the RAFT transfer agent is free in the continuous monomer phase. As a consequence, according to the well established mechanism of the RAFT-mediated free-radical polymerization, and assuming transfer of radicals occurred throughout polymerization, the theoretical molar ratio of bound to unbound polystyrene $[PS]$ chains can be calculated as shown in Equation 5.1.

$$\frac{[PS]_{BOUND}}{[PS]_{UNBOUND}} = \frac{2f[I]_0(1-e^{-k_d t})}{[R]_0}. \qquad \textbf{Equation 5.2}$$

Where f = initiator efficiency, k_d = initiator dissociation constant, $[\mathrm{I}]_0$ = Initial initiator concentration, $[R]_0$ = Initial RAFT agent concentration and t = time.

The efficiency of the clay-bound initiator is likely to be low and the initial ratio of RAFT agent to initiator is always greater than 0.5. Consequently, most of the polymer chains are unbound after the initialization time of the polymerization.

Among the different RAFT-mediated nanocomposites the thermal stabilities at similar clay loadings at 50% and 90% decompositions were found to be comparable. At 10% clay loading, however, differences are clearly visible, depending on the molar mass of the polymer, e.g. at 2.4% and 2.6% clay loading for PCDBDCP and BACTUA, where the molar masses are the same at 9,000 g/mol, the stabilities are the same. At 1% loading for PCDBDCP and DCTBTCD, where the molar masses are 10,370 and 8,020 g/mol respectively, their thermal stabilities differ by 16 ºC. This clearly shows that the onset of decomposition is very much dependent on the molar mass.[34]

Table 5.7. Thermal decomposition rates of controlled PS-VA060-MC nanocomposites mediated by PCDBDCP, DCTBTCD and BCTUA.

Polymer	$\frac{[R]_0}{[I]_0}$	*Exp. clay load (%)*	*Exp. Mn (g/mol)*	*Tº at 10% decomp. (ºC)*	*Tº at 50% decomp. (ºC)*	*Tº at 90% decomp. (ºC)*
PS	-	-	168,000	362.0	412.0	436.0
PS-P0	-	-	20,340	410.0	441.0	456.0
PS-VA060-P1	5.07	1.00	10,370	382.0	437.0	475.0
PS-VA060-P2	2.51	2.60	9,128	378.0	441.0	475.0
PS-VA060-P3	1.02	4.50	6,672	390.0	447.0	470.0
PS-D0	-	-	20,800	401.0	435.0	454.0
PS-VA060-D1	5.30	1.00	8,021	366.0	442.0	476.0
PS-VA060-D2	2.61	3.30	7,317	370.0	441.0	471.0
PS-VA060-D3	0.54	14.20	6,878	364.0	452.0	480.0
PS-B0	-	-	19,950	399.0	437.0	458.0
PS-VA060-B1	5.46	0.50	13,720	399.0	443.0	466.0
PS-VA060-B2	2.74	2.40	9,371	383.0	443.0	470.0
PS-VA060-B3	0.56	8.80	9,703	409.0	456.0	471.0

5.4. Conclusions

Difunctional initiator (VA060) bound onto clay platelets was successfully used to initiate the polymerization of styrene to yield PS–CNs. The initiator-modified-clay was used to initiate the polymerization of styrene, yielding PS–CNs with low conversions and intercalated morphology, as also obtained when RAFT transfer agents were used. The conversions observed were found to be a function of the clay content: an increase in clay content resulted in a lower conversion. This was attributed to the glassy effect of polystyrene coupled to the clay layers, which resulted in restriction of diffusion of monomer and thus a slow polymerization. The VA060 initiator-modified-clay was found to be less effective in initiating the polymerization inside clay galleries

because of radical–radical coupling (the cage effect). On the other hand, the low initiator efficiency was found to allow the preparation of nanocomposites with controlled molar masses even at high initiator concentration. Use of the RAFT technique was indeed successfully used to control the molar mass of polystyrene by *in situ* free-radical polymerization of styrene in the presence of clay. Polystyrene clay nanocomposites displayed enhanced thermal stability relative to virgin polystyrene. The thermal stability of polymers was found to be a function of the molar mass distribution, molar mass and clay loading. However, a limiting amount of clay was found to be sufficient to attain an optimum thermal stability. The molar masses were found to be critical in determining the onset of degradation taken at 10% decomposition, and broad molar masses (PDI values) resulted in less stable polymers due to early decomposition of short chains initiating the earlier than usual decomposition of longer chains. In addition the lower viscosity of the small chains can release gas easier.

5.6. References

[1] W. A. Braunecker, K. Matyjaszewski. *Prog Polym Sci* **2007**, *32*, 93-146.

[2] A. Favier, M. T. Charreyre. *Macromol Rapid Commun* **2006**, *27*, 653-692.

[3] G. Moad, E. Rizzardo, S. H. Thang. *Aus J Chem* **2005**, *58*, 379-410.

[4] S. Perrier, P. Takolpuckdee. *J Polym Sci Part A: Polym Chem* **2005**, *43*, 5347-5393.

[5] G. Moad, K. Dean, L. Edmond, N. Kukaleva, G. X. Li, R. T. A. Mayadunne, R. Pfaendner, A. Schneider, G. P. Simon, H. Wermter. *Macromol Mater Eng* **2006**, *291*, 37-52.

[6] J. Pyun, K. Matyjaszewski. *Chem Mater* **2001**, *13*, 3436-3448.

[7] M. W. Weimer, H. Chen, E. P. Giannelis, D. Y. Sogah. *J Am Chem Soc* **1999**, *121*, 1615-1616.

[8] P. A. Wheeler, J. Z. Wang, L. J. Mathias. *Chem Mater* **2006**, *18*, 3937-3945.

[9] J. Baussard, J. Habib-Jiwan, A. Laschewsky, M. Mertoglu, J. Storsberg. *Polymer* **2004**, *45*, 3615-3626.

[10] G. Levesque, P. Arsene, V. Fanneau-Bellenger, T. Pham. *Biomacromolecules* **2000**, *1*, 400-406.

[11] G. Levesque, P. Arsene, V. Fanneau-Bellenger, T. Pham. *Biomacromolecules* **2000**, *1*, 387-399.

[12] A. Samakande, R. D. Sanderson, P. C. Hartmann. *Synthetic Commun* **2007**, *37*, 3861-3872.

[13] G. Moad, G. Li, E. Rizzardo, S. H. Thang, R. Pfaendner, H. Wermter. *Polym Prepr* **2005**, *46*, 376.

[14] G. Moad, K. Dean, L. Edmond, N. Kukaleva, G. X. Li, R. T. A. Mayadunne, R. Pfaendner, A. Schneider, G. Simon, H. Wermter. *Macromol Symp* **2006**, *233*, 170-179.

[15] G. Moad, G. Li, R. Pfaendner, A. Postma, E. Rizzardo, San.Thang, H. Wermter. *ACS Symp Ser* **2006**, *944*, 514-532.

[16] N. Salem, D. A. Shipp. *Polymer* **2005**, *46*, 8573-8581.

[17] C. Zeng, L. J. Lee. *Macromolecules* **2001**, *34*, 4098-4103.

[18] J. B. Di, D. Y. Sogah. *Macromolecules* **2006**, *39*, 1020-1028.

[19] A. Samakande, J. J. Juodaityte, R. D. Sanderson, P. C. Hartmann. *Macromol Mater Eng* **2008**, 293, 428-437.

[20] B. Q. Zhang, C. Y. Pan, C. Y. Hong, B. Luan, P. J. Shi. *Macromol Rapid Commun* **2006**, *27*, 97-102.

[21] H. G. G. Dekking. *J Appl Polym Sci* **1965**, *9*, 1641-1651.

[22] H. G. G. Dekking. *J Appl Polym Sci* **1967**, *11*, 23-26.

[23] X. W. Fan, C. J. Xia, R. C. Advincula. *Langmuir* **2003**, *19*, 4381-4389.

[24] X. W. Fan, C. J. Xia, T. Fulghum, M. K. Park, J. Locklin, R. C. Advincula. *Langmuir* **2003**, *19*, 916-923.

[25] L. P. Meier, R. A. Shelden, W. R. Caseri, U. W. Suter. *Macromolecules* **1994**, *27*, 1637-1642.

[26] A. Bluimstein. *J Polym Sci A* **1965**, *3*, 2665-2673.

[27] M. Alexandre, P. Dubois. *Mater Sci Eng A* **2000**, *28*, 1-63.

[28] M. Okamoto. *Encyclopedia of Nanoscience and Nanotechnology*; American Scientific Publishers: California, 2004.

[29] S. S. Ray, M. Okamoto. *Prog Polym Sci* **2003**, *28*, 1539-1641.

[30] W. A. Zhang, D. Z. Chen, H. Y. Xu, X. F. Shen, Y. E. Fang. *Eur Polym J* **2003**, *39*, 2323-2328.

[31] E. Giannelis. *Adv Mater* **1996**, *8*, 29-31.

[32] J. W. Gilman, T. Kashiwagi, A. B. Morgan, R. H. Harris, L. D. Brassell, M. R. Vanlandingham, C. L. Jackson. *NISTIR 6531* **2000**, 1-55.

[33] A. Samakande, P. C. Hartmann, V. Cloete, R. D. Sanderson. *Polymer* **2007**, *48*, 1490-1499.

[34] J. Bicerano. *Prediction of Polymer Properties*; Marcel Dekker: New York, 1993.

[35] J. B. Di, D. Y. Sogah. *Macromolecules* **2006**, *39*, 5052-5057.

[36] B. Trathnigg, M. Kollroser. *J Chromatogr A* **1997**, *768*, 223-238.

[37] P. C. Hartmann, P. Dieudonne, R. D. Sanderson. *J Colloid Interface Sci* **2005**, *284*, 289-297.

[38] L. Biasci, M. Aglietto, G. Ruggeri, F. Ciardelli. *Polymer* **1994**, *35*, 3296-3304.

[39] T. D. Fornes, D. L. Hunter, D. R. Paul. *Macromolecules* **2004**, *37*, 1793-1798.

[40] X. Fu, S. Qutubuddin. *Polymer* **2001**, *42*, 807-813.

[41] M. Kawasami, N. Hasegawa, M. Kato, A. Usuki, A. Okada. *Macromolecules* **1997**, *30*, 6333-6338.

[42] M. Xu, Y. S. Choi, Y. K. Kim, K. H. Wang, I. J. Chung. *Polymer* **2003**, *44*, 6387-6395.

[43] S. Sadhu, A. K. Bhowmick. *J Appl Polym Sci* **2004**, *92*, 698-709.

[44] C. Tseng, J. Wu, H. Lee, F. Chang. *J Appl Polym Sci* **2002**, *85*, 1370-1377.

[45] M. K. Wang, F. Zhao, Z. H. Guo, S. J. Dong. *Electrochim Acta* **2004**, *49*, 3595-3602.

[46] H. M. Jung, E. M. Lee, B. C. Ji, Y. L. Deng, J. D. Yun, J. H. Yeum. *Colloid and Polymer Science* **2007**, *285*, 705-710.

[47] G. Moad, J. Chiefari, B. Y. K. Chong, Julia Krstina, R. T. A. Mayadunne, A. Postma, E. Rizzardo, S. H. Thang. *Polym Int* **2000**, *49*, 993-1001.

[48] Y. L. Zhao, S. Perrier. *Macromolecules* **2006**, *39*, 8603-8608.

[49] J. B. McLeary. University of Stellenbosch: Stellenbosch, 2004; p 223.

[50] A. Postma, T. P. Davis, G. X. Li, G. Moad, M. S. O'Shea. *Macromolecules* **2006**, *39*, 5307-5318.

[51] A. B. Morgan, J. W. Gilman. *J Appl Polym Sci* **2003**, *87*, 1329-1338.

[52] M. Rosorff. *Nano Surface Chemistry*; Marcel Dekker: New York-Basel, 2002.

[53] J. Wang, J. Du, J. Zhu, C. A. Wilkie. *Polym Degrad Stabil* **2002**, *77*, 249-252.

[54] J. G. Doh, I. Cho. *Polym Bull* **1998**, *41*, 511-518.

[55] Y. Zhong, Z. Y. Zhu, S. Q. Wang. *Polymer* **2005**, *46*, 3006-3013.

[56] Y. S. Choi, I. J. Chung. *Macromol Res* **2003**, *11*, 425-430.

[57] A. Leszczynska, J. Njuguna, K. Pielichowski, J. R. Banerjee. *Thermochim Acta* **2007**, *453*, 75-96.

[58] E. A. Turi. *Thermal Characterization of Polymeric Materials*, 2nd ed.; Academic Press: San Diego, 1997; Vol. 1.

[59] P. Ding, M. Zhang, J. Gai, B. Qu. *J Mater Chem* **2007**, *17*, 1117-1122.

[60] G. Chigwada, C. A. Wilkie. *Polym Degrad Stabil* **2003**, *80*, 551-557.

[61] D. Yei, S. Kuo, Y. Su, F. Chang. *Polymer* **2004**, *45*, 2633-2640.

[62] B. Zhang, G. Chen, C. Pan, B. Luan, C. Hong. *J Appl Polym Sci* **2006**, *102*, 1950-1958.

Chapter 6: Novel cationic RAFT-mediated polystyrene–clay nanocomposites: Synthesis, characterization, and thermal stability

The work described in this chapter has been published in the following paper:

Novel cationic RAFT-mediated polystyrene–clay nanocomposites: Synthesis, characterization, and thermal stability

Austin Samakande, J. J. Juodaityte, Ronald D. Sanderson and Patrice C. Hartmann

Macromol Mater Eng 2008, 293, 428–437.

Abstract

Two novel cationic RAFT agents, N,N-dimethyl-N-(4-(((phenylcarbonothioyl)thio)-methyl)benzyl)ethanammonium bromide (PCDBAB) and N-(4-((((dodecylthio)carbo-nothioyl)thio)methyl)benzyl)-N,N-dimethylethanammonium bromide (DCTBAB), were anchored onto MMT clay to yield RAFT-modified-MMT (RAFT-MMT) clays. The RAFT-MMT clays were dispersed in styrene after which thermal self-initiation polymerization of styrene was carried out to give rise to exfoliated PS-clay nanocomposites (PS–CNs). The RAFT agents anchored onto the clay layers successfully controlled the polymerization process, resulting in products with controlled molar masses and narrow polydispersity indices. The nanocomposites prepared showed enhanced thermal stability, which was a function of the clay loading, clay morphology and on molar mass.

6.1 Introduction

The preparation of polymer–clay nanocomposites (PCNs) with the morphology of clay, varying from an intercalated to a fully exfoliated structure, is now a fully developed concept.[1-8] However, much research still needs to be carried out before proposals can be made as to what is required, particularly in terms of materials and reaction conditions, to obtain a particular clay morphology in a final PCN. Several researchers have made various proposals for this; for example, the need for complete compatibility between the clay or modified-clay and the monomer/polymer,[9] copolymerization of the main monomer with polymerizable surfactants bound to the clay layers,[8,10-15] (this idea has resulted in many successful exfoliated PCNs being reported), use of hyperbranched polymers,[16] and inter-gallery initiation of polymerization,[17-23] that results in the promotion of inter-gallery polymerization/crosslinking at the expense of bulk polymerization. Uncontrolled inter-gallery polymerization was reported as early as 1965, by Dekking, who anchored an azo initiator, azo*bis*isobutyramidine hydrochloride (AIBA), onto clay layers, thus forming an initiator-modified-clay, which he subsequently used in the initiation of polystyrene and poly(methyl methacrylate), and yielded PCNs with polymer chains attached to the clay layers.[17,24] Fan *et al*. and Meier *et al*. also reported a similar approach to the synthesis of polystyrene–clay nanocomposites (PS–CNs) initiated by clay bound initiators.[18,19,22]

Another important issue that is yet to be thoroughly investigated is the polymer architecture in the PCNs. To date, most of the research into the polymer architecture that has been undertaken has focused on uncontrolled radical polymerization reactions.[3,6,8,25] The few articles available on controlled living radical polymerization in PCNs focused on nitroxide mediated polymerization (NMP).[26,27] This is easy to understand, as in NMP the control of polymerization is based on a nitrogen containing species that can easily be quaternized and anchored on clay surfaces, resulting in modified-clay, and which can then subsequently be used in a polymerization reaction. This leads to nanocomposites with both the polymer and clay architectures being controlled. This idea was pioneered by Weimer *et al*., who synthesized PS–CNs with controlled molar masses by first anchoring a 2,2,6,6-tetramethyl-1-piperidinyloxy free-radical (TEMPO) derivative onto clay layers, and used the modified-clay in the nanocomposite synthesis.[27] Di and Sogah prepared

their nanocomposites based on this idea, with minor changes in the nitroxide mediating species. They also prepared block copolymers.[26]

To date, other types of controlled living polymerization methods, such as ionic polymerization,[28,29] atom transfer radical polymerization (ATRP),[30,31] borane chemistry,[32,33] and reversible addition–fragmentation chain transfer (RAFT) techniques,[33-37] have not been widely used. There are several reasons for this, particularly the techniques' susceptibility to impurities; e.g. the propagating species in ionic polymerization is destroyed by even small amounts of water (small amounts of water are always present in clays).[34] Notwithstanding the disadvantages of ionic polymerization in the presence of clay, Fan *et al*. and Advincula *et al*. synthesized PS–CNs under harsh conditions of high temperature and vacuum in order to remove any moisture in the system.[28,29] ATRP suffers from the presence of redox species,[20] the presence of which in clays is well known, as these might lead to the undesired reduction of the ionic copper species to copper zero. ATRP also suffers from the limited number of monomers that can be successfully synthesized under controlled conditions, as well as the presence of toxic copper in the final product.[38] Very little is known about controlling polymerization using borane chemistry, however, Yang *et al*. did use this technique to synthesize PS–CNs with controlled molar masses.[32] The RAFT technique is one of the fastest growing and most robust controlled radical polymerization techniques.[39,40] This is due to its versatility, such as tolerance to impurities, and the numerous types of monomers that can be used. Furthermore, the experimental setup required for RAFT controlled radical polymerization is relatively simple. The RAFT technique owes its success to a family of organic molecules containing the thio-carbonyl-thio group, known as RAFT agents.[41-43] There are however shortcomings: the thio-carbonyl-thio group can be hydrolyzed by basic species such as hydroxide ions, primary and secondary amines.[38,44-47] Thus, the synthesis of positively charged RAFT agents is a great challenge because of the inherent instability of the thio-carbonyl-thio group in a basic environment, since most of the positively charged organic species originate from amines.

Clay in its native state is hydrophilic and incompatible with hydrophobic monomers. Consequently, a prerequisite in preparing most PCNs is to modify the surface of clay in order to make it compatible with the monomer/polymer system involved. This is generally done by ion-exchange, using positively charged species such as quaternary ammonium surfactants.[8] The fixing of a RAFT agent within the clay

galleries ensures growth of polymer chains from clay surfaces in a controlled manner.[34] Despite the difficulty in synthesizing positively charged RAFT agents,[45] they are potentially very interesting, as they could allow the synthesis of RAFT-mediated PCNs, where the polymer growth takes place from the clay surfaces. Because of the advantages of the RAFT technique over other controlled radical polymerization techniques we considered it worthwhile to endeavour to synthesize positively charged RAFT agents and apply the technique to the synthesis of PCNs to control both the clay morphology and the polymer architecture. Most of the work reported in literature to date is on the use of free RAFT agents (i.e. the RAFT agent is not attached to the clay layers).

Moad *et al*. have used RAFT-mediated polar polymers that are miscible with polypropylene and then melt blended both polymers (i.e. polymers and polypropylene) in the presence of sodium montmorillonite to yield polypropylene-clay nanocomposites.[36] Salem and Shipp have shown the ability of free RAFT agents to control the polymerization in the preparation of polystyrene-, poly(methyl methacrylate)- and poly(butyl acrylate)-clay nanocomposites by the *in situ* polymerization method.[35] They used polymerizable surfactant-modified-clays and copolymerized these anchored polymerizable surfactants with the main monomer in a controlled manner. The monomer-clay system they investigated had previously been studied and results showed that the nanocomposite structure obtained was not changed by the presence of the RAFT agent. PCNs synthesized using positively charged RAFT agents have been reported by Zhang *et al* who anchored a cationic RAFT agent 10-Carboxylic acid-10-dithiobenzoate-decyltrimethylammonium bromide (CDDA) onto clay and then used the modified-clay for the controlled solution-based *in situ* intercalative polymerization of styrene, and obtained exfoliated PCNs.[48] Di and Sogah used a dithiocarbamate-based modified-clay.[34] Dithiocarbamates are well known for their poor ability to control polymerization in most cases, save for the polymerization of specific monomer systems. The poor control is because the dithiocarbamyl radicals generated undergo several side reactions.[38] The use of positively charged RAFT agents based on the more general and versatile dithiocarbonates and trithiocarbonates have still to be well documented.

This chapter reports on anchoring two different, positively charged novel RAFT agents (i.e. a dithiobenzoate and a trithiocarbonate) onto the surface of the clay layers via their cationic R groups, and the subsequent use of the obtained modified-

clays in the preparation of PS–CNs by the *in situ* polymerization of styrene. Thermal stability of the nanocomposites was investigated and is also discussed, with regards to their morphology, the amount of clay used, and the molar mass of the polymer.

6.2 Materials and methods

6.2.1 Reagents

Styrene (99%, Aldrich) was purified by washing with 0.3M KOH, followed by distillation at 40 ºC under reduced pressure. Sodium montmorillonite (Na-MMT) was obtained from Southern Clay Products (Texas, USA). Deionized water was obtained from a Millipore Super Q System. N,N-dimethyl-N-(4-(((phenylcarbonothioyl)thio)-methyl)benzyl)ethanammonium bromide (PCDBAB) and N-(4-((((dodecylthio) carbono-thioyl)thio)methyl)benzyl)-N,N-dimethylethanammonium bromide (DCTBAB) were synthesized as described in a previous paper of mine.[45]

6.2.2 Typical modification of sodium montmorillonite clay (ion-exchange reaction)

Na-MMT (3.06 g) was dispersed in water (300 ml) over a period of 1 h. A solution of DCTBAB (1.435 g, 2.721 10^{-3} mol) in a mixture of acetonitrile and deionized water (30 ml:180 ml) was slowly added to the dispersion over 30 min. The mixture was stirred for a further 3 h and then filtered. The precipitate was washed until a negative test to a silver nitrate solution was obtained.[8] The filtrate was analyzed by high performance liquid chromatography (HPLC). The washed solids were then freeze-dried for 5 days to yield very fine, loose DCTBAB modified-clay (DCTBAB-MMT). A similar procedure was followed for the preparation of modified PCDBAB clay (PCDBAB-MMT). The yields in both cases were over 90%.

6.2.3 Typical polymerization of styrene

Predetermined quantities of RAFT agent and styrene were placed in a Schlenk tube. The contents of the tube were freeze-vacuum-thawed three times and then the tube was placed in an oil bath at 90 ºC. The polymerization was carried out for 72 h at 90 ºC. The obtained solid was dissolved in chloroform and then precipitated in a 10-fold excess of methanol. The obtained monomer-free polystyrene polymer was dried in an oven at 55 ºC overnight to yield a powdered polymer.

A similar procedure was used for the synthesis of the nanocomposites, the only difference being that RAFT-modified-clay was included instead of a free RAFT agent. Overnight stirring of the monomer clay suspension was performed prior to polymerization so as to allow the monomer in the clay galleries to swell.

6.2.4 Analyses

6.2.4.1 High performance liquid chromatography (HPLC)

HPLC was carried out using a using a Kontron Instruments HPLC system, automatically controlled by Geminyx software. It was equipped with a C12 (250 x 460 mm, 4 µm) column in reverse-phase mode. Detection of analytes was done using a quasi online evaporative light scattering (ELS) detector system, model PL-ELS 2100, purchased from Polymer Laboratories. The detector parameters were set as follows: evaporator 50 ºC, nebuliser 30 ºC and N_2 gas flow rate 1.60 ml/min. A mixture of two solvents was used as the mobile phase: 94.53/4.97/0.5 v/v/v HPLC grade acetonitrile/water/trifluoroacetic acid (B solvent) and 4.97/94.53/0.5 v/v/v acetonitrile/water/trifluoroacetic acid (A solvent), at 1 ml min^{-1} flow rate. The analyte injection volume was set at 20 µl. The filtrates from the ion-exchange reaction of clay were analyzed by HPLC, using the solvent composition B:A. The solvent composition was optimized for each transfer surfactant (transurf) as follows. For the DCTBAB transurf, the initial ratio of B:A = 70:30 was linearly ramped up to 100% B within 25 min, held there for 5 min, and then linearly ramped down to B:A = 70:30 within 5 min, giving an elution time of 17.73 min. For the PCDBAB, the initial ratio of B:A = 40:60 was linearly ramped to 100% B in 20 min, held for 5 min, and then linearly ramped down to B:A = 40:60 within 5 min, giving an elution time of 9.15 min. Once the parameters for each different analyte were optimized, calibration curves were plotted, using various RAFT agent concentrations. The calibration curves that were obtained were non-linear. This was not surprising, given that the ELS detector's response is non-linear against concentration. Unknown concentrations of analytes were determined by extrapolation from the calibration curves.[49]

6.2.4.2 Size-exclusion chromatography (SEC)

SEC was carried out using a Waters 600E system controller equipped with a Waters 610 Fluid Unit pump and a Waters 410 Differential Refractometer as detector. Prior to analysis, samples were vigorously stirred in tetrahydrofuran (THF) for a week. The

samples were then filtered through a 0.20-μm filter membrane. However, it was soon discovered that even after filtering the polymer-clay suspension through Celite particles and a 0.20-μm filter membrane some polymer that was still attached to the clay particles passed through and was detected in the RI signal. Thus, prior to SEC analysis, the samples were reverse ion-exchanged as follows. Quantities of PS–CNs (0.2 g) and LiCl (0.06 g) were dissolved in THF (10 ml) and refluxed at 70 ºC for 3 h. The solution was filtered through Celite and thereafter the polymer was precipitated in methanol and dried. SEC analysis, using THF as mobile phase and an initial polymer concentration of 5 mg/mL, was performed on clay-free polymer solutions. Dynamic light scattering (DLS) showed no peak/s characteristic of clay particles.

6.2.4.3 Small angle X-ray scattering (SAXS)

SAXS measurements were performed in a transmission configuration at 298 K. A copper rotating anode X-ray smyce (functioning at 4 kW), with a multilayer focusing "Osmic" monochromator giving high flux (10^8 photons/sec) and punctual collimation, was used. An "image plate" 2D detector was used. Scattering patterns were obtained, giving scattered intensity as a function of the wave vector q. The calculation of q values is described elsewhere.[50]

6.2.4.4 Transmission electron microscopy (TEM)

TEM was used to directly visualize the morphology of the clay particles in PS–CNs at the nanometer level. Bright field TEM images were recorded using a LEO 912 transmission electron microscope, at an accelerating voltage of 120 kV. Prior to analysis, samples of PS–CNs were embedded in epoxy resin and cured for 24 h at 60 ºC. The embedded samples were then ultra-microtomed with a diamond knife on a Reichert Ultracut S ultra microtome at room temperature. This resulted in sections with a nominal thickness of ~100 nm. The sections were transferred from water at room temperature to 300-mesh copper grids, which were then transferred to the TEM apparatus.

6.2.4.5 Thermogravimetric analysis (TGA)

TGA measurements were done on a TA Instruments Q 500 thermogravimetric analyzer. Samples of less than 15 mg were used for all analyses. They were analyzed from ambient temperature to 600 ºC, using a heating rate of 20 ºC/min. All

TGA analyses were carried out under a nitrogen atmosphere. Nitrogen was purged at a flow rate of 50 ml/min.

6.3 Results and discussion

6.3.1 Modification of clay

The modification of clay was carried out using an equimolar amount of the modifier relative to the cation-exchange capacity (cec), with the cec value being 92.6 meq/100g clay for the Na-MMT used. Clay modification was monitored using TGA, HPLC and SAXS. From TGA results (see Fig. 6.1), the difference between the percentage weight loss of the virgin clay and the modified-clay is attributed to the amount of cationic organic species ion-exchanged.[8,9,13,51-53] The FTIR spectra of Na-MMT and the modified-clays are shown in Fig. 27 in Appendix. The appearance of new peaks in the spectra of the modified-clays is a qualitative indication that the ion-exchange process was indeed successful.

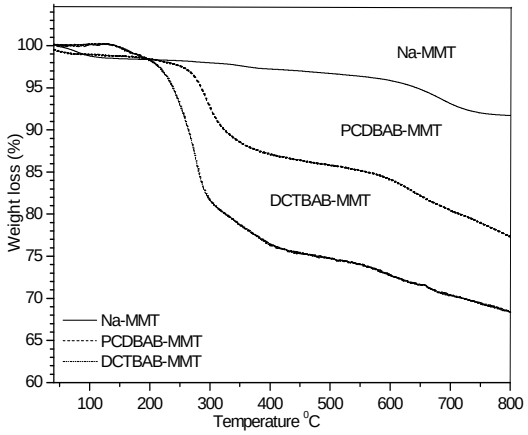

Fig. 6.1 TGA thermograms of Na-MMT and the modified-clays.

HPLC analysis of the water phase was carried out in order to determine the amount of non-ion-exchanged surfactant remaining in solution after the ion-exchange process. Given that Na-MMT is a type of swelling clay, the ion-exchange of the Na^+ by organic cationic species causes an increase of the inter-gallery spaces, which can be conveniently monitored by SAXS.[15]

HPLC analysis showed that after the ion-exchange reaction PCDBAB and DCTBAB had no characteristic HPLC peaks. This implies that when quantities of modifier of up to 100% cec were used the ion-exchange occurred quantitatively. HPLC results were further corroborated by TGA results, as PCDBAB-MMT and DCTBAB-MMT showed

weight losses that were in good agreement with the expected ones. The amount of modifier successfully ion-exchanged was calculated from the experimental weight loss determined by TGA. Results tabulated in Table 6.1 show ion-exchanged modifiers slightly above the theoretical limit of 100% cec. These overestimated values are probably due the weight loss contribution of any remaining hydration water present in the modified-clay, even after drying. Alternatively, they could be due to the catalytic hydrolysis of the hydroxyl groups on clay edges by the byproducts of the degrading RAFT molecules anchored onto clay. An increase in the *d* spacing from the SAXS patterns of these modified-clays further confirmed (qualitatively) that ion-exchange had occurred.

Table 6.1 HPLC, TGA and SAXS analyses of the modified-clays

	Na-MMT	***PCDBAB-MMT***	***DCTBAB-MMT***
A/%cec		103	110
B/%cec		100	100
d (nm)	1.19	1.62	2.03

Key: A% and B% are the amounts of ion-exchanged surfactant given as a percentage relative to cec, from TGA and HPLC analyses, respectively. *d (*nm) is the *d* spacing of the clays as measured by SAXS analysis.

6.3.2 RAFT-modified-clay-mediated bulk polymerization of styrene

In RAFT, the control of polymerization is significantly influenced by both the leaving group (R) and the stabilizing group (Z), which makes their choice, to match the desired monomer, very important.[54,55] (See Scheme 6.1).

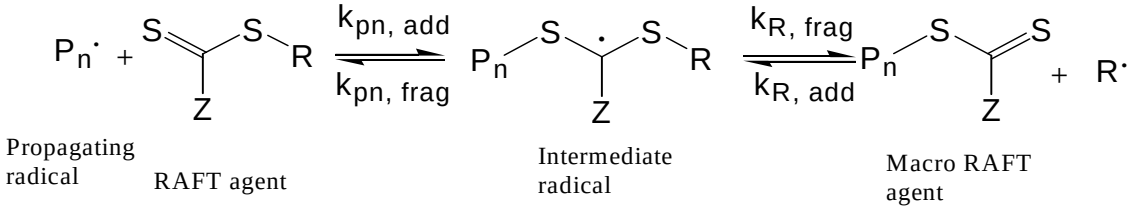

Scheme 6.1 Addition–fragmentation equilibrium between propagating radicals in a RAFT reaction.

The (Z) group acts as an activator for the thiocarbonyl group to react with radicals. It also acts as a stabilizer of the transition state radical that is formed between the thiocarbonyl group and a free-radical. On the other hand, the (R) group should be a good leaving group by undergoing a homolytic fission; once it leaves the main RAFT agent as a radical it should be able to reinitiate polymerization by reacting with monomer units. In both DCTBAB and PCDBAB the (R) group is the same para-modified benzyl group. The benzyl group is known as an efficient candidate to

reinitiate the polymerization of styrene after fragmentation.[56] The (Z) group was varied from a phenyl (for PCDBAB) to a thioalkyl group (for DCTBAB), as phenyl- and dodecylthio- (Z) groups have been reported to effectively control the polymerization of styrene,[55,56] (see Scheme 6.2).

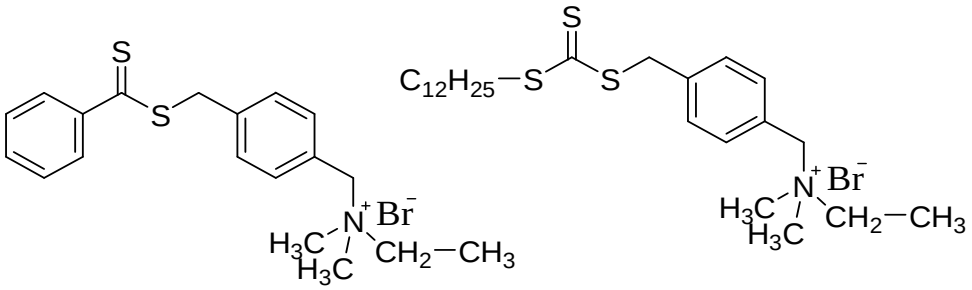

Scheme 6.2 Structures of RAFT agents PCDBAB (left) and DCTBAB (right).

The RAFT-mediated bulk polymerization of styrene using the RAFT agent DCTBAB (in the absence of clay) showed that this RAFT agent was indeed able to control the polymerization process. Fig. 28 in Appendix shows a linear increase in molar mass with conversion. The value of the polydispersity index (PDI) of the final polymer was 1.30 and the experimental M_n was comparable to the theoretical calculated one, indicating control of the polymerization. However, the conversions did not reach 100%, even after 72 h, due to an increase in viscosity that occurred at high conversions (see Table 6.2). When the polymerization was performed in the absence of a RAFT agent, typical broad molar mass distributions with high PDI values were recorded.

Table 6.2 RAFT polystyrene DCTBAB-MMT nanocomposites mediated bulk polymerization of styrene at 90 ºC

Polymer	$\frac{[MC]_0}{[S]_0}\%$	$\frac{[S]_0}{[R]_0}$	*Conv (%)*	*Calc M_n*	*Exp M_n*	*PDI*
PS	-	-	92.0	-	168 032	2.99
PS-D0	-	238.7	83.8	25 412	15 938	1.30
PS-D-MC1	0.51	2547.8	91.5	242 972	145 349	2.83
PS-D-MC2	1.01	1277.3	88.7	118 231	175 108	1.87
PS-D-MC3	2.50	515.9	42.0	22 680	44 825	1.59
PS-D-MC4	3.48	370.8	48.5	19 166	23 580	1.39

Key: $\frac{[MC]_0}{[S]_0}$ initial mass ratio of modified-clay to styrene; $\frac{[S]_0}{[R]_0}$ initial molar ratio of styrene to RAFT , *Calc M_n* = theoretical mass calculated using the Equation $M_n = \frac{[S]_0 M_S x}{[RAFT]_0} + M_{RAFT}$,[57] where $[S]_0$ = initial styrene concentration, M_S = molar massof styrene, x = conversion, M_{RAFT} = molar massof RAFT, $[RAFT]_0$ = initial concentration of RAFT; *Exp M_n* = experimental molar mass; *PDI* = polydispersity indices of the polymer obtained, as determined by SEC.

Table 6.3 RAFT polystyrene PCDBAB-MMT nanocomposites mediated bulk polymerization of styrene at 90 ºC

Polymer	$\frac{[MC]_0}{[S]_0}$ %	$\frac{[S]_0}{[R]_0}$	*Conv (%)*	*Calc M_n*	*Exp M_n*	*PDI*
PS	-	-	92	-	168 032	2.99
PS-P-MC1	0.50	2491.0	57.7	149 842	136 103	3.04
PS-P-MC2	1.04	1202.5	55.8	69 946	94 241	2.07
PS-P-MC3	2.49	499.8	43.0	22 680	53 285	1.50
PS-P-MC4	3.60	346.7	18.5	7 000	37 519	1.59

Since PCDBAB is not soluble in styrene, the PCDBAB-mediated free-radical polymerization of styrene in bulk could not be performed. However, when the PCDBAB-modified-clay was dispersed in the monomer an increase in viscosity was observed. This is explained by the fact that once ion-exchanged on clay surfaces, the tails of the hydrophobic phenyl ring radiate away from the clay surface, making the modified-clay compatible with the non-polar styrene monomer/polymer.

From Tables 6.2 and 6.3 it is evident that the nanocomposites synthesized using either DCTBAB or PCDBAB showed three main trends, namely: (1) a decreasing conversion as the clay level increases; (2) a decreasing polydispersity index as the clay level increases; and (3) at [monomer]/[RAFT] ratio greater than 1000, i.e. at low clay loadings, the PDI values are greater than the theoretical limit value of 1.5 above which the polymerization is theoretically no longer considered to be controlled.[35]

The decreasing conversion has been reported before by Choi and Chung.[58] They reported that an increasing clay content at the same monomer content results in a decrease in relative amount of monomer, thus a decrease in the molar mass of the obtained PCN. The decreasing conversion could also be explained by the contribution of the clay content, as modified-clays are well-known for leading to increased viscosities.[8,52,59] In this study there is an increase in the $[MC]_0/[S]_0$ ratio, thus we would expect the conversion to decrease with an increase in clay loading, as is observed. The conversion was found to be lower in the PCDBAB-MMT system relative to the DCTBAB-MMT system. This could be due to inhibition, retardation, and side reactions (termination) that are prevalent in dithio systems, as opposed to trithiocarbonates.[60,61] Zhao and Perrier also found that the polymerization of dithiobenzoates is generally slower than that of trithiocarbonates.[62] Furthermore, the effect of retardation brought about by the RAFT agent could also be the reason for a decrease in conversion, as more clay loading resulted in an increase in the RAFT agent concentration.

In RAFT-mediated systems the ratio [styrene]/[RAFT] is rarely above 1000,[63] causing the RAFT chain transfer constant (CT) to be several orders of magnitude greater than ratio [styrene]/[RAFT]. This scenario ensures that the probability of multiple monomer additions becomes negligible.[64] In other words, there is one monomer addition to a growing chain before transfer to a RAFT agent, implying control of polymerization. In our case, at low clay loadings the [styrene]/[RAFT] is well above 1000, which implies that the probability of multiple monomer addition occurring becomes more pronounced, and thus there is partial loss of control of polymerization, as depicted by the high PDI values obtained. Accordingly, control of the polymerization was found to increase as the clay loading increased, as evidenced by the decrease in the PDI values as the clay loading (and concomitantly RAFT agent concentration) increased. Pham *et al*. observed a similar decrease in PDI as the RAFT concentration increased,[65] however, the system that they studied was clay free.

In most cases the experimental molar masses were greater than the theoretically expected ones. Jesberger *et al.* also observed such results when they used a multifunctional-RAFT polyester as a macro RAFT agent for the synthesis of core shell particles.[66] A similar trend was also observed by Di and Sogah for dithiocarbamate-anchored-mediated polymerizations: higher PDI values at low clay levels and molar masses higher than expected were obtained. They attributed their findings to a low initiator efficiency of the attached RAFT system, although the efficiency was found to increase as the clay loading increased.[34] Zhang *et al*. did however report lower PDI values for their nanocomposites, which they attributed to the ability of the 10-Carboxylic acid-10-dithiobenzoate-decyltrimethylammonium bromide (CDDA) RAFT agent to promote diffusion of oligo-radicals into the clay galleries.[48] The PDI values they reported are comparatively lower than the PDI values of our system. This is because they polymerized in solution, which generally results in lower PDI values than when the polymerization is performed in bulk.

The loss of control of the polymerization in our system could also be related to the uneven repartition of the RAFT agent in the monomer phase, as the RAFT concentration is locally high in the clay galleries, whereas it is theoretically locally equal to zero outside the clay galleries (i.e. in the pure monomer phase). This effect could increase the probability of multiple monomer addition before the propagating radical encounters a RAFT agent. However, as polymerization progresses and the

molar mass increases, and thus the ability of the growing chain ends to radiate away from the clay surface increases its likelihood to diffuse freely in the monomer continuous phase. As a consequence, the polymerization gains in terms of control of molar mass. This implies that the hybrid system requires more clay loading (i.e. more RAFT agent) for better control of polymerization, as is observed in the present study.

On a closer look at the two series it is evident that the DCTBAB bound to clay is a more efficient RAFT agent as it yielded better control of the polymerization of styrene (i.e. PDI value of 1.39 for PS-D-MC4) relative to the PCDBAB bound to clay system (i.e. PDI not lower than 1.50). It is of interest to note that the anchoring of the RAFT agent onto the clay platelets did not have an effect on the RAFT agent's ability to control polymerization (see Fig. 6.2).

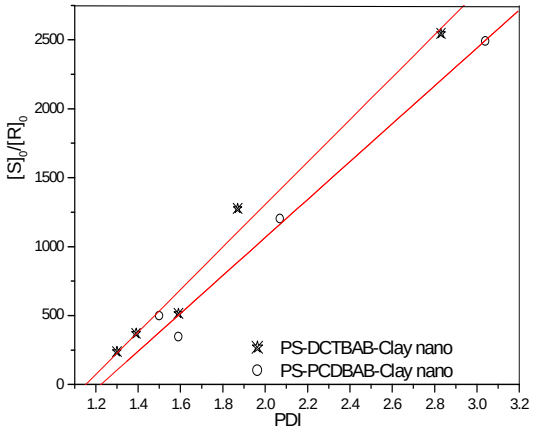

Fig. 6.2 Ratio of initial styrene to RAFT concentration as a function of PDI.

The curves show a linear fit between the $[S]_0/[R]_0$ ratio and the PDI of the polymer. In the DCTBAB system the last point, i.e. PDI = 1.3, which corresponds to a polymer made using free RAFT agent (i.e. not anchored onto clay), fits well with the linear curve of RAFT anchored onto clay. Unfortunately such a point could not be obtained for the PCDBAB system because PCDBAB is not compatible with styrene monomer when unanchored to clay.

6.3.3 Morphology of polystyrene–clay nanocomposites

6.3.3.1 TEM analysis

The TEM images of PS–CNs, clearly show exfoliated structures with homogeneously dispersed single clay platelets in both systems. Two examples, namely (a) polystyrene–DCTBAB-clay nanocomposites and (b) polystyrene–PCDBAB-clay

nanocomposites, are shown in Fig. 6.3. This implies that the PS–CNs were of exfoliated morphology. The exfoliated structure has also been obtained by many other researchers who recorded polymer growth taking place from the clay surface.[26,27,30,34] The exfoliated structure is mainly created by the pressure exerted on the clay sheets by the growing polymer chains within the interlayer space.[67] Since TEM imaging gives a picture of only a very small portion of the sample,[68] the exfoliated morphology was further confirmed by SAXS, as it allows one to look at the average morphology of the whole sample.

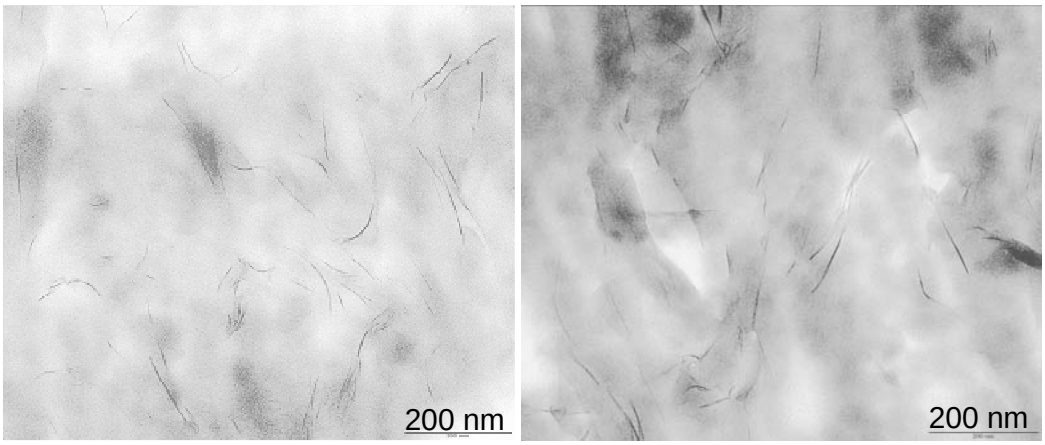

Fig. 6.3 TEM images of (a) polystyrene-DCTBAB-clay nanocomposites and (b) polystyrene–PCDBAB-clay nanocomposites (scale bar = 200 nm) at 1.7 and 1.3% clay loadings, respectively.

6.3.3.2 SAXS analysis

The SAXS patterns were found to be similar to those obtained using a regular XRD apparatus. In SAXS a decreasing q value is equivalent to a decreasing 2θ value, implying an increasing inter-gallery distance. The *d* spacings were found to increase from unmodified-clay (i.e. 1.19 nm, as reported elsewhere,[7,11,15,52,69]) to modified-clays (i.e. about 2 nm, see Fig. 6.4(i-iii)), whereas no Bragg peak was observed with the polymer–clay nanocomposites(see Fig. 6.4(iv-v)). The absence of Bragg peaks could be due to either loss of order (i.e. exfoliation) or to the dilution factor of the clay in the polymer matrix.[48] However, TEM imaging seems to favour the exfoliation hypothesis, as no regularly oriented clay particles were observed. Exfoliated morphologies were accordingly obtained for the entire range of PCN compositions prepared, i.e. up to an experimental clay content of 12.9%. Preparation of PCNs with even higher clay contents was not undertaken for reason of dispersion inhomogeneity, due to the viscosity of the RAFT-MC-monomer system being too high

prior to polymerization. The fact that exfoliated structures were obtained is in line with the accepted model, where polymerization within the clay galleries generates pressure on the clay platelets from the growing chains, eventually leading to the exfoliated structure.[67] However, thermodynamic compatibility of the monomer/polymer with the modified-clay is still required to allow an efficient exfoliation.[9,52] In the present system, good compatibility between the modified-clay and the styrene monomer was achieved due to the non-polar character of the organic RAFT agent once grafted onto the clay surface.

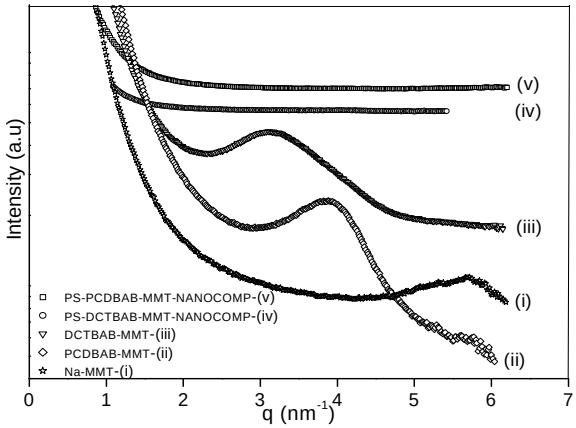

Fig. 6.4 SAXS patterns of PS–clay nanocomposites.

6.3.4 Thermal stability of polystyrene–clay nanocomposites

The first report on thermal stability of PCNs was published as early as 1965, by Bluimstein.[70] The general notion on the issue of thermal stability in PCNs is the following: an increase in clay loading results in an increase in thermal stability.[1,3,5] This is due to an increase in the number of clay platelets hindering diffusion of gasified polymers because almost all nanocomposite samples become homogeneous and almost all the polymer chains are in contact with the clay particles.[8,15,71] Improvement in thermal stability has also been attributed to restricted thermal motion of the polymer between the clay galleries.[70] Since most of the available literature is based on uncontrolled free-radical polymerization, many researchers attribute the net increase in thermal stability to only clay loading. In some cases researchers did try to relate the morphology of clay in the nanocomposites to the thermal stability. The general agreement on this is that an exfoliated clay structure results in better thermal stability.[15] There were however certain cases reported where an intercalated clay structure resulted in better thermal stability.[8,72,73]

As shown in Table 6.4 and Fig. 6.5, nanocomposites prepared using DCTBAB and PCDBAB modified-clays showed enhanced thermal stability relative to virgin polystyrene. This is in general agreement with what is reported in the literature.[8,11,15,35,48,52,74,75]

Table 6.4 Thermal stabilities and molecular weights of PS–DCTBAB and PS–PCDBAB-PCNs (values in brackets were obtained for clay-free polymers obtained after a reverse ion-exchange reaction)

Polymer	*Exp M_n*	*Clay Load $_{exp.}$ (wt.%)*	*T (^{0}C) @ 10% wt loss*	*T (^{0}C) @ 50% wt loss*	*T (^{0}C) @ 90% wt loss*
PS	168 032	-	393	415	428
PS-D-MC1	145 349	0.5	409 (395)	444 (422)	460 (437)
PS-D-MC2	175 108	0.8	408 (395)	440 (422)	453 (439)
PS-D-MC3	44 825	1.7	407 (389)	429 (420)	442 (437)
PS-D-MC4	23 580	4.6	400 (391)	426 (423)	437 (446)
PS-P-MC1	136 103	0.9	425 (394)	448 (428)	548 (481)
PS-P-MC2	94 241	1.3	413 (393)	441 (421)	457 (436)
PS-P-MC3	53 285	4.1	404 (390)	433 (423)	444 (441)
PS-P-MC4	37 519	12.9	368 (377)	397 (422)	408 (442)

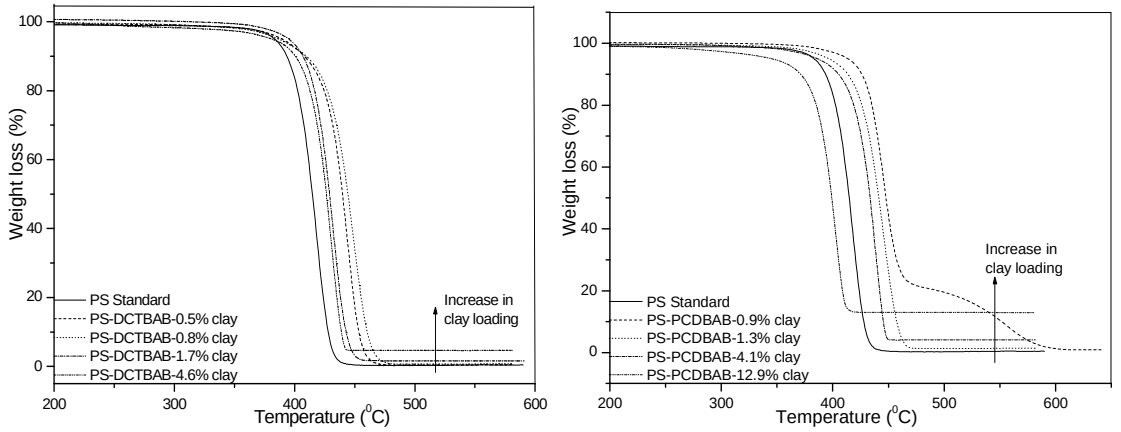

Fig. 6.5 Variation of weight loss (%) with temperature of the polymer–clay nanocomposites.

Upon closer inspection of the thermal stability trends, the nanocomposites yielded unexpected results: in general, as the clay loading increased, and concomitantly the molar mass decreased, so the thermal stability decreased. This agrees with the results of Choi and Chung, who observed a decrease in thermal stability as clay loading increased.[58] They attributed this to a low yield of polymerization. This is in stark contradiction to the general notion that an increase in clay loading leads to an increase in thermal stability.[1,3,5] The decreasing thermal stability as clay loading increases is more pronounced in the PCDBAB-MMT nanocomposites series, where a very clear decrease in thermal stability with an increase in clay content was seen. There are three possible reasons for this: (1) molar mass effects,[76] (2) the ratio of

chains attached to clay relative to those unattached, given that if the whole sample is indeed a near interface then a large increase in thermal stability would be expected, and (3) the extent of clay exfoliation as the clay level increases.

We therefore proceeded to try to separate the unattached chains from the attached ones, but were unsuccessful. This attempt included separating these chains by filtering through Celite and the smallest pore size filter membrane, i.e. 0.20 μm, and also by centrifuging the nanocomposites sample suspended in THF solution at the highest speed (4400 rpm) for 4 h. The clay particles could however still be detected by dynamic light scattering (DLS).

The second effect, i.e. measurement of the effect of molar mass on thermal stability, was performed after a reverse ion-exchange process, followed by filtration through Celite, and then carrying out TGA analysis. For both the DCTBAB-MMT and PCDBAB-MMT series (c.f. Table 6.4), most of the polymers had roughly the same thermal stability, within experimental error. However a decrease in the stability of the clay-free samples relative to the nanocomposites was observed. The difference was attributed to the presence of clay in the nanocomposites. Thus the molar mass seems not to be significantly affecting the thermal stability or it has a minimal effect, as the differences in the clay-free samples are very small and do not show a very pronounced trend when compared to the trends for the PCNs. Ding *et al*. also acknowledged the effect of the molar mass on the thermal stability; they postulated a decrease in thermal stability as molar mass decreased.[33] However, in our case the effect of molar mass should indeed be minimal, given all the molar masses under investigation were above critical molar mass, i.e M_c. At molar masses greater than M_c entanglements start to form, beyond which thermal stability is relatively independent of molar mass. The M_c of styrene has been reported to be ~18 000 $gmol^{-1}$.[77] Moreover, the low polydispersity indices eliminates the presence of small chains that have the propensity of degrading first and then catalyze the degradation of longer chains.[78]

The degree of exfoliation as the clay loading increases could indeed have an effect, given that the morphology of clay particles has already been shown to influence the properties of the final nanocomposites. Thus, the determination of the exact degree of exfoliation is ambiguous as XRD determinations only focus on an average of the

sample whereas TEM focuses on a small portion of the sample. As such, XRD could not detect small differences between the samples under investigation.

Overall, we propose that the number of attached chains relative to unattached chains, the levels of clay exfoliation, clay distribution and, to some extend, the molar mass, could all have an effect on the thermal stability of the nanocomposites, and, there is a balance between these competing effects. However, it is evident that for the two nanocomposites series investigated here that there is a decrease in thermal stability as clay loading increases, and a concomitant decrease in molar mass.

6.4 Conclusions

Novel positively charged RAFT agents DCTBAB and PCDBAB were successfully anchored onto clay layers and then the modified-clays were subsequently used to control the polymerization of styrene in bulk. The degree of control of polymerization increased with the RAFT/clay content relative to styrene. The degree of conversion was found to decrease as the RAFT/clay loading increased. This was attributed to the presence of clay layers, which increased the viscosity of the system, although this could also be due to an increased retardation brought about by the increased RAFT agent as clay loading increased. The trithiocarbonate system, i.e. DCTBAB-mediated styrene polymerization, resulted in better conversion and control relative to the more retarding dithiocarbonate system, i.e. PCDBAB-mediated styrene polymerization. The thermal stability of the nanocomposites decreased with an increase in clay loading. This behaviour was attributed to two competing effects, i.e. the number of attached chains relative to the unattached chains, and the level of clay exfoliation and clay distribution. The overall thermal stability was found to be only slightly dependent on the molar mass of the polystyrene, which decreased as the clay level increased.

6.5 References

[1] M. Alexandre, P. Dubois. *Mater Sci Eng A* **2000**, *28*, 1-63.

[2] M. Biswas, S. S. Ray. *Adv Polym Sci* **2001**, *155*, 170-221.

[3] M. Okamoto. *Encyclopedia of Nanoscience and Nanotechnology*; American Scientific Publishers: California, 2004.

[4] P. Pinnavaia. *Appl Clay Sci* **1999**, *15*, 11-29.

[5] S. S. Ray, M. Okamoto. *Prog Polym Sci* **2003**, *28*, 1539-1641.

[6] M. Rosorff. *Nano Surface Chemistry*; Marcel Dekker:: New York-Basel, 2002.

[7] S. Sadhu, A. K. Bhowmick. *J Appl Polym Sci* **2004**, *92*, 698-709.

[8] A. Samakande, P. C. Hartmann, V. Cloete, R. D. Sanderson. *Polymer* **2007**, *48*, 1490-1499.

[9] T. D. Fornes, D. L. Hunter, D. R. Paul. *Macromolecules* **2004**, *37*, 1793-1798.

[10] C. I. Park, H. Kim, O. O. Park. *Polymer* **2004**, *45*, 1267-1273.

[11] C. Tseng, J. Wu, H. Lee, F. Chang. *J Appl Polym Sci* **2002**, *85*, 1370-1377.

[12] C. A. Wilkie, J. Zhang. *Polym Degrad Stabil* **2004**, *83*, 301-307.

[13] M. Xu, Y. S. Choi, Y. K. Kim, K. H. Wang, I. J. Chung. *Polymer* **2003**, *44*, 6387-6395.

[14] J. Zhu, A. B. Morgan, F. J. Lamelas, C. A. Wilkie. *Chem Mater* **2001**, *13*, 3774-3780.

[15] W. A. Zhang, D. Z. Chen, H. Y. Xu, X. F. Shen, Y. E. Fang. *Eur Polym J* **2003**, *39*, 2323-2328.

[16] M. Rodlert, C. J. G. Plummer, L. Garamszegi, Y. Leterrier, H. J. M. Grunbauer, J. A. E. Manson. *Polymer* **2004**, *45*, 949-960.

[17] H. G. G. Dekking. *J Appl Polym Sci* **1967**, *11*, 23-26.

[18] X. W. Fan, C. J. Xia, R. C. Advincula. *Langmuir* **2003**, *19*, 4381-4389.

[19] X. W. Fan, C. J. Xia, T. Fulghum, M. K. Park, J. Locklin, R. C. Advincula. *Langmuir* **2003**, *19*, 916-923.

[20] P. Bera, S. K. Saha. *Polymer* **1998**, *39*, 1461-1469.

[21] I. J. Chin, T. Thurn-Albrecht, H. C. Kim, T. P. Russell, J. Wang. *Polymer* **2001**, *42*, 5947-5952.

[22] L. P. Meier, R. A. Shelden, W. R. Caseri, U. W. Suter. *Macromolecules* **1994**, *27*, 1637-1642.

[23] N. Negrete-Herrera, J. L. Putaux, L. David, E. Bourgeat-Lami. *Macromolecules* **2006**, *39*, 9177-9184.

[24] H. G. G. Dekking. *J Appl Polym Sci* **1965**, *9*, 1641-1651.

[25] B. Ray, Y. Isobe, K. Morioka, S. Habaue, Y. Okamoto, M. Kamigaito, M. Sawamoto. *Macromolecules* **2003**, *36*, 543-545.

[26] J. B. Di, D. Y. Sogah. *Macromolecules* **2006**, *39*, 5052-5057.

[27] M. W. Weimer, H. Chen, E. P. Giannelis, D. Y. Sogah. *J Am Chem Soc* **1999**, *121*, 1615-1616.

[28] X. W. Fan, Q. Y. Zhou, C. J. Xia, W. Cristofoli, J. Mays, R. Advincula. *Langmuir* **2002**, *18*, 4511-4518.

[29] R. Advincula, Q. Y. Zhou, Y. Nakamura, S. Inaoka, M. K. Park, Y. F. Wang, J. Mays. *Abstr Pap Am Chem Soc* **2000**, *219*, U498-U498.

[30] P. A. Wheeler, J. Z. Wang, J. Baker, L. J. Mathias. *Chem Mater* **2005**, *17*, 3012-3018.

[31] P. A. Wheeler, J. Z. Wang, L. J. Mathias. *Chem Mater* **2006**, *18*, 3937-3945.

[32] Y. Y. Yang, J. C. Lin, W. T. Yang, G. J. Jiang. *Polym Prepr* **2003**, *44*, 855-856.

[33] P. Ding, M. Zhang, J. Gai, B. Qu. *J Mater Chem* **2007**, *17*, 1117-1122.

[34] J. B. Di, D. Y. Sogah. *Macromolecules* **2006**, *39*, 1020-1028.

[35] N. Salem, D. A. Shipp. *Polymer* **2005**, *46*, 8573-8581.

[36] G. Moad, G. Li, E. Rizzardo, S. H. Thang, R. Pfaendner, H. Wermter. *Polym Prepr* **2005**, *46*, 376.

[37] Y. Zhao, S. Perrier. *Macromolecules* **2007**, *40*, 9116-9124.

[38] W. A. Braunecker, K. Matyjaszewski. *Prog Polym Sci* **2007**, *32*, 93-146.

[39] G. Moad, E. Rizzardo, S. H. Thang. *Aus J Chem* **2005**, *58*, 379-410.

[40] E. Rizzardo, J. Chiefari, R. Mayadunne, G. Moad, S. Thang. *Macromol Symp* **2001**, *174*, 209-212.

[41] J. Chiefari, R. T. A. Mayadunne, G. M. Catherine L. Moad, E. Rizzardo, A. Postma, M. A. Skidmore, S. H. Thang. *Macromolecules* **2003**, *36*, 2273-2283.

[42] B. Y. K. Chong, J. Krstina, T. P. T. Le, G. Moad, A. Postma, E. Rizzardo, S. H. Thang. *Macromolecules* **2003**, *36*, 2256-2272.

[43] S. H. Thang, B. Y. K. Chong, R. T. A. Mayadunne, G. Moad, E. Rizzardo. *Tetrahedron Lett* **1999**, *40*, 2435-2438.

[44] J. Baussard, J. Habib-Jiwan, A. Laschewsky, M. Mertoglu, J. Storsberg. *Polymer* **2004**, *45*, 3615-3626.

[45] A. Samakande, R. D. Sanderson, P. C. Hartmann. *Synthetic Commun* **2007**, *37*, 3861-3872.

[46] G. Levesque, P. Arsene, V. Fanneau-Bellenger, T. Pham. *Biomacromolecules* **2000**, *1*, 400-406.

[47] G. Levesque, P. Arsene, V. Fanneau-Bellenger, T. Pham. *Biomacromolecules* **2000**, *1*, 387-399.

[48] B. Q. Zhang, C. Y. Pan, C. Y. Hong, B. Luan, P. J. Shi. *Macromol Rapid Commun* **2006**, *27*, 97-102.

[49] B. Trathnigg, M. Kollroser. *J Chromatogr A* **1997**, *768*, 223-238.

[50] P. C. Hartmann, P. Dieudonne, R. D. Sanderson. *J Colloid Interface Sci* **2005**, *284*, 289-297.

[51] L. Biasci, M. Aglietto, G. Ruggeri, F. Ciardelli. *Polymer* **1994**, *35*, 3296-3304.

[52] X. Fu, S. Qutubuddin. *Polymer* **2001**, *42*, 807-813.

[53] M. Kawasami, N. Hasegawa, M. Kato, A. Usuki, A. Okada. *Macromolecules* **1997**, *30*, 6333-6338.

[54] S. Perrier, P. Takolpuckdee. *J Polym Sci Part A: Polym Chem* **2005**, *43*, 5347-5393.

[55] A. Favier, M. T. Charreyre. *Macromol Rapid Commun* **2006**, *27*, 653-692.

[56] G. Moad, J. Chiefari, B. Y. K. Chong, Julia Krstina, R. T. A. Mayadunne, A. Postma, E. Rizzardo, S. H. Thang. *Polym Int* **2000**, *49*, 993-1001.

[57] A. Postma, T. P. Davis, G. X. Li, G. Moad, M. S. O'Shea. *Macromolecules* **2006**, *39*, 5307-5318.

[58] Y. S. Choi, I. J. Chung. *Macromol Res* **2003**, *11*, 425-430.

[59] H. M. Jung, E. M. Lee, B. C. Ji, Y. L. Deng, J. D. Yun, J. H. Yeum. *Colloid and Polymer Science* **2007**, *285*, 705-710.

[60] A. Bowes, J. B. McLeary, R. D. Sanderson. *J Polym Sci Part A: Polym Chem* **2007**, *45*, 588-604.

[61] S. Muthukrishnan, E. H. Pan, M. H. Stenzel, C. Barner-Kowollik, T. P. Davis, D. Lewis, L. Barner. *Macromolecules* **2007**, *40*, 2978-2980.

[62] Y. L. Zhao, S. Perrier. *Macromolecules* **2006**, *39*, 8603-8608.

[63] J. B. McLeary. University of Stellenbosch: Stellenbosch, 2004; p 223.

[64] H. De-Brouwer. Eindhoven University of Technology: Eindhoven, 2001; p 219.

[65] B. T. T. Pham, D. Nguyen, C. J. Ferguson, B. S. Hawkett, A. K. Serelis, C. H. Such. *Macromolecules* **2003**, *36*, 8907-8909.

[66] M. Jesberger, L. Barner, M. H. Stenzel, E. M. M, T. P. Davis, C. Barner-Kowollik. *J Polym Sci Part A: Polym Chem* **2003**, *41*, 3847-3861.

[67] F. Gardebien, J. Bre´Das, R. Lazzaroni. *J Phys Chem B* **2005**, *109*, 12287-12296.

[68] A. B. Morgan, J. W. Gilman. *J Appl Polym Sci* **2003**, *87*, 1329-1338.

[69] J. Cui, W. Wang, Y. You, C. Liu, P. Wang. *Polymer* **2004**, *45*, 8717-8721.

[70] A. Bluimstein. *J Polym Sci A* **1965**, *3*, 2665-2673.

[71] J. Wang, J. Du, J. Zhu, C. A. Wilkie. *Polym Degrad Stabil* **2002**, *77*, 249-252.

[72] E. Giannelis. *Adv Mater* **1996**, *8*, 29-31.

[73] J. W. Gilman, T. Kashiwagi, A. B. Morgan, R. H. Harris, L. D. Brassell, M. R. Vanlandingham, C. L. Jackson. *NISTIR 6531* **2000**, 1-55.

[74] G. Chigwada, C. A. Wilkie. *Polym Degrad Stabil* **2003**, *80*, 551-557.

[75] D. Yei, S. Kuo, Y. Su, F. Chang. *Polymer* **2004**, *45*, 2633-2640.

[76] J. Bicerano. *Prediction of Polymer Properties*; Marcel Dekker: New York, 1993.

[77] J. X. Ren, A. S. Silva, R. Krishnamoorti. *Macromolecules* **2000**, *33*, 3739-3746.

[78] E. A. Turi. *Thermal Characterization of Polymeric Materials*, 2nd ed.; Academic Press: San Diego, 1997; Vol. 1.

Chapter 7: Encapsulated clay particles in polystyrene prepared by RAFT-mediated miniemulsion polymerization

The work described in this chapter has been published in the following paper:

Encapsulated clay particles in polystyrene prepared by RAFT-mediated miniemulsion polymerization.

Austin Samakande, Ronald D. Sanderson and Patrice C. Hartmann

J Polym Sci Part A: Polym Chem. 2008, 46, 7114–7126.

Abstract

RAFT grafted montmorillonite (MMT) clays, N,N-dimethyl-N-(4-(((phenylcarbonothioyl)thio)methyl)benzyl)ethanammonium-MMT (PCDBAB-MMT) and N-(4-((((dodecylthio)carbonothioyl)thio)methyl)benzyl)-N,N-dimethylethanammonium-MMT (DCTBAB-MMT), of various loadings were dispersed in styrene (S) monomer and the resultant mixtures emulsified and sonicated in the presence of a hydrophobe (hexadecane) into miniemulsions. The stable miniemulsions thus obtained were polymerized to yield encapsulated polystyrene–clay nanocomposites (PS–CNs). The molar mass and polydispersity index (PDI) of the PS–CNs depended on the amount of RAFT agent in the system, in accordance with the features of the RAFT process. The morphology of the PS–CNs ranged from partially exfoliated to an intercalated morphology, depending on the percentage clay loading. The thermo-mechanical properties of the PS–CNs were better than those of the neat PS polymer, and were dependent on the molar mass, PS–CN morphology and clay loading. The similarities and differences of the PS–CNs prepared here by miniemulsion

polymerization were compared to those prepared using the same RAFT agents and polymer system by bulk polymerization (as reported by us in a previous paper).

7.1 Introduction

Rapid advances in controlled/living polymerization have led to the preparation of polymers with tailored polymer architecture. Various controlled polymerization techniques are available, including: ionic polymerization,[1] stable free-radical polymerization (SFRP),[2] reverse iodine transfer polymerization (RITP),[3-10] atom transfer radical polymerization (ATRP),[11,12] and reversible addition–fragmentation chain transfer (RAFT).[13-17] These techniques differ from each other in their mechanisms of polymerization, the monomers that can be polymerized under controlled conditions, tolerance to impurities, inclusion of inorganic particles, the architectures that can be achieved, and applicability to homogeneous and heterogeneous polymerization conditions. The RAFT technique has been found to be the most robust and versatile to date, hence its tremendous growth since its discovery in the late 1990s.[15,16]

Miniemulsion polymerization offers many advantages over other polymerization methods: it is environmentally friendly; the system has a high heat transfer, which prevents local heat build up; high conversions and high molar masses are achieved; a high solids content can be used; high rates of polymerization are achieved, due to compartmentalization; the viscosity remains low; inorganic particles can be incorporated into the system; it is compatible with highly hydrophobic monomers; and kinetic parameters are easy to predict.[18,19] The many advantages of miniemulsion polymerization over other polymerization methods make it attractive to combine it with controlled polymerization techniques.[20] Hence it is not surprising that the RAFT technique has been applied to miniemulsions.

There are however reports on the shortcomings of the RAFT technique in heterogeneous media such as miniemulsions.[18,21] The leaving group (i.e. R group) of the RAFT agent has been found to desorb out of the growing polymer particles, leading to aqueous phase polymerization (i.e. secondary particle nucleation), loss of control of polymerization and retardation of polymerization. In order to avoid this, use can be made of polymeric RAFT agents with R groups that have very limited solubility in water and thus reduce the exit of the R group to the aqueous phase.[21-24] Amphiphilic RAFT agents can be used, which leads to the partitioning and locking of

the RAFT agent at the water-oil interface and thus minimization of the radical exit.[25] In attempts to tailor-make the hydrophilic-lipophilic balance (HLB) and thus minimize secondary particle nucleation use has been made of polymeric surfactants such as Igepal and Brij.[22] The initiator-derived chains have also been linked to secondary particle nucleation,[26] and to minimize the initiator-derived chains some researchers used aqueous phase radical traps.[27,28] Recently, several reports claimed the anomalies in the RAFT-mediated miniemulsions to be due to a super-swelling effect.[29-33] Super-swelling leads to phase separation and, in some cases, coagulation. In order to avoid this many researchers propose the use of higher levels of surfactants and hydrophobe, use of non-ionic surfactants and careful choice of a suitable RAFT agent.[29,31,32,34] All these factors are claimed to lead to a better miniemulsion stability, an increase in polymerization rate, control of the polymerization process, and narrow particle size distributions.[29]

Due to miniemulsions' compatibility with hydrophobic species it can be used for the synthesis of polymer–clay nanocomposites(PCNs) using modified-clays, which will result in the clay particles being encapsulated inside the polymer particles.[35] Clay particles are layered materials that occur naturally and synthetically, in good purity. The surfaces of clay platelets are negatively charged and hydrated alkali or alkaline earth metals counterbalance the negative charges. These countercharge balancing cations reside between the clay platelets, in a region commonly known as the intergallery region. The distance between adjacent clay platelets is known as the interlayer distance, or the *d* spacing. The weak van der Waals forces that hold the clay platelets together allows adjacent clay platelets to move away from each other to accommodate alien species in-between the clay galleries. This results in variations in the *d* spacing, depending on the size of the species that is present in-between the clay layers. The presence of inorganic hydrated cations in-between the clay platelets makes the clays in their natural state miscible with only hydrophilic species. However, for the compatibility of clay with hydrophobic species (polymers); the hydrated cations are replaced by organic cations thus making the clay hydrophobic and hence compatible with hydrophobic species. The organic cations that can replace the hydrated alkali or alkaline earth metals include conventional cationic surfactants and/or functional cationic surfactants.[36-38]

Our findings,[37] and those of many other research groups,[39,40] have however, shown that the use of simple organic cations in the modification of clay layers, and the

subsequent use of the modified-clays in the preparation of nanocomposites, results in PCNs with only moderately enhanced properties e.g. thermo-mechanical. For exceptional property enhancement, functional surfactants are required. These include polymerizable surfactants (surfmers), initiator surfactants (inisurfs) and transfer surfactants (transurfs). These participate in the polymerization process and lead to chains becoming attached to clay layers and, in most cases, exfoliated PCNs, i.e., the individual clay layers/platelets are randomly distributed within the polymer matrix.[37,39,40]

Our research group has been investigating the use of functional surfactants for the modification of clay and the resultant PCNs properties.[37,41] we have shown the effectiveness of surfmers in the preparation of exfoliated nanocomposites with enhanced properties. Lately the focus has been on the use of transurfs in particular functionalized RAFT agents, which can attach to clay layers as well as control the polymerization process.[42] The attachment of RAFT agents onto clay layers leads to polymer growth from the surfaces of the clay layers in accordance with the RAFT mechanism. Together with other researchers we have reported on the use of these attached RAFT agents in bulk.[42-45]

In this chapter we now report, for the first time, on the use of these clay-anchored RAFT agents in miniemulsion polymerization. We intend to show that the use of the attached RAFT agents minimizes exit problems of the R group to the aqueous phase, i.e., there is little radical exit to the aqueous phase and moreover, that there is no phase separation when the RAFT agents are attached to clay platelets, due to little or no super-swelling effect, and thus close to monomodal polymer particle size distribution is achieved. We also report on the thermo-mechanical properties of the PS–CNs and compare our findings to the molar mass, clay morphology and clay loading of PS–CNs prepared by miniemulsion polymerization to previous results that we obtained for PS–CNs prepared by bulk polymerization.[42]

To date, there are no reports in the open literature on the use of RAFT agents anchored onto clay platelets in miniemulsion, other than reports on uncontrolled radical polymerization techniques.[35,46,47] Reports on the use of RAFT agents attached to spherical and flat surfaces, and other controlled radical techniques such as ATRP and SFRP in various homogeneous and heterogeneous polymerization media, are however available.[2,12,48-63]

We hypothesize that the use of an anchored RAFT agent will result in controlled living radical polymer growth from the clay surface, as we have already shown in bulk polymerization.[42] This will lead to polymer chains attached to the clay platelets. A strong interfacial region between the polymer and the clay platelets has been reported to result in enhancement of the thermo-mechanical properties.[64,65] Reports on the thermo-mechanical properties of PCNs have shown that an increase in clay loading results in better properties, and an exfoliated structure also generally gives better properties.[64,65]

The successful encapsulation of clay platelets inside polymer particles could lead to materials with niche applications in areas such as paints and coatings, and in biomedical applications where controlled drug delivery is essential.[66]

7.2 Experimental

7.2.1 Reagents

Styrene (99%, Aldrich) was purified by washing with aqueous 0.3M KOH, followed by distillation at 40 ºC under reduced pressure. Sodium dodecyl sulphate (SDS) (99%, Aldrich), hexadecane (99%, Aldrich), and azo*bis*isobutyronitrile (AIBN) were obtained from Aldrich. AIBN was purified by recrystallization from methanol. Sodium montmorillonite (Na-MMT) was obtained from Southern Clay Products (Texas, USA). Deionized water was obtained from a Millipore Milli-Q-purification water system. *N*,*N*-dimethyl-*N*-(4-(((phenylcarbonothioyl)thio)methyl)benzyl)-ethanammonium bromide (PCDBAB), *N*-(4-((((dodecylthio)carbonothioyl)thio)-methyl)benzyl)-*N*,*N*-dimethyletha-nammonium bromide (DCTBAB), PCDBAB-MMT and DCTBAB-MMT were prepared as we described in previous chapters.[42,67]

7.2.2 Typical preparation of PS–CNs using RAFT-mediated free-radical miniemulsion polymerization

Predetermined quantities of modified-clay (RAFT-MMT), AIBN, styrene and hexadecane (oil phase) were stirred together overnight in a three-neck round-bottomed flask to allow effective swelling of the clay galleries by the monomer. An aqueous solution of SDS (water phase) was added to the oil phase and the mixture stirred for a further 30 min in order to obtain a pre-emulsion. The pre-emulsion was then sonicated for 30 min using a Sonics Vibra Cell Autotune series 750VCX high intensity ultrasonic processor, in a water jacketed vessel. The amplitude was set at 90%, and the temperature cut off for the probe set at 40 ºC. The average energy

expended was ~180 kJ. The flask containing the resultant miniemulsion was then immersed in an oil bath. The flask was fitted with a condenser, a nitrogen gas inlet and a septum. The content of the flask was then nitrogen purged for 30 min before the temperature was raised rapidly to 75 ºC to start the polymerization. The polymerization was carried out for 6 h at 75 ºC. Samples were periodically extracted from the reaction mixture, through the septum, and the conversion determined gravimetrically.

A similar procedure was used for the synthesis of clay-free RAFT-mediated styrene by miniemulsion polymerization, the only difference being that the oil and the water phases were mixed after having been stirred separately for 1 h.

7.2.3 Analyses

7.2.3.1 Size-exclusion chromatography (SEC)

SEC was carried out using a Waters 600E system controller equipped with a Waters 610 fluid unit pump and a Waters 410 differential refractometer as detector. Prior to SEC analysis, the samples were reverse ion-exchanged as follows. Quantities of PS–CN (0.2 g) and LiCl (0.06 g) were dissolved in THF (10 ml) and boiled under reflux at 70 ºC for 3 h. The solution was filtered through Celite and thereafter the polymer was precipitated in methanol and dried. SEC analysis, using THF as mobile phase and an initial polymer concentration of 5 mg/mL, was performed on the clay-free polymer solutions. Dynamic light scattering (DLS) of the polymer in THF showed no peak/s characteristic of clay particles, thus proving that the chains were completely detached from the clay particles prior to SEC analysis.

7.2.3.2 Small angle X-ray scattering (SAXS)

SAXS measurements were performed in a transmission configuration at 298 K. A copper rotating anode X-ray source (functioning at 4 kW) with a multilayer focusing 'Osmic' monochromator giving high flux (10^8 photons/sec) and punctual collimation was used. An 'image plate' 2D detector was used. Scattering patterns were obtained, giving diffracted intensity as a function of the wave vector q. The calculation of q values is described elsewhere.[68]

7.2.3.3 Transmission electron microscopy (TEM)

TEM was used to directly visualize the morphology of the clay particles in PS–CNs at the nanometer level. Bright field TEM images were recorded using a LEO 912

transmission electron microscope, at an accelerating voltage of 120 kV. Prior to analysis, miniemulsion samples were diluted with water and then placed on 300-mesh copper grids, which were then transferred to the TEM machine. A portion of the PS–CN miniemulsion samples were dried and then embedded in epoxy resin and cured for 24 h at 60 ºC. The embedded samples were then ultra-microtomed with a diamond knife on a Reichert Ultracut S ultra microtome at room temperature. This resulted in sections with a nominal thickness of ~100 nm. The sections were transferred from water at room temperature to 300-mesh copper grids, which were then transferred to the TEM apparatus.

7.2.3.4 Thermogravimetric analysis (TGA)

TGA measurements were carried out on a TA instruments Q500 thermogravimetric analyzer. Samples of less than 15 mg were used for all analyses. They were analyzed from ambient temperature to 600 ºC at a heating rate of 20 ºC/min. All TGA analyses were carried out under a nitrogen atmosphere. Nitrogen was purged at a flow rate of 50 ml/min.

7.2.3.5 Dynamic mechanical analysis (DMA)

DMA measurements were carried out under nitrogen atmosphere, using a Perkin Elmer DMA 7e instrument that employs a parallel plate measuring system equipped with a 1-mm probe. Polymer samples were pressed into discs by using a hydraulic press. The discs were then taken for DMA analysis as follows, cooling to –20 ºC for 1 min, and then the temperature raised to 200 ºC at a heating rate of 5 ºC/min and a frequency of 1 Hz while recording the mechanical properties.

7.2.3.6 Dynamic light scattering (DLS)

DLS was used to determine the particle size. A Zeta sizer ZS 90 (Malvern Instruments, United Kingdom) was used. Miniemulsion samples were first diluted with deionized water before they were analyzed.

7.3 Results and discussion

7.3.1 Polymer matrix characterization

The formulations used for polymerization of PS–CNs are tabulated in Table 7.1.

The polymerization process resulted in high conversions in relatively short time relative to *in situ* intercalative bulk polymerization systems.[42] This is a direct result of the compartmentalization phenomenon,[47] where the average number of radicals of the whole system is greater than that in the bulk system. However, the conversion generally decreased with an increase in clay loading (c.f. Fig. 7.1).

Table 7.1. Initial quantities of reagents used in the miniemulsions to prepare polystyrene–clay nanocomposites

Polymer	*RAFT (g)*	*MC (g)*	*S (g)*	*AIBN (g)*	*SDS (g)*	*HD (g)*
PS-D-St	0.085	-	7.022	0.014	0.176	0.355
PS-D-1		0.07	7.015	0.005	0.178	0.351
PS-D-2		0.149	7.038	0.011	0.177	0.353
PS-D-3		0.253	7.001	0.018	0.176	0.354
PS-D-5		0.349	7.000	0.022	0.178	0.352
PS-P-St	0.080	-	7.035	0.017	0.115	0.352
PS-P-1		0.070	7.000	0.003	0.117	0.351
PS-P-2		0.140	7.011	0.009	0.116	0.353
PS-P-3		0.253	7.002	0.014	0.118	0.362
PS-P-5		0.350	7.012	0.017	0.117	0.354

Key: MC = modified-clay, S = styrene monomer, SDS = sodium dodecyl sulphate and HD = hexadecane

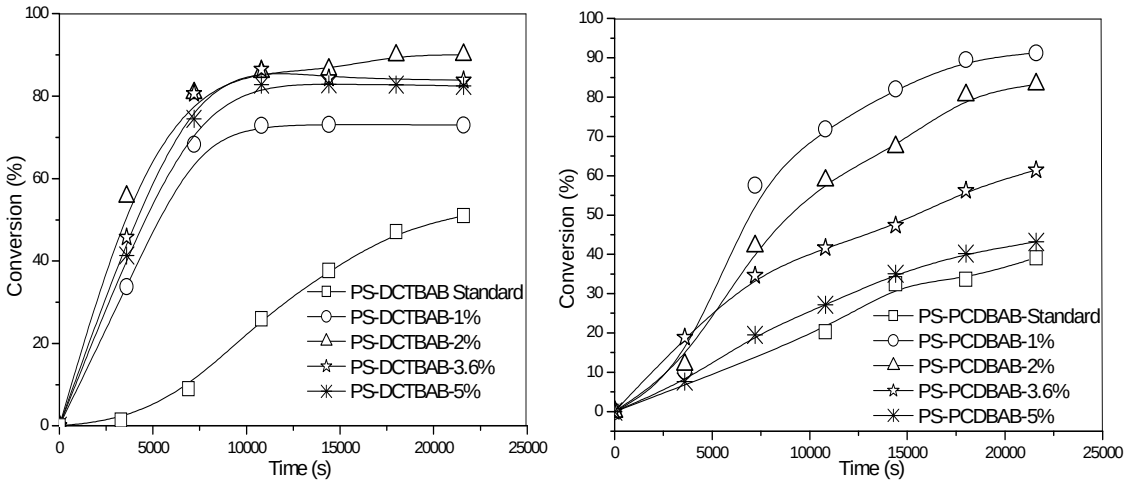

Fig. 7.1 Conversion (%) against time plots for the nanocomposites prepared.

The phenomenon of a decrease in conversion with increased clay loading has been reported before.[42,69] According to Bon *et al.,*[47] when a radical is incident on a clay surface it reacts irreversibly with the functionalities there, hence the more clay layers there are the greater are the chances of termination. (They did however not give details of the species on the clay surface that were involved in the termination process). Our findings are however in disagreement with those of other researchers, who observed no change in conversion with an increase in clay loading,[35,70]

although it should be noted that they used uncontrolled radical polymerization whereas we used a controlled radical polymerization approach.

On the other hand, the presence of the RAFT agent on the clay surfaces was found to affect the polymerization process. As shown in Fig. 7.1, the non-clay-containing RAFT standards reached lower conversions. Retardation, side reactions and inhibition are some of the reasons for the slow polymerization progress in RAFT-mediated polymerization reactions.[22,71] Luo *et al*.,[30] observed a decreasing polymerization rate with increasing RAFT agent concentration. In our present case studies, retardation was more pronounced for dithiobenzoate (PCDBAB) mediated systems than for trithiocarbonate (DCTBAB) mediated systems.[71,72] This is in agreement with the findings of Yang *et al*.,[29] who also proposed that the extent of polymerization retardation is a function of the RAFT agent type.

The molar masses, polydispersity indices and T_g values of the nanocomposites that were prepared by us are tabulated in Table 7.2.

Table 7.2. Molar masses, polydispersity indices and T_g values of PS–clay nanocomposites

Polymer	$\frac{[MC]_0}{[S]_0}$ %	$\frac{[S]_0}{[R]_0}$	*Calc Mn (g/mol)*	*Exp Mn (g/mol)*	*PDI*	**Tg*
PS-D-St	-	425.76	23 082	55 935	1.40	85.83
PS-D-1	1.00	1424.08	104 057	149 521	1.70	88.60
PS-D-2	2.00	709.37	74 047	114 366	1.44	96.90
PS-D-3	3.61	393.17	34 717	55 955	1.40	102.00
PS-D-5	4.99	285.02	24 934	45 044	1.39	102.34
PS-P-St	-	346.70	14 486	35 456	1.53	86.75
PS-P-1	1.00	1302.58	119 277	106 185	1.73	91.87
PS-P-2	2.00	651.29	51 839	65 247	1.56	98.15
PS-P-3	3.61	360.40	22 375	47 306	1.59	104.62
PS-P-5	5.00	260.52	11 602	27 057	1.54	105.87

Key: PS-D- and PS-P- are abbreviations for PS–DCTBAB- and PS–PCDBAB-clay nanocomposites respectively. $\frac{[MC]_0}{[S]_0}$ initial mass ratio of modified-clay to styrene; $\frac{[S]_0}{[R]_0}$ initial molar ratio of styrene to RAFT, *Calc* M_n = theoretical mass calculated using the Equation $M_n = \frac{[S]_0 M_S x}{[RAFT]_0} + M_{RAFT}$,[73] where $[S]_0$ = initial styrene concentration, M_S = molecular weight of styrene, x = conversion, M_{RAFT} = molecular weight of RAFT, $[RAFT]_0$ = initial concentration of RAFT; Exp M_n = experimental molecular mass; *PDI* = polydispersity indices of the polymer obtained, as determined by SEC. *Tg = glass transition temperature as measured using DMA.

An increase in clay loading resulted in a decrease in molar mass. This was expected, as the concentration of RAFT agent increases with the amount of RAFT-modified-clay incorporated. It is an established fact that an increase in RAFT agent concentration results in a decrease in molar mass. The PDI values reached

asymptotic values of 1.5 and 1.4 respectively, as the clay loading increased for the PCDBAB-and DCTBAB-mediated polymerizations. The higher PDIs recorded at low clay loadings and concomitantly low RAFT concentrations are mainly attributed to the fact that our system is highly heterogeneous. The monomer is emulsified in the water system and the modified-clay on which the RAFT is anchored is suspended in the monomer phase. Thus the RAFT is not homogeneously distributed in the monomer phase; there are regions of high and low RAFT agent concentration.[20,42] Hence the probability of a growing polymeric radical to encounter a RAFT molecule, and thus control of polymerization, increases with an increase in clay loading, i.e., an increase in RAFT agent concentration. Di and Sogah observed this phenomenon in their dithiocarbamate-anchored RAFT-mediated bulk polymerizations.[43] They found that the PDI values increased at low clay levels and molar masses were higher than expected. They attributed their findings to a low transfer efficiency of the attached RAFT system, although the efficiency was found to increase as the clay loading increased.[43] Pham *et al*.,[23] who studied a non-clay-containing system, observed a similar decrease in PDI as the RAFT concentration increased.

In our present study, the best control is achieved at about 2% clay loadings, which seems to be the threshold clay concentration at which good control starts to be observed. Another possible reason for the loss of control at very low clay loadings could arise from the fact that at high molar masses the efficiency of addition and fragmentation of the RAFT agent is sterically reduced. On a closer look at the two systems it is seen that the DCTBAB system shows better control than the PCDBAB system.

Our earlier observations made for bulk polymerization,[42] agree well with the results presented here. Under bulk polymerization, conversion also decreased with an increasing clay loading. Similar PDI trends were also seen, although lower PDI values were recorded for bulk system. An initiator was used for miniemulsion polymerization whereas thermal initiation was used for bulk polymerization. Use of initiator leads to the presence of initiator derived chains for miniemulsion, thus higher PDI values will result. The differences between the two systems in terms of the theoretical and the observed Mn values are, attributed to the low efficiency and availability of the bound RAFT agents.[24]

7.3.2 PS–CN colloidal miniemulsion and morphological characterization

The particle size of the PS–CN miniemulsion lattices increased as the clay loading increased. An increase in clay content implies that more space is required to accommodate the swelling clay within the polymer particle. Fig 7.2 shows the evolution of particle size as the clay loading increases, as measured by DLS.

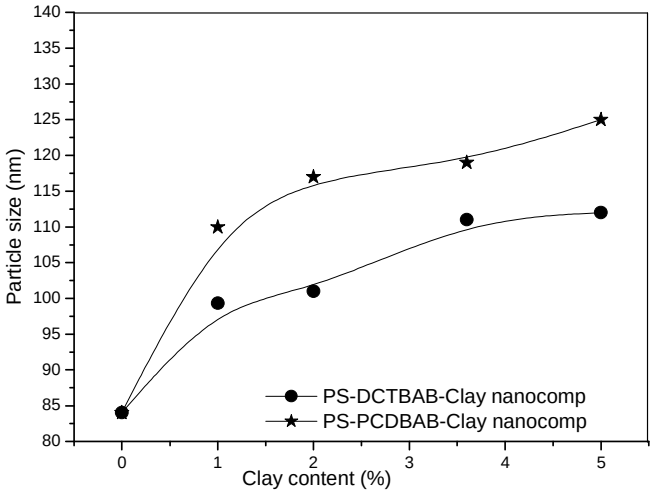

Fig. 7.2 Particle sizes of the nanocomposites as a function of clay loading (clay content %).

The PCDBAB system had greater polymer particle size values compared to the DCTBAB system. This may be because a slightly lower amount of surfactant was used in the PCDBAB than in DCTBAB. More surfactant in a miniemulsion system results in smaller polymer particle size.[19,74] More SDS was used because DCTBAB-MMT clay is very hydrophobic and difficult to emulsify. The particle sizes of the latices obtained did not change over a period of six months, which illustrated the stability of the PS–CNs latices prepared.

The particle sizes as determined by DLS analysis were further confirmed by TEM analysis (c.f. Fig 7.3). However, the particle sizes of the miniemulsions as measured by TEM were found to be slightly smaller than those determined by DLS. This difference was however, attributed to the different modes of analysis between the two techniques, as the same trends in particle sizes were nonetheless obtained.

The TEM images in Fig 7.3 show that the particle size distribution is fairly narrow, which is an indication that little to no secondary particle nucleation occurred during the polymerization process. This was expected in our system for the following two reasons. First, the clay layers form a physical barrier and make it difficult for species, e.g. growing radicals, to be transported towards the particle surface prior to the exit

into the water phase. Second, most of the R groups are electrostatically bound to the clay surfaces, which prevents them from escaping into the continuous aqueous phase. Moreover, there was little or no super-swelling effect, given that the clay layers are excellent physical barriers and thus effectively prevent any monomer diffusion to other particles.

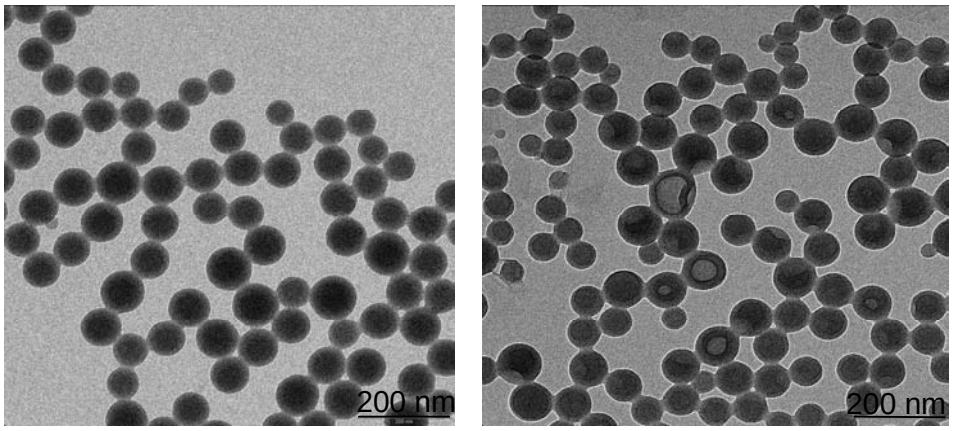

Fig. 7.3 TEM images of PS–PCDBAB-2%-MMT clay nanocomposite (left) and PS–DCTBAB-2%-MMT clay nanocomposite (right).

In addition, a higher level of hexadecane than normally used in literature was used in all the experiments, which further reduced any super-swelling effect.[29,31,32] Thus there was no loss of colour and no appearance of a coloured layer (at the top of the reaction vessel), commonly reported in RAFT-mediated free-radical polymerization in miniemulsion.[34,75]

However, as clay loading increased a few small particles started to appear (c.f. Fig 7.4). The appearance of these secondary particles was attributed to initiator derived chains emanating from a small amount of AIBN that dissolves in the aqueous phase. The AIBN concentration was increased as the clay/RAFT level increased in order to maintain a constant $[RAFT]_0/[AIBN]_0$ ratio. On the other hand, an appreciable number of secondary particles were observed in the case of the clay-free RAFT-mediated miniemulsion. There are many possible reasons for this including super-swelling effect, initiator derived chains and R group exit. The exit of the R group and super-swelling affects possibilities are however unlikely because we used ionic and bound R groups, and a higher level of the hydrophobe limits the radical exit and the super-swelling effect.[25,29]

Surprisingly, the clay platelets could not be observed in the nanocomposites of PS by TEM analysis (c.f. Fig 7.3). Even when 11% of hexadecane was used during the

polymerization and core shell morphologies were observed, the clay particles were still not visible (c.f. Fig.7. 4).

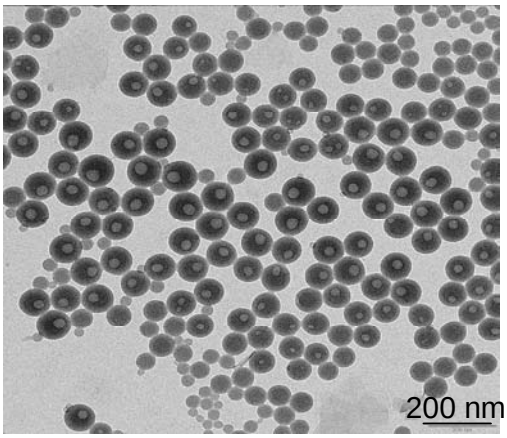

Fig. 7.4 TEM image of the miniemulsion latex of PS–PCDBAB-3.6%-MMT nanocomposite with 11% hydrophobe.

As hexadecane phase separates, when used in high quantities, in polystyrene,[76] we had hoped that some of the clay platelets would become visible on the hexadecane-polystyrene interface, but this did not happen.

However the clay platelets did became visible in TEM images when dried latices were embedded into epoxy resin (c.f. Fig. 7.5). Furthermore, most of the clay platelets (Fig. 7.5 left and right) were of intercalated morphology, with the exception of some areas that contained a few exfoliated clay platelets.

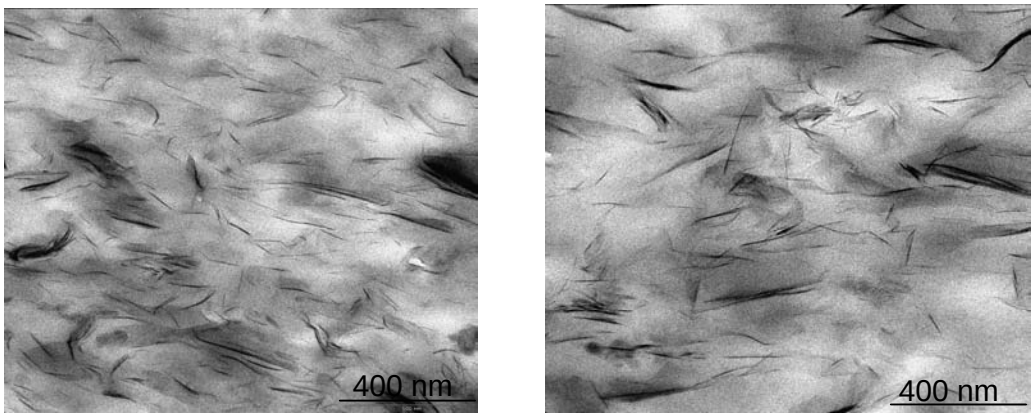

Fig. 7.5 TEM pictures of PS–PCDBAB-3.6%-MMT clay nanocomposite (left) and PS–DCTBAB-3.6%-MMT clay nanocomposite (right).

The SAXS patterns of the nanocomposites were in agreement with our expectations namely, that the morphology of the nanocomposites changes as the molar mass decreases, whilst the clay loading increases. Fig 7.6 shows SAXS patterns of the PS–CNs. There are broad peaks at low clay loadings, which is an indication of partial

exfoliation. This is in agreement with the TEM results. At higher clay loadings (i.e. 5% clay loading), more defined peaks, although still broad which are characteristic of intercalated morphology, were observed.

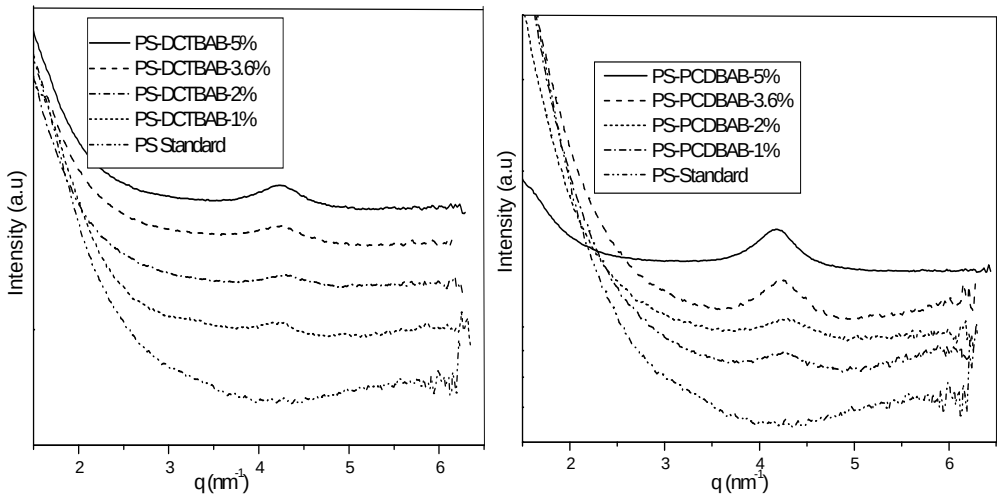

Fig. 7.6 SAXS patterns of PS–CNs.

7.3.3 Thermal stability

Fig. 7.7 shows the TGA thermograms of PS–DCTBAB- and PS–PCDBAB-clay nanocomposites. PS does not contain volatile products below 300 °C, but random main chain scission occurs in this temperature range. Above 300 °C volatile products comprising monomer and oligomers begin to form. Early degradation has been attributed to labile chain ends.[77] Only a slight improvement in the thermal stability of PCNs was observed above 50% degradation relative to the neat polymer standard (see Fig 7.7). Jan *et al.*[78] also reported that epoxy-clay nanocomposites only showed enhanced thermal stability from 40–50% weight degradation. The thermal stability of PS–CNs was also found to increase slightly when the clay loading increased. This is in accordance with literature.[37,39,70,79-83]

The formation of clay char, which acts as a mass transport barrier and insulator between the polymer and the superficial zone where the polymer decomposition takes place, is the cause of the improvements in the thermal stability of the nanocomposites.[37,80,83,84] Concurrently, the restricted thermal motion of the polymer chains localized in the clay galleries can also bring about thermal stability improvements.[37,85]

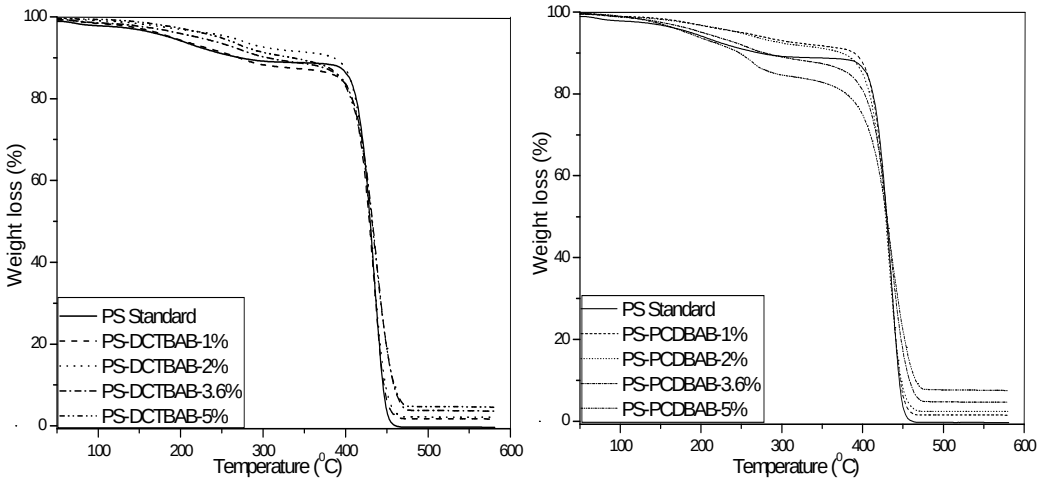

Fig. 7.7 TGA thermograms of PS–DCTBAB-clay nanocomposites (left) and PS–PCDBAB-clay nanocomposites (right).

The labile thio-carbonyl-thio moeity is also believed to play a role in the thermal stability of the PCNs. We found that PCNs made using DCTBAB are more stable, especially in the 200–300 ^{0}C region where degradation starts to occur, than PCNs made using PCDBAB. This temperature range coincides with that used by Postma *et al.* for the removal of the thio-carbonyl-thio group from polymers by thermolysis.[86]

Surprisingly, the results we obtained in miniemulsion polymerization were not the same as those we obtained in bulk.[42] For bulk polymerization, it was observed that an increase in clay loading led to a decrease in thermal stability. The reasons for the discrepancies are not exactly known, but it is suggested that the differences in the clay exfoliation in the two systems, the ratio of clay attached to unattached polymer chains, and the end group effect (i.e. no initiator was used for bulk polymerization whereas AIBN was used in miniemulsion), all play a part in thermal stability.

7.3.4 Mechanical properties

The dynamic mechanical properties (DMA) of the dried samples showed that all the nanocomposites had enhanced storage moduli in the glassy state relative to the neat polymer standard (see Fig 7.8).

The enhancement in storage modulus is caused by the high aspect ratio of the dispersed clay platelets and the interaction between polymer chains and clay layers. This results in a decrease in the polymer segments' mobility near the polymer-clay interface.[87] However, within the two series of nanocomposites, the storage modulus was seen to decrease with an increase in clay loading, save for the DCTBAB-2%

clay loading that has a slightly higher storage modulus in the glassy state than for the DCTBAB-1% clay loading.

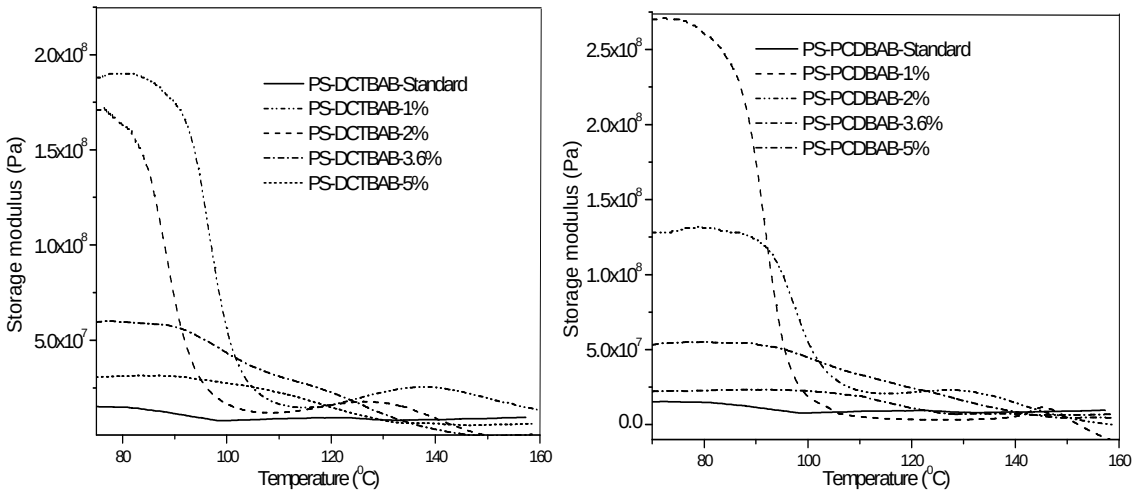

Fig. 7.8 Storage modulus as a function of temperature of PS–DCTBAB-clay nanocomposites (left) and PS–PCDBAB-clay nanocomposites (right), at 1, 2, 3.6, and 5% clay loadings.

These results differ from those of other researchers, who observed an increase in storage modulus with increasing clay loading.[39,88-90] The difference between their findings and ours is mainly attributed to the fact that in their systems they either used polymers of the same molar mass and varied the clay loading alone, or they used uncontrolled radical polymerization which normally yields high molar mass polymers. In our study, the two main factors that contribute to a decrease in the storage modulus as the clay loading increase are: (i) a decrease in the molar mass and (ii) a change in the nanocomposite morphology from semi-exfoliated to intercalated as the percentage clay increases.[80] Figure 7.8 also shows that at 3.6 and 5% clay loadings the transition of the storage modulus from the glassy state to the rubbery state is relatively broad. This is attributed to the presence of nanoclay within the polymer matrix.[77] The broad peaks are also seen in Fig. 7.9, which shows the changes in the loss modulus with temperature. The maximum points of the loss modulus peaks were used for the measurement of the glass transition temperature (T_g) as opposed to the normally used tan delta peak, which overestimates the value.[77] The T_g data are tabulated in Table 7.2

The T_g value is affected by the molar mass,[91,92] presence of plasticizers, crosslinking density and filler content. T_g increases with increasing M_n up to a certain value of M_n above which the T_g becomes invariable with the molar mass.

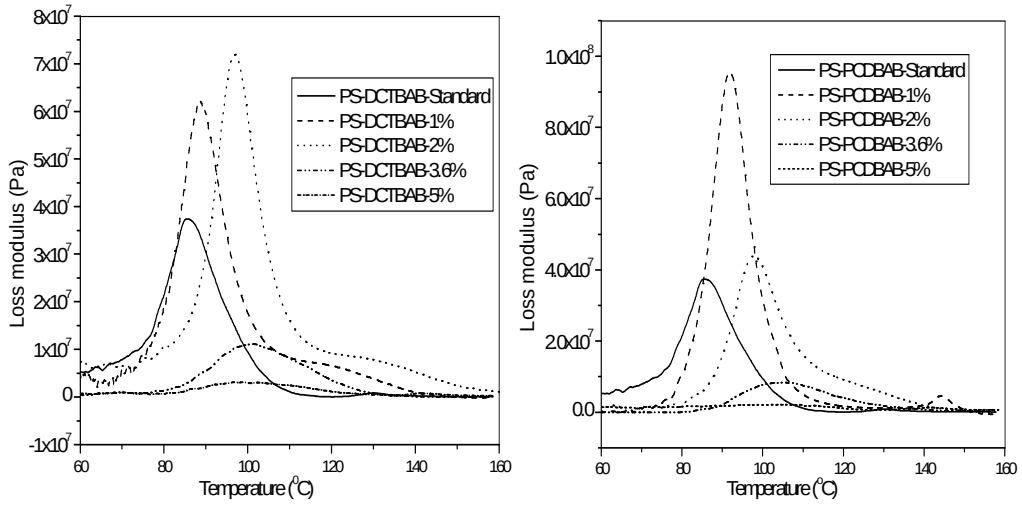

Fig. 7.9 Loss modulus as a function of temperature for PS–clay nanocomposites, DCTBAB and PCDBAB respectively at 1, 2, 3.6, and 5% clay loading.

The increase of the T_g with increasing molar mass is due to a reduction of the relative number of polymer chain ends.[91] In the two nanocomposites series that we studied T_g was seen to increase with increasing clay loading, regardless of the fact that the molar mass was decreasing (c.f. Table 7.2). Thus the contribution of the clay nanofiller outweighed the opposing molar mass effect. An increase in T_g with an increasing clay loading has also been reported in literature.[83,88] Moreas *et al*.[35] reported that the clay addition did not alter the T_g of their polystyrene-co-butyl acrylate nanocomposites. On the other hand, Fu and Qutubuddin,[39] reported a decrease in T_g with an increase in clay loading, which they attributed to a decrease in molar mass. In our system we used a controlled free-radical polymerization approach, which eliminates the presence of low molar mass or even oligomeric chains, which adversely reduces the T_g. The slightly lower T_g of DCTBAB relative to PCDBAB is attributed to the plasticizing effect of the slightly higher surfactant amount used in the DCTBAB system.

Fig 7.10 shows variation of tan δ with temperature. The tan δ peak is associated with partial loosening of the polymer structure so that small groups and chain segments can move. In the phase transition zone tan δ measures imperfections in the elasticity of a material.

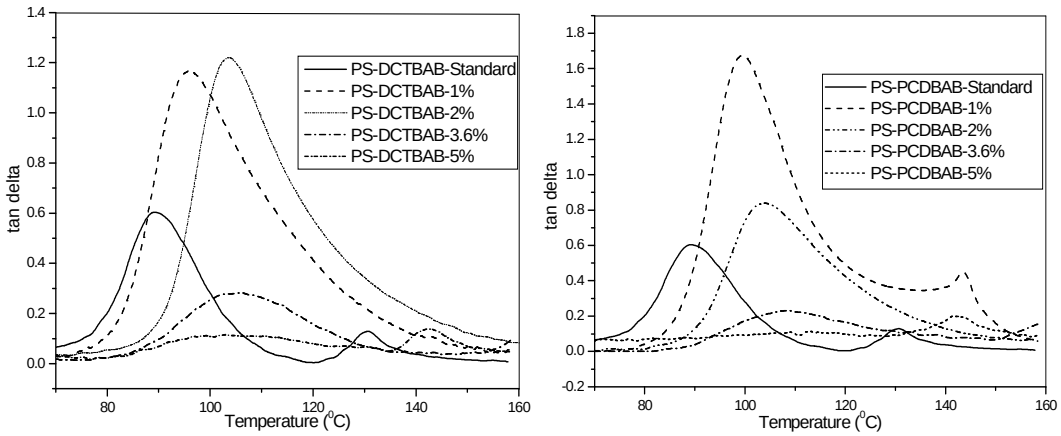

Fig. 7.10 Tan δ as a function of temperature for PS–clay nanocomposites, DCTBAB and PCDBAB at 1, 2, 3.6 and 5% clay loading.

Peak broadening and a shift of the tan δ peaks of the nanocomposites to higher temperatures relative to polystyrene standards were recorded. These shifts are a result of the restricted chain mobility brought about by the clay filler.[93,94] The peak broadening effects are more pronounced for the low clay loadings. i.e. 1% and 2%. The level of peak broadening is directly attributed to the different levels of exfoliation and the higher PDI occurring at low clay loadings.

7.4 Conclusions

Encapsulated PS–DCTBAB-clay nanocomposites and PS–PCDBAB-clay nanocomposites were successfully synthesized by RAFT-mediated miniemulsion polymerization. The RAFT agents that were successfully anchored onto the clay controlled the polymerization process. The miniemulsion polymerization process resulted in polymers with decreasing molar mass and low polydispersity indices as the RAFT concentration increased, as expected for RAFT-mediated polymerization. Because the R groups of the RAFT agents were electrostatically bound to the clay platelets, the occurrence of radical exit to the aqueous phase was significantly hindered. Radical exit was further minimized by the clay platelets that act as physical barriers preventing radical exit. This resulted in relatively narrow PS particle size distribution. The nanocomposites were of partially exfoliated morphology at low clay loadings, and changed to intercalated morphology as the clay loading increased. The change in morphology was attributed to the decreasing molar mass and the increasing clay loading. Changes in morphology manifested themselves in the thermo-mechanical properties, which were found to depend on the molar mass, PS–CN morphology and clay loading.

7.5 References

[1] M. Szwarc. *J Polym Sci Part A: Polym Chem* **1998**, *36*, IX-XV.

[2] C. Konn, F. Morel, E. Beyou, P. Chaumont, E. Bourgeat-Lami. *Macromolecules* **2007**, *40*, 7464-7472.

[3] C. Boyer, P. Lacroix-Desmazes, J. J. Robin, B. Boutevin. *Macromolecules* **2006**, *39*, 4044-4053.

[4] P. Lacroix-Desmazes, R. Severac, B. Boutevin. *Macromolecules* **2005**, *38*, 6299-6309.

[5] P. Lacroix-Desmazes, R. Severac, B. Otazaghine, B. Boutevin. *Abstr Pap Am Chem Soc* **2003**, *226*, U398-U398.

[6] B. Nottelet, P. Lacroix-Desmazes, B. Boutevin. *Polymer* **2007**, *48*, 50-57.

[7] J. Tonnar, P. Lacroix-Desmazes, B. Boutevin. *Abstr Pap Am Chem Soc* **2005**, *230*, U4126-U4126.

[8] J. Tonnar, P. Lacroix-Desmazes, B. Boutevin. *Macromol Rapid Commun* **2006**, *27*, 1733-1738.

[9] J. Tonnar, P. Lacroix-Desmazes, B. Boutevin. *Macromolecules* **2007**, *40*, 6076-6081.

[10] J. Tonnar, P. Lacroix-Desmazes, B. Boutevin. *Macromolecules* **2007**, *40*, 186-190.

[11] H. Y. Zhao, D. A. Shipp. *Chem Mater* **2003**, *15*, 2693-2695.

[12] L. Bombalski, K. Min, H. C. Dong, C. B. Tang, K. Matyjaszewski. *Macromolecules* **2007**, *40*, 7429-7432.

[13] W. A. Braunecker, K. Matyjaszewski. *Prog Polym Sci* **2007**, *32*, 93-146.

[14] A. Favier, M. T. Charreyre. *Macromol Rapid Commun* **2006**, *27*, 653-692.

[15] G. Moad, E. Rizzardo, S. H. Thang. *Aus J Chem* **2005**, *58*, 379-410.

[16] G. Moad, E. Rizzardo, S. H. Thang. *Aust J Chem* **2006**, *59*, 669-692.

[17] S. Perrier, P. Takolpuckdee. *J Polym Sci Part A: Polym Chem* **2005**, *43*, 5347-5393.

[18] H. Matahwa, J. B. McLeary, R. D. Sanderson. *J Polym Sci Part A: Polym Chem* **2006**, *44*, 427-442.

[19] K. Landfester. *Annu Rev Mater Res* **2006**, *36*, 231-279.

[20] A. Butte´, G. Storti, M. Morbidelli. *Macromolecules* **2001**, *34*, 5885-5896.

[21] J. B. McLeary, M. C. Hermant, H. Matahwa, B. Klumperman, R. D. Sanderson. *Abstr Pap Am Chem Soc* **2005**, *230*, U4238-U4238.

[22] A. Bowes, J. B. McLeary, R. D. Sanderson. *J Polym Sci Part A: Polym Chem* **2007**, *45*, 588-604.

[23] B. T. T. Pham, D. Nguyen, C. J. Ferguson, B. S. Hawkett, A. K. Serelis, C. H. Such. *Macromolecules* **2003**, *36*, 8907-8909.

[24] We. Uzulina, N. Gaillard, A. Guyot, J. Claverie. *C. R. Chimie* **2003**, *6*, 1375-1384.

[25] H. J. Lee, J. M. Lee, S. E. Shim, B. H. Lee, S. Choe. *Polymer* **2005**, *46*, 3661-3668.

[26] C. Autran, J. C. De La Cal, J. M. Asua. *Macromolecules* **2007**, *40*, 6233-6238.

[27] Y. W. Luo, F. J. Schork. *J Polym Sci Part A: Polym Chem* **2002**, *40*, 3200-3211.

[28] P. J. Blythe, E. D. Sudol, M. S. Elaasser. *J Polym Sci Part A: Polym Chem* **1997**, *35*, 807-811.

[29] L. Yang, Y. W. Luo, B. G. Li. *Polymer* **2006**, *47*, 751-762.

[30] Y. W. Luo, R. Wang, L. Yang, B. Yu, B. G. Li, S. P. Zhu. *Macromolecules* **2006**, *39*, 1328-1337.

[31] L. Yang, Y. W. Luo, B. G. Li. *J Polym Sci Part A: Polym Chem* **2006**, *44*, 2293-2306.

[32] X. D. Zhou, P. H. Ni, Z. Q. Yu. *Polymer* **2007**, *48*, 6262-6271.

[33] Y. Luo, H. Gu. *Macromol Rapid Comm* **2006**, *27*, 21-25.

[34] X. Y. Huang, E. D. Sudol, V. L. Dimonie, C. D. Anderson, M. S. El-Aasser. *Macromolecules* **2006**, *39*, 6944-6950.

[35] R. P. Moraes, A. M. Santos, P. C. Oliveira, F. C. T. Souza, M. Amaral, T. S. Valera, N. R. Demarquette. *Macromol Symp* **2006**, *245-246*, 106-115.

[36] J. W. Jordan. *J Phys Colloid Chem* **1949**, *53* 294-306.

[37] A. Samakande, P. C. Hartmann, V. Cloete, R. D. Sanderson. *Polymer* **2007**, *48*, 1490-1499.

[38] P. A. Wheeler, J. Z. Wang, L. J. Mathias. *Chem Mater* **2006**, *18*, 3937-3945.

[39] X. Fu, S. Qutubuddin. *Polymer* **2001**, *42*, 807-813.

[40] X. A. Fu, S. Qutubuddin. *J Colloid Interf Sci* **2005**, *283*, 373-379.

[41] N. Greesh, P. C. Hartmann, V. Cloete, R. D. Sanderson. *J Colloid Interf Sci* **2008**, *319*, 2-11.

[42] A. Samakande, J. J. Juodaityte, R. D. Sanderson, P. C. Hartmann. *Macromol Mater Eng* **2008**, 293, 428-437.

[43] J. B. Di, D. Y. Sogah. *Macromolecules* **2006**, *39*, 1020-1028.

[44] P. Ding, M. Zhang, J. Gai, B. Qu. *J Mater Chem* **2007**, *17*, 1117-1122.

[45] B. Q. Zhang, C. Y. Pan, C. Y. Hong, B. Luan, P. J. Shi. *Macromol Rapid Commun* **2006**, *27*, 97-102.

[46] B. Z. Putlitz, K. Landfester, H. Fischer, M. Antonietti. *Adv Mater* **2001**, *13*, 500-503.

[47] S. A. F. Bon, P. J. Colver. *Langmuir* **2007**, *23*, 8316-8322.

[48] J. Cui, W. Wang, Y. You, C. Liu, P. Wang. *Polymer* **2004**, *45*, 8717-8721.

[49] X. W. Fan, Q. Y. Zhou, C. J. Xia, W. Cristofoli, J. Mays, R. Advincula. *Langmuir* **2002**, *18*, 4511-4518.

[50] J. Pyun, K. Matyjaszewski. *Chem Mater* **2001**, *13*, 3436-3448.

[51] J. Couet, M. Biesalski. *Macromolecules* **2006**, *39*, 7258-7268.

[52] Z. L. Lei, S. X. Bi. *Mater Lett* **2007**, *61*, 3531-3534.

[53] N. Negrete-Herrera, J. L. Putaux, L. David, E. Bourgeat-Lami. *Macromolecules* **2006**, *39*, 9177-9184.

[54] X. W. Pei, J. C. Hao, W. M. Liu. *J Phys Chem C* **2007**, *111*, 2947-2952.

[55] Q. Peng, D. M. Y. Lai, E. T. Kang, K. G. Neoh. *Macromolecules* **2006**, *39*, 5577-5582.

[56] D. J. Voorn, W. Ming, A. M. Van Herk. *Macromolecules* **2006**, *39*, 4654-4656.

[57] D. J. Voorn, W. Ming, A. M. Van Herk. *Macromolecules* **2006**, *39*, 2137-2143.

[58] G. J. Wang, S. Z. Huang, Y. Wang, L. Liu, J. Qiu, Y. Li. *Polymer* **2007**, *48*, 728-733.

[59] G. Xu, W.-T. Wu, Y. Wang, W. Pang, Q. Zhu, P. Wang, Y. You. *Polymer* **2006**, *47*, 5909-5918.

[60] Y. Yang, D. Wu, C. Li, L. Liu, X. Cheng, H. Zhao. *Polymer* **2006**, *47*, 7374-7381.

[61] Y. Zhao, S. Perrier. *Macromolecules* **2007**, *40*, 9116-9124.

[62] R. Advincula, Q. Y. Zhou, Y. Nakamura, S. Inaoka, M. K. Park, Y. F. Wang, J. Mays. *Abstr Pap Am Chem Soc* **2000**, *219*, U498-U498.

[63] S. Blomberg, S. Ostberg, E. Harth, A. W. Bosman, B. Van Horn, C. J. Hawker. *J Polym Sci Part A: Polym Chem* **2002**, *40*, 1309-1320.

[64] M. Alexandre, P. Dubois. *Mater Sci Eng A* **2000**, *28*, 1-63.

[65] M. Okamoto. *Encyclopedia of Nanoscience and Nanotechnology*; American Scientific Publishers: California, 2004.

[66] S. H. Cypes, W. M. Saltzman, E. P. Giannelis. *J Control Release* **2003**, *90*, 163-169.

[67] A. Samakande, R. D. Sanderson, P. C. Hartmann. *Synthetic Commun* **2007**, *37*, 3861-3872.

[68] P. C. Hartmann, P. Dieudonne, R. D. Sanderson. *J Colloid Interface Sci* **2005**, *284*, 289-297.

[69] Y. S. Choi, We. J. Chung. *Macromol Res* **2003**, *11*, 425-430.

[70] T. H. Kim, L. W. Jang, D. C. Lee, H. J. Choi, M. S. Jhon. *Macromol Rapid Commun* **2002**, *23*, 191-195.

[71] S. Muthukrishnan, E. H. Pan, M. H. Stenzel, C. Barner-Kowollik, T. P. Davis, D. Lewis, L. Barner. *Macromolecules* **2007**, *40*, 2978-2980.

[72] Y. L. Zhao, S. Perrier. *Macromolecules* **2006**, *39*, 8603-8608.

[73] A. Postma, T. P. Davis, G. X. Li, G. Moad, M. S. O'Shea. *Macromolecules* **2006**, *39*, 5307-5318.

[74] K. Landfester. *Macromol Rapid Commun* **2001**, *22*, 896-936.

[75] G. Qi, F. J. Schork. *Langmuir Lett* **2006**, *22*, 9075-9078.

[76] Z. H. Tong, Y. L. Deng. *Polymer* **2007**, *48*, 4337-4343.

[77] E. A. Turi. *Thermal Characterization of Polymeric Materials*, 2nd ed.; Academic Press: San Diego, 1997; Vol. 1.

[78] We. N. Jan, T. M. Lee, K. C. Chiou, J. J. Lin. *Ind Eng Chem Res* **2005**, *44*, 2086-2090.

[79] C. Tseng, J. Wu, H. Lee, F. Chang. *J Appl Polym Sci* **2002**, *85*, 1370-1377.

[80] W. A. Zhang, D. Z. Chen, H. Y. Xu, X. F. Shen, Y. E. Fang. *Eur Polym J* **2003**, *39*, 2323-2328.

[81] G. Chigwada, C. A. Wilkie. *Polym Degrad Stabil* **2003**, *80*, 551-557.

[82] D. B. Zax, D. K. Santos, H. Hegemann, E. P. Giannelis, E. Manias. *J Chem Phys* **2000**, *112*, 2945-2951.

[83] T. H. Kim, S. T. Lim, C. H. Lee, H. J. Choi, M. S. Jhon. *J Appl Polym Sci* **2003**, *87*, 2106-2112.

[84] J. Wang, J. Du, J. Zhu, C. A. Wilkie. *Polym Degrad Stabil* **2002**, *77*, 249-252.

[85] A. Bluimstein. *J Polym Sci A* **1965**, *3*, 2665-2673.

[86] A. Postma, T. P. Davis, R. A. Evans, G. X. Li, G. Moad, M. S. O'Shea. *Macromolecules* **2006**, *39*, 5293-5306.

[87] J. Luo, We. M. Daniel. *Compos Sci Technol* **2003**, *63*, 1607-1616.

[88] H. Tyan, K. Wei, T. Hsieh. *J Polym Sci Part B: Polym Phys* **2000**, *38*, 2873-2878.

[89] M. Xu, Y. S. Choi, Y. K. Kim, K. H. Wang, We. J. Chung. *Polymer* **2003**, *44*, 6387-6395.

[90] W. Zhang, D. Z. Chen, Q. B. Zhao, Y. Fang. *Polymer* **2003**, *44*, 7953-7961.

[91] J. M. G. Cowie. *Eur Polym J* **1975**, *11*, 297-300.

[92] F. H. Sanchez, J. M. M. Duenas, J. L. G. Ribelles. *J Therm Anal Calorim* **2003**, *72*, 631-640.

[93] M. W. Noh, D. C. Lee. *Polym Bull* **1999**, *42*, 619-626.

[94] Y. Yu, J. Yeh, S. Liou, Y. Chang. *Acta Mater* **2004**, *52*, 475-486.

Chapter 8 Rheological properties of RAFT-mediated poly(styrene-co-butyl acrylate)–clay nanocomposites (P(S-co-BA)-PCNs)with, emphasis on the effect of the structural parameters on thermo-mechanical and melt flow behaviours

The work described in this chapter has been published in the following paper:

Rheological properties of RAFT-mediated poly(styrene-co-butyl acrylate)–clay nanocomposites (P(S-co-BA)-PCNs)with, emphasis on the effect of the structural parameters on thermo-mechanical and melt flow behaviours.

Austin Samakande, Ronald D. Sanderson and Patrice C. Hartmann

Polymer (DOI:10.1016/j.polymer.2008.10.150)

Abstract

RAFT-mediated random poly(styrene-co-butyl acrylate)-[*N*-(4-((((dodecylthio)-carbonothioyl)thio)methyl)benzyl)-*N*,*N*-dimethylethanammonium]-clay nanocomposites (P(S-co-BA)–DCTBAB-PCNs) and poly(styrene-co-butyl acrylate)-[*N*,*N*-dimethyl-*N*-(4-(((phenylcarbonothioyl)thio)methyl)benzyl)ethanammonium]-clay nanocomposites (P(S-co-BA)–PCDBAB-PCNs) were prepared by miniemulsion free-radical polymerization. The RAFT agents, (i.e. DCTBAB and PCDBAB) were anchored onto the clay layers prior to polymerization, and were able to control the polymerization process, as evident from the decreasing molar mass and polydispersity index (PDI) values as the relative amount of RAFT agent to monomer in the system increased.

The efficiency of control of polymerization of the anchored RAFT agents increased as the RAFT agent concentration in the system increased, i.e. as the clay loading increased, due to the inhomogeneous distribution of the RAFT agent. At the beginning of the polymerization reaction the RAFT agent molecules were concentrated on the clay platelets to which they were attached. The nanocomposites that were prepared were found to have a partially exfoliated morphology at low clay loadings, as determined by SAXS and TEM, whereas, at high clay loadings the morphology changed to become predominantly intercalated. The thermo-mechanical properties of the nanocomposites were found to be a function of the molar mass, PDI, PCN morphology, and clay loading. In the glassy state, the storage modulus was seen to effectively decrease as clay loading increased, whereas the opposite was true for the loss modulus and tan delta. At low clay loadings the melt rheological properties were dominated by the matrix effects, whereas at high clay loadings the effect of the clay filler dominated, resulting in pseudo solid–liquid-like behaviour.

8.1 Introduction

The discovery of the nylon 6 polymer–clay nanocomposite (Nylon 6-PCN) by the Toyota research group in the early 1990s marked the dawn of a new era in the field of PCNs.[1] The Nylon 6-PCN that they prepared had better thermal and mechanical properties than neat nylon 6 polymer, which resulted in Nylon 6-PCN's use in the automotive industry. Toyota's landmark discovery has subsequently led to concerted efforts in research and development towards various aspects of PCNs from their synthesis to their applications. A vast amount of literature on PCNs has appeared over only a decade. Of particular interest is PCN characterization and the rheological properties of PCNs. The most widely studied rheological properties include dynamic mechanical analysis (DMA) and polymer melt rheology.

Polymer melt rheological studies provide information that is similar to that of DMA but, importantly, they also provides more valuable information pertaining to the behaviour of a polymer under processing conditions prior to the formation of the final product. The melt rheological properties of PCNs are dependent on their molar mass, polydispersity index (PDI), clay loading and the PCN morphology.[2-8] The complex viscosity of PCNs has been shown to be typically non-Newtonian in behaviour, as a result of the nanodispersion of the clay platelets.[2,8] The storage and loss moduli have been reported to show non-terminal solid-like behaviour at low frequencies due

to the presence of the clay platelets,[4,5,7-12] while in the high frequency region monotonic increases in storage modulus (G^{I}) and loss modulus (G^{II}) are observed as clay loading increases.[4,5,7,9,13] However, most of the PCNs that have been prepared and characterized to date have been synthesized by uncontrolled radical polymerization. Hence, the various explanations they provided for the physical and chemical properties of the PCNs they investigated did not fully take into account the effects of molar mass, polydispersity index and the changing PCN morphology.

This chapter describes the preparation of poly(styrene-co-butyl acrylate)-[*N*-(4-((((dodecylthio)carbonothioyl)thio)methyl)benzyl)-*N*,*N*-dimethylethanammonium]–clay nanocomposites (P(S-co-BA)–DCTBAB-PCNs) and poly(styrene-co-butyl acrylate)-*[N*,*N*-dimethyl-*N*-(4-(((phenylcarbonothioyl)thio)methyl)benzyl)ethanammonium]–clay nanocomposites (P(S-co-BA)–PCDBAB-PCNs) by RAFT-mediated free-radical polymerization. The impact of molar mass, PCN morphology and clay loading on thermo-mechanical and melt flow properties is investigated and discussed.

8.2 Experimental

8.2.1 Reagents

Styrene (99%, Aldrich) was purified by washing with 0.3M KOH, followed by distillation at 40 ºC under reduced pressure. Sodium dodecyl sulphate (SDS) (99%, Aldrich) and hexadecane (99%, Aldrich) were used as received. Azo*bis*isobutyronitrile (AIBN, Aldrich) was purified by recrystallization from methanol. Sodium montmorillonite (Na-MMT) was obtained from Southern Clay Products (Texas, USA). Deionized water was obtained from a Millipore Milli-Q-purification water system. *N*,*N*-dimethyl-*N*-(4-(((phenylcarbonothioyl)thio)methyl)benzyl)ethan-ammonium bromide (PCDBAB), *N*-(4-((((dodecylthio)carbonothioyl)thio)methyl)-benzyl)-*N*,*N*-dimethylethanammonium bromide (DCTBAB), PCDBAB-MMT and DCTBAB-MMT, (i.e. RAFT-MMT) clays were prepared as described in chapters 4 and 6.[14,15]

8.2.2 Typical preparation of P(S-co-BA)-PCNs using RAFT-mediated free-radical miniemulsion polymerization

Predetermined quantities of RAFT-MMT, AIBN, a mixture of styrene and n-butyl acrylate (50:50 by mass) and hexadecane (oil phase) (c.f. Table 8.1) were stirred

together overnight in a three-necked round-bottomed flask, to allow effective swelling of the clay galleries by the monomers.

Table 8.1. Quantities of reagents used in the preparation of P(S-co-BA)-PCNs by RAFT-mediated free-radical miniemulsion polymerization

Polymer	*RAFT (g)*	*MC (g)*	*S (g)*	*BA (g)*	*AIBN (g)*	*SDS (g)*	*HD (g)*
PS-D-St	0.080	-	3.543	3.506	0.016	0.174	0.357
PS-D-1		0.100	4.910	4.914	0.009	0.248	0.487
PS-D-2		0.198	4.914	4.900	0.012	0.248	0.499
PS-D-3		0.356	4.917	4.917	0.027	0.248	0.503
PS-D-5		0.497	4.900	4.906	0.030	0.248	0.492
PS-P-St	0.075	-	3.515	3.537	0.018	0.115	0.350
PS-P-1		0.101	4.909	4.908	0.010	0.164	0.508
PS-P-2		0.198	4.892	5.030	0.014	0.164	0.509
PS-P-3		0.356	4.923	4.909	0.023	0.164	0.489
PS-P-5		0.490	4.900	4.899	0.024	0.164	0.488

Key: MC = modified-clay, S = styrene monomer, BA = butyl acrylate monomer, SDS = sodium dodecyl sulphate and HD = hexadecane

To the oil phase, SDS solution (water phase) was added and the resulting biphasic mixture was stirred for a further 30 min to obtain a pre-emulsion. The pre-emulsion was then sonicated for 30 min using a Sonics Vibra Cell Autotune series 750VCX high intensity ultrasonic processor, in a water jacketed vessel. The amplitude was set at 90%, and the temperature cut off for the probe was set at 40 ºC. The average energy expended was ~180 kJ. The resultant miniemulsion was then immersed in an oil bath. The three necks of the round-bottomed flask were fitted with a condenser (main neck), a nitrogen gas inlet and a septum (side necks). The miniemulsion sample was then purged with nitrogen for 30 min before the temperature was rapidly increased to 75 ºC to start the polymerization. The polymerization was carried out for 6 h at 75 ºC.

A similar procedure was used for the synthesis of clay-free RAFT-mediated styrene-co-butyl acrylate miniemulsion polymerization, the only difference now being that the oil and the water phases were mixed after being stirred separately for 1 h.

8.2.3 Analyses

8.2.3.1 Size-exclusion chromatography (SEC)

SEC was carried out using a Waters 600E system controller equipped with a Waters 610 fluid unit pump and a Waters 410 differential refractometer as detector. Prior to analysis, samples were reverse ion-exchanged as follows. Quantities of P(S-co-BA)-

PCN (0.2 g) and LiCl (0.06 g) were dissolved in THF (10 ml) and refluxed at 70 ºC for 3 h. The solution was filtered through Celite, and the polymer was precipitated from methanol and dried. GPC analysis, using THF as mobile phase and an initial polymer concentration of 5 mg/mL, was performed on clay-free polymer solutions. Dynamic light scattering (DLS) measurements of the polymer in THF solution showed no peak/s characteristic of clay particles, thus proving that the chains were completely detached from the clay particles before SEC analysis.

8.2.3.2 Small angle X-ray scattering (SAXS)

SAXS measurements were performed in a transmission configuration at 298 K. A copper rotating anode X-ray source (functioning at 4 kW), with a multilayer focusing Osmic monochromator giving high flux (10^8 photons/sec) and punctual collimation, was used. An image plate 2D detector was used. Scattering patterns were obtained, giving diffracted intensity as a function of the wave vector *q*. The calculation of the *q* values is described elsewhere.[16]

8.2.3.3 Transmission electron microscopy (TEM)

TEM was used to directly visualize the morphology of the clay particles in polystyrene–clay nanocomposites at the nanometer level. Bright field TEM images were recorded using a LEO 912 transmission electron microscope, at an accelerating voltage of 120 kV. Prior to analysis the P(S-co-BA)-PCNs miniemulsion samples were dried, embedded in epoxy resin and cured for 24 h at 60 ºC. The embedded samples were then ultra-microtomed with a diamond knife on a Reichert Ultracut S ultra microtome at room temperature. This resulted in sections with a nominal thickness of ~100 nm. The sections were transferred from water at room temperature to 300-mesh copper grids, which were then transferred to the TEM apparatus.

8.2.3.4 Dynamic mechanical analysis (DMA) and rheology

Determinations of the DMA and the rheology of the P(S-co-BA)-PCN films were carried out using a Physica MCR 501 apparatus (Anton Paar, Germany). For DMA measurements, parallel-plate geometry (diameter 25 mm) was used, with a 1-mm gap distance and a constant strain of 0.1%. Measurements were carried out from 90 ºC to –20 ºC, at a heating rate of –5 ºC/min, an oscillation frequency of 1 Hz, and a normal force of 5 N.

Rheology measurements were carried out at 95 ºC, using an angular frequency range of 600–0.01 rad/sec. Parallel-plate geometry (diameter 25 mm), with a gap distance of 1-mm. A constant strain of 1% was obtained from the strain-sweep experiments were used, an example is given in Fig 29 in Appendix, in order to carry out measurements within the linear viscoelastic (LVE) range. The initial normal force was set to 5N.

8.3 Results and discussion

8.3.1 Synthesis of P(S-co-BA)-PCNs

Styrene and n-butyl acrylate were copolymerized, initially using a 50:50 (by mass) monomer ratio. This ratio has already been shown to yield a random polystyrene-co-butyl acrylate that can film form at room temperature.[12] Moraes *et al*.[12] reported on the preparation of P(S-co-BA) in the presence of clay by miniemulsion free-radical polymerization and obtained random P(S-co-BA)-PCNs. It is hence believed that we also obtained a random copolymer. Moreover, Fildermann *et al.*[17] reported that the inclusion of a RAFT agent does not significantly change the copolymer composition and the respective reactivity ratios of the comonomers.

The molar masses and the PDI values of the copolymers we synthesized decreased as the clay loading increased, as expected in RAFT-mediated polymerization systems (see Table 8.2).

Table 8.2. Molar masses, polydispersity indices and percentage conversions for various P(S-co-BA)-PCNs prepared

Polymer	$\frac{[MC]_0}{[M]_0}$ %	$\frac{[M]_0}{[R]_0}$	*Calc M_n (g/mol)*	*Exp M_n (g/mol)*	*PDI*	*Conv (%)*
P(S-co-BA) St	-	-	-	235 826	3.75	86.73
P(S-co-BA) P-St	-	331.60	9 898	12 248	1.34	23.84
P(S-co-BA)-P-1%	1.02	1133.40	101 750	114 215	2.09	87.73
P(S-co-BA)-P-2%	2.00	537.22	53 521	73 495	1.94	86.68
P(S-co-BA)-P-3.6%	3.62	351.40	24 285	42 196	1.68	69.98
P(S-co-BA)-P-5%	5.00	233.19	15 549	28 297	1.73	60.28
P(S-co-BA)-D-St	-	406.77	26 401	35 748	2.28	71.07
P(S-co-BA)-D-1%	1.02	1249.73	114 825	191 824	2.42	91.15
P(S-co-BA)-D-2%	2.02	630.53	61 186	91 265	2.51	89.81
P(S-co-BA)-D-3.6%	3.62	322.04	31 354	49 075	2.22	86.50
P(S-co-BA)-D-5%	5.07	250.99	23 389	36 837	2.16	84.96

Key: $\frac{[MC]_0}{[M]_0}$ initial mass ratio of modified-clay to monomer; $\frac{[M]_0}{[R]_0}$ initial molar ratio of monomer to RAFT, *Calc M_n* = theoretical molar mass calculated using the Equation $M_n = \frac{[M]_0 M_S x}{[RAFT]_0} + M_{RAFT}$,[18] where $[M]_0$ = initial monomer concentration, M_S = molar mass of monomer, x = conversion, M_{RAFT} =

molar mass of RAFT, $[RAFT]_0$ = initial concentration of RAFT; Exp M_n = experimental molecular mass; *PDI* = polydispersity indices of the polymer obtained, as determined by SEC. P(S-co-BA)-P and P(S-co-BA)-D refer to PCNs based on PCDBAB and DCTBAB respectively.

The experimental molar masses were higher than the theoretically calculated ones in all cases. This is explained by the relatively poor efficiency of the anchored RAFT agent that is not initially homogeneously dispersed in the monomer system.[15,19] On the other hand, the PDI values of the random copolymers were above 1.5 (i.e. the threshold PDI for controlled radical polymerizations) for all clay loadings. Such PDI values are not surprising, given that RAFT-mediated random copolymers and block copolymers have been shown to have relatively higher PDI values than the standard 1.5. This does however not mean that there was a loss of control of the polymerization process.[20,21] The phenomenon of a decrease in conversion with increased clay loading has been reported before.[15,22,23] According to Bon and Colver, when a radical is incident on a clay surface it reacts irreversibly with the functionalities there.[24] However, they did not give details of the species on the clay surface that are involved in the termination process. Thus, the more clay layers there are the greater are the chances of termination. Our findings are however in disagreement with those of other researchers who observed no change in conversion with an increase in clay loading for uncontrolled systems.[12,25] (It should however be mentioned that they used uncontrolled radical polymerization as opposed to our controlled polymerization).

Moreover, the presence of the RAFT agent on the clay surfaces might be affecting the polymerization process. Retardation, side reactions and inhibition are some of the reasons for the slow polymerization progress in RAFT-mediated polymerization reactions. This was more pronounced for dithiobenzoate (PCDBAB) than for trithiocarbonate (DCTBAB) mediated systems, in accordance with literature.[26,27]

8.3.2 Morphology of polymer-clay nanocomposites

8.3.2.1 TEM analysis

The particle sizes (as determined by DLS) were similar to those obtained for PS–CNs homopolymers in Chapter 7. Monitoring size and shape of particles obtained by miniemulsion polymerization using TEM was difficult since the particles coalesced under the effect of the high energy beam used for TEM analysis (c.f. Fig 8.1).

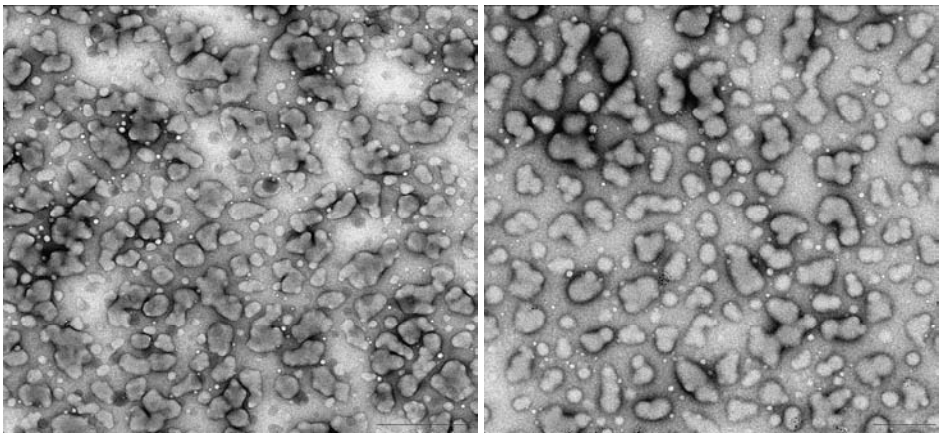

Fig.8.1. TEM images of P(S-co-BA)-DCTBAB-1% (left) and P(S-co-BA)-PCDBAB-1% (right)

The TEM images of dried samples (films) of P(S-co-BA)-DCTBAB (1%) and P(S-co-BA)-PCDBAB-1% (c.f. Fig. 8.2) showed predominantly a partially exfoliated structure, with a typical dispersion in the polymer matrix of both individual clay platelets and stacks of a few intercalated ones.

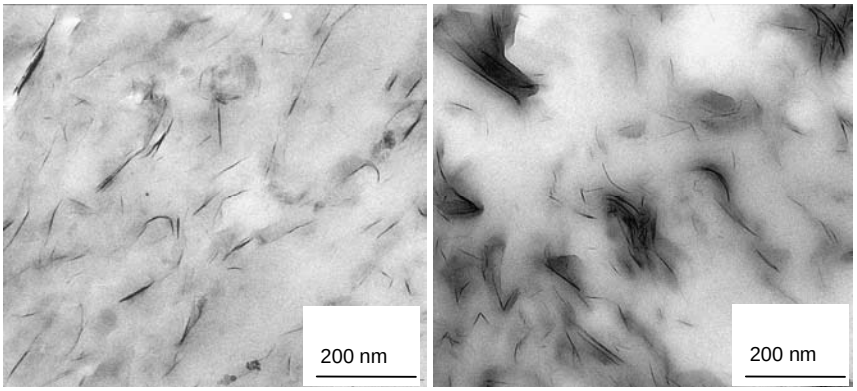

Fig. 8.2 TEM images of P(S-co-BA)-DCTBAB-1% (left) and P(S-co-BA)-PCDBAB-1% (right).

8.3.2.1 SAXS analysis

The SAXS patterns of P(S-co-BA)-PCNs are shown in Fig. 8.3. The peak of particular interest is the broad peak at the q value of 4.14. This peak at low clay loadings is very broad and of very low intensity, indicating a partially exfoliated structure. At higher clay loadings (5% clay loading) the peak is well defined and intense, indicating an intercalated morphology. The change in the nanocomposite morphology is ascribed to a decreasing molar mass. As the polymer chains grow they exert pressure on the clay platelets, causing them to move apart, which results in an exfoliated structure.[28] However, in our case, as the clay loading is increased there is a reduction in the effective molar mass of the chains. This results in intercalated morphology at high clay loading and, concomitantly, lower molar mass polymer chains relative to low clay loadings.

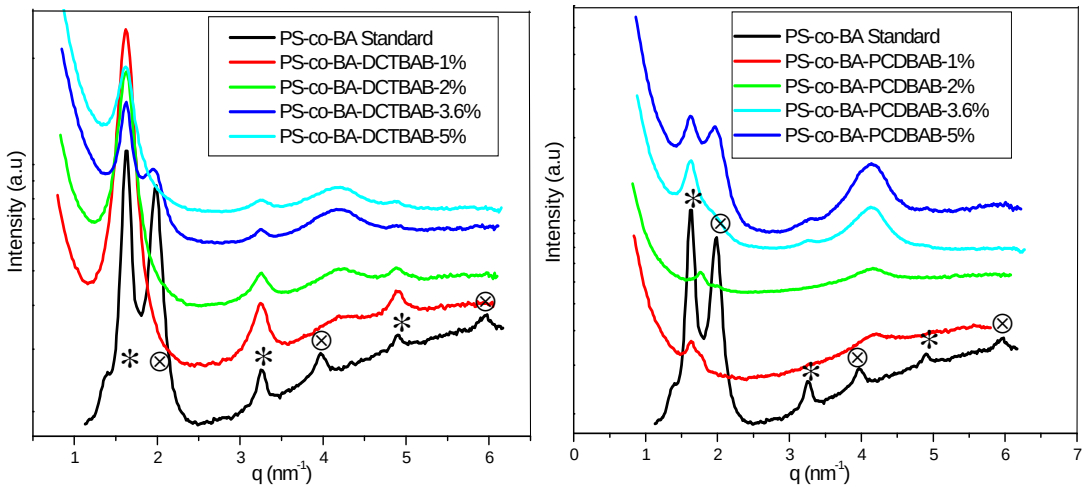

Fig 8.3. SAXS patterns of P(S-co-BA)-PCNs.

Surprisingly, two groups of relatively sharp peaks were seen in the SAXS patterns of the P(S-co-BA)-PCNs as well as in the P(S-co-BA) non-clay containing blank sample, (i.e. P(S-co-BA) without RAFT standard). The q values and the respective *d* spacing are given here in brackets: (∗) [1.64 (3.83nm), 3.27 (1.92 nm); 4.90 (1.28 nm)] and (⊗) [1.99 (3.16nm), 3.97 (1.58 nm); 5.98 (1.05 nm)]. In each group of peaks the absolute *d* spacing values follow the pattern $1:\frac{1}{2}:\frac{1}{3}$ typical of a lamellar structure. These lamellar structures are believed to be due to the self assembly of hexadecane and SDS in the presence of P(S-co-BA). The self assembly behaviour of SDS and hexadecane reported in literature shows that they can both form lamellar structures.[29-32] However, and even more surprisingly, the amount of the clay layers seems to affect this self assembly. Moreover, the RAFT agent used for surface modification prior to polymerization influenced the extent of self assembly. Reasons for this behaviour are still unclear, although it is likely to be due to the difference in the chemical structure of the Z group of the RAFT agents used.

8.3.3 Thermal stability

P(S-co-BA) nanocomposites showed no improvements in thermal stability when compared to neat copolymer standards, as shown in Fig. 8.4. The absence of thermal improvement of P(S-co-BA)-PCNs can be due to the presence of low molar mass oligomers in the nanocomposites as the PDI values of the nanocomposites are high, and these small oligomers could be accelerating further decomposition of the PCNs.[15,22,33,34]

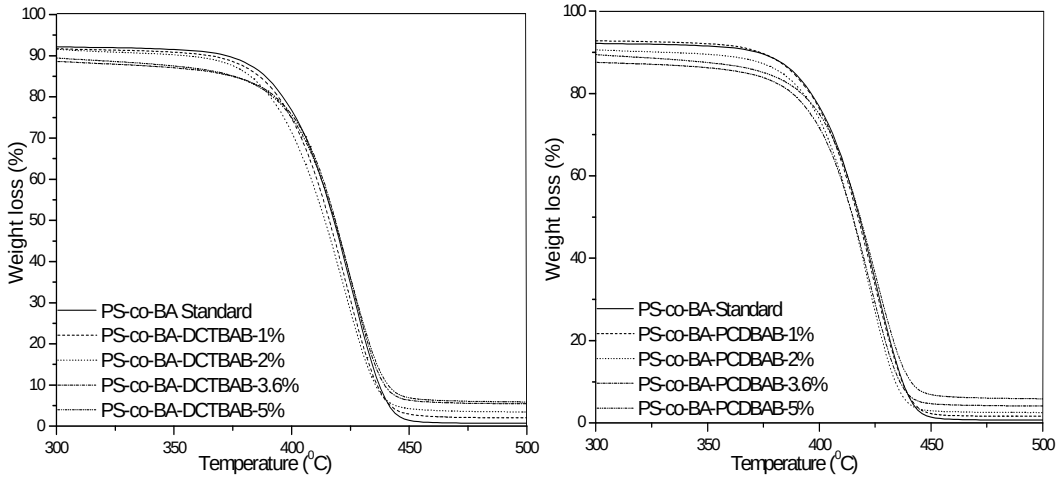

Fig. 8.4 TGA thermograms of P(S-co-BA)-PCNs, DCTBAB based (left) and PCDBAB based (right), at 1, 2, 3.6 and 5% clay loadings.

The thermal interaction of the hydrophobe, SDS, RAFT agent and the distribution of the styrene units relative to the butyl acrylate in the copolymer are also speculated to play a critical role in the thermal stability of the P(S-co-BA) nanocomposites.

8.3.4 Mechanical properties

8.3.4.1 Dynamic mechanical analysis (DMA)

The three main parameters of DMA measurements are (i) the storage modulus (G^{I}), which is a measure of elastic response to the deformation; (ii) the loss modulus (G^{II}), which is a measure of the flow response, and (iii) tan δ, i.e. the ratio of G^{II}/G^{I}. Tan δ is also used to determine molecular mobility. The interactions taking place at the interface between the polymer matrix and clay's silicate layers decrease the macromolecule's mobility in the polymer segments near the interface,[35] which leads to improved mechanical properties. In general, G^{I} values increase with an increase in the clay loading of nanocomposites below the glass transition temperature (T_g) (i.e. in the glassy state). The same effect occurs in the rubbery region.[6,36-38] This is attributed to the large aspect ratio of the structural hierarchy on the nanoscale level. Nanocomposites with exfoliated morphologies have been shown to have exceptionally enhanced thermo-mechanical properties relative to the intercalated and the conventional microcomposites. When nanoclay is present in a PCN sample the G^{II} and tan δ peaks have been shown to broaden and shift to higher temperatures. This has been attributed to restricted chain mobility,[9,37,39,40] associated with an increase in the T_g of the PCN relative to the neat polymer. The broadness of the T_g peak can be attributed to the distance of a polymer segment from the clay-polymer

interface. Different distances from a clay-polymer interface results in different sensitivity towards an applied force that causes polymer chain's movement.

The storage moduli of P(S-co-BA)-PCNs as a function of temperature (c.f. Fig. 8.5) were found to be superior to those of the non-clay-containing random copolymer. However, as the clay loading increased, and concurrently the molar mass decreased, the storage modulus effectively decreased. This behaviour was similar to that of RAFT-mediated PS–CNs prepared in a similar manner.[41]

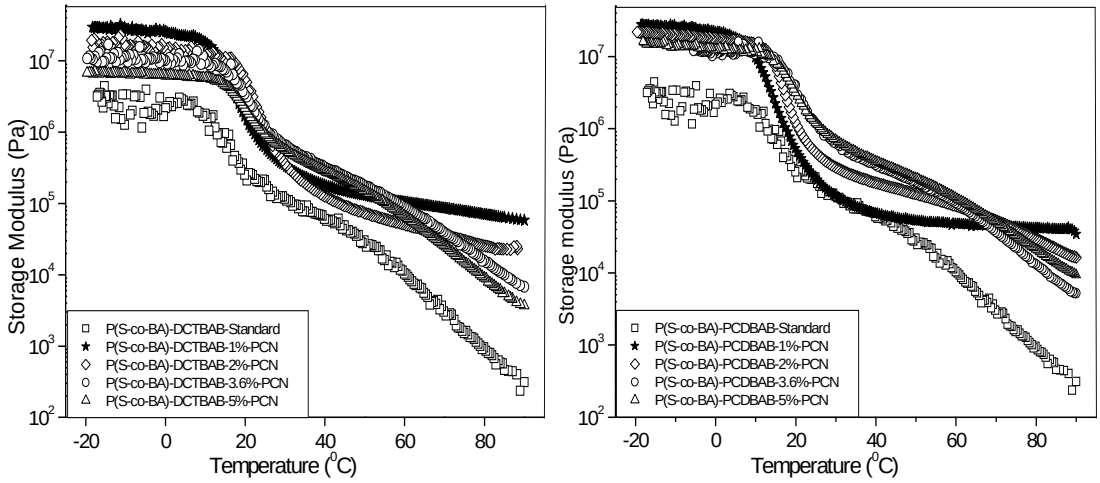

Fig. 8.5 Storage modulus as a function of temperature of P(S-co-BA)–DCTBAB-PCNs (left) and P(S-co-BA)–PCDBAB-PCNs (right), at 0% (□), 1% (∗), 2% (◊), 3.6% (○) and 5% (Δ) clay loadings respectively.

Thus the effect of both molar mass and PCN morphology seems to have a dominant effect on G^{I}. It was expected that an increase in clay loading would result in an increase in the storage modulus. The recorded storage moduli of the P(S-co-BA)-PCN films also showed interesting effects of the molar mass and clay loading effects in the profiles of the variation of G^{I} against temperature curves. The width of the rubbery plateau (i.e. at temperatures above the transition from the glassy state and below the final transition into the viscous liquid state) is indicative of the molar mass of the polymer.[7,34] It is seen that the width of the rubbery plateau becomes narrower with increasing clay loading, further confirming our deductions that the molar mass decreases with increasing clay loading. This is also an indication that the RAFT agents within the clay galleries effectively control the polymerization process. Moreover, the extent (drop) of the transition from the glassy state to the rubbery region decreases with increasing clay loading, further proving that the clay layers are indeed acting in a similar way as crosslinkers towards the polymer chains. The

presence of crosslinkers in a polymer sample is known to decrease the length of the transition from the glassy state to the rubbery region.[7,34]

The loss moduli peaks of the P(S-co-BA)-PCNs as a function of temperature shifted to higher temperature, relative to the standard neat copolymers, indicating an increase in T_g. This is due to the incorporation of clay layers that act as mobility retarders in the polymer network. The presence of clay leads to the presence of interfacial material that has different properties to bulk. However, as the clay loading increased the peak maximum did not shift significantly further to higher temperatures (see Fig. 8.6).

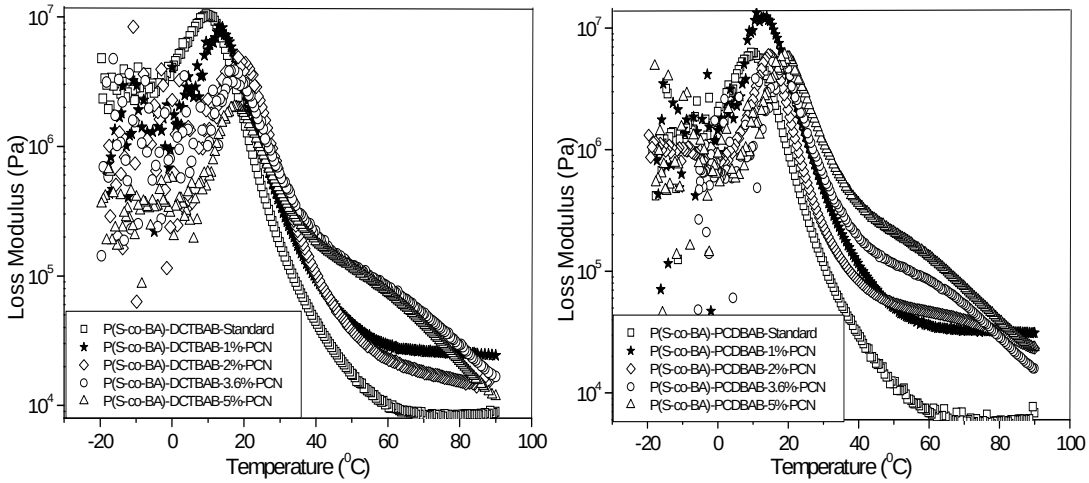

Fig. 8.6 Loss modulus as a function of temperature of P(S-co-BA)–DCTBAB-PCNs (left) and P(S-co-BA)–PCDBAB-PCNs (right), at 0% (□), 1% (∗), 2% (◊), 3.6% (O) and 5% (Δ) clay loadings respectively.

These results indicate that the T_g of the P(S-co-BA)-PCNs did not significantly change as the clay loading increased and, simultaneously, the molar mass decreased. These results are indicative of a balance of effects of the clay loading and the molar mass. Our results are in agreement with those of Moraes *et al*.[12] who also prepared P(S-co-BA)-PCNs using miniemulsion polymerization, although their nanocomposites were prepared using an uncontrolled free-radical polymerization method.

The tan δ peaks of the P(S-co-BA)-PCNs were also shifted to higher temperature relative to the neat P(S-co-BA) standard (see Fig. 8.7). The molar mass and clay loading effects were also evident in these tan δ peaks, as seen by the shape of the peaks above the transition.[34] As the clay loading increased and molar mass decreased the transition peak became small and the values of tan δ after the

transition peak increased monotonously. As opposed to previous reports that the tan δ peak broadens as clay loading increases, in our case the reverse is true, probably due to the decreasing PDI in the PCNs as clay loading increases.

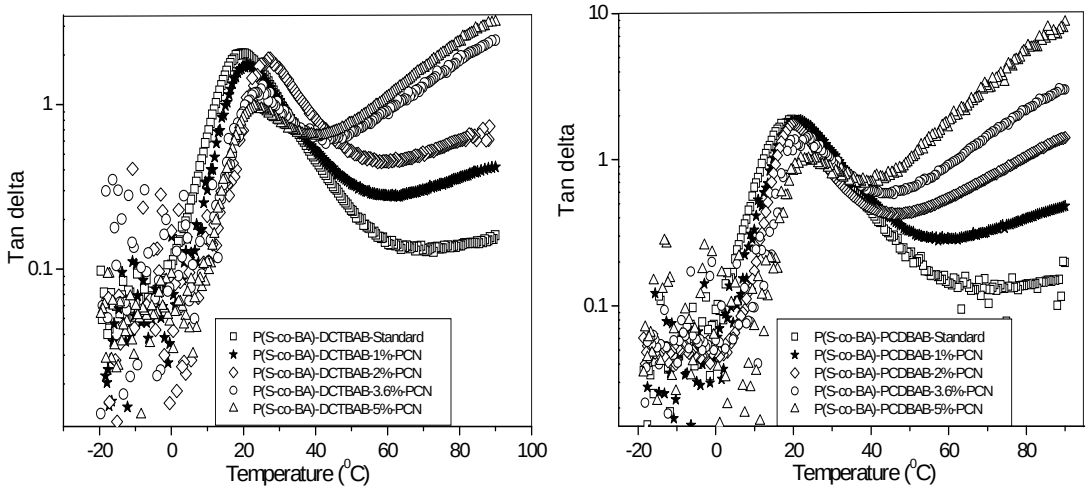

Fig. 8.7 Tan δ as a function of temperature for P(S-co-BA)-PCNs, based on DCTBAB (left) and PCDBAB (right) respectively, at 0% (□), 1% (∗), 2% (◊), 3.6% (O) and 5% (Δ) clay loadings respectively.

The effect of the percentage clay loading on the relative values of tan δ seem to have an opposite effect, depending on whether the temperature is below or above the T_g. In the glassy state (below T_g) the presence of clay enhances the solid–like character of the material, as tan delta gradually decreases as the percentage clay loading increases. On the contrary, in the viscous state (above T_g), the presence of clay enhances further the softness character of the material, as tan delta gradually increases with the clay loading. Although this latter effect is due to a decrease of the molar mass as the clay loading increases, the resulting overall effect is of particular interest for industrial processability, as an increase in clay loading seems to enhance the toughness of the material below T_g.

8.3.4.2 Melt rheology

Melt rheological properties of the PCNs are important in the consideration of their possible processing. The complex viscosity of PCNs with various clay loadings at 95 ºC was plotted as a function of angular frequency for both series PCDBAB and DCTBAB (see Fig. 8.8). The DCTBAB- and PCDBAB-mediated P(S-co-BA) polymer standards without clay showed typical Newtonian behaviour.[5] The complex viscosity (η^*) increased linearly with a decrease in the angular frequency up to about 10 rad/s, whereas at lower frequencies η^* tends to become independent of the angular

frequency. This Newtonian behaviour at low frequencies is typical of unfilled polymers, as reported in literature[2,8].

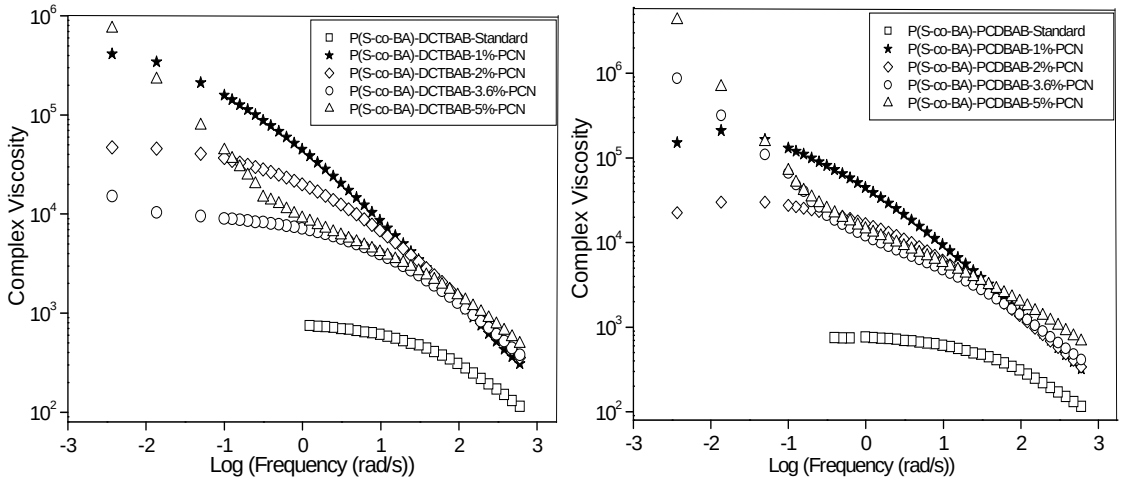

Fig. 8.8 Complex viscosity as a function of angular frequency for P(S-co-BA)–DCTBAB-PCNs (left) and P(S-co-BA)–PCDBAB-PCNs (right), at 0% (□), 1% (∗), 2% (◊), 3.6% (O) and 5% (Δ) clay loadings respectively.

The complex viscosities of both P(S-co-BA)–DCTBAB-PCNs and P(S-co-BA)–PCDBAB-PCNs are dependent on a number of factors: (i) molar mass, (ii) clay loading and (iii) PCN morphology. The value of the onset of the complex viscosity (high frequency region) was found to increase monotonously with an increase in clay loading. The complex viscosity as a function of frequency for 1% and 2% clay loadings were found to be dominated by the molar mass and showed little dependence on the clay loading and morphology. Here the increase in complex viscosity observed as the angular frequency decreased was more pronounced for the PCNs with 1% clay loading, and which ultimately had higher molar mass than the PCNs with 2, 3.6 and 5% clay loadings. Viscosities of the samples with 1% clay loading became independent of angular frequency for values below 0.01 rad/sec, whereas at 2% clay loading this effect was observed for angular frequencies below 0.1 rad/sec. This showed the dependency of the viscosity on molar mass and PCN morphology. At 3.6% clay loading and above, the complex viscosity curves showed a different pattern, as the complex viscosity continuously increased even at very low angular frequencies. This showed their typical non-Newtonian behaviour, i.e. pseudo solid–like behaviour, as reported in literature.[2,8] For frequencies above 0.3 rad/sec the melt flow properties of the nanocomposites were dominated by the molar mass, as they tend to be close to Newtonian in behaviour, i.e. there is a tendency to be independent of clay loading, by showing pseudo plateaus.

The variation of G^{I} and G^{II} of the P(S-co-BA) with angular frequency at 95 ºC followed a similar pattern to the complex viscosity: the onset (high frequency region) of both storage and loss moduli increases monotonously with clay loading, as reported in literature.[4,5,7,9,13,42] This clearly shows that the presence of clay increases the stiffness of the material. However, storage and loss moduli of the nanocomposites at 1 and 2% clay loadings were dominated by the molar mass of the polymer matrix as they do not show the solid–liquid character typical of PCNs (c.f. Fig. 8.9).[2-4,7]

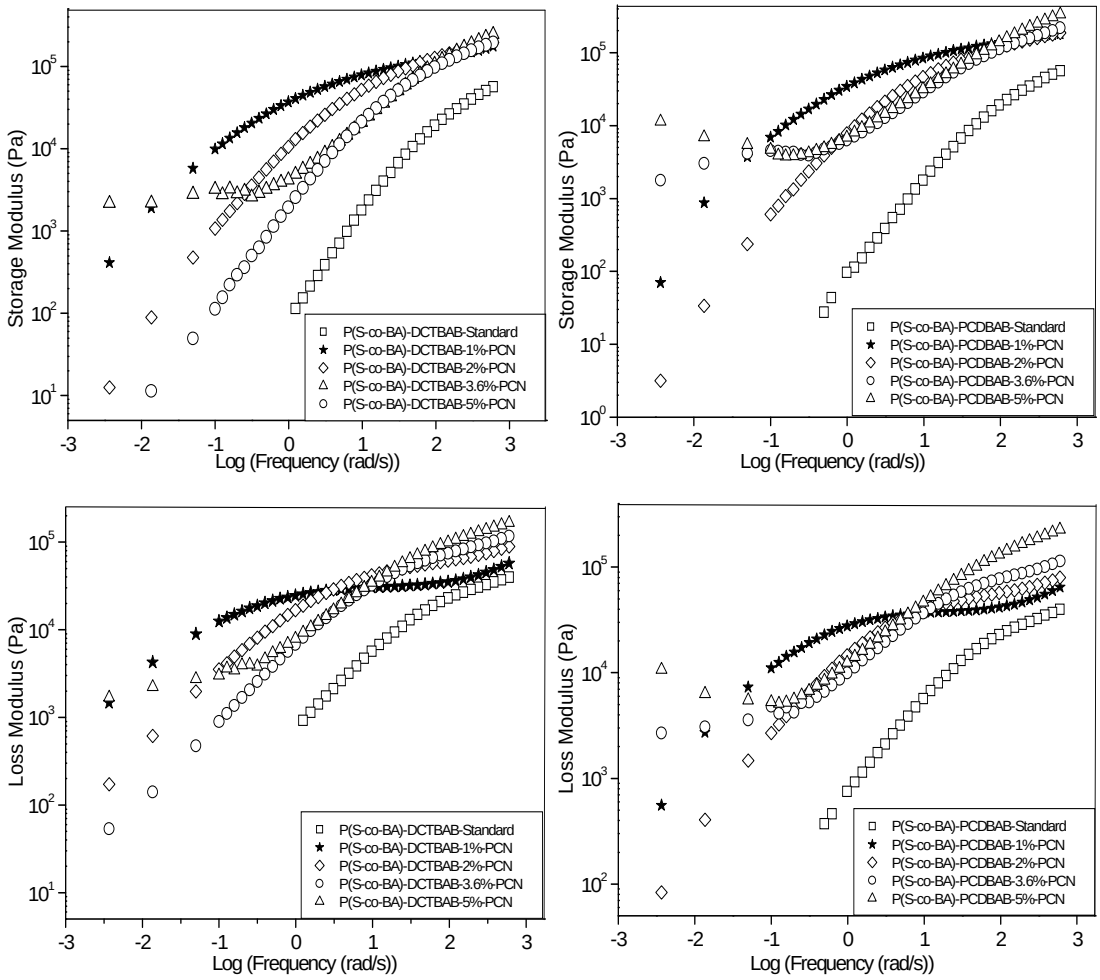

Fig. 8.9 Variation of storage modulus (G^{I}) and loss modulus (G^{II}) with angular frequency (ω) for (left) P(S-co-BA)–DCTBAB-PCNs and (right) P(S-co-BA)–PCDBAB-PCNs, at 0% (□), 1% (⋆), 2% (◊), 3.6% (O) and 5% (Δ) clay loadings respectively.

Fig. 8.9 shows that 1% and 2% clay contents tend to flattern in the high angular frequency region, before they start to decrease. This is more pronounced for the 1% clay loading. For the 3.6 and 5% clay loadings the loss and storage moduli quickly decrease with decreasing angular frequency. This is an indication of the dependence of the rheological properties on the molar mass of the matrix.[6,42] Ma *et al.* have reported very small differences in the storage and loss moduli of the acrylonitrile-

butadiene-styrene (ABS) and acrylonitrile–butadiene–styrene grafted maleic anhydride (ABS–graft–MAH)-PCNs in the high frequency region.[11] This shows that in the high frequency region matrix effects are dominant. At low angular frequency PCNs with 1% and 2% clay loadings show a fast decreasing loss and storage moduli with decreasing angular frequency, which is characteristic of molecular movement. This indicates that at low clay loadings the melt flow properties of PCNs are not significantly influenced by the clay loading but rather by the matrix and the polydispersity indices. At the 3.6 and 5% clay loadings, for both PCNs, pseudo non-terminal, pseudo solid–liquid-like behaviour is observed.[2-5,7,8,10-12,43] The dependency of the storage and loss moduli on angular frequency diminishes and becomes more dependent on the clay loading.[7,10] This effect is a result of the increased frictional interactions of the clay particles, as well as the strong polymer–clay interactions.[3,5] Our results of pseudo solid–liquid-like behaviour at clay loadings of greater than 3% agree well with those of Krishnamoorti *et al.,*[7] who also observed similar effects for their clay attached (end-tethered) poly(ε-caprolactone)–clay nanocomposites, as in our case, whereas Ren *et al.*[14] only observed this effect at 6.7% clay loading for non-clay-attached polystyrene–polyisoprene–clay nanocomposites. The differences in the clay levels where pseudo solid–liquid-like behaviour is observed can thus be attributed to whether the polymers are attached or not to the clay layers.

Another important parameter related to the melt rheology of PCNs is the crossover frequencies (i.e. frequencies at which values of storage and loss moduli are equal). These angular frequency points give an indication of the relaxation times of the polymer chains in the PCNs (see Table 8.3). The number of these crossover points also gives an indication of the arrangement of the clay platelets relative to each other, and of the number density of the clay platelets.[8] On the other hand, the terminal slope of the storage and loss moduli versus angular frequency gives an indication of the clay morphology and the polydispersity of the polymers. Monodisperse unfilled polymers obey the following relationships in the low angular frequency region, $G^{I} \propto \omega^{2}$ and $G^{II} \propto \omega^{1}$. In essence, the terminal gradient of the variation of storage modulus with angular frequency, should be theoretically equal to 2 and the terminal slope of the loss modulus equal to 1, for a homogeneous and monodisperse homopolymer.[3,4,7] Deviations from these values, (i.e. terminal

gradients) may be due to polydispersity, the P(S-co-BA)-PCNs morphology, and/or clay loading.

Table 8.3. Terminal gradients and the associated relaxation times of P(S-co-BA)-PCNs

Polymer	$\frac{\Delta G^I}{\Delta\omega}$	$\frac{\Delta G^{II}}{\Delta\omega}$	ω_1 (rad/s)	T_1 (s)	ω_2 (rad/s)	T_2 (s)
P(S-co-BA) St	1.46	0.94	151.92	0.04	-	-
P(S-co-BA)-P-1%	1.93	1.21	0.50	12.57	-	-
P(S-co-BA)-P-2%	1.86	1.22	6.16	1.02	-	-
P(S-co-BA)-P-3.6%	0.41	0.10	24.33	0.26	0.16	39.27
P(S-co-BA)-P-5%	0.25	0.05	76.44	0.08	0.05	125.66
P(S-co-BA)-D-1%	1.38	0.82	0.25	25.13	-	-
P(S-co-BA)-D-2%	1.50	0.97	3.90	1.61	-	-
P(S-co-BA)-D-3.6%	0.73	0.93	24.33	0.26	-	-
P(S-co-BA)-D-5%	0.00	0.21	76.44	0.08	0.03	209.44

Key: $\frac{\Delta G^I}{\Delta\omega}$ = terminal gradient, i.e. increase in storage modulus/increase in angular frequency; $\frac{\Delta G^{II}}{\Delta\omega}$ = terminal gradient i.e. increase in loss modulus/increase in angular frequency; ω_1= first crossover angular frequency and the associated relaxation time (T_1); then ω_2= second crossover angular frequency and the associated relaxation time (T_2). T_1 and T_2 were calculated using the relation $T = 2\pi/\omega$.

G^I and G^{II} crossover frequencies and corresponding relaxation times are reported in Table 8.3. The relaxation times of all P(S-co-BA)-PCNs were found to be greater than that of the neat P(S-co-BA) copolymer standard, although within the same series of P(S-co-BA)-PCNs, the relaxation time decreases as the clay loading increases. This is surprising, as the presence of clay was expected to increase the relaxation time of the polymer chains of the matrix.[10] However, the decrease of molar mass with increasing clay loading ought to have a dominating effect; hence decreasing the relaxation time to a greater extent than the clay loading contributes to it. The presence of two crossover frequencies (the second being at low angular frequency) for the P(S-co-BA)–P-3.6%-PCN, P(S-co-BA)–P-5%-PCN and P(S-co-BA)–D-5%-PCN show that for these nanocomposites there is long-range relaxation process taking place, which is caused by the presence of clay. This is to be expected, since an increase in clay loading results in highly confined polymer chains; as such long-range relaxation processes take place over a longer period of time. Moreover, two crossover angular frequencies are an indication of the clay platelets having reached

the percolation threshold.[8] A phenomenon where clay platelets will be touching each other, i.e. a clay network. These results also indicate that the clay platelets were more thoroughly dispersed in the PCDBAB based nanocomposites relative to the DCTBAB ones as clay platelets formed a network at 3.6% clay loading for PCDBAB relative to 5% clay loading in the DCTBAB system.

The terminal gradients of both the PCDBAB and DCTBAB based nanocomposites decreased with an increase in clay loading, as reported by others.[5,9,11] The terminal gradients decreased from those typical of homopolymer behaviour, i.e. $G^{I} \alpha \sim \omega^{2}$ and $G^{II} \alpha \omega^{1}$, to levels where the solid–liquid behaviour dominates, here $G^{I} > G^{II}$ at higher clay loadings, which is in agreement with literature.[8] The PDI values of the two series appeared to be important: the narrow PDI values of PCDBAB based nanocomposites resulted in better adherence to the expected relationships between G^{I} and G^{II} as a function of ω.

8.4 Conclusions

RAFT-mediated free-radical copolymerization of styrene and butyl acrylate was successfully achieved in miniemulsion using clay modified with either *N*-(4-((((dodecylthio)-carbonothioyl)thio)methyl)benzyl)-*N*,*N*-dimethylethanammonium (DC-TBAB) or *N*,*N*-dimethyl-*N*-(4-(((phenylcarbonothioyl)thio)methyl)benzyl)ethanamm-onium (PCDBAB). The resulting stable lattices were P(S-co-BA)-PCNs with a morphology varying from semi-exfoliated to intercalated as the clay loading increased. The RAFT agents anchored onto clay, (i.e. DCTBAB and PCDBAB), resulted in polymers with molar masses and polydispersity indices that decreased as the clay loading increased. The control of the polymerization process increased with RAFT agent concentration. The melt rheological properties of PCNs were found to be dependent on molar mass, PDI, clay loading, clay morphology and whether the polymer chains are attached to clay platelets or not.

8.5 References

[1] A. Usuki, Y. Kojima, M. Kawasumi, A. Okada, Y. Fukushima, T. Kurauchi, O. Kamigaito. *J Mater Res* **1993**, *8*, 1179-1184.

[2] T. D. Fornes, P. J. Yoon, H. Keskkula, D. R. Paul. *Polymer* **2001**, *42*, 9929-9940.

[3] G. Galgali, C. Ramesh, A. Lele. *Macromolecules* **2001**, *34*, 852-858.

[4] R. Krishnamoorti, E. P. Giannelis. *Macromolecules* **1997**, *30*, 4097-4102.

[5] K. Okada, T. Mitsunaga, Y. Nagase. *Korea-Aust Rheol J* **2003**, *15*, 43-50.

[6] M. Xu, Y. S. Choi, Y. K. Kim, K. H. Wang, I. J. Chung. *Polymer* **2003**, *44*, 6387-6395.

[7] J. X. Ren, A. S. Silva, R. Krishnamoorti. *Macromolecules* **2000**, *33*, 3739-3746.

[8] J. Zhao, A. B. Morgan, J. D. Harris. *Polymer* **2005**, *46*, 8641-8660.

[9] T. H. Kim, S. T. Lim, C. H. Lee, H. J. Choi, M. S. Jhon. *J Appl Polym Sci* **2003**, *87*, 2106-2112.

[10] S. T. Lim, C. H. Lee, H. J. Choi, M. S. Jhon. *J Polym Sci Part B: Polym Phys* **2003**, *41*, 2052-2061.

[11] H. Y. Ma, L. F. Tong, Z. B. Xu, Z. P. Fang. *Polym Degrad Stabil* **2007**, *92*, 1439-1445.

[12] R. P. Moraes, A. M. Santos, P. C. Oliveira, F. C. T. Souza, M. Amaral, T. S. Valera, N. R. Demarquette. *Macromol Symp* **2006**, *245-246*, 106-115.

[13] M. J. Solomon, A. S. Almusallam, K. F. Seefeldt, A. Somwangthanaroj, P. Varadan. *Macromolecules* **2001**, *34*, 1864-1872.

[14] A. Samakande, R. D. Sanderson, P. C. Hartmann. *Synthetic Commun* **2007**, *37*, 3861-3872.

[15] A. Samakande, J. J. Juodaityte, R. D. Sanderson, P. C. Hartmann. *Macromol Mater Eng* **2008**, 293, 428-437.

[16] P. C. Hartmann, P. Dieudonne, R. D. Sanderson. *J Colloid Interface Sci* **2005**, *284*, 289-297.

[17] A. Feldermann, A. A. Toy, H. Phan, M. H. Stenzel, T. P. Davis, C. Barner-Kowollik. *Polymer* **2004**, *45*, 3997-4007.

[18] A. Postma, T. P. Davis, G. X. Li, G. Moad, M. S. O'Shea. *Macromolecules* **2006**, *39*, 5307-5318.

[19] J. B. Di, D. Y. Sogah. *Macromolecules* **2006**, *39*, 1020-1028.

[20] S. Perrier, P. Takolpuckdee. *J Polym Sci Part A: Polym Chem* **2005**, *43*, 5347-5393.

[21] A. Bowes, J. B. McLeary, R. D. Sanderson. *J Polym Sci Part A: Polym Chem* **2007**, *45*, 588-604.

[22] Y. S. Choi, I. J. Chung. *Macromol Res* **2003**, *11*, 425-430.

[23] H. M. Jung, E. M. Lee, B. C. Ji, Y. L. Deng, J. D. Yun, J. H. Yeum. *Colloid and Polymer Science* **2007**, *285*, 705-710.

[24] S. A. F. Bon, P. J. Colver. *Langmuir* **2007**, *23*, 8316-8322.

[25] T. H. Kim, L. W. Jang, D. C. Lee, H. J. Choi, M. S. Jhon. *Macromol Rapid Commun* **2002**, *23*, 191-195.

[26] S. Muthukrishnan, E. H. Pan, M. H. Stenzel, C. Barner-Kowollik, T. P. Davis, D. Lewis, L. Barner. *Macromolecules* **2007**, *40*, 2978-2980.

[27] Y. L. Zhao, S. Perrier. *Macromolecules* **2006**, *39*, 8603-8608.

[28] F. Gardebien, J. Bre´Das, R. Lazzaroni. *J Phys Chem B* **2005**, *109*, 12287-12296.

[29] I. D. Leigh, M. P. Mcdonald, R. M. Wood, G. J. T. Tiddy, M. A. Travethan. *J Chem Soc Farad T 1* **1981**, *77*, 2867-2876.

[30] E. Leontidis, T. Kyprianidou-Leodidou, W. Caseri, P. Robyr, F. Krumeich, K. C. Kyriacou. *J Phys Chem B* **2001**, *105*, 4133-4144.

[31] V. Metivaud, A. Lefevre, L. Ventola, P. Negrier, E. Moreno, T. Calvet, D. Mondieig, M. A. Cuevas-Diarte. *Chem Mater* **2005**, *17*, 3302-3310.

[32] K. Smith, G. A. El-Hiti, M. E. W. Hammond, D. Bahzad, Z. Q. Li, C. Siquet. *J Chem Soc Perk T 1* **2000**, 2745-2752.

[33] A. Leszczynska, J. Njuguna, K. Pielichowski, J. R. Banerjee. *Thermochim Acta* **2007**, *453*, 75-96.

[34] E. A. Turi. *Thermal Characterization of Polymeric Materials*, 2nd ed.; Academic Press: San Diego, 1997; Vol. 1.

[35] J. Luo, I. M. Daniel. *Compos Sci Technol* **2003**, *63*, 1607-1616.

[36] X. Fu, S. Qutubuddin. *Polymer* **2001**, *42*, 807-813.

[37] H. Tyan, K. Wei, T. Hsieh. *J Polym Sci Part B: Polym Phys* **2000**, *38*, 2873-2878.

[38] W. Zhang, D. Z. Chen, Q. B. Zhao, Y. Fang. *Polymer* **2003**, *44*, 7953-7961.

[39] M. W. Noh, D. C. Lee. *Polym Bull* **1999**, *42*, 619-626.

[40] Y. Yu, J. Yeh, S. Liou, Y. Chang. *Acta Mater* **2004**, *52*, 475-486.

[41] A. Samakande, P. C. Hartmann, R. D. Sanderson. *J Polym Sci Part A: Polym Chem* ***Submitted***.

[42] O. Meincke, B. Hoffmann, C. Dietrich, C. Friedrich. *Macromol Chem Physic* **2003**, *204*, 823-830.

[43] T. T. Chastek, A. Stein, C. Macosko. *Polymer* **2005**, *46*, 4431-4439.

Chapter 9: Conclusions and recommendations for future work

9.1. Conclusions

Three neutral and two cationic RAFT agents, 11-(((benzylthio)carbonothioyl)thio)undecanoic acid (BCTUA), 1,4-phenylenebis(methylene)dibenzenecarbodithioate (PCDBDCP), dodecyl-1,4-phenylenebis(methylene)bistrithiocarbonate (DCTBTCD) and *N*, *N*-dimethyl-*N*-(4-(((phenylcarbonothionyl)thio)methyl)benzyl)ethanammonium bromide (PC-DBAB), *N*-(4-((((dodecylthio)carbonothioyl)thio)-methyl)benzyl)-*N*,*N*-dimethyl-ethanammonium bromide (DCTBAB) respectively were successfully synthesized in appreciable yields and purity. The amphiphilic behaviour of the two cationic RAFT agents, PCDBAB and DCTBAB, in dilute aqueous environments was influenced by the presence of the thio-carbonyl-thio group on the surfactants. The thio-carbonyl-thio group promote micellization and contribute favourable to the thermodynamic parameters of micellization (i.e. free energy, entropic and enthalpy of micellization). The thermodynamic parameters of micellization were amplified by the usual factors that govern the behaviour of surfactants in dilute aqueous environments such as, the surfactant's chemical structure, chain length and head group size.

A cationic initiator, VA060 was successfully used to modify montmorillonite (MMT) clay to yield VA060-MMT clay. The VA060-MMT clay was less effective as a macro initiator for *in situ* intercalative free-radical bulk polymerization of styrene to yield polystyrene clay nanocomposites (PS–CNs). As such, PS–CNs of low conversions and predominantly intercalated morphologies were obtained as a result of radical–radical coupling (the cage effect) inside the clay galleries. Incorporation of neutral RAFT agents synthesized above to the reaction media led to PS–CNs of controlled molar masses and low polydispersity indices. However, the PS–CNs had the same morphologies and similar trends in conversions as those prepared in the absence of the RAFT agents. The PS–CNs prepared resulted in better thermal stability relative to neat PS.

Similarly cationic RAFT agents were successfully anchored onto MMT clay to yield RAFT-modified-clays. Polystyrene clay nanocomposites (PS–CNs) were subsequently synthesized using the RAFT-Modified-clays. The PS–CNs obtained had exfoliated morphology and the polymer chains had controlled

molar mass and low polydispersity indices. The degree of control of polymerization was dependant on the amount of RAFT agent in the reaction media. Trends in the monomer to polymer conversion were found to be similar to those prepared using the initiator-modified-clay above. Similarly the PS–CNs had improved thermal stability relative to neat PS.

The RAFT-modified-clays described above were used to make PCNs in miniemulsion based polymerization. Colloidally stable, PS–CNs and polystyrene-co-butyl acrylate (P(S-co-BA))-PCNs, miniemulsions lattices were obtained. The control of polymerization was not as good as that in the bulk system due to the prevalence of termination reactions. The morphologies of the nanocomposites varied from partial exfoliation at low clay loadings and higher molar masses to intercalated structure at higher clay loadings and low molar masses. The nanocomposites in miniemulsion had slight or no thermal stability enhancement relative to the neat polymers. However, they had improved mechanical properties that were dependent on the molar mass, clay loading and the morphology of the nanocomposite. P(S-co-BA)-PCNs showed enhanced rheological properties relative to unfilled polymers. The rheological properties where found to be dependent on molar mass, PDI, clay loading, clay morphology and whether the polymer chains are attached to clay platelets or not.

Therefore this study effectively combined the RAFT technology and clay nanotechnology for the synthesis of PCNs.

9.2 Recommendations for future work

- Study of PCDBAB and DCTBAB cationic RAFT agent's self assembly in concentrated aqueous environments.
- Study of the cationic RAFT's ability to control various aqueous based solution and dispersed media polymerization in the absence of clay, as the resulting polymers could have niche applications.
- Study of the kinetics of the RAFT-mediated polymerization of PCNs. Study of kinetics of polymerization are useful for the academic understanding of the reaction process and for industrial PCN preparation.

- Synthesize new RAFT agents that can control the polymerization of a range of monomers, including methacrylates and vinyl acetates in the presence of clay.

- Produce ranges of PCNs of increasing clay loadings all at the same molar mass.

- The on line coupling of TEM and XRD *in situ* so as to look at the changing morphology of the nanocomposites with conversion. The obtained results are then correlated to those of SEC from which the molar mass at which exfoliation takes place is elucidated. Such a study will also provide vital information about the PCN formation, hence factors that affect PCN formation.

Appendix

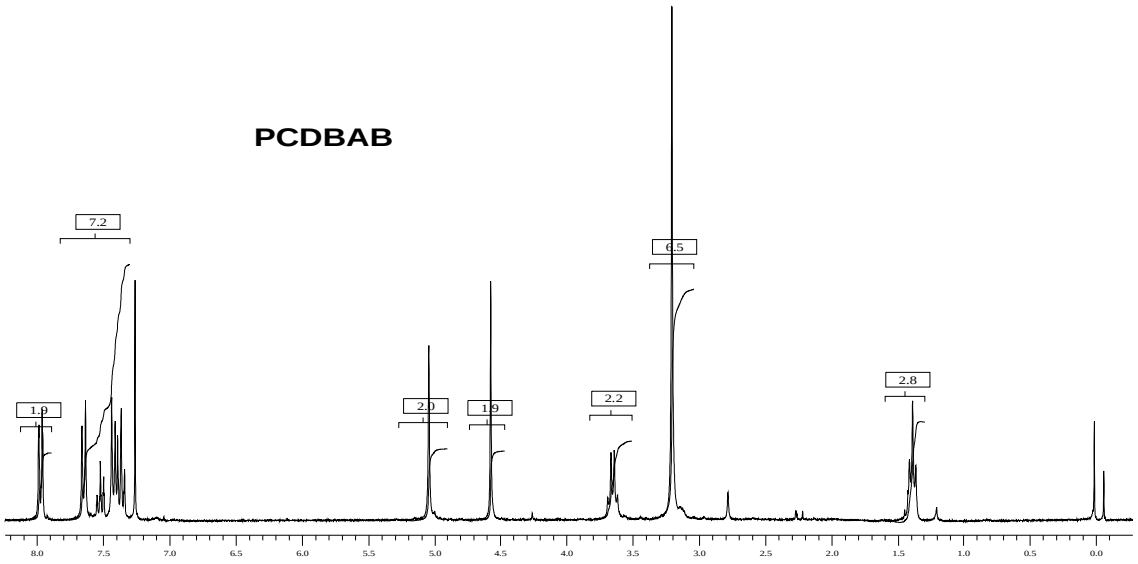

Fig. 1 ^{1}H NMR spectrum of PCDBAB

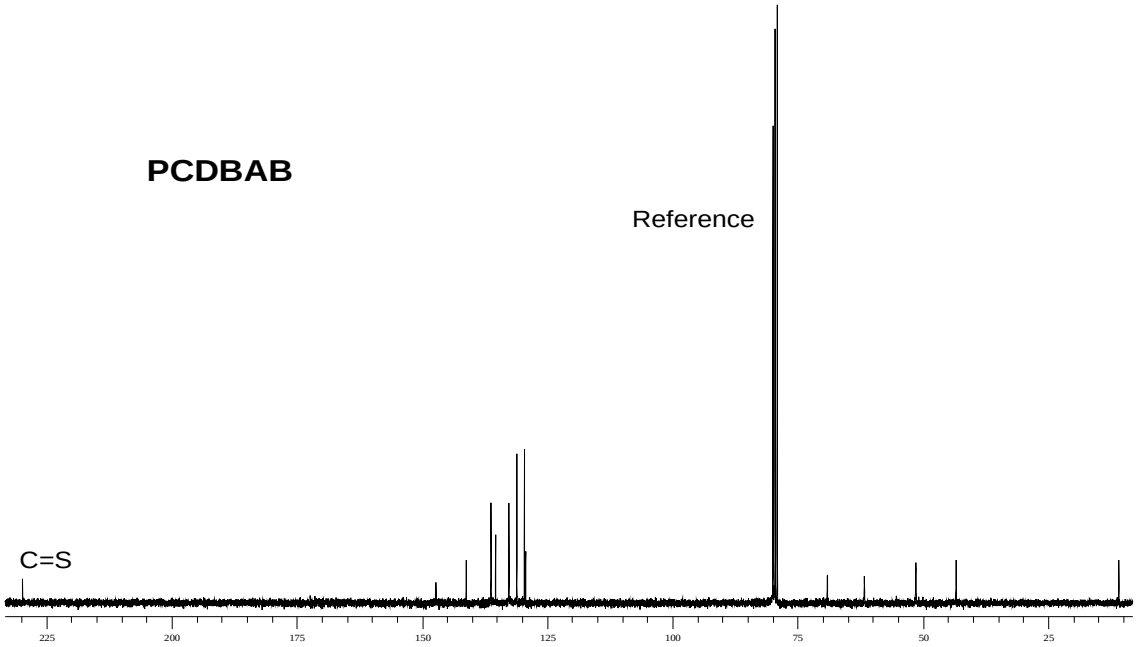

Fig. 2 ^{13}C NMR spectrum of PCDBAB

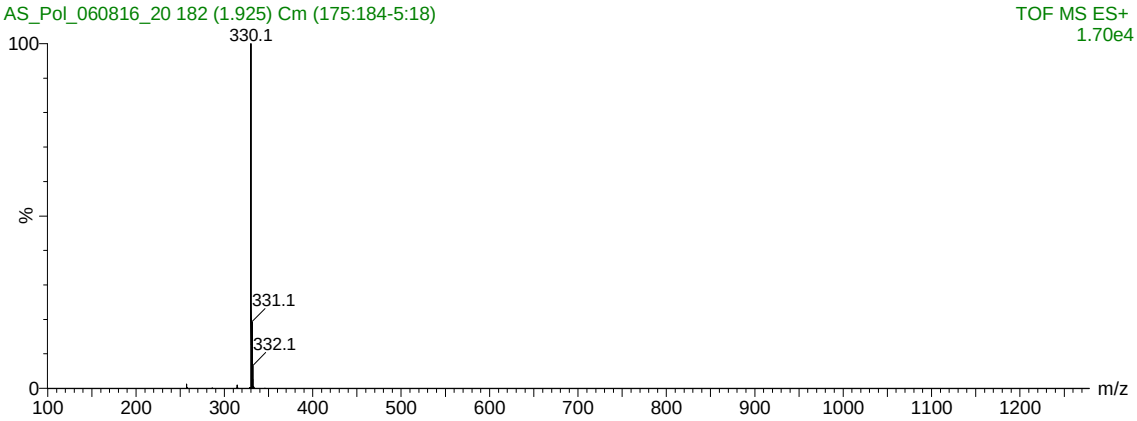

Fig. 3 ESMS spectrum of PCDBAB

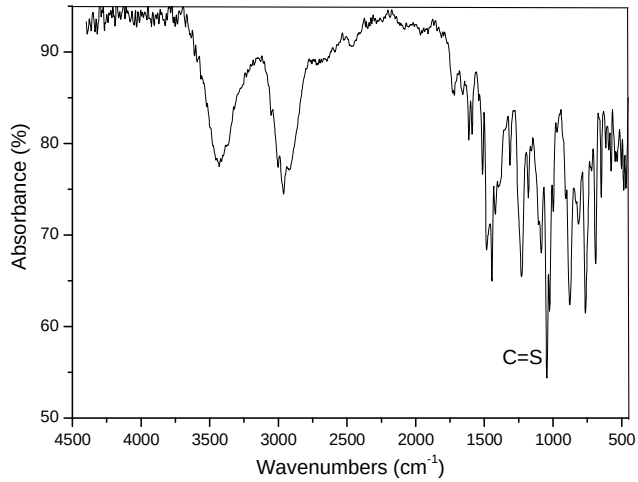

Fig. 4 PAS-FTIR spectrum of PCDBAB

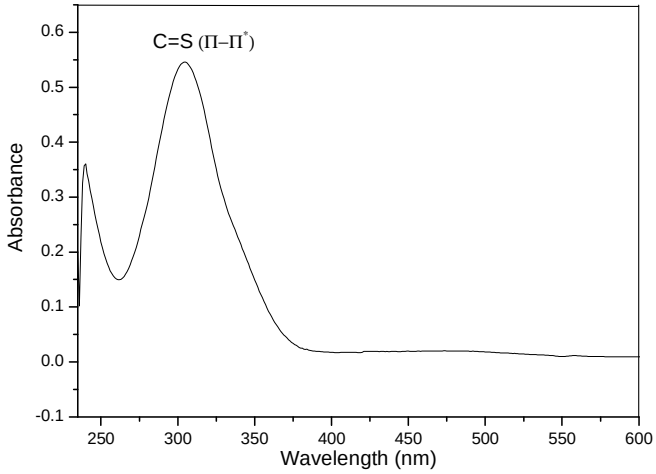

Fig. 5 UV spectrum of PCDBAB

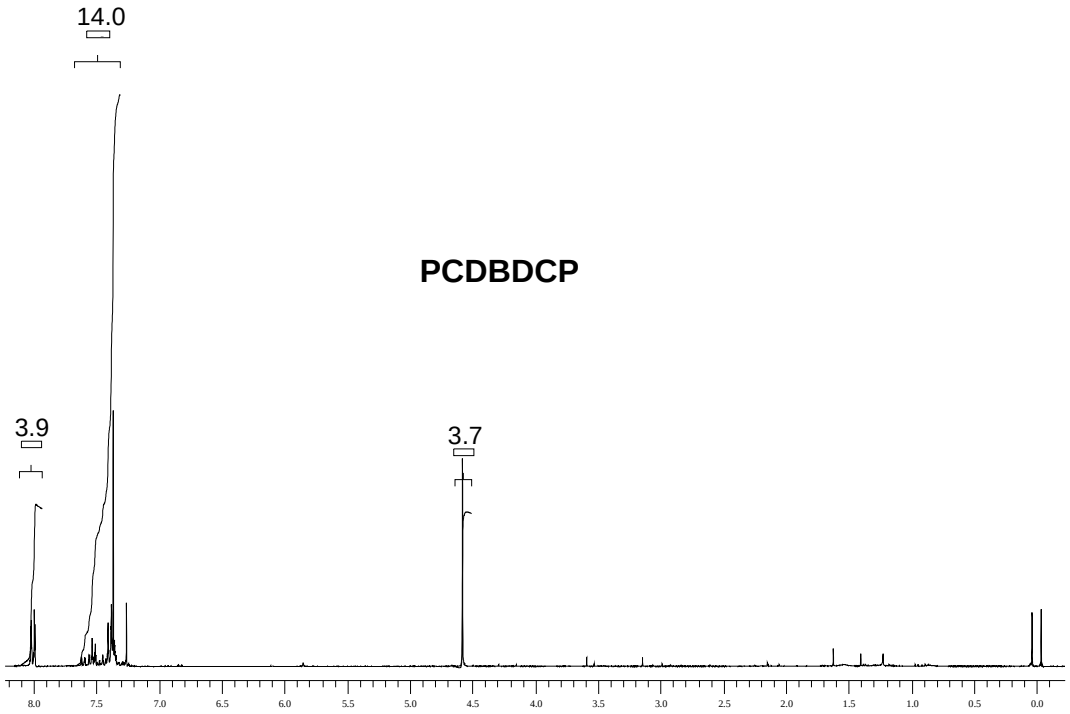

Fig. 6 ^{1}H NMR spectrum of PCDBDCP

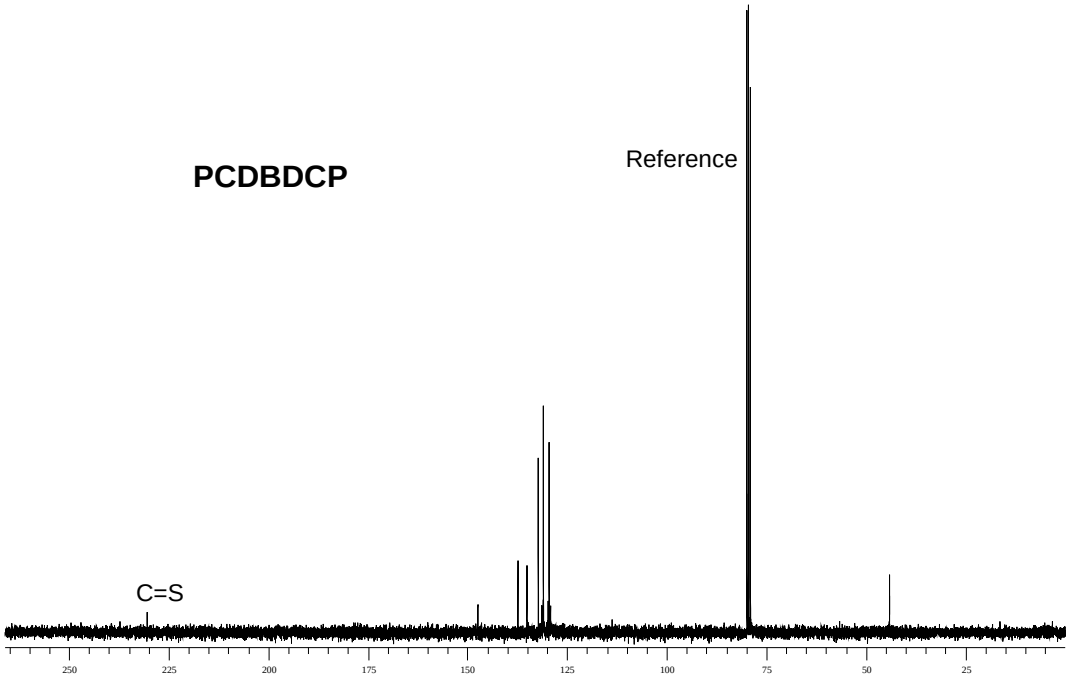

Fig. 7 ^{13}C NMR spectrum of PCDBDCP

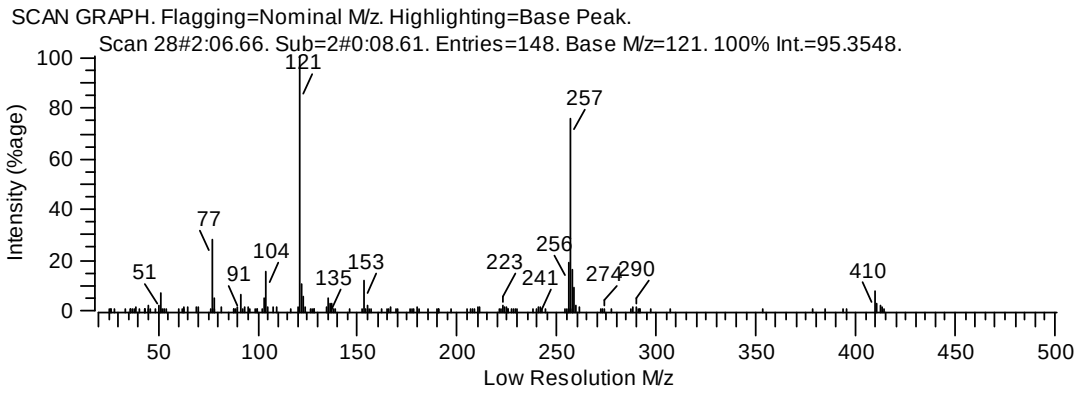

Fig. 8 EIMS spectrum of PCDBDCP

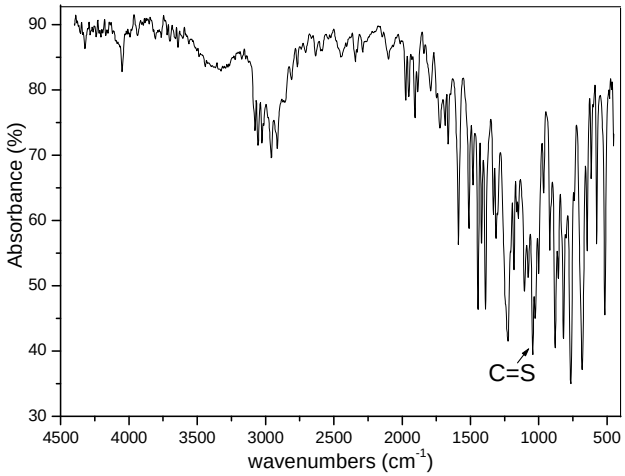

Fig. 9 PAS-FTIR spectrum of PCDBDCP

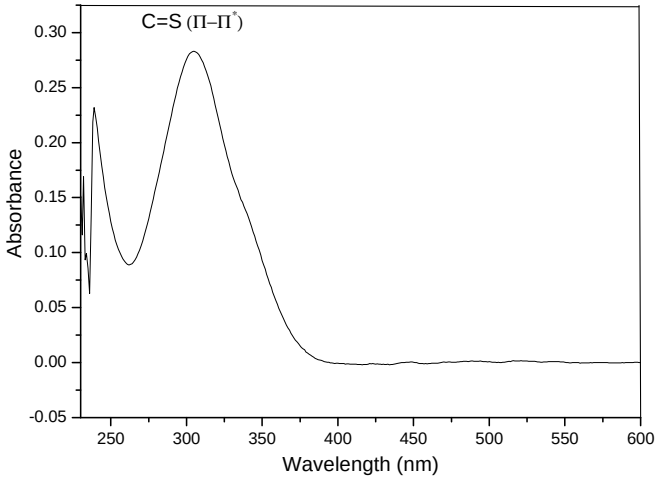

Fig. 10 UV spectrum of PCDBDCP

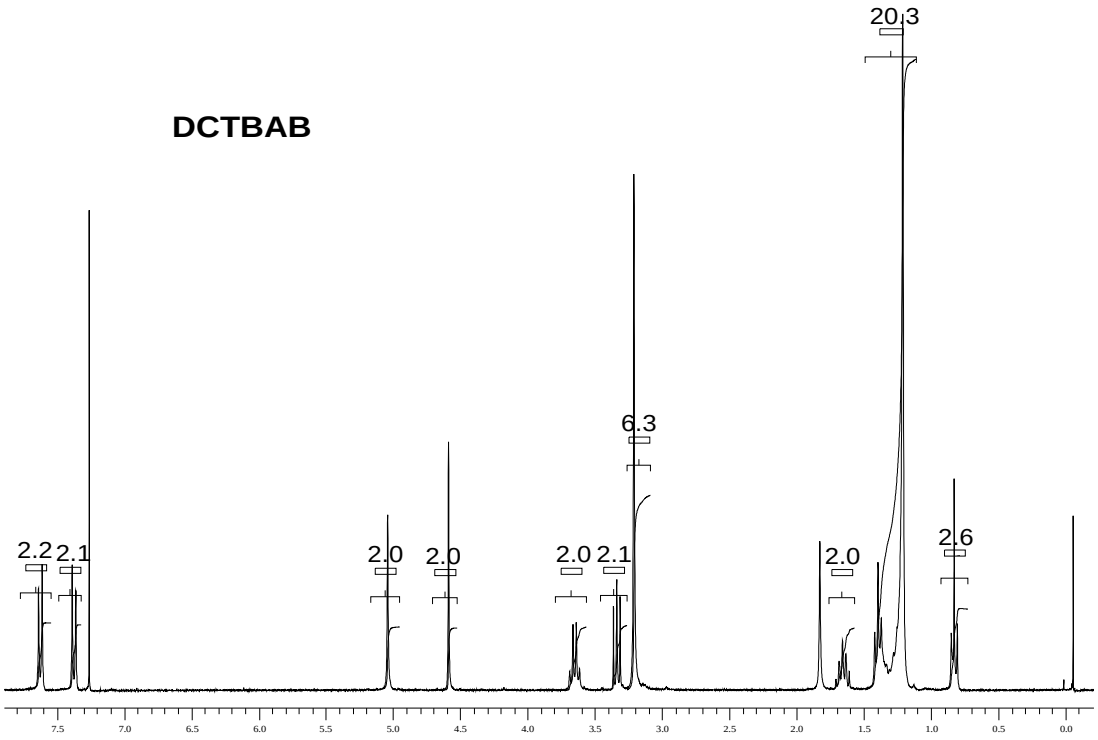

Fig. 11 ^{1}H NMR spectrum of DCTBAB

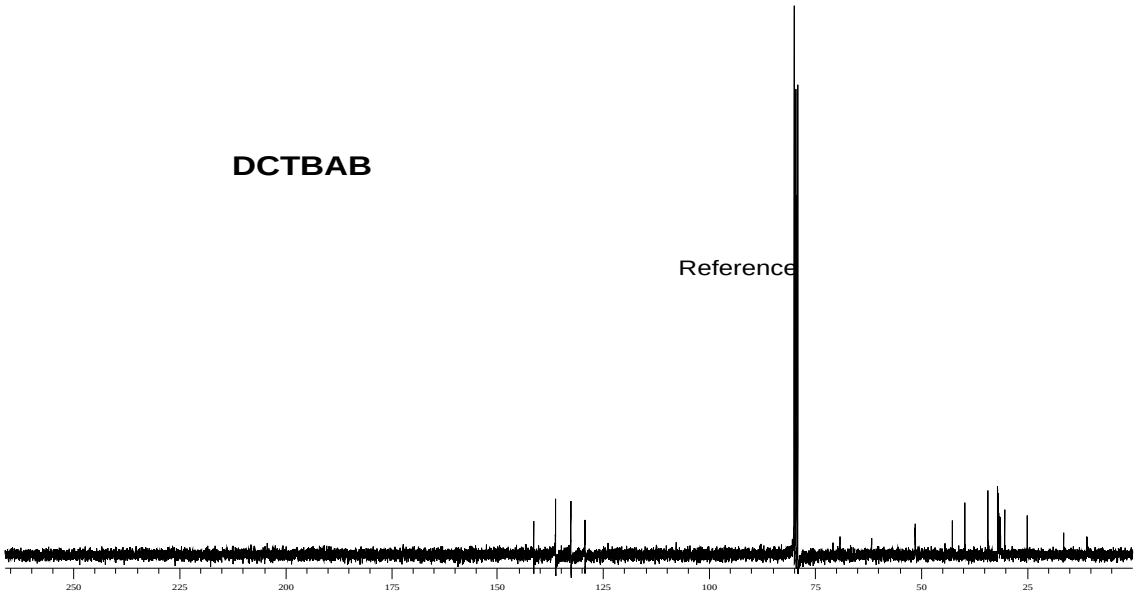

Fig. 12 ^{13}C NMR spectrum of DCTBAB

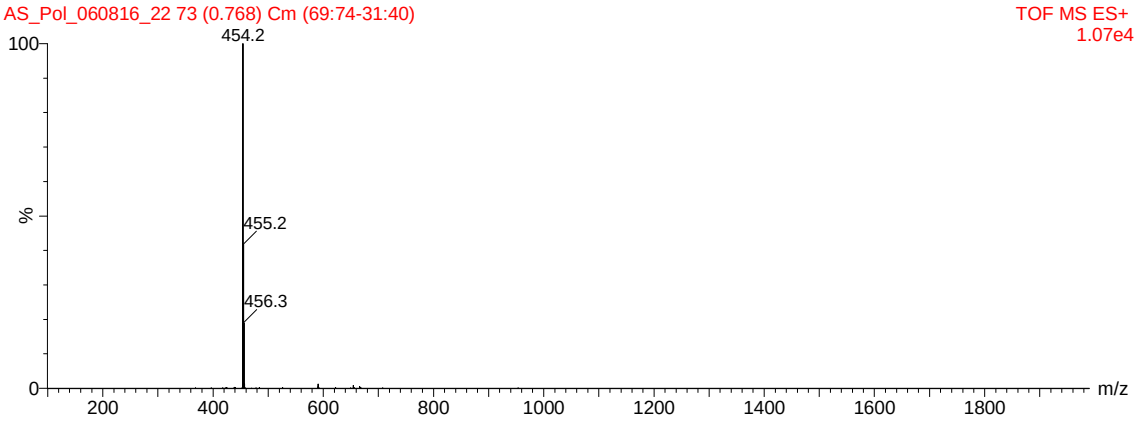

Fig. 13 ESMS spectrum of DCTBAB

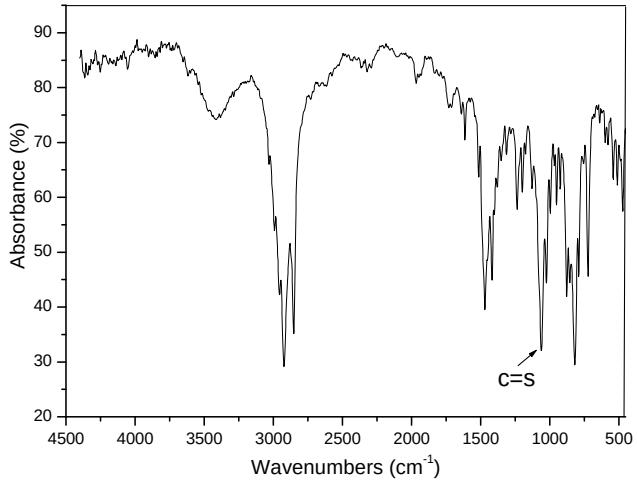

Fig. 14 PAS FTIR spectrum of DCTBAB

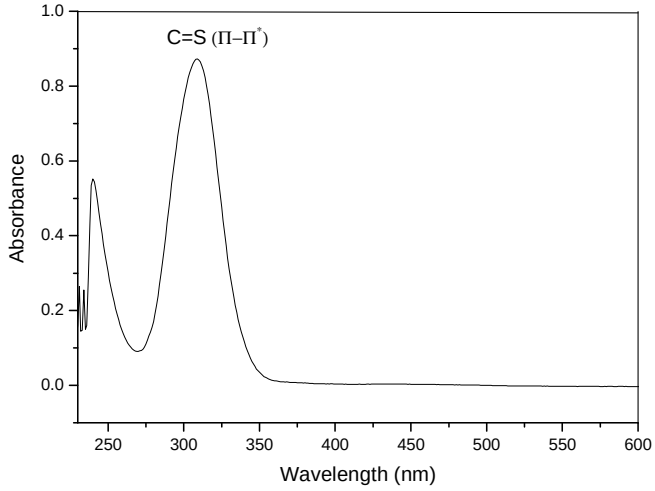

Fig. 15 UV spectrum of DCTBAB

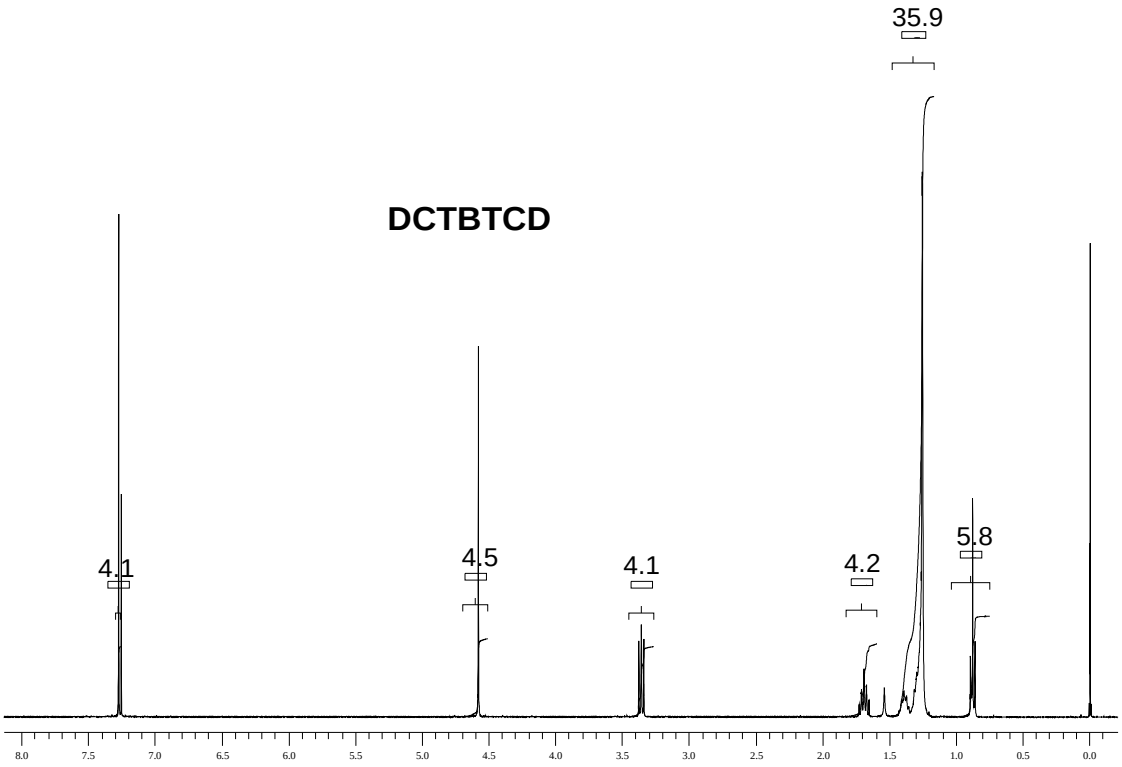

Fig. 16 ^{1}H NMR spectrum of DCTBTCD

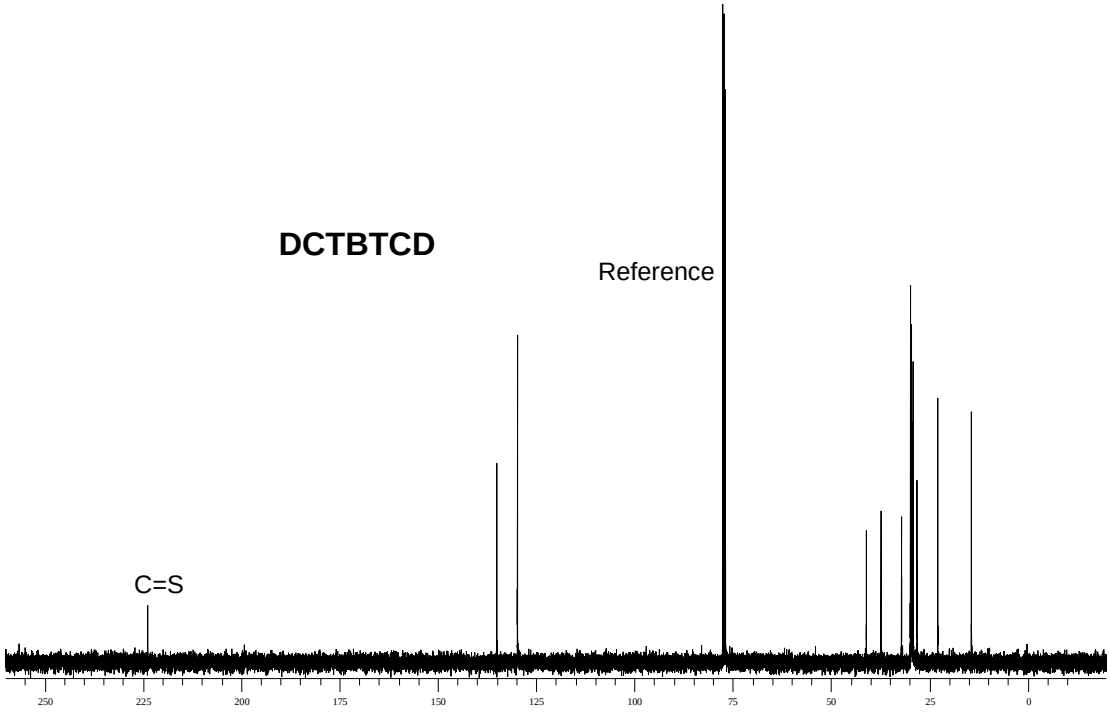

Fig. 17 ^{13}C NMR spectrum of DCTBTCD

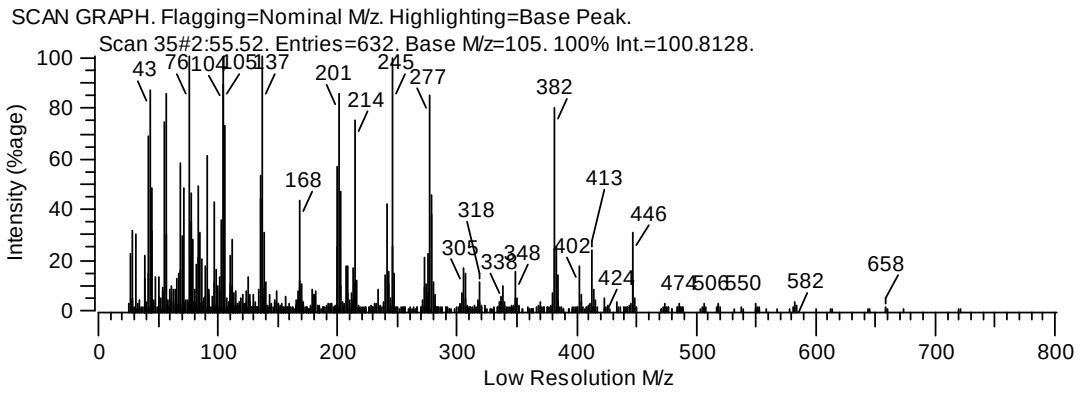

Fig. 18 EIMS spectrum of DCTBTCD

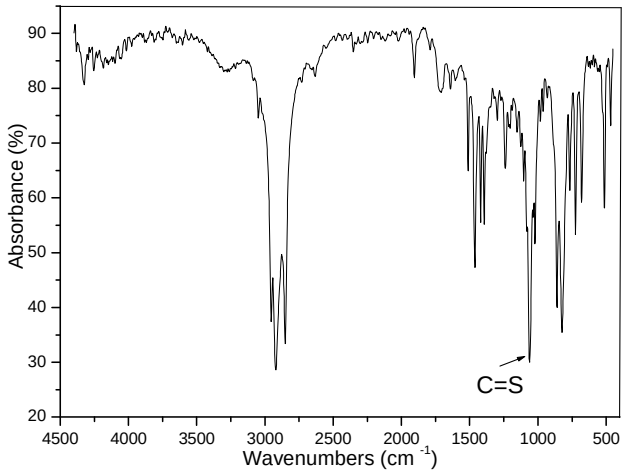

Fig. 19 PAS-FTIR spectrum of DCTBTCD

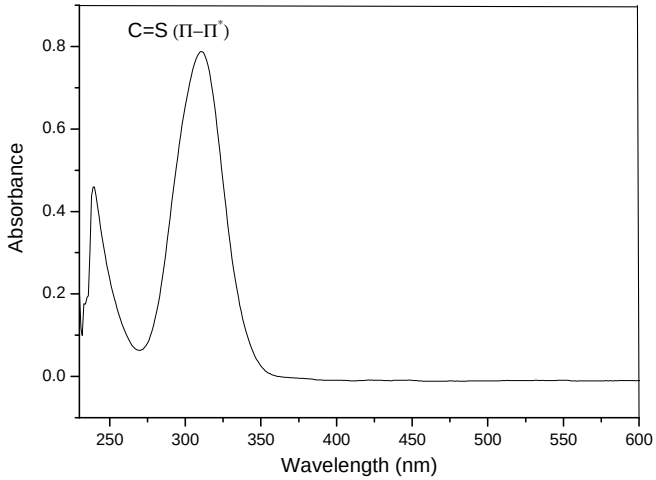

Fig. 20 UV spectrum of DCTBTCD

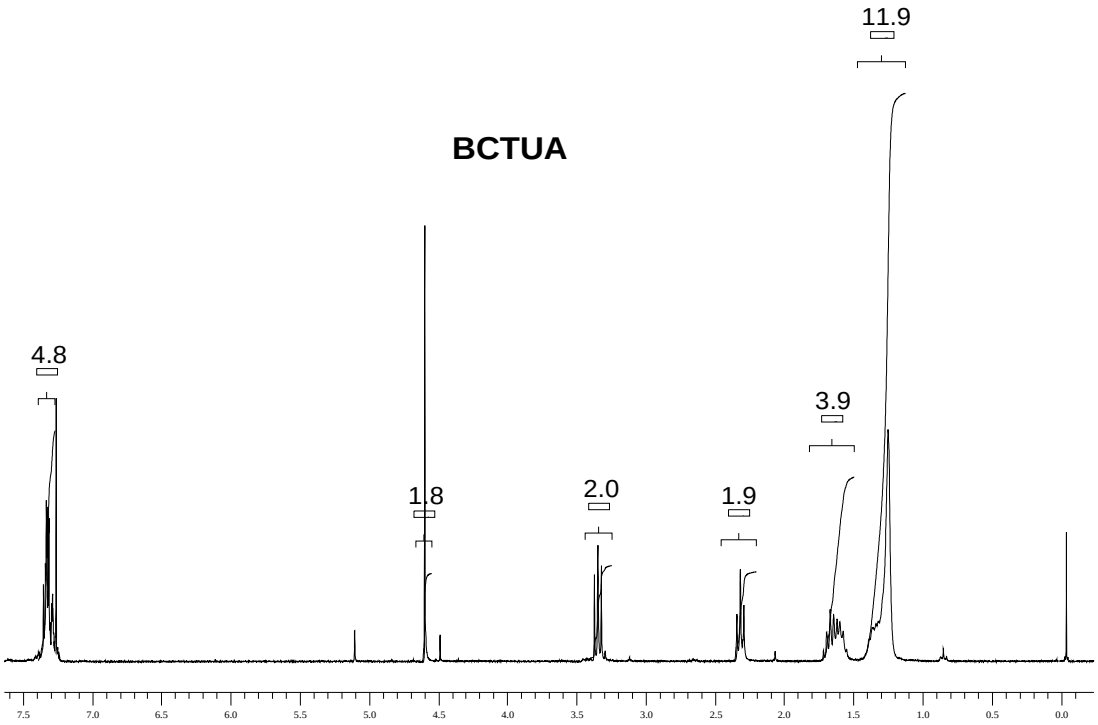

Fig. 21 ^{1}H NMR spectrum of BCTUA

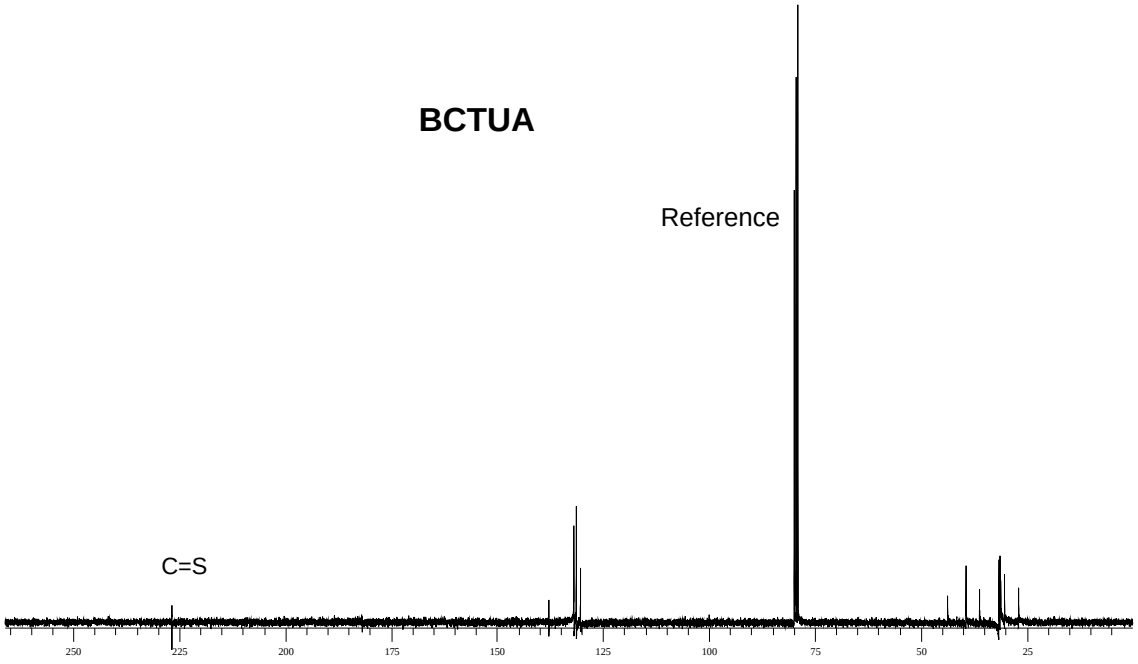

Fig. 22 ^{13}C spectrum of BCTUA

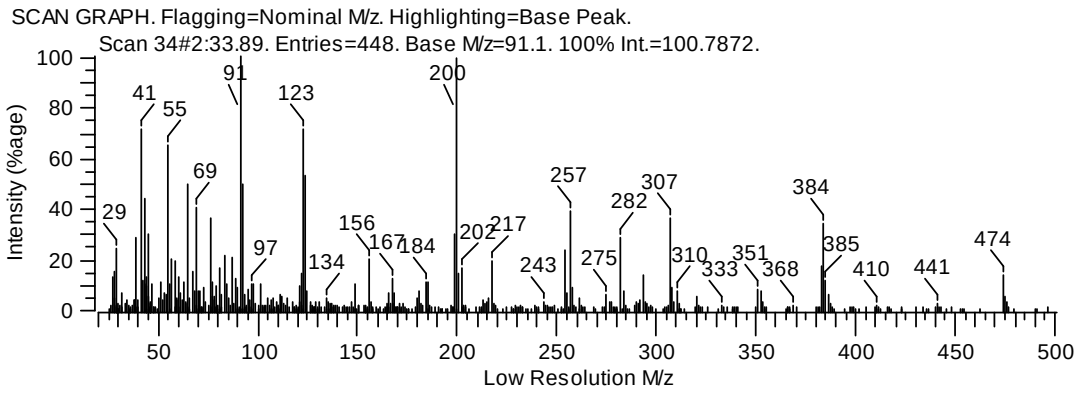

Fig. 23 EIMS spectrum of BCTUA

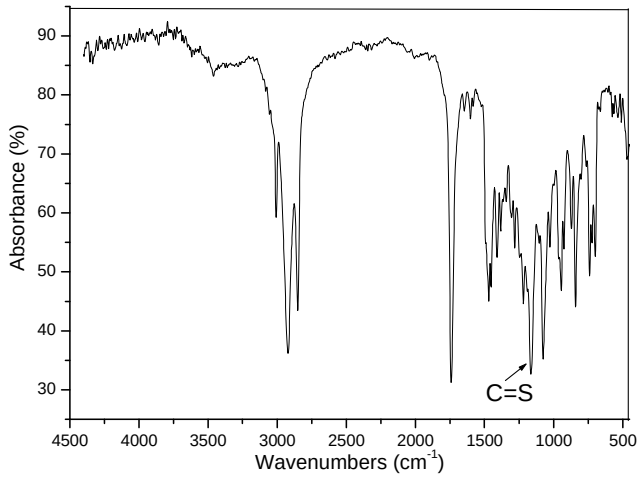

Fig. 24 PAS-FTIR spectrum of BCTUA

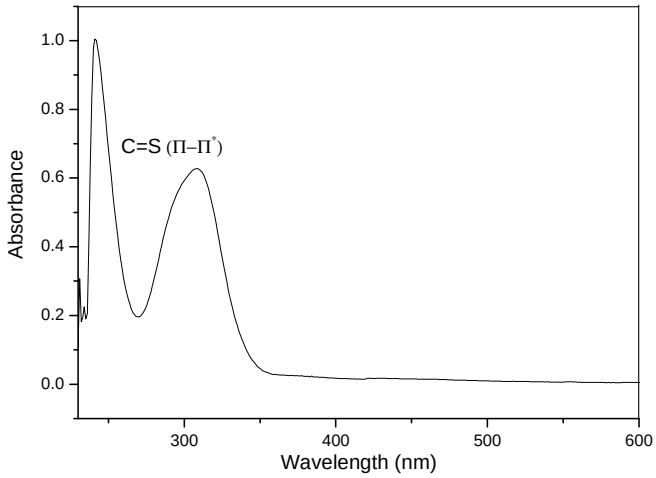

Fig. 25 UV spectrum of BCTUA

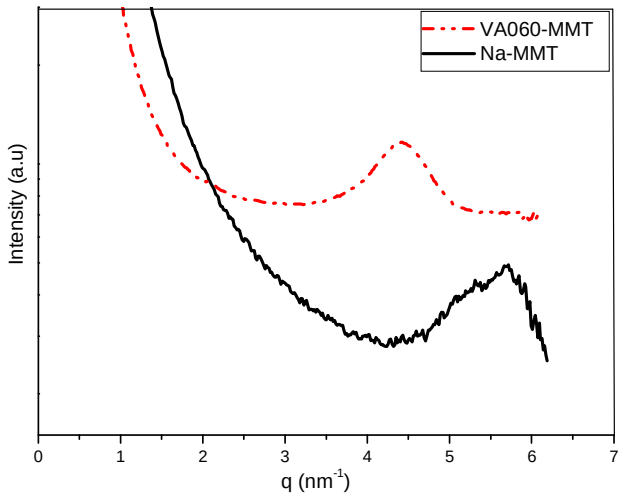

Fig. 26 SAXS pattern of Na-MMT and VA060-MMT clays

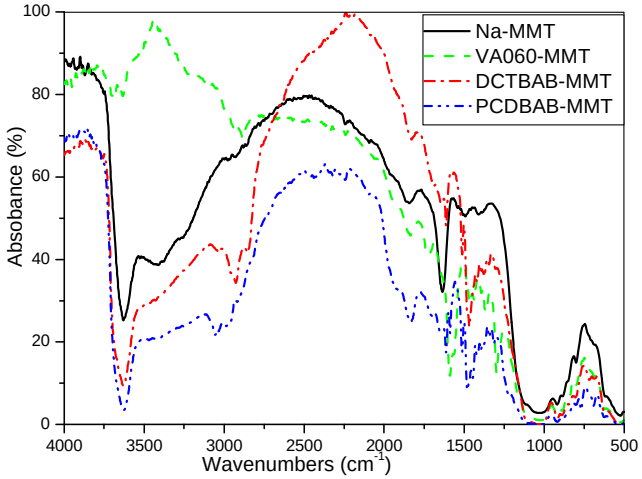

Fig. 27 PAS-FTIR spectra of modified-clays

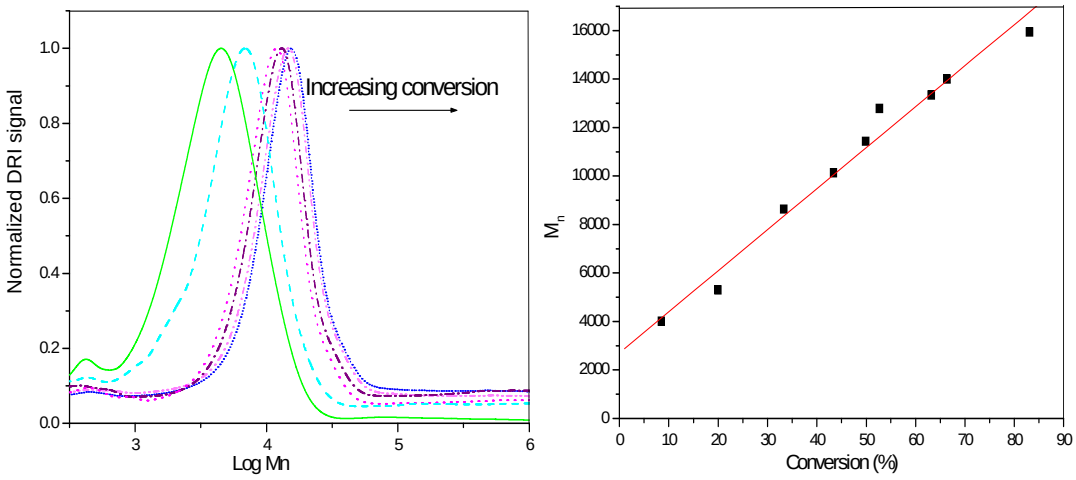

Fig. 28 Variation of molecular mass with conversion for DCTBAB mediated bulk polymerization of styrene

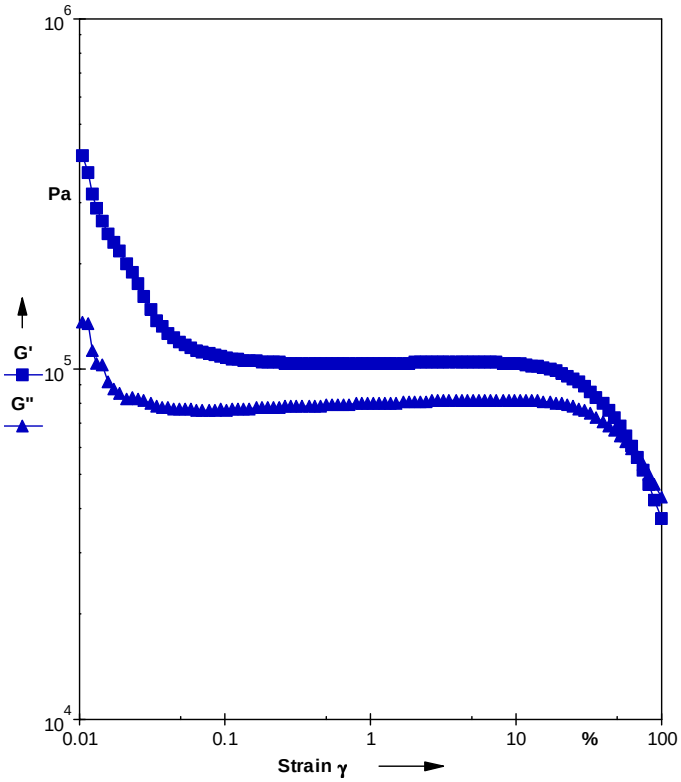

Fig. 29 Variation of Storage modulus (G^{I}) and Loss modulus (G^{II}) as a function of Strain, i.e. strain-sweep experiment, for P(S-co-BA)-PCDBAB-2% clay loading